UNIVERSITÀ DEGLI STUDI DI MILANO

DIPARTIMENTO DI INFORMATICA

DOCTORAL PROGRAM IN COMPUTER SCIENCE

Novel approaches in color assessment: from point-wise colorimetry to film restoration

---

Doctoral Dissertation of:
Alice PLUTINO

Supervisor:
Prof. Alessandro RIZZI

Co-Supervisor:
Dr. Barbara Rita BARRICELLI

The Chair of the Doctoral Program:
Prof. Paolo BOLDI

A.A. 2019/2020 - Cycle XXXIII

"When I heard the learn'd astronomer,
When the proofs, the figures, were ranged in columns before me,
When I was shown the charts and diagrams, to add, divide, and measure them,
When I sitting heard the astronomer where he lectured with much applause in the lecture-room,
How soon unaccountable I became tired and sick,
Till rising and gliding out I wander'd off by myself,
In the mystical moist night-air, and from time to time,
Look'd up in perfect silence at the stars."

Walt Whitman

"[...] senza la bellezza non avrà assolutamente nulla da fare al mondo! Tutto il segreto è qui, tutta la storia è qui! La scienza stessa non si reggerà neanche un minuto senza la bellezza, lo sapete questo, voi che ridete? Si convertirà in trivialità, non inventerete nemmeno un chiodo!"

Fëdor Michajlovič Dostoevskij

Abstract

Colorimetry is the science which studies the quantification, reproduction and management of color from its optical, chemical, physical, but also physiological and perceptual point of view. Today, colorimetry has been standardized and color management can count on a robust workflow in point-wise conditions, thus when a color stimulus is considered under specific constraints (e.g., standard illumination and observation). As a consequence, the rigorous application of standard colorimetry is insufficient to reproduce and manage color in real conditions with non-uniform illumination and with complex spatial arrangements. This work of research is organized into three threads of work, which follow the standard pipeline of color signal evaluation: color assessment, color acquisition and processing, and quality assessment.

In the first Part of this study, the assumptions and constraints of standard colorimetry are recalled, together with specific comments on their limits in non-standard and practical applications. The open problems and misuses of colorimetry discussed from the theoretical point of view are supported by preliminary tests and experiments, aiming at highlighting the limits of the application of standard colorimetry in cultural heritage field.

In the second Part of this work, the standard digitization workflow is analyzed, and the issues and effects which could affect the acquisition of contrast and tones in imaging systems are discussed. In particular, the limits of hyperspectral imaging have been tested and examined, in order to assess the main source of noise in the acquisition and to evaluate the reliability of the acquired data. Subsequently, an implementation of the digitization protocol for film restoration is proposed and different methods to perform image enhancement and processing have been examined. For this aim, the family of Spatial Color Algorithms (SCAs), derived from Retinex, has been found successful for cultural heritage applications and a novel approach to film restoration is proposed. This specific family of algorithms, enhance colors according to the spatial distribution of pixel values in the scene, thus include the visual spatial mechanisms in color computation, overcoming the main constraints of standard colorimetry. Nevertheless, SCAs present high computational costs. To address this problem, in this Thesis a new speed-up algorithm is presented in order to allow the enhancement of video streams.

Regarding quality assessment thread, an overview of image quality metrics is presented, and different metrics and measures have been examined and tested, to define which metrics could be the most effective and usable for cultural heritage applications. In this context, a new framework of image quality measures has been presented and applied on historical images and videos.

The field of cultural heritage has been particularly suitable to underline the limits in the application of standard colorimetry, because, in this context, color is never observed as isolated phenomenon, but always inside a spatial arrangement. In this work, film digital restoration has been the main field of application and different approaches and alternative methods have been proposed to overcome the limits of standard color analysis. Anyway, the highlighted limits and solutions are applicable to film restoration, as well as to many other fields, where color sensation cannot be limited to point-wise colorimetry.

Contents

Chapter 1

Introduction

1.1 Research Context

Color is not only a physical quantity, but also a quality of the visual sensation. It is subjective and incommunicable. Nevertheless, different people can agree asserting that different physical radiations produce similar color sensations. Colorimetry is based on the univocal correspondence of these two phenomena, which is possible thanks to the properties of the Human Visual System (HVS).

Human vision is a complex phenomenon which involves color perception together with many other elements like forms, movements, lights, shadows, surfaces texture, light polarization, which can interact among them. For this reason colorimetry aims at studying color as isolated phenomenon and is based on a strict set of conventions. From this, it is wrong to consider colorimetry as the science used to *quantify and describe physically the human color perception* [1]. This definition is an oxymoron, because it uses the ostensible contradiction of quantifying and describing physically something which cannot be controlled and quantified, the human color perception. It is better to define colorimetry, as the:

[...] measurement of color stimuli based on a set of conventions. [2]

From the general mistaken idea of colorimetry derive all the issues and problem presented in this work; above all, the application of colorimetry in non-standard conditions. Colorimetry, is used to study color quantification, reproduction and management from optical, chemical, physical, but also physiological and perceptual points of view. In 1931, CIE (Commission Internationale de l'éclairage, or International Commission on Illumination) published the first version of the spectral sensitivity curves of the human eye [3], which allowed for the first time to create a correlation between the physical nature of color and the human perception. In this publication, the *CIE 1931 RGB* and *CIE 1931 XYZ* color spaces have been presented and thanks to the experiments of Wright and Guild the colorimetry was born. Today, this science has been standardized and the color management can count on a robust pipeline which allow identifying and reproducing colors in standard conditions of illumination and observation [4]. Following this idea, color sensation can be resumed as the result of three main phenomena: (1) the radiation emitted by a light source, (2) the interaction between the emitted light and the surface of an object (3) the elaboration of the signal reflected by an object in the Human Visual System [5]. Thus, color sensation depends on: the light source spectrum, the optical properties of the object surface and the elaboration of the visual system.

Since the birth of colorimetry, many studies focused on light sources characterization have been made [2], [6]–[8]. The field of spectroscopy made developments and innovations in materials properties analysis [9]–[11] and today, colorimetry is a useful science to manage color through different systems (from monitors to printers) and, more in general, to specify color through numbers. Nevertheless, the studies

concerning the third phenomena of color vision (i.e. color perception and appearance) are limited [12]–[14] and a complete model of the human visual system still does not exist. As a consequence, when colorimetry is applied in non-standard conditions or for non-standard observers (e.g., color blind people), this science is no more appropriate to model color perception. As a consequence, colorimetry is extremely useful and correct for color analysis, management and reproduction in point-wise conditions, but in scenes and contexts where the human visual system performs a higher-level elaboration of the signal, it fails. Colorimetry is widely used in many fields of application and has become a fundamental science in the study and analysis of cultural heritage. In this field, the study of colors is fundamental, because color has not only an expressive role, but it is also a physical part of the historical objects and must be identified, conserved, restored and promoted. In cultural heritage, the use of spectroscopy is widely spread to identify the materials composing the works of art (e.g., pigments identification in paintings), but also for restoration and retrieval. Therefore, it is applied mainly for the analysis of the physical and chemical properties of the materials, without considering the appearance and psycho-physical process of color perception. The use of colorimetry in cultural heritage application is limited to the numerical definition of point-wise color, in order to assess the color fading on a surface, monitor aging processes, evaluate innovative protective or cleaning products, among other things. In this context, the wrong use of spectral data and the application of point-wise colorimetry in non-standard conditions can lead to problems in the computation of colorimetric spatial coordinates and color perception modeling [15], [16].

These limits comes out especially when point-wise spectral data are used to make two-dimensional or three-dimensional colorimetric reconstruction, where the standard conditions of observation and illumination are no more preserved, and as results the colors of the reconstructions are no more coherent with the visual color perception of the original objects. In 2D or 3D contexts, in fact, the HSV performs an higher-level elaboration and spatial processing [17], [18], which is not considered by standard colorimetry, that models the human visual system just to the transduction level (i.e., retinal level). The limits of colorimetry in acquisition and color reproduction in 2D and 3D contexts are well known and some technical solutions have been proposed and developed in recent years. Nevertheless, in the field of cultural heritage and, more specifically, for photo and film restoration, the adopted solutions are based mainly on the visual assessment and the restoration is performed subjectively [19], [20].

1.2 Motivation and Aims

Starting from the current literature and the colorimetry research context, this thesis underlines and analyzes the main limits and constraints of standard colorimetry in cultural heritage applications, and proposes novel approaches and methods to measure, render and control color. This work has been divided in three main threads: color assessment, color acquisition and processing, and quality assessment. In the first thread, the main limits of colorimetry will be presented and discussed from the theoretical point of view, and through practical experiments, in order to focus on the development of new protocols and modelings.

In this Part, an overview of the color specifications available through the standard colorimetry (i.e., color matching, color difference and appearance) are presented, together with the constraints related to their practical use. A series of open

problems and misuses of colorimetry will be discussed and supported by practical experiments.

Considering color acquisition and processing, different open questions can be underlined and it is fundamental to deal with them. Today, different standardized instruments can be used to calibrate and assess the performance of an acquisition setup or to manage color reproduction. Nevertheless, for many applications, the standard calibration protocols and guidelines have been found inadequate, especially when an accurate acquisitions is needed, and the correlated metrics have been found insufficient [21]. Thus, there is the need to examine the main source of error in the acquisition workflow and propose new metrics to measure them, together with new protocols and guidelines. Concerning the field of cultural heritage, color acquisition and processing are a fundamental step for many application, including film restoration. In this field, the lack of commonly shared digitization procedures together with the common problems of noise and error propagation in the acquisition, led to the need of more control during film scanning. Furthermore, digital restoration, today, is performed subjectively and is dependent on commercial softwares. Thus, there is the need to define the different approaches to film restoration and provide innovative technical methods to restore and enhance film frames taking into account the materials and the origin of films.

In conclusion, to assess the quality of the final results of a restoration or an image enhancement process, different image quality metrics exists. Despite the subjective evaluation is very popular in many applications, an objective quality assessment is desirable, since it guarantees the reproducibility of the results and enables automation. In the literature, many full-, no- or reduced- reference image quality metrics have been proposed. Due to the complexity of image quality assessment, a single metric and a single quality value may not be robust enough to summarize all the aspects occurring to a complete quality evaluation. Furthermore with a single numerical output it is hard to understand why an image gives a good or a bad quality value. In this context, the evaluation of image quality in film restoration is even harder, because in many cases a reference does not exists and the quality of the results is evaluated visually by the film curator. Thus, it is mandatory to find new tools and solutions to assess the global quality of a restoration or an image enhancement process, which could be complete, usable and easy to understand for film experts and restorers. Today, there are no commonly shared solutions to overcome the presented issues. With this work I propose new approaches and preliminary strategies, as well as rising the awareness of the scientific community in this field, in order to find new solutions leading to a more correct and accurate color management and assessment.

1.3 Research Method

In order to identify the contexts and application fields in which standard colorimetry is applied improperly, different experiments have been carried out and different approaches have been proposed. After a general overview on standard colorimetry (Chapter 2), in order to support the theoretical dissertation on the open problems in the assessment of color appearance, different psychophysical experiments requiring human observers have been made (Chapter 3). In these tests, quantitative and qualitative methods have been used to obtain a complete and detailed description of color assessment measures and methods and to get a broaden understanding of this

phenomenon. Subsequently, after a broad analysis of all the guidelines and methods to digitize and acquire signals and images (Chapter 4), different tests have been conducted on a hyperspectral acquisition system, to assess the limits and potentials of digital acquisitions in the analysis and reproduction of colors (Section 4.3). The obtained data have been analyzed using in existing methods and innovative metrics and measurements, in order to assess the main source of noise in the acquisition and the reliability of the acquired data. In the context of cultural heritage and film restoration, a systematic review of the existing methods to enhance color images has been made (Chapter 6), and from it, different techniques for the restoration of old films have been tested and examined (Chapter 5). In this context, a speed-up to apply some of the most suitable algorithms for image enhancement on videos has been proposed, tested end evaluated (Section 5.5). To give a compete and trustworthy evaluation of the results a novel framework of image quality metrics has been proposed, tested and applied on different datasets (Chapter 7). The work carried out in this thesis is both theoretical and practical.

Core application of this work is the digital film restoration, thus a multidisciplinary and complex field in which the color sensation cannot be limited to the set of conventions imposed by standard colorimetry. In this context, the colorimetric constraints are often not considered, and the lack of scientific research caused weaknesses and problems between color measurements and color sensations, which are often solved resorting to subjectivity. The presented and discussed limits of standard colorimetry characterize the field of film restoration as well as many other field of application, in which color analysis can not be limited to the transduction level of the HSV, but is the results of an higher-level elaboration. For this reason, color assessment is presented also in museums lighting application and in gems color evaluation (Chapter 2), but it is applicable to any context in which color analysis is performed without applying the colorimetry constraints and set of conventions.

1.4 Thesis Contribution

This thesis is intended to contribute to the research field with necessary information and tools to measure, render and control color in cultural heritage applications, with a specific focus on film restoration. The thesis is organized in three main parts.

Part I: Color assessment: after an overview of the background knowledge in colorimetry and the presentation of the standard colorimetric computational models, the main limits of standard point-wise colorimetry are presented. Here, two psychophysical experiments are used to demonstrate the main limits of colorimetry and novel approaches to analyze color in non-standard conditions are proposed. This study led to the publication of the following scientific journal papers:

> [21] Plutino A. and Simone G., "The Limits of Colorimetry in Cultural Heritage Applications", Coloration Technology, Volume 137, Issue 1, Special Issue: Challenges and Open Problems in Colorimetry Special Issue, February 2021, Pages 56-63. DOI: https://doi.org/10.1111/cote.12500.
>
> [22] De Meo S., Plutino A. and Rizzi A., "Assessing colour of gemstones", Color Research and Application 2020, pp. 1-11, Wiley Periodicals Inc., 2020, DOI: 10.1002/col.22472.
>
> [8] Plutino A., Grechi L., Rizzi A., "Evaluation of the perceived colour difference under different lighting for museum applications", Color Culture and Science Journal Vol. 11 (2), 2019, DOI: 10.23738/CCSJ.110210.

Part II: Color acquisition and processing: a preliminary overview of the standard acquisition workflow is presented and a practical experiment is proposed to measure and assess the main source of error in imaging systems. Subsequently, after a detailed introduction on film restoration, an implementation of film digitization protocol has been proposed and different methods to perform image enhancement and processing have been examined. In this context, the family of Spatial Color Algorithms, has been found successful for film restoration applications and a new speed-up to effectively apply these algorithms on videos is presented. This study led to the publication of the following scientific journal papers:

> [23] Signoroni A., Conte M., Plutino A. and Rizzi A., "Spatial-spectral evidence of glare influence on hyperspectral acquisitions", Sensors 2020, 20(16), 4374; DOI: https://doi.org/10.3390/s20164374.

> [24] Plutino A, Rizzi A. "Research directions in color movie restoration", Coloration Technol, Volume 137, Issue 1, Special Issue: Challenges and Open Problems in Colorimetry Special Issue, February 2021, Pages 78-82, DOI: https://doi.org/10.1111/cote.12488.

Part III: Quality assessment: an overview of the research area related to quality in imaging is presented and different image quality metrics have been tested for film restoration assessment. Here, a new framework for the evaluation of image and videos of historical value is exposed, tested and applied on different datasets. This study led to the publication of the following scientific journal papers:

> [25] Barricelli B. R., Casiraghi E., Lecca M., Pluino A., and Rizzi A., "A cockpit of multiple measures for assessing film restoration quality", Pattern Recognition Letters, Pattern Recognition and Artificial Intelligence Techniques for Cultural Heritage special issue, available online: 8 January 2020, DOI: 10.1016/j.patrec.2020.01.009.

> [26] Plutino A., Lanaro M. P., Liberini S., Rizzi A., "Work memories in Super 8: Searching a frame quality metric for movie restoration assessment", Journal of Cultural Heritage, 2019, DOI: 10.1016/j.culher.2019.06.008.

Other publication on the specified topics are reported after the thesis conclusions in Section 8.1.

Part I

Color assessment

Chapter 2

Color and colorimetry

2.1 Introduction

In the real physical world, color does not exist. Color vision is the interpretation of the world made by our brain, which has evolved to acquire and elaborate the different frequencies of the visible radiation entering in our visual system. This phenomenon is originated by the photo-receptors in the retina, which convert the light in nerve signals, subsequently sent to the brain (i.e., thalamus and visual cortex) through the optical nerve, where they are interpreted as images (see Section 2.2).

As presented in this Chapter, standard colorimetry focus in the study of color as result of the cones transduction, thus as isolated stimulus observed in standard conditions. As a consequence, in colorimetry, the color specification is determined by defined constraints: the Standard Observer, the light source, the direction of observation and of illumination, the type of spectral data and the technique applied in the colorimetric computation (see Section 2.3). Therefore, colorimetry can be very precise and accurate in measuring color under specific conditions of observation and illumination (see *aperture mode* in Section 2.3), but fails if applied in complex spatial contexts, where color is not isolated, but is the result of an higher level elaboration in the HVS.

Over the course of colorimetry history, different models and systems have been presented, to measure and assess color in complex scenes and in non-standard configurations (see Section 2.3.3). Nevertheless, all those models restrict the scene complexity to a defined set of conditions, are based on their own constraints, do not consider the spatial arrangement, and the consequent elaboration made by the brain in the process of vision. As a consequence, still today, there is the need to develop new color vision models which considers the contribution of the whole HVS, including the higher-level elaboration and not just the retinal transduction level. Furthermore, colorimetry must develop new models and systems to assess color in complex spatial arrangements, considering edges, gradients and spatial interactions (i.e., the entire scene and not just the isolated color stimulus).

Due to the physical and perceptive nature of color, it is important to understand the complexity of the mechanisms of color vision, and define on which constraints and assumptions colorimetry is based. In this Section, after a brief overview of color vision physiology and the presentations of the different colorimetric phases, the assumptions and constraints of colorimetry are recalled, together with specific comments on their limits in non-standard and practical applications.

Successively in Chapter 3, the open problems and misuses of colorimetry presented in this Chapter will be supported by psychophysical experiments, aiming at highlighting the limits of the application of standard colorimetry in cultural heritage field.

2.2 Overview of color vision physiology

The phenomenon of vision is a complex process, and today still not completely understood, despite years of studies and modeling. The retina is the sensible layer of the eye, in which the nervous signals are generated in response to the visual stimuli coming from the surrounding environment. It is the innermost tissue in the eye, where the image of the visual world is focused and converted in electrical neural impulses sent to the brain. The neural retina consists of several layers of neurons interconnected by synapses, and is supported by an outer layer of pigmented epithelial cells. The primary light-sensing cells in the retina are the photo-receptor cells, which are of two types: rods and cones. Rods are typically long and thin, differently of the cones that are more round. The external part of photo-receptors is composed by a layer containing the photopigment, a chemical substance that isomerizes when absorbs light. From this, the electric signal is generated as the first neural response to the visual stimuli. The signal is then transmitted through the retina's neural networks (see Figure 2.1a).

In the central area of the retina, there is the *fovea*, that contains only cones. The bipolar and ganglion cells ar not in front of the cones, as happens in all the other retina regions, but are placed on the fovea borders. This is the only region in the retina where the photo-receptors receive directly the radiations coming from external objects and focused by the eye. In fact, in the other regions of the retina, the radiations must pass through cells of the most external layers before reaching the photo-receptors. Furthermore, in the fovea, for each cone there is one bipolar and one ganglion cell. Due to this, the fovea is the region in the retina that allows the best vision of thin details, so the best *visual acuity* [28].

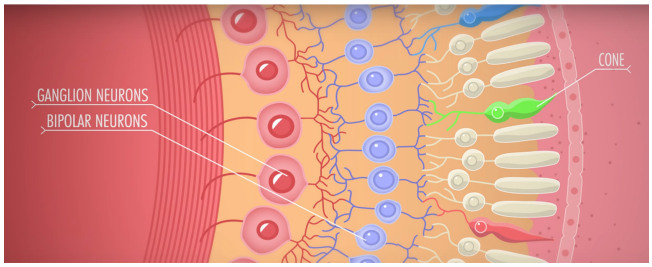

(A)

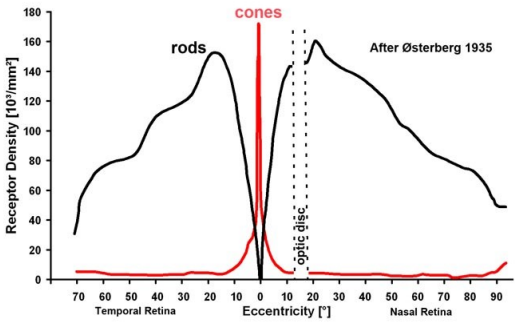

(B)

FIGURE 2.1: In Figure 2.1a a graphical representation of the retina. In Figure 2.1b Rods and cones densities along the horizontal median. Figure reproduced from [29]

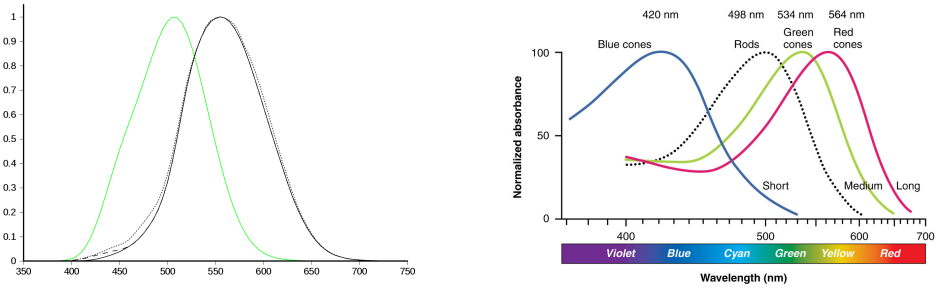

(A) (B)

FIGURE 2.2: In Figure 2.2a a graph of photopic luminosity function (black) including CIE 1931 (solid), Judd-Vos modified (dashed), and Sharpe, Stockman, Jagla and Jägle 2005 (dotted); and scotopic luminosity function, CIE 1951 (green). In Figure 2.2a the normalized human photoreceptor absorbances for different wavelengths of light. Figures reproduced from:[31]

The two kinds of photo-receptors, rods and cones, have different functions: the rods are responsible for the night vision (*scotopic vision*) and the cones are responsible for the daily vision (*photopic vision*). Rods are usually found concentrated at the outer edges of the retina and are also used in peripheral vision. On average, there are approximately 92 million rod cells in the human retina [30]. Cone cells are densely packed in the *fovea centralis*, a 0.3 mm diameter rod-free area with very thin, densely packed cones which quickly reduce in number towards the periphery of the retina. There are about six to seven million cones in a human eye and are most concentrated towards the *macula*, a rounded pigmented area axial to the retina center. The commonly cited figure of six million cone cells in the human eye was first reported by Osterberg in 1935 [29] (See Figure 2.1b).

The photopic vision is characterized by the curve of *Luminous efficiency* $V(\lambda)$. This curve describes how the eye sensitivity varies for monochromatic radiations of different wavelengths λ (at photopic level). The sensitivity is normalized to its maximum value (555 nm) and is referred to the *Standard Observer* defined by the CIE (International Commission on Illumination) in 1924 (see Figure 2.2a) [32]. The sensitivity curve drops below 400 nm and above 700 nm, that are generally considered the limits of the visible spectrum. A similar function $V'(\lambda)$ describes the eye scotopic vision. This curve was defined by CIE in 1951 [33]. The main differences between the scotopic sensitivity curve and the photopic are that the peak of maximum sensitivity in night vision is at 507 nm, instead of 555 nm, and that the scotopic sensitivity is moderately bigger for shot wavelengths and smaller for long wavelengths [32]. Ability to see colors is a capability of the photopic vision and is due to the cones. There are three kinds of cones, and each kind contains a different pigment that absorbs in different percentage the radiations of the visible spectrum, and each cone contains just one of those pigments. Due to this, the cones can be classified in: *Cones L* that cover the region of long and medium wavelengths with a maximum at 560 nm; *Cones M* that absorb medium wavelengths with a maximum at 530 nm and; *Cones S* that absorb shot wavelength with a maximum at 420 nm [29]. Note in Figure 2.2b that the curves of L and M cones are more overlapping, in contrast to the S curve that is well separate from the others. In the retina, the cones L and M, are more numerous than the cones S. The S cones can be very few or completely absent in the center of the fovea and globally they are approximately the 10% of all the cones in the retina. The photopic sensitivity curve results in the sum of the responses of the

cones L and M. Thus, just those two classes of cones defines how luminous a stimulus appears to an observer. However, the S cones give a significant contribute to the chromatic vision [32].

2.3 Colorimetry: computational modeling and digitization

Since the phenomenon of color vision is extremely complex and, still today, not fully understood, colorimetry mainly focuses on the study of color at the retinal transduction level (i.e., as isolated phenomenon observed in standard conditions) [34]. Because of this simplification of the color vision process, colorimetry presents many open problems, even if they have been simplified during the last decades through the introduction of specific constraints. Aim of colorimetry is the color specification through numbers, and this happens (and is happened) with different methods and with different meanings.

Oleari in [32], splits colorimetry in three historical phases, with the associated vision level, Standard Observer and CIE systems (see Table 2.1).

Historical phases/vision level/systems			
	1st historical phase: "color matching" 1st vision level: transduction Psychophysical system	2nd historical phase: "color difference" 2nd vision level: adaptation Psychometric system	3rd historical phase: "color appearance" 3rd vision level ...
Foveal vision (field of view $< 4^\circ$)	CIE 1931 Standard Observer (X,Y,Z) Judd-Vos observer (L,M,S)	CIELUV (L*, u*, v*) CIELAB (L*, a*, b*)	CIECAM Retinex ...
Extrafoveal vision (field of view 10°)	CIE 1964 Supplementary Standard Observer (X_{10}, Y_{10}, Z_{10})	CIELUV $(L*_{10}, u*_{10}, v*_{10})$ CIELAB $(L*_{10}, a*_{10}, b*_{10})$	...

TABLE 2.1: Colorimetry outline according to historical phases, vision level with the associated CIE standard system. Table reproduced from [32].

Similarly, Rizzi in [35] analyzes the colorimetric practice from the *scene type*, i.e. the assumptions and constraints on which the scholar color analysis is based (see Table 2.2).

	Description	Model	Input	Goal	Output	HVS
Scene type 0	single light spot	XYZ	single light spot	aperture mode	colorimetry match	cone
Scene type 1	single light spot	CIELAB	single light spot + illuminant	object mode	appearance	cone + spatial
Scene type 2	2D scene	CIECAM	single spot taken isolated from a 2D scene + illuminant + parameters	object mode	appearance	cone + spatial
Scene type 3	3D scene	?	?	object mode	appearance	cone + spatial

TABLE 2.2: Scene types characteristics. Table reproduced from [35].

Following the summaries proposed by Oleari and Rizzi, in Table 2.3 I propose a further outline of colorimetry. In this table, the historical phases of colorimetry and the development of the CIE standard system are correlated with a more practical description of the assumptions and constraints that every phase involves.

As previously stated, Colorimetry aims at studying color as isolated phenomenon, therefore it requires standard conditions of observation and illumination. In this context, *aperture mode* is used to present color. Here, the definition given by CIE [2]:

Aperture Mode: color seen through an aperture which prevents its association with a specific object or source.

The aperture mode, has been defined more specifically by Oleari [32] as:

Perceived color typical of the radiation that, before entering the eye, passes through the aperture of a diaphragm and the eye is focused on the edge of the diaphragm in order to avoid associating the radiation with an object or a source. In this way, the observer loses any information that denotes the object (or source), such as surface nonuniformity, polish, texture, type of lighting (grazing, diffused, etc.), and the light that enters the eye on the retina has at any point the same spectral decomposition. In this case, the field of vision is totally dark with the exclusion of the part within the aperture of the diaphragm.

Using the aperture mode constraints, just the intensity of the color stimuli and its spectral decomposition are considered, thus the *psychophysical* color, which can be specified numerically.

As presented in Table 2.3, the first phase of colorimetry, the *color matching*, is based on observations in aperture mode (see Section 2.3.1). The second and third phases, *color difference* (see Section 2.3.2) and *color appearance* (see Section 2.3.3), try to overcome some limits of aperture mode constraints, anyway are still based on observations in simple and controlled visual conditions.

Phase	**Systems and Models**	**Characteristics**
Color matching	CIE1931 Standard Observer CIE 1964 Standard Observer XYZ	Vision level: cones transduction Input: color stimuli in aperture mode Output: colorimetric match Description: color in aperture mode
Color difference	CIELAB CIELUV	Visual mechanism: cones transduction Input: color stimuli and illuminant chromaticity Output: color appearance Description: color appearance in aperture mode
Point-wise color appearance Single object color appearance	CIECAMs ...	Vision mechanism: cones transduction and parameters Input: color stimuli isolated from a 2D scene, illuminant chromaticity and parameters Output: point-wise / single object color appearance Description: color inside a context under specific constraints
Color appearance	Retinex ...	Vision mechanism: cones transduction and spatial mechanism Input: 2D scene (image) Output: 2D scene appearance. Description: color inside a context.

TABLE 2.3: Outline and description of colorimetric phases, with the associated CIE standard system.

2.3.1 Color matching

Color matching is based on observations in aperture mode. In this context, the ways in which the color signal is generated, are not considered. In aperture mode, if a color signal is generated by a light source, an object surface or both, it is not worth considering, because the color signal is the same [35].

Color matching, is the easiest operation to characterize the human observer and in this phase to the viewer is asked only the evaluation of equality in the comparison of different isolated color stimuli. The vision level, which is characterized in this phase is the transduction, thus the conversion of the light radiation into a nerve signal, which took place in the retina. Thus, the subsequent levels of elaboration are not considered.

Since the tristimulus value in the human eye, depends by the field of view, the CIE defined in 1931 a *Standard Observer* to represent the average chromatic response within a visual field of 2° [3] (see Figure 2.3). In 1964, a *Supplementary Standard Observer* was defined by CIE, for a visual field of 10°. The 2° observer, in fact, concerns just the foveal vision (i.e. a vision restricted to a visual field underlying a solid angle whose maximum section is less than 4°). In this way the observation is made with the retinal portion intended for vision with great acuity, without rods. Outside this region the retinal tissue changes and with it the color vision changes without the observer becoming aware of it. Thus, to deal with a field of view wider than 4° the Supplementary Standard Observer is recommended, although less-used than the CIE 1931.

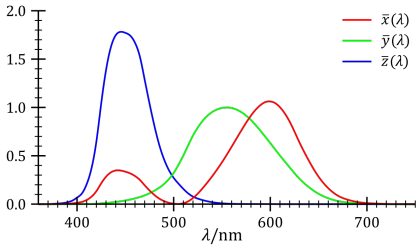

FIGURE 2.3: CIE 1931 Color Matching Functions

Limits of color matching

In this Section color matching has been presented together with the psychophysical system and its representation in the tristimulus space. In this phase of colorimetry all the phenomena consequent to the cones activation are not considered. In particular, the psychophysical specification of color is inadequate to represent color differences, in fact in any reference system of the tristimulus space equal distances represent equal differences in color perception. This is the main limit of the tristimulus space.

The aperture mode can precisely model the transduction level of color vision and, as a consequence, this constraint has strongly influenced color analysis and color matching. Nevertheless, aperture mode heavily limits the application of color matching systems and models to real conditions, like digital imaging. Moreover, the application of color matching in non-aperture mode, produces errors and mismatches between measures and color sensation. As a consequence, in order to represent color differences and characterize complex scenes, it is necessary to overcome color matching.

As will be presented in Chapter 3, in many fields of application like cultural heritage, color matching is used when spectroscopy analysis are applied to compute tristimulus values or whenever a tristimulus colorimeter is used to measure a color (see Section 2.4). In this context, psychophysical colorimetry can be used to objectively assess and measure a color or a color variation e.g., after a restoration or to monitor the aging of a surface. Anyway, it is important to remember that the tristimulus values have a meaning just if the color under analysis is considered in aperture mode. Otherwise, if the psychophysical colorimetry is used to assess a color in a complex scene or in a different context, the measure could lead to errors and mismatches.

2.3.2 Color difference

In psychophysical colorimetry (i.e., color matching), the color simuli is considered in absolute way and associated to a spectral radiance observed in aperture mode. On the other hand, *psychometric colorimetry* (i.e., color difference) considers *related colors*. Main goal of this phase is to have the color specification on uniform perceived scales, in order that different color specifications represents different colors. Furthermore, color difference phase aims at specifying color depending on the illuminant.

The psychometric system is a first limited answer to the problems of color appearance. In this phase, the perceived color is related to the illuminant, to which the HVS is supposedly adapted, and the aperture mode can be overtaken. In this case, the color can be defined as *object color*, which can be non-self-luminous (*surface mode*) or self-luminous. To those two situations correspond the CIELAB and CIELUV systems.

The CIELAB and CIELUV are defined for the Standard Observer and for the Supplementary Standard Observer. Moreover, CIELUV and CIELAB are obtained partially and totally, by non-linear transformations of the tristimulus space. Thus, these spaces aims to be *metric* and it is possible to quantify the color difference.

Light sources evaluation and Color Rendering Index

The evaluation of a light source is made in relation with the black-body radiation, a continuous frequency spectrum which depends only on the body temperature, called Plank spectrum. Since the light sources are evaluated in relation with an ideal illuminant, these measures are included in the color difference phase, thus in psychometric colorimetry. For thermal effect, the emitted spectrum of a black-body goes from *red* (1000 K), to *yellow* (2000 K), to *white* (6000 K) and to *light blue* (over 6000 K). The spectral distribution of a black-body radiator is descried by the Plank formula and is the result of a theoretical model [36].

Following the CIE guidelines, the recommended illuminants to make colorimetric measurements, according to importance, are: the blackbody radiation, the Daylight illuminants, the standard light sources and the fluorescent lamps. The Plankian radiators are not practical light sources, which have an emission different from the one of the full radiator. In this context, when the chromaticity of those light sources is similar to the one of the black body it is possible to talk about *Correlated Color Temperature* (T_{cp}). It is the temperature of the black body which color is the nearest to the one of the considered light source in the CIE chromaticity diagram (see Figure 2.4).

As said the illuminant and the light source are defined by their SPD, which can be *absolute* S_λ [W/nm] or *relative* $S(\lambda)$. The relative quantity is referred to the value at 590 nm of wavelength, which is conventionally 100. Usually the spectral range to

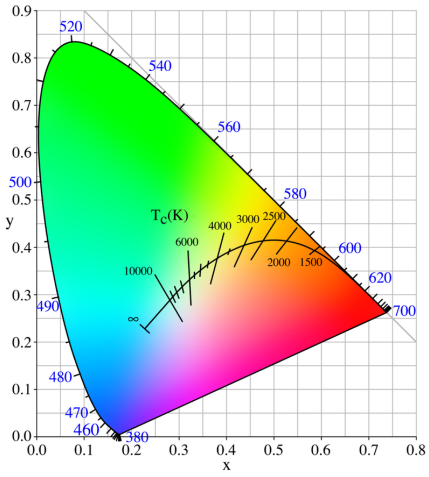

FIGURE 2.4: Chromaticity of the black body radiation in the CIE 1931 chromaticity diagram.

define the illuminant goes from 300 nm to 830 nm, in fact the extension to the UV region is particularly useful to evaluate the fluorescence phenomena.

The comparison between the SPD of a light source and the black body radiation permits to obtain an objective information about how well a light renders the colors of an object. This measure is called Color Rendering Index (CRI) and was defined for the first time in 1987 by CIE [2]. The CRI determines how well a light source illuminate 14 defined samples compared to the illumination provided by an ideal full radiator.The highest CRI value (R_a) is 100, and represents a light source identical to the one of reference.

Limits of color difference

The CIELAB and CIELUV psychometric systems are extremely practical and derive from a compromise between the still limited scientific knowledge of the HVS and the needs of the market. Those systems are extensively used in color science and engineering applications and are so well established that the introduction of new systems and algorithms is still arduous [37].

CIELAB and CIELUV consider color in relation to the illuminant limited to the case in which the object is surrounded by a medium gray background and where the illuminant is similar to the average daylight. The first issue in this models is the consideration of a medium gray background as neutral. In fact, as demonstrated by many experiments and visual illusions of simultaneous contrast, illustrated for the first time by Chevreul in [38], a gray background produces an effect on color perception, and could influence the final color appearance [34]. For what concerns the illuminant definition in CIELAB and CIELUV systems, in standard point-wise colorimetry, this problem is overcome expressing the systems quantities relatively to a reference white, specified by setting the luminance at 100 and the chromaticity equal to the one of the considered illuminant [32]. Anyway, the use of non-standard conditions or the substitution of the real illuminant values, with the values of a standard illuminant may lead to errors and approximations in real conditions, and could cause a lack of matching between the computed and perceived colors and color differences [34], [35].

From these consideration is derived that, nevertheless the high diffusion of the psychometric colorimetry and the overcome of the aperture mode, these systems

introduce new requirements and constraints, and are still not applicable in complex visual contexts (i.e., images, real scenes). In fact, color is still considered as isolated phenomenon, and colorimetry is still point-wise.

Considering the psychometric system colorimetry to assess the quality of a light source, the CRI index has been used for years, and still today on every light bulb package is possible to find the respective color rendering index. Nevertheless, since the introduction of LED light sources in the market, this index started presenting some criticism. In fact CRI does not always correlates with the subjective color rendering, especially for light sources with spiky emission spectra (e.g., LEDs) [39]. As consequence, new measures based on color appearance models like CIECAM02 [40] or CIE Metamerism Indexes [41] have been adopted but none of them effectively substituted the previous one, or was adopted as standard.

2.3.3 Color appearance

Color appearance, in psychophysical studies, is defined as: *Visual perception in which the spectral aspects of a visual stimulus are integrated with its illuminating and viewing environment.*

In this context, scene content complexity can be very high and model every possible content configuration can be very difficult. Visual illusions (see an example in Figure 2.5) demonstrate the importance of spatial configuration of a scene, and confirm the idea that color sensation depends not only by a point-wise stimulus, but by the spatial arrangement.

After the presentation of CIELAB and CIELUV systems, different models have been developed, but they rarely consider the mechanisms whole visual elaboration,

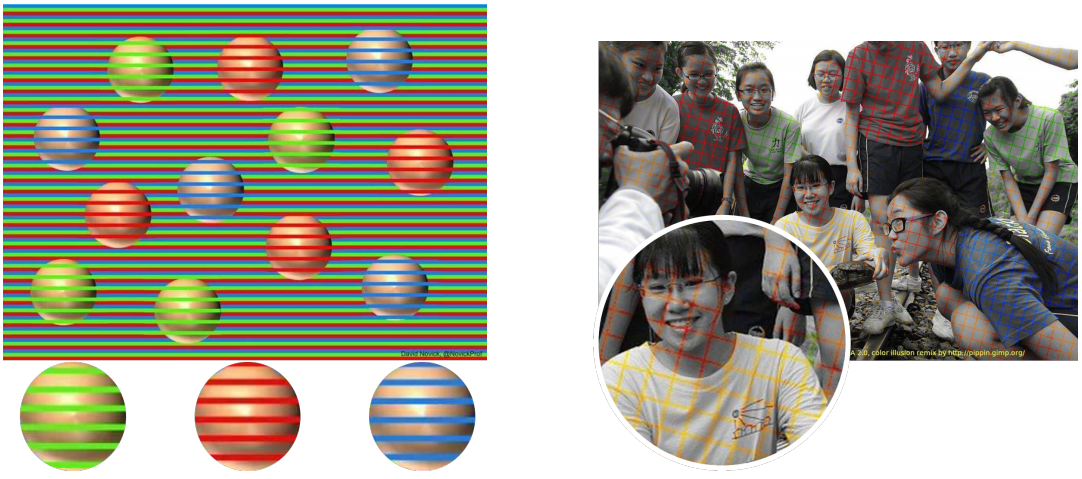

(A) (B)

FIGURE 2.5: In 2.5a the three-color confetti illusion designed by David Novick. Looking at this image from a distance the circles appear to be in different hues (green, red and blue), but looking at the magnifications it is possible to see that them are all the same color. In 2.5b an example of the Bezold effect (visual illusion), where from a distance the image appear to be in color, but looking at the magnification it is possible to see that it is in black and white and the color is present just on small stripes above the image.

where the effect of spatial arrangements, edges and gradients have a fundamental role in the process of color perception [42], [43].

In recent years, the Color Appearance Models (CAMs) have been developed. Those models tries to overcome the limits of color matching and color difference phases, but, as all the previous systems, are based on their own constraints and have significant limits in real-condition applications [44]–[47]. CAMs, in fact, restrict the scenes content complexity to a set of defined configurations, like background, lighting and field of view [48]. As a consequence, even these more elaborated models, are not applicable in many real conditions, and the application without considering the CAMs constraints lead to errors and excessive approximations [34].

An innovative approach to color appearance has been introduced with the Retinex theory proposed in 1971 by E.H. Land and J.J. McCann [12]. Retinex theory, together with the related models, will be presented and discussed more thoroughly in Section 5.3.1. In general, the idea at the base of this model is to join the mechanisms of the retinal transduction level with the cortex elaboration level, to adjust the colors in a scene depending on their distribution in the scene (spatial arrangement).

The Retinex model is a first attempt to introduce spatial mechanisms to model HVS and its success underlines the need to develop more complete and robust systems to model color appearance. In this context, one strong improvement could be done starting considering and modeling the elaboration level of our HVS and, more specifically, considering the spatial mechanisms of vision.

2.4 Measuring instruments

The instruments used in colorimetry can be divided in: light measurement device and light modulation devices (reflectance and transmittance). This difference is enhanced by the geometry of signal capture and by the spectral responsivity of the detector. In [32] the instruments are classified as:

- *Radiometers*: for the measurement of *radiant flux* $[W]$, *radiant intensity* $[W/sr]$ or *radiance* $[W/(m_2 x sr)]$. The response is in radiant intensity.
- *Spectroradiometers*: for the measurement of spectral densities in the radiometric units defined by the radiometers.
- *Photometers*: to measure the light physical quantities like luminous flux (*illuminance*) $[lm]$, *luminous intensity* $[cd]$ and *luminance* $[cd/m_2]$. The spectral response depends by the function of relative luminous efficiency $V(\lambda)$.
- *Tristimulus colorimeters*: to measure the spectral trichromatic characteristics. The response depends by Color Matching Functions of the Standard Observer ($\bar{x}(\lambda)$, $\bar{y}(\lambda)$ and $\bar{z}(\lambda)$).
- *Visual Colorimeters*: for the visual comparison of colors. These instruments can work in additive or subtractive synthesis.
- *Spectrophotometers*: to measure the ratio between spectral densities like *reflectance*, *transmittance*, *reflectance factor* and *transmittance factor*.

In general, the light modulation devices have an internal standard light source. Among the classified instruments, the spectroradiometers and spectrophotometers makes measures of spectral densities and the photometric and colorimetric units are obtained through the computation of spectral data. Thus, all the other instruments

makes spectral weighting functions, using optical filters to obtain the spectral response in function of $V(\lambda)$, for photometric measures, or of $\bar{x}(\lambda)$, $\bar{y}(\lambda)$ and $\bar{z}(\lambda)$ for colorimetric measures.

2.4.1 Spectral Imaging

Among all the measuring instruments used in colorimetry, particular attention should be given to spectral imaging techniques. Imaging techniques are all those methods which provide an image of the object studied as final result. In general, among the imaging techniques, the most used in Cultural Heritage domain are:

- X-ray radiography
- Gamma radiography
- UV-Vis luminescence
- UV reflectance imaging
- Spectral imaging
- False-Color IR Photography (IRFC)
- B& W infrared photography
- Infrared reflectography
- Trans-illumination and trans-irradiation
- Raking light
- Thermal imaging / thermography

Nowadays, one of the most interesting technique is spectral imaging. This method allows the simultaneous acquisition of hundred wavelengths bands for each pixel in an image. Thus, the captured spectrum can include single regions of the electromagnetic spectrum, or combinations of them.

Multispectral Imaging (MSI) is part of the spectral imaging family. A technique which allows to capture image data within specific wavelength ranges across the electromagnetic spectrum. Multispectral images are obtained using different filters sensitive to specific regions of the electromagnetic radiation, or changing the light source. Typically, the multispectral technique captures from 3 to 15 spectral bands.

The *Hyperspectral Imaging* (HSI) is a particular case of spectral imaging, which permits the collection of hundred of images corresponding to narrow bands (e.g., less than 10 nm), in order to allow the generation of a reflectance spectrum at each pixel in the image. The image produced by this technique is called *hyperspectral cube*, because of the typical three-dimensional representation of data, where x and y are the image spatial dimensions and z represents the spectral dimension (λ). The hyperspectral cubes are obtained through specific cameras, which hardware captures hundreds of spectral bands for each pixel. The hyperspectral imaging techniques can be divided in four categories: spatial scanning, spectral scanning, non-scanning and spatio-spectral scanning (see. Figure 2.6).

In spatial scanning the image is analyzed line per line capturing a spectrum (λ) for every pixel along the x axis. The third dimension (y) is obtained through the movement of the scanner. In the spectral scanning technique a bidimensional image

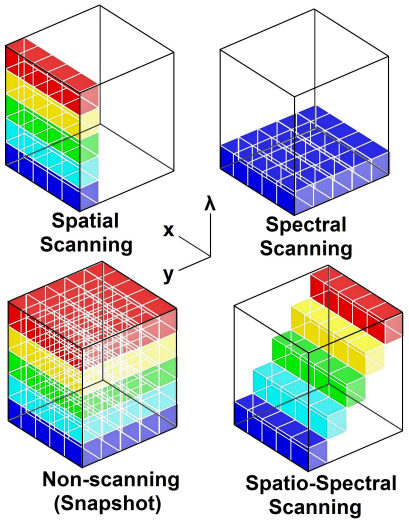

FIGURE 2.6: Representation of the different acquisition techniques in hyperspectral imaging: spatial scanning, spectral scanning, non-scanning and spatiospectral scanning. Figure reproduced from: Sascha Grusche.

is acquired, but it is composed by the x, y map of the scene for one single wavelength. Then, the 3-D hyperspectral cube is obtained using different filters sensitive to subsequent wavelengths. The non-scanning technique is the only method which allows to obtain in a snapshot a 3-D hyperspectra cube, using a sensor capable to acquire all the spatial (x, y) and spectral (λ) data. In conclusion, the spatio-spectral scanning is an innovative method introduced as prototype in 2014 able to obtain a wavelength-coded $(\lambda = \lambda(y))$ spatial (x, y) map [49].

MSI and HSI today are widely used in Cultural Heritage domain [50]–[52]. These techniques permit a non-invasive analysis of different materials (i.e. frescoes, paintings, paper materials and films) and enables the identification and analysis for restoration and preservation purpose.

Chapter 3

Colorimetry in cultural heritage applications

3.1 Introduction

In the previous Chapter color sensation was described as the result of optical and psycho-physical process. Moreover, the main phases of colorimetry were presented, together with their relative assumptions, constraints and limits of application.

In the last decades, colorimetry has become a fundamental subject in the study of cultural heritage. Thus, colors started being considered as physical materials to be restored and preserved, and not just as expressive tools [53]. As result, in cultural heritage, has widely spread the use of spectroscopy, together with other analytical techniques, to analyze and characterize the physical and chemical nature of colors [54]–[56].

The use of colorimetry in cultural heritage applications is limited to the numerical definition of color in aperture mode (see Section 2.3.1) or under the strict constraints of psychometric colorimetry (see Section 2.3.2). In this context, colorimetry is used to characterize color punctually and out of context, for example to study color fading on surfaces [57] or to asses the quality of innovative products to clean or protect surfaces [58], [59]. Furthermore, since the beginning of the current Century, the traditional colorimetric measurements and instruments did not evolve and the acquirable data are still the same. Even today, colorimetric studies start from data (e.g. reflectance and transmittance spectra) aimed at providing information on chemical and physical properties of materials, without considering the psycho-physical process which underlies color vision. In conservation science, the acquired spectrophotometric data are unlikely converted into trichromatic coordinates, since their mainly purpose is to allow the identification of colorants (e.g. for the restoration through the same materials).

In this context, the widespread use of digital technologies required the use of colorimetry for digital acquisitions and reconstructions. These approaches may have a conservation and valorization purpose [60]–[62], supporting the archiving and cataloging process [63] and test the dependence on different devices [64]. In digital applications, where entire objects are acquired, standard colorimetric constraints cannot be respected and the scene content complexity and spatial arrangement cannot be longer ignored. In fact, in real 3D scenes, many phenomena like a non-uniform illumination, inter-reflections or surface light scattering cause wide shift in color appearance, and the constraints of modern colorimetry are not respected. Since colorimetry requires specific constraints, colorimetric measures are strictly point-wise, thus colorimetry is extremely precise just when the standard conditions are respected, but fails when data are reported in more complex context [42], [65], [66].

As presented in Chapter 1 colorimetry works under strict assumptions and constraints, color is modeled at the sensory input and it is not considered the subsequent spatial processing of the signal. Different recent works have demonstrated the complex role of the retinal input where a spatial processing occurs [18].

The inappropriate use of a point-wise approach in complex contexts raises many challenges in the colorimetric field and today this issue is solved using subjective color assessments and manual color corrections and enhancement. Considering the cultural heritage field, the limits of colorimetry in assessing color in complex scenes and including the spatial arrangement can be particularly dangerous, leading to a color reconstruction defined by subjective opinion. This is the case of every non point-wise 2D or 3D physical or digital color restoration or retrieval, where the final evaluation is left to the *expert eye*, and can not be assessed objectively.

The main limits of standard colorimetric measures in cultural heritage applications are demonstrated in the following Chapters considering digital film restoration as main application (see Chapters 4, 5, 6 and 7). However, the problems of color appearance are always present whenever a color is inserted in a context, and standard colorimetry constraints cannot be applied. For this reason, in the following Sections some experiments to underline the limits of standard colorimetry measures and to propose new approaches will be presented.

3.2 Measurement and assessment of color rendering for museum applications

The evaluation, modeling and measurement of the perceived color difference in museum environments is fundamental to guarantee the correct illumination and fruition of objects of historical importance. As demonstrated in the previous Chapter, light influences the perception of colors and space, therefore any type of lighting must be adequately analyzed to confirm a stable and undistorted color rendering. In this preliminary study, I carried out a two-stage perceptual test asking to 20 participants to evaluate the colors of a Gretag Macbeth Color Checker [67] under different light sources according to the criteria of color brilliance, lighting pleasantness and overall satisfaction. Subsequently, the participants have been asked to quantify the efficiency of the light sources for the identification of color differences between an original and a printed Color Checker. Thanks to this test it was possible to characterize and analyze the most commonly used color rendering indexes and color difference models.

3.2.1 Lighting for museums and collections

In museums, the role of light is fundamental to create an immersive and evocative experience. The definition of the optimal illumination is still an open issue for museums and collections, which aim at exposing objects of historical relevance to a public. In fact, museums and collections need to find a balance among the public, the works of art and the building architecture. First, the light can strongly affect the experience of the visitors, so it must be correctly designed, but must also be safe for the people working and visiting the museum [68], [69]. Second, the amount of light per year and the range of light intensities to which each artwork and historical object can be subject is defined by specific national and international regulations. In this context, it is fundamental to use light sources which do not induce fading and damage the objects (see for example Italian regulations about this problem [70]–[72]). The third

FIGURE 3.1: An example of two exposition rooms of the Sforza Castle Museum. On the left a view of the tapestries in the Room of the Standard ("Sala del Gonfalone"). This is an example of balance among the needs of the tapestries, which are considered high sensitive to light, and the building architecture, which presents large windows. On the right, a view of the new exposition of the Rondanini's Pity in the ancient Spanish Hospital in the Castle Courtyard of Arms [54]. Here the natural light is used in harmony with an artificial light to enhance the emotional and iconic aspect of the statue as suggested by architect De Lucchi. Figure reproduced from [21]

aspect to consider when working on museum lighting, is that the illumination conditions can not always be controlled, because many museums are inside historical buildings e.g., castles, villas or factories, that cannot be modified because are cultural heritages themselves (see Figure 3.1).

In such a complex domain, the assessment of objects' color rendering is considered of secondary importance. This lack of awareness is caused, among several motives, by the lack of guidelines and regulations and sometimes also by the absence of experts in conservation science among the personnel. One of the main problems is the lack of objective measures, which can correlate objects final color with the complex scenes in which they are located and with the behavior of the Human Visual System (HVS).

In recent years, several experiments have been carried out in order to evaluate the color perception of museum objects under different light sources [73]–[75], these studies focus mainly on color temperature and LEDs. Furthermore, in literature numerous studies can be found aimed at determining which source guarantees the best color rendering and if there are more suitable light sources to be used for lighting of specific museum objects [76]–[80].

In these studies, a light source is defined by its spectral power distribution, and as explained in Chapter 2 this measure is extremely limited because it does not give any information concerning the light spatial distribution. Furthermore, as previously described, many studies evaluate the light rendering index based on the CRI. As said, the main limit of this index is that it not always correlate with the subjective color rendering. Since then, different rendering indexes have been developed, but none of them have been able to effectively replace the original one. As consequence, today there is still the need to develop new systems and models to evaluate the color rendering taking into account the visual perception in complex scenes and not just focused on the spectral analysis [81].

3.2.2 Experimental set-up

In order to preliminarily test the efficiency of the most used color rendering indexes and metrics of color difference, I carried out a psychophysical test on 20 people.

The obtained results have been published in [8]. Aim of this experiment is to discover the limits and weaknesses of the modeling based on point-wise colorimetry. In particular, in this test, I compared the CRI, the TM-30 Fidelity Index and TM-30 Gamut Index with the perceived brilliance, pleasantness and satisfaction, and the ΔE (referred to the CIELAB76 ΔE) and $DeltaE00$ (referred to the CIEDE2000) color differences with the perceived color difference.

The objects of this experiment have been two Gretag Macbeth Colur Checker, one in original and one printed (Figure 3.2). The printed Color Checker has been obtained from a standard image of the target [82], which has been printed using the default gamut mapping of a LaserJet Pro 400 color printer. Both Color Checkers have been positioned within a Light Booth, model The Judge II, equipped with 4 different types of light sources: CIE D65, Cool White Fluorescent, U30TL84 and Illuminant A. Two LED lights have been added to the Light Booth: one 'cold' (LED 1, 5000K) and one 'warm' (LED 2, 2500K). The uniformity of the light diffusion was verified on the basis of the Light Booth for all the lights. The emission spectra of each source have been measured with a CL-500A spectrophotometer (see the spectra in Figure 3.3 and the measurement set-up in Figure 3.2). The following indexes have been computed: CRI [53] , TM-30 Fidelity Index [6] and TM-30 Gamut Index [6].

To measure and analyze the color difference between the two Color Checkers, the reflectance spectra of each patch has been measured through an Ocean Optics HR4000 spectrophotometer and the data have been processed to obtain the colorimetric values in the CIELAB color space simulating the illumination under the various light sources present in the Light Booth. Then, the chromatic differences (values ΔE and $DeltaE00$) between the original and printed Color Checker have been calculated.

The perceptual test has been carried out involving 20 people, in a dark room. The test was composed by two phases. In the first phase, named *Color rendering assessment*, it has been asked to the participant to quantify from 0 to 100 the brilliance of the colors, the degree of pleasantness referred to the light source and the degree of general satisfaction of the setting. This first step has been performed alternating and evaluating one Color Checker at the time, to avoid a comparison between the two objects. In the second phase, named *Color difference assessment* the perceived color difference has been evaluated. In this step it has been asked to the participants to indicate with a number from 1 to 5 (where 1 was associated to identical patches and 5 to absolutely different patches), the perceived color difference between 15 couples of patches one from the original Color Checker and one from the printed Color Checker.

3.2.3 Results and discussion

The results of the experiment presented in the previous Section have been compared with the most common color rendering and color difference indexes. The applicability of the obtained results has been evaluated specifically for the application in museums and exhibitions, where lighting is considered in terms of conservation, design and safety.

Color rendering assessment

In the table below are listed the CRI, the color temperature and the TM-30 values of the Fidelity Index (Table 3.1) of each light source used in the experiment. Figure 3.4 shows the results of the subjective evaluation of brilliance, pleasantness and

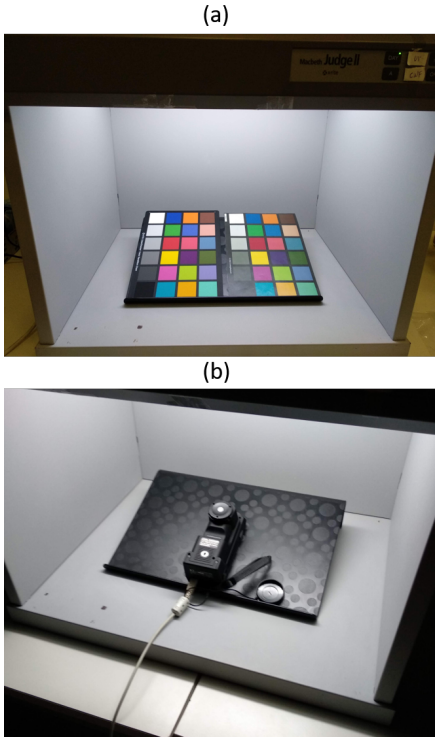

FIGURE 3.2: In Figure 3.2a the original (left) and printed (right) Color Checker inside the Light Booth. In Figure 3.2b the set-up of the CL-500A spectrophotometer during measurements. Figure reproduced from [8]

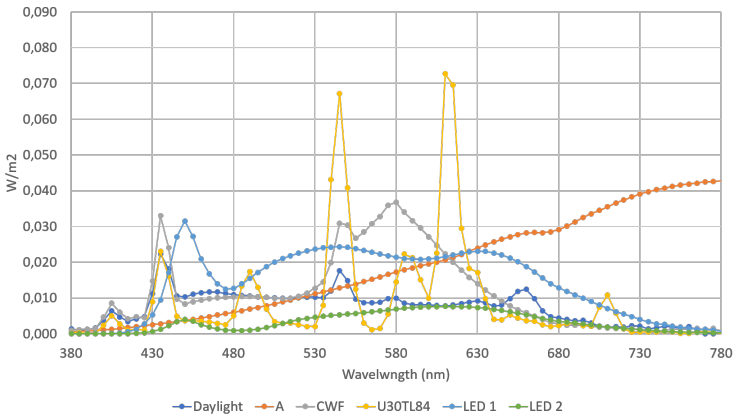

FIGURE 3.3: Emission spectra of sources. Figure reproduced from [8]

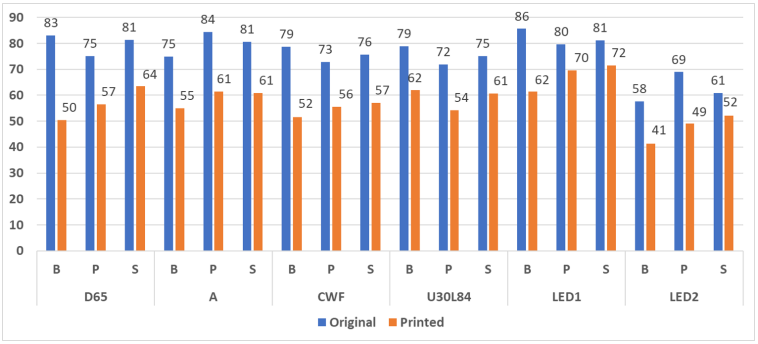

FIGURE 3.4: User-assigned values in % for three parameters: B = Brilliance, P= Pleasantness, S = Satisfaction. Figure reproduced from [8]

satisfaction for each light source.

	Daylight	**A**	**CWF**	**U30TL84**	**LED 1**	**LED 2**
CRI (Ra)	94	99	59	87	94	83
Color Temperature (K)	7000	2600	3900	3000	4800	3000
Fidelity Index (Rf)	94	99	67	82	93	84

TABLE 3.1: CRI, Color Temperature and Fidelity Index of the considered light sources. Table reproduced from [8]

In general, comparing Figure 3.4 and Table 3.1, it is interesting to note that the values of brilliance, pleasantness and satisfaction assigned by the participants never reach the scores measured by the CRI index. Furthermore, looking at the results it is clear that the original version of the Color Checker under all the light sources is more appreciated by the participants (than the printed version) in terms of brilliance, pleasantness and satisfaction. This indicates that the support and materials used for any colored object have a fundamental role in color rendering.

Now, considering the value of satisfaction, the light sources that received the highest scores are D65, A and LED1. This evaluation is consistent with the values of CRI and TM-30 Fidelity. For what concerns the values of brilliance and pleasantness, there are major discrepancies between the subjective judgment and the color rendering indexes. LED1 presents the highest value of brilliance for the original Color Checker, followed by the A source, CWL and U30TL84. Nevertheless, for the printed Color Checker the highest value of brilliance is reached by U30TL84 and LED1 source. Now, considering the feature of pleasantness, the original Color Checker presents the highest value together with the A source followed by LED1. The printed Color Checker obtains the highest score of pleasantness for LED1, followed by A source.

The high discrepancies of these results demonstrate that the modeling performed by the most diffuse Color Rendering indexes, tend to approximate and simplify the process of color perception, as well as the basic phenomena of eyes light adaptation and spatial variability. Both this preliminary experiment and the study made by Rizzi et al. in [81] query the adequacy of color rendering indexes to give an estimate of the perceptive quality of a light source or of an illumination set-up, especially for complex scenes like museums or expositions.

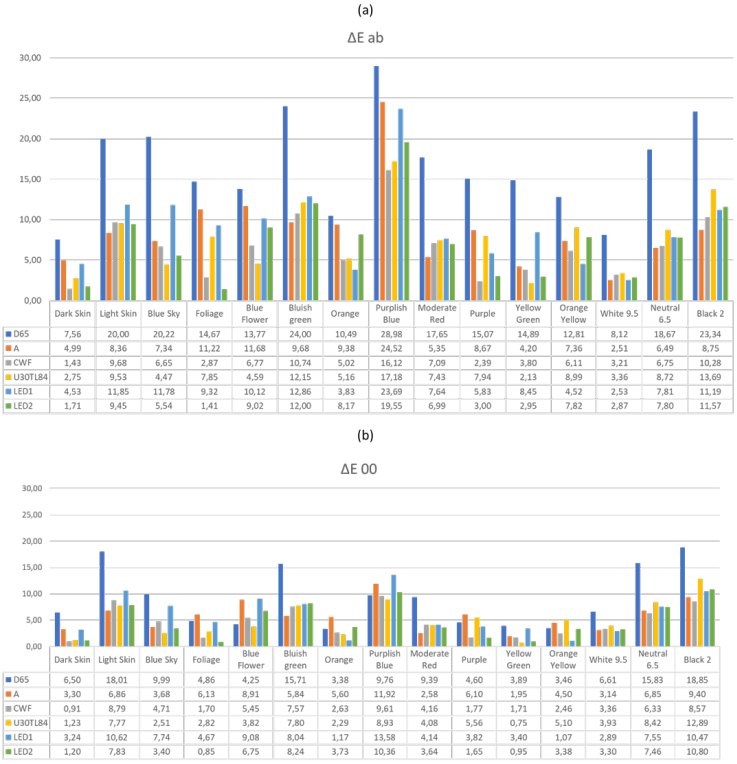

	Dark Skin	Light Skin	Blue Sky	Foliage	Blue Flower	Bluish green	Orange	Purplish Blue	Moderate Red	Purple	Yellow Green	Orange Yellow	White 9.5	Neutral 6.5	Black 2
D65	7,56	20,00	20,22	14,67	13,77	24,00	10,49	28,98	17,65	15,07	14,89	12,81	8,12	18,67	23,34
A	4,99	8,36	7,34	11,22	11,68	9,68	9,38	24,52	5,35	8,67	4,20	7,36	2,51	6,49	8,75
CWF	1,43	9,68	6,65	2,87	6,77	10,74	5,02	16,12	7,09	2,39	3,80	6,11	3,21	6,75	10,28
U30TL84	2,75	9,53	4,47	7,85	4,59	12,15	5,16	17,18	7,43	7,94	2,13	8,99	3,36	8,72	13,69
LED1	4,53	11,85	11,78	9,32	10,12	12,86	3,83	23,69	7,64	5,83	8,45	4,52	2,53	7,81	11,19
LED2	1,71	9,45	5,54	1,41	9,02	12,00	8,17	19,55	6,99	3,00	2,95	7,82	2,87	7,80	11,57

	Dark Skin	Light Skin	Blue Sky	Foliage	Blue Flower	Bluish green	Orange	Purplish Blue	Moderate Red	Purple	Yellow Green	Orange Yellow	White 9.5	Neutral 6.5	Black 2
D65	6,50	18,01	9,99	4,86	4,25	15,71	3,38	9,76	9,39	4,60	3,89	3,46	6,61	15,83	18,85
A	3,30	6,86	3,68	6,13	8,91	5,84	5,60	11,92	2,58	6,10	1,95	4,50	3,14	6,85	9,40
CWF	0,91	8,79	4,71	1,70	5,45	7,57	2,63	9,61	4,16	1,77	1,71	2,46	3,36	6,33	8,57
U30TL84	1,23	7,77	2,51	2,82	3,82	7,80	2,29	8,93	4,08	5,56	0,75	5,10	3,93	8,42	12,89
LED1	3,24	10,62	7,74	4,67	9,08	8,04	1,17	13,58	4,14	3,82	3,40	1,07	2,89	7,55	10,47
LED2	1,20	7,83	3,40	0,85	6,75	8,24	3,73	10,36	3,64	1,65	0,95	3,38	3,30	7,46	10,80

FIGURE 3.5: In Figure 3.5a the ΔE and in Figure 3.5b the $\Delta E00$ values calculated under the different light sources in the Light Booth. Figure reproduced from [8]

Color difference assessment

For what concerns the evaluation of color difference the following tables summarizes the values of ΔE and $\Delta E00$ computed from the reflectance spectra of each patch of the Color Checker under each light source (Figure 3.5). The ΔE values have been compared with the average values of perceived difference assigned by the participants, as shown in Figure 3.6.

Considering the results displayed in the plots, it can be noticed that the perceived color difference between the two Color Checkers is quite always higher than the measured values ΔE and $\Delta E00$. Furthermore, the perceived difference in each light source presents high variability. Some discrepancies and divergences between the measured and perceived color differences could derive from noise in the acquisitions (e.g., the way in which fiber optics are placed and moved). Nevertheless, the perceived differences using standard background and a controlled illumination, are heavily higher than the effect of noise in the acquisition. A particular case is given by the D65 source, where the measured color differences are significantly higher than the perceived ones. On the other hand, the CWF and LED2 light sources are the ones with the smallest values of perceived difference.

For what concerns the perceived difference of specific colors, the highest difference is noticed when comparing patches with a strong blue component (Bluish Green, Purplish Blue, Blue Sky, Blue Flower) while, the perceived difference decreases for patches an high red component (Orange and Moderate Red) and in the gray levels (White 9.5, Neutral 6.5, Black 2). The patches with red component and the gray levels obtain lower values in both ΔE measurements.

Now, analyzing each light source it can be noticed that, in the D65 source (Tables

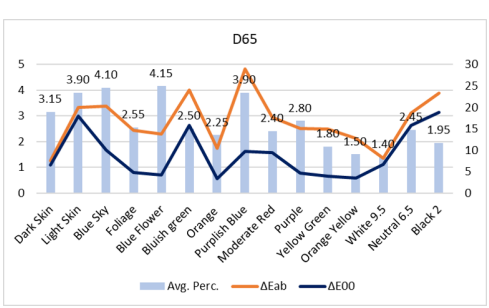

(A)

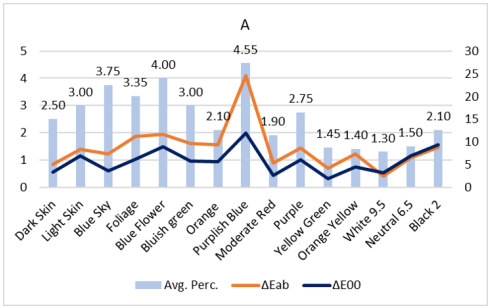

(B)

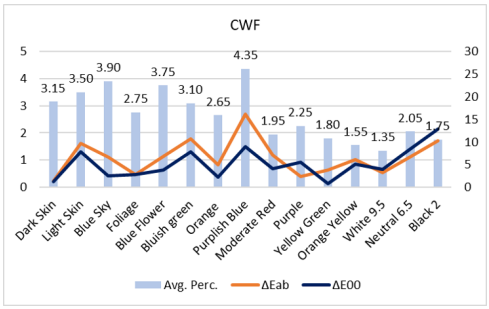

(C)

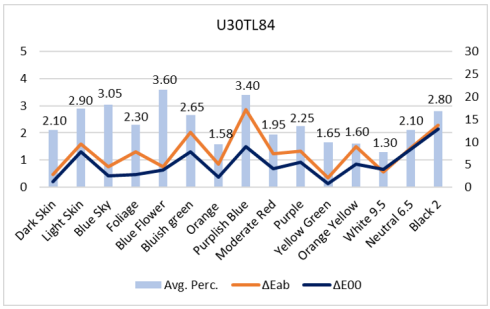

(D)

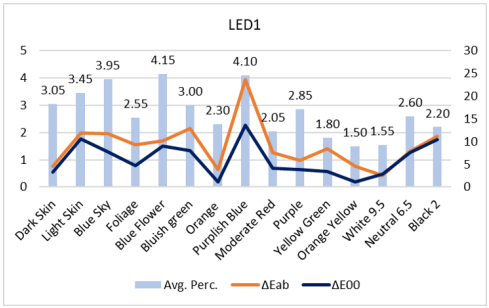

(E)

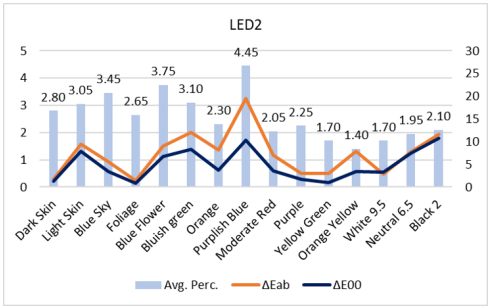

(F)

FIGURE 3.6: Representation of the average perceived color difference compared with the measured values of ΔE and $\Delta E00$ for the light sources: D65 (Figure 3.6a), A (Figure 3.6b), CWF (Figure 3.6c), U30TL84 (Figure 3.6d), LED1 (Figure 3.6e) and LED2 (Figure 3.6f). Figures reproduced from [8]

in Figure 3.6a), the perceived differences are always greater than 2, with a peak for the Purplish Blue, which assumes a value close to 5. Looking the A source (Figure 3.6b), there is a general decrease in the perceived difference, but the peak in the Purplish Blue remains also if it decreases from 5 to 4.3. For the White, Yellow Green and Moderate Red under the A source, the values of perceived difference are close to 1.5, so them are considered perceptually very close to the ones of the original Color Checker.

Considering the illuminant CWF (Figure 3.6c), the values of Dark Skin and Purple have a lowest perceived difference in comparison to all the other light sources. In this light source, the perceived difference assumed by Purplish Blue returns back to 4.5. In this case, the values of ΔE and $\Delta E00$ are much lower than in the case of D65 and A.

Similarly for U30TL84 source (Figure 3.6d) the perceptual difference in Yellow Green and Dark Skin is around 1.5, and the values of ΔE and $\Delta E00$ decrease for Purplish Blue but still remaining around 4.5. Finally, in LED1 (Figure 3.6e), the perceptual differences between the original and the printed Color Checker increase compared to the other light sources and present a similar trend to D65, even if lowered by 1 point circa. In LED2 (Figure 3.6f) the perceived differences are very close to LED1.

Starting from these results and evaluations, it is possible to identify and analyze the strong discrepancies between measured and perceived differences. The ΔE and $\Delta E00$ are colorimetric values derived from the lights SPD and are extremely useful for a point-wise assessment in standard observation conditions, but their model is limited in complex scenes. The model on which these measures are based do not consider the spatial arrangement of colors in the space, as well as the adaptation of the human visual system to the different light sources.

3.2.4 Final considerations

Thanks to this experiment it is possible to assert that the current colorimetric measures to evaluate a light source still do not consider the behavior of the human visual system and its adaptation, thus them must be modified and re-modeled to include some of those aspects. It is also interesting to notice that, when evaluating the color differences between patches, some color remains perceptually constant under different light sources, thus the color metamerism is preserved.

In conclusion it can be said that all the considered limits must be taken into account especially when designing the lighting for a museum or an exhibition, where the objects are made of different materials and where the public is immersed in a complex scene, of non standard illumination and observation.

3.3 Physical objects color assessment

In cultural heritage field, physical and chemical analysis are used to support operations of restoration, retrieval and conservation. In this context, spectral acquisitions can be used to identify and characterize different materials, among which pigments and colorants. When spectral data are acquired respecting constraints of geometry of illumination / observation and standard lighting [53], them can be used to numerically specify colors through CIE Standard Systems (see Chapter 1). However, during this procedure it is possible to occur in some errors, linked to the instruments

[16]. The main problems in color identification and measurements is an inappropriate calibration of the instruments or the uncontrolled conditions of measurement, which could lead to errors in spectral acquisitions and to its propagation during the colorimetric conversions [15]. Also in this context, the need of standard illumination conditions and direction of observation, makes the measurement point-wise, and the colorimetric measurements fails when the object under analysis presents a complex structure.

A case study, where the limits of the point-based colorimetric approach are presented is reported in the following Subsection. In this work, the colorimetric and subjective approaches to assess the colors in gemstones are compared. The gems, in fact, have particular refractive properties, enhanced by the cuts, and a standard colorimetric evaluation is limited when compared to the visual assessment.

3.3.1 Case Study: Assessing color of gemstones

The use of gemstones in the field of jewelery has been attested by many archaeological finds and date back to the Bronze Age. Gems have been used along the history to affirm power and royalty and today are integral part of many objects of cultural and historical relevance. All the gemstones evaluation systems, define color as a fundamental parameter for the evaluation of the market price [83]. Nevertheless, still today, there is a lack of standards for gemstone color assessment and the color identification is exclusively based on the direct visual observation, in some cases with lenses and microscopes. This lack of guidelines concerns not only commercial gemstones, but also the stones which are already part of cultural heritage. Thus, there is the need to define a more general and objective system for gemstones color assessment.

The only standard and widely used color classification system has been made for the assessment of diamonds value, which is a priority for market and trade, thus, since 1950s, it is diffuse the use of GIA Color Grading System [84]. This standard do not concerns the gemstones different from diamonds, and also if many color classification systems have been tested since 1970s, none of them have been successfully adopted as a standard and specific instruments for gemstone color identification still do not exist.

The most common issues against the development of a color evaluation system for gemstones can be resumed in three points. First, the gemstones sellers fear that this system could reduce their role. Second, the jewelers do not want to invest money in complex instruments, and due to safety and economic issues, they do not want to send the gemstones to external laboratories. Third, many sellers do not want the market of colored gemstones to become similar to the diamond commerce, where the stones are traded without a proper knowledge of their characteristics.

It is clear that, despite these considerations, the development of a reliable standard color assessment system for gemstones would bring advantages for characterization and trade. The main limit in the application of classic colorimetry for the assessment of gemstones color is that light hitting a gemstone surface produces scattering and multiple reflecting phenomena. This fact puts the process of gemstone color assessment out of the scope of standard point-wise colorimetric measures.

Starting from this issue, in this key study I have investigated the relationship between the use of color measuring instruments and visual inspection, for the assessment of gems color appearance. In this perceptual experiment I asked participants to correlate the measured and the perceived colors of a set of gemological samples.

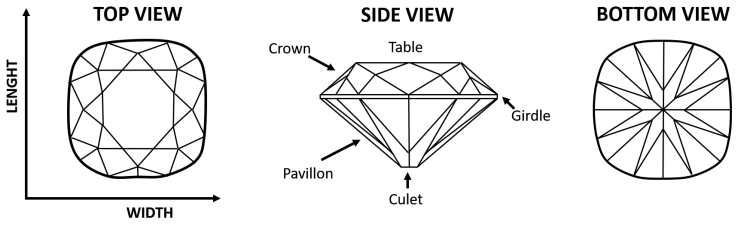

FIGURE 3.7: Scheme of the sections of a faceted gemstone [83]. Figure reproduced from [22].

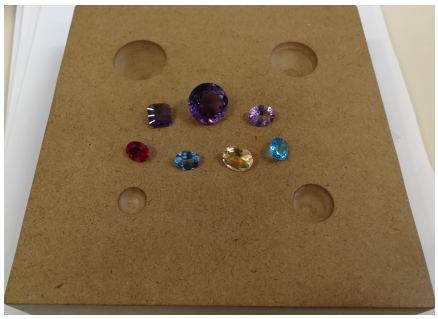

FIGURE 3.8: The analyzed gemstones. Figure reproduced from [22].

Results report the correlations between instrumental measures and the visual assessment of gemstones color appearance and can be a potential base for a future standard method for gemstones color assessment.

Experimental set-up

Gemstones are often transparent, and their color is non-uniform. Aim of this experiment is the evaluation of the overall gemstones appearance arising from the interaction of color coverage, brilliance and dispersion. I published the results of this experiment in [22].

For this experiment 7 gemstones have been selected to be of different colors, without inclusions and transparent (see Figure 3.8). The stones are faceted with different cuts and have similar ratio values *width x highness x thickness*. The gemstones characteristics are summarized in Table 3.2. All the factors listed in the table contribute to make these samples very hard to measure with standard optical measuring devices and with standard colorimetry [85]. For this reason, an alternative measurement set-up based on subjective assessment has been proposed and tested.

Gemstone	Sample	Measure (mm)	Form	Chromophore	Cause of color
Synth. ruby	RUB	10 x 8 x 4.7	Oval	Cr^3+	Trace element
Synth. aquamarine	ACQ	10 x 8 x 4.5	Oval	Fe^2+-Fe^3+	Charge transfer
Topaz	TOP	9.9 x 8.2 x 5	Oval	Structural defect (vacancy)	Gamma rays irradiation
Amethyst	AM1	17 x 10.2	Round	Fe^3+ - Na^+/H^+	Trace element and charge transfer
Amethyst	AM2	9.9 x 9.9 x 4.7	Squared	Fe^3+ - Na^+/H^+	Trace element and charge transfer
Amethyst	AM3	11 x 9 x 5.2	Oval	Fe^3+ - Na^+/H^+	Trace element and charge transfer
Citrine	CIT	11.9 x 10 x 6	Oval	Fe^2+-Fe^3+	Trace element and charge transfer

TABLE 3.2: Characteristics of the samples. Table reproduced from [22].

The Munsell color atlas [86] has been chosen as reference for the subjective assessment, due to its diffusion as a standard and to its perceptual uniformity. As

Sample	2nd choice of hue	%	3rd choice of hue	%
AM1	19	90.5	7	33.3
AM 2	16	76.2	7	33.3
AM3	19	90.5	8	38.1
ACQ	19	90.5	6	28.6
TOP	17	81.0	6	28.6
CIT	18	85.7	6	28.6
RUB	8	38.1	2	9.5

TABLE 3.3: Percentage of subjects that have chosen a second and a third hue

already said the Munsell color patches and the gemstones presents dissimilar characteristics of transparency and non-uniformity. This difference in color spatial distribution is useful to force the observer to summarize the whole visual assessment into an unique color value. In this way, the visual system has been used to perform the integration instead of performing this step through an instrument or a computation. Furthermore, the variance among the observers matches produces a fine tuning of the subjective final appearance value and it is a sort of low-pass filtering of anomalous values generated by the misinterpretation of the task.

The subjective assessment test has been designed to obtain a color evaluation through the direct observation of gemstones. In the experimental set-up, gemstones have been observed under a daylight illuminant (D65), in a The Judge II lighting box. This choice was made because daylight sources, both natural and artificial, are commonly and traditionally used in gemology and in gemstones trade for color evaluation. Furthermore, D65 is recommended as the best daylight source for gemstone color evaluation [87]. The participants of the subjective assessment tests have been people aged between 20 and 54 years, with normal or lens corrected visus. In the experimental set-up the gemstones have been compared with pre-selected pages of the Munsell atlas placed into a D65 source in a the Judge II Light Booth. To each participant has been asked to report from 1 to 3 color patches to characterize the color appearance of each observed gem. The possibility to give up to 3 preferences refers to the traditional color evaluation method, in which the first color refers to the main hue, with a maximum of two shades. The choice of the second and third color patch was not mandatory. However, as visible in Table 3.3, the majority of subjects reported more than one preference. The ideal sequence of sample observation was established as AM1 – ACQ – AM3 – CIT – RUB – TOP – AM2 to reduce the possible effects of assimilation/similarity caused by the close observation of samples with similar colors.

The subjective color assessment has been compared with instrumental measures. The measurements have been made with a spectrophotometer Konica Minolta CM-2600d, which measures the reflectance spectrum of the sample for the illuminant D65. The samples rotation was realized with 4 turnings of 90° made moving the whole support. To solve the problems of direction of observation and background, all the colorimetric measures have been taken placing the samples into the cavities of a support, visible in Figure 3.8, filled with powdered titanium dioxide (TiO_2). This solution allowed to keep the samples always in the same position and to have a standard matte white background. In this experiment, a standard white background has been chosen due to titanium dioxide physical properties, in order to avoid chromatic shifts linked to the use of non-standard background colors. The 10° CIE observer has been used to accomplish with a slightly larger field of view and subsequently, the

analysis in the CIELAB color space has been performed. The instrument was set in SCE mode (Specular Component Excluded) to compensate the high reflectivity of the sample surfaces. The instrument has been placed at an average distance of 2.5 cm from the samples and a black opaque matte extension tube have been used to minimize the contribution of the external reflected light.

Results and discussion

Color instrumental measures

The measures obtained with the spectrophotometer demonstrate the issues of pleochroism in the selected samples. In fact, significant hue variations have not been detected when the direction of measurement was changed. The obtained L*a*b* coordinates are very similar in each rotation, with variations below 3%. In Table 3.3 are reported the mean values of the four measures performed for each sample.

	AM1	AM2	AM3	CIT	RUB	TOP	ACQ
L*	8.65 ± 3.06	41.70 ± 8.07	52.82 ± 1.30	72.52 ± 2.90	22.17 ± 0.73	61.32 ± 3.56	59.32 ± 1.49
a*	29.14 ± 2.71	18.69 ± 7.99	11.03 ± 2.14	6.80 ± 1.33	52.36 ± 3.83	-19.51 ± 6.53	-13.82 ± 0.18
b*	-26.29 ± 3.29	-8.91 ± 21.99	-9.18 ± 3.68	35.07 ± 9.38	15.28 ± 0.49	-24.65 ± 7.54	-10.94 ± 0.37

TABLE 3.4: L*a*b* coordinates from the spectra measured with the Konika Minolta 2600 spectrophotometer. Table reproduced from [22].

Subjective color assessment

The results of the subjective color assessment are presented in Tables 3.5. The use of the Munsell Color Space has been straightforward to analyze the visual assessment results separated in Value and Chroma, given a certain Hue. In this application, Chroma is the most interesting result for this color assessment test, since Value characterizes the lightness. In Figure 3.9 it is possible to see the correlation between the perceived and the measured Chroma. The L*a*b* values obtained through the CM 2600d have been converted in Munsell HSV coordinates [88]. Further material about perceived and measured Chroma values in the second and third color choice can be fund in [22]. Table 3.5 reports the measures L*a*b* values (the same of Table 3.4) and the perceived average values of the first, second and third color choice transformed from Munsell HSV to L*a*b*. The second color choice, for some samples, has been particularly debated, so the two most frequent answers are reported (labeled respectively “2nd choice – a” and “2nd choice - b”).

Considering just the value of Chroma, in the boxplots of Figure 3.9, it is evident that for some stones, like AM1, CIT and RUB, the perceived and the measured Chroma is the same. A particular case is represented by RUB, where the variance of the perceived color is almost null.

In the other stones the perceived Chroma is always higher than the measured one, moreover, the variance of the first color choice is significant, in fact, for some stones like AM3 the chroma variance is around value 5. In some gemstones RUB and CIT, the variance of visual assessment is low, while it grows for gemstones like AM1, AM2 and AM3. In this context, it is interesting to notice that the resulting Chroma of the first color choice is the nearest to the spectrometric result in only RUB and TOP, while in all the other samples the second and/or the third color choices are the nearest to the spectrometric results.

The CIT perceived color, which in Chroma is very similar to the measured one and it can be assessed that the appearance of this gemstone is coherent with the colorimetric measure. On the other hand, the RUB stone, which Chroma resulted very

AM1				
	Measure	**1st choice**	**2nd choice**	**3rd choice**
L*	8.65	41.01	30.64	51.42
a*	29.14	37.07	24.93	29.11
b*	-26.29	-25.99	-17.86	-20.38
ΔE	-	33.32	23.93	43.18

AM2				
	Measure	**1st choice**	**2nd choice - a**	**2nd choice - b**	**3rd choice**
L*	41.70	41.01	61.52	41.06	51.38
a*	18.69	37.07	35.01	29.93	35.77
b*	-8.91	-25.99	-24.23	-21.23	-24.87
ΔE	-	25.11	29.90	16.69	25.31

AM3				
	Measure	**1st choice**	**2nd choice**	**3rd choice**
L*	52.82	61.56	71.5	81.29
a*	11.03	23.38	16.15	9.67
b*	-9.18	-23.94	-17.61	-11.31
ΔE	-	21.75	22.37	29.98

CIT					
	Measure	**1st choice**	**2nd choice -a**	**2nd choice -b**	**2nd choice -c**
L*	72.57	91.18	91.13	86.28	86.3
a*	6.80	-4.26	-2.23	-3.41	-3.82
b*	35.07	45.19	16.7	30.43	44.47
ΔE	-	23.89	27.63	17.71	19.74

RUB			
	Measure	**1st choice**	**2nd choice**
L*	22.17	41.05	51.41
a*	52.36	55.28	54.53
b*	15.28	7.77	9.61
ΔE	-	20.53	29.86

TOP				
	Measure	**1st choice**	**2nd choice**	**3rd choice**
L*	61.32	61.61	81.33	51.47
a*	-19.51	-15.38	-7.59	-14.29
b*	-24.65	-37.61	-13.91	-38.64
ΔE	-	13.61	25.64	17.89

ACQ				
	Measure	**1st choice**	**2nd choice**	**3rd choice**
L*	59.32	71.56	61.66	71.58
a*	-13.82	-10.75	-10.07	-7.34
b*	-10.94	-21.33	-22.08	-13.72
ΔE	-	16.35	11.99	14.14

TABLE 3.5: Table of measured and perceived L*a*b* values. The difference between the perceived and measured colors is reported using the ΔE (referred to the CIELAB76 ΔE) color difference. Tables reproduced from [22].

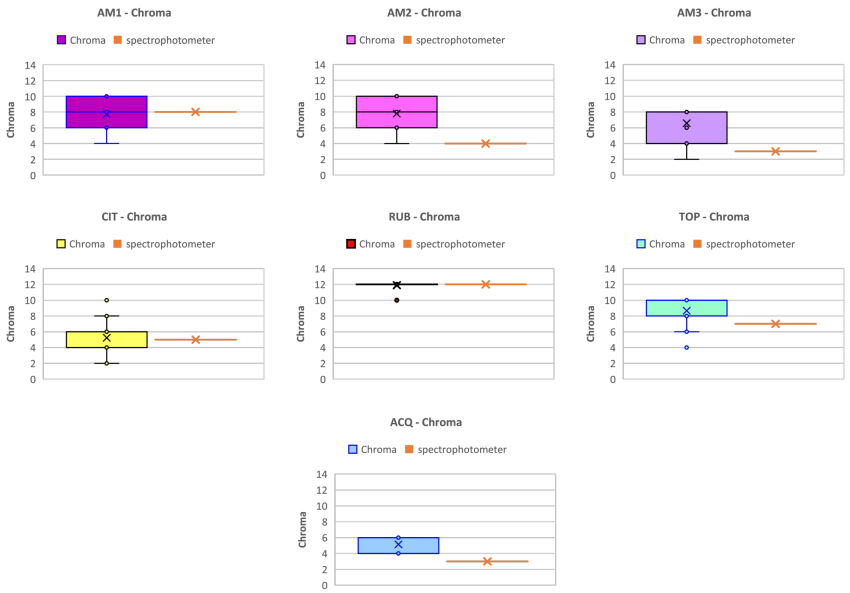

FIGURE 3.9: Boxplot with average and variance of the perceptual Chroma of the first choice for each gemstone. Figure reproduced from [22].

similar to the measured one with a very low variance, it results quite different from the colorimetric measure, when considering the Value data. The TOP gemstone has different values from the measured ones, and the ACQ stone appears distant from the first color choice. The same tendency can be observed considering the ΔE values in Table 3.9. One limit of this experiment which must be considered into account

is the gamut constraints of the Munsell Atlas, which presents a limit in the highly saturated colors. Considering this, for AM1, AM2, TOP and RUB some choices lays on the upper limit of saturation in the Munsell Atlas. Nevertheless this limit, this experiment it has been useful to perform the task of appearance assessment and, in any case, it has been able to outperform the instrumental measures. In fact, the most saturated gems (AM1 – RUB) are the ones with lowest difference between measured and perceived values. Furthermore, even if colored gemstones do not present uniform color, the visual color assessment forced observers to make an average of the overall perceived colors that leads to an overall final precision. Those consideration underlines the importance of subjective visual assessment in gemstones color assessment compared to the limits of instrumental colorimetric measures.

Thanks to the comparison between the subjective assessment and the point-wise colorimetry it has been possible to set a starting point for the development of a general and more accurate system for gemstone color assessment. In this application, a subjective color assessment has been fund more successful than an objective colorimetric measurement. In fact gemstones optical characteristics make impossible the application of standard colorimetry, since a gemstone color can not be approximated to the color measured in aperture mode or setting a specific illumination.

Gemstones, are a peculiar example of objects widely used in cultural heritage (e.g., jewelry, ornaments, decorations), which color can not be assessed objectively. In this application, as in many other field, the subjective color assessment is still a standard evaluation system and, in the literature, different applications confirm the biggest fidelity of a subjective assessment compared to the actual point-wise colorimetric measures [89]–[92]. The prevalence of subjective assessments and the use of subjectivity to solve problems of color management are the clear warning of color measurement inaccuracy, and underline the need to develop new models of HVS behavior.

In the following Chapters the limits of standard colorimetry in cultural heritage applications will be evaluated mainly in film restoration field. Anyway, the presented case study is useful to demonstrate that color measurements presents limits of applicability whenever color is the result of a complex interaction which cannot be approximated by colorimetry constraints. This is a matter of fact which must be considered when analyzing optically complex objects (i.e., gemstones), colors inserted in spatial arrangement (i.e., museum expositions) or 2D/3D scenes (i.e., images).

Part II

Color acquisition and processing

Chapter 4

Color and contrast acquisition

4.1 Introduction

In Chapter 1, different CIE Standard Systems have been introduced and colorimetry has been presented through the phases of color matching, color difference and color appearance. In summary, it is possible to assess that to measure color in aperture mode or in relation to an illuminant (object color) is mandatory to respect strict constraints and assumption, thus considering color at the retinal transduction level. In Chapter 2, some limits of applicability of these constraints have been presented, and the need to develop new color computing methods applicable to real and complex scenes has been underlined. In fact, when a color is observed in a way different from aperture mode, spatial interactions occur and must be considered in the formation of color sensation.

Starting from the examples and experiments presented in the previous Sections, I aim at showing that it is quite impossible to deal with cultural heritage in aperture mode, or using specific and defined constraints, because the colors of objects of historical and cultural relevance, are never observed in isolation, but always inside a context.

From this point forward, I will focus on image acquisition, processing and assessment using digital film restoration as main application. It is a peculiar field, where the colorimetric constraints are often not considered, and the lack of scientific research caused weaknesses and problems between color measurements and color sensations, which are often solved resorting to subjectivity (see Chapter 6).

In this Chapter, after a brief overview of image acquisition, I will focus on the issues and effects which could affect the acquisition of contrast and tones, I will present the limits of an imaging techniques widely used in cultural heritage field and I will underline the colorimetric constraints linked to the applicability of the acquirable data. Successively all those considerations will be useful in Chapter 6 to present an alternative approach for contrast and color restoration, which could help to starting overcome the limits of standard colorimetry.

4.2 Overview of image acquisition

Digitization is a conversion process, allowing to move from physical continuous values to discrete values. In digital imaging, the process of digitization is performed by scanners and cameras (see Figure 4.1). When a camera is used to make acquisitions, the incident radiation must first pass through the camera optics (i.e., lenses) and then hits the sensor. Here, the photons are picked up by an active sensing area, integrated for the exposure time and then are passed to a set of amplifiers. The imaging sensors are the core of the systems pipeline for image acquisitions and generally can be of

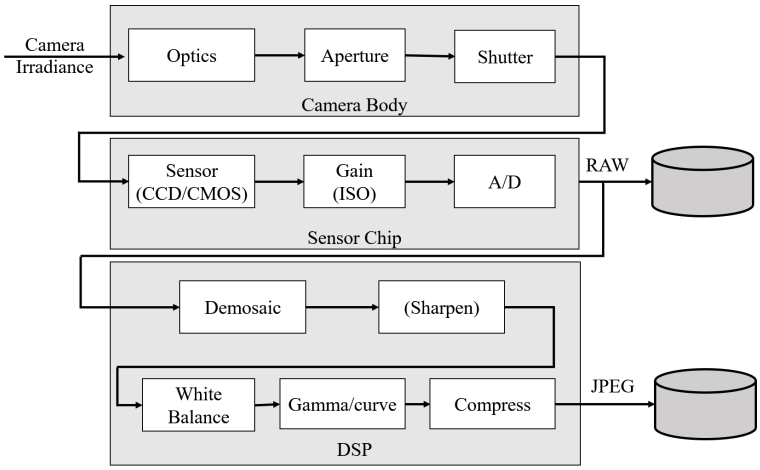

FIGURE 4.1: Example of image sensing pipeline. Figure reproduced from: [94] and developed from the model of [95]–[97].

two types: the Charge-Coupled Device (CCD) and the Complementary Metal Oxide on Silicon (CMOS). The CCDs consist of an integrated circuit formed by a grid or a row of semiconductors elements (*photosite*), capable of accumulating an electric charge proportional to the intensity of the radiation hitting the system. By sending a timed sequence of impulses to the camera device, an electrical signal is obtained and the matrix of image pixels can be reconstructed. The image matrix can be used directly in its analog form, to reproduce the image on a monitor or to record it on magnetic media, or it can be converted into digital format for future reuse (thanks to analog-to-digital converter - ADC) [93], [94].

In the CMOS, the photons hit the sensor, affecting directly the conductivity (i.e., gain) of a photodetector. This last element can be modulated to control the exposure time and can be locally amplified before being read.

In general, the CCD sensor outperforms CMOS in quality sensitive applications, although the CMOS is used, today, in most digital cameras due to its performance in low-power applications [94].

Nevertheless, the characteristics of the imaging system sensor errors and noise can be produced from various sources, during the digitization process. The most common are: fixed pattern noise, dark current noise, shot noise, amplifier noise and quantization noise [95], [96]. The amount of noise in the final image will depend on these quantities, but also on the exposure defined by the scene radiance, diaphragm aperture, time, and sensor gain. To overcome some errors in the acquisition and model the noise in a single image, the authors demonstrated that the Poisson model can be more appropriate than the Gaussian in [97]. Alternatively, it is useful to pre-calibrate the *Noise Level Function* (NLF) of the camera using targets such as the Color Checker. Nevertheless, the pre-calibration process must be repeated for different exposures and acquisition settings.

In conclusion, an important aspect to consider in the camera sensing pipeline is that, before compressing and storing the pixel values, many systems perform Digital Signal Processing (DSP) operations. Thus, the acquired RAW image can be filtered, balanced and enhanced automatically by the system (e.g., white balancing, gamma correction, color filtering).

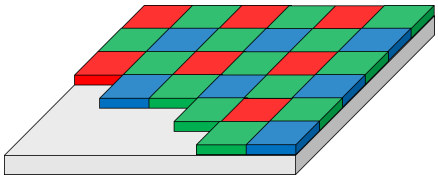

FIGURE 4.2: Graphical representation of a Bayer pattern.

4.2.1 Tones and color reproduction

Today, to acquire colors the imaging systems use *Color Filters Arrays* (CFA), where alternating sensors are covered by different filters. The *Bayer* pattern is one of the most common scheme for CFA (see Figure 4.2) and it places green filters in half of the sensors and the red and blue ones over the remaining ones [94]. When the Bayer pattern is exploited, it is necessary to interpolate the missing color values to re-construct RGB values for all the pixels in the image; this is done in a process called *demosaicing*.

Alternatively to the Bayer pattern, some new generation imaging systems (e.g., film scanners) acquire directly three full resolution R, G and B images, to overcome the demosaicing step and obtain images of higher quality.

Before encoding the sensed RGB values, many systems for image acquisition apply a preliminary image processing pipeline. Generally, a color image processing pipeline consists of: 1.Exposure determination, 2.Pre-processing (e.g. noise removal, primary color correction), 3.Linearization, 4.Dark current compensation, 5.Flare compensation, 6.White balance, 7.Demosaicking, 8.Color transformation (in un-rendered and rendered color spaces) 9.Post-processing. In digital cameras, the acquired RAW image is converted in a representation of the original scene, which must be as faithful as possible. Considering the work presented in [98], the main module responsible for the accuracy of color rendering in a digital camera are: the module responsible for the evaluation and correction of the light source and the module of color matrix transformation. First, the color constancy characteristics of the HVS are simulated; second the image is transformed in a colorimetric color space. In [99], the authors, aiming at designing a new and more robust color correction pipeline, substitute the first module using a different illuminating estimation and correction algorithms which are automatically selected on the image content. In this way, in the second module, the error propagation is alleviated and the accuracy of color rendering is limited. In 2016, a more efficient pipeline was presented in [100]. This work focuses particularly on noisy images and is composed by two steps: color correction and denoising. First, a spatial color correction algorithm is used to adaptively calculate a color correction matrices for each local image block considering the noise effect. Second, a spatially variable noise level process produces an effective noise canceling effect on the image divided into blacks.

In addition to these models, in the past literature, many algorithms for color correction have been proposed including: polynomial model [101], polynomial regression [102], [103], LUT and interpolation [104] and neural networks [105].

Gamma correction is used to encode linear luminance or RGB values in an analog video signal or in discrete digital video values. Gamma expansion is the inverse process and has its motivation in the non-linearity of the relationship between current and voltage of the electronic beams of the CRTs, which act as a natural decoder. The relationship between the voltage and the resulting brightness was characterized

by the *gamma*:

$$B = V^{\gamma}, \tag{4.1}$$

with a γ of 2.2. To compensate this effect,it was necessary to map the luminance Y through an inverse gamma:

$$Y' = Y^{\frac{1}{\gamma}}, \tag{4.2}$$

with $\frac{1}{\gamma}$ of 0.45.

The gamma value is generally used to quantify the contrast, for example of photographic film (see Chapter 6). It represents the derivative of the relationship between input and output in a logarithmic space:

$$\gamma = \frac{dlog(V_{out})}{dlog(V_{in})}, \tag{4.3}$$

In the case of photographic film, non-linearity is called the *sensitometric curve*, where the gamma values below 1 are typical of the negative film and the values above 1 are characteristic of the invertible films.

In modern systems, gamma correction is applied during compression, so the gamma encoding and decoding is still useful, but in some other applications might be problematic. Once that a computation or an enhancement is made, the appropriate gamma should be applied before the visualization on a display; unfortunately, many computer systems operate directly in RGB mode and display the values without a proper correction. In this context it is fundamental to preserve the gamma used by the imaging system in the acquisition avoiding to incur in further errors and approximations.

4.2.2 Compression

Many cameras and scanners allow to acquire images using lossless compression schemes (e.g., RAW, PNG, DPX), anyway generally the last step in the acquisition pipeline is the image compression. Since the HVS is more sensitive to variations in luminance than in chrominance, all compression algorithms converts the system in YCbCr (YUV color model). After the subsampling of the image in luminance and chrominance images, a *block transform* stage is performed, generally, applying a 2D Discrete Cosine Transform (2D-DCT). The 2D-DCT is the most widespread function that provides spatial compression, capable of detecting the variations of information between an area and the contiguous one of a digital image, neglecting repetition, and it is a variant of the Discrete Fourier Transform (DFT). E.g., both MPEG and JPEG uses an 8x8 2D-DCT transform [106], [107]. The block transform coding is followed by the quantization of the coefficient values into a set of smaller integers. This coding can be performed using a variable bit length scheme such as Huffman code or an arithmetic code [106].

The quality of a compression is usually assessed through the *Peak Signal-to-Noise Ratio* (PSNR), derived from the Mean Square Error (see Chapter 7).

4.2.3 System performance assessment

In [108] Don Williams et al. propose an imaging performance taxonomy and relate the image metrics with the imaging characteristics. In fact, the imaging performance metrics are one fundamental aspect to assess how an imaging system or a single component acts in front of an input scene, and this is decisive to perform a correct

digital reproduction. Measuring the imaging performance is fundamental and allows to: evaluate the equipment, benchmark, quantify and identify the influence of image processing and perform a quality control. In order to evaluate the system performances it is mandatory to set up the adequate test conditions and acquire targets and charts (e.g., IT8, Color Checkers). This system allows to evaluate the accuracy and variations of the imaging and the targets are intended for system calibration and performance testing. Following the ISO standards, in [109] the mandatory aspects to get a sufficient characterization of an imaging system are summarized as:

1. Opto Electronic Conversion Function (OECF)
2. white balancing
3. dynamic range (related scene contrast)
4. used digital values
5. noise (signal to noise ratio)
6. resolution (limiting resolution center,corner)
7. sharpness

In [109], the recommended values are: distortion, shading/vignetting, chromatic aberration, color reproduction quality, unsharp masking, shutter lag, aliasing artifacts, compression rates, exposure and exposure time accuracy and constancy, ISO speed.

4.3 Glare effect in image acquisitions

Glare (or flare) is an unwanted optical veiling caused by the presence of lenses and optics in the acquisition system. This phenomenon is still unclear and less studied if compared with other source of noise or error in the acquisition (e.g. uneven receptor sensitivity, dark current, interference pattern, non-uniform lighting, atmospheric and topographic effects, parasitic images, reflections and shadows), but it can cause greater errors in the output. Glare is not just noise. The effect of glare is systematic, unpredictable and unavoidable and in many acquisition can weight much more that other sources of noise.

Glare is a phenomenon well known in the optics domain caused by the scattering of light in the eye-bulb and in the retina, which reduces the ability to see details and a general vision loss [2], [110]. Please notice that in this case the term *glare* is used to identify its effect and not the cause of this phenomenon. In this thesis, I will refer with the term *glare* to the unwanted effect in imaging acquisitions. In some studies, it has been found that the cortical processing of the optical glare change the general appearance of the observed scene, which rarely correlates with its luminance [111], [112]. For what concerns the imaging domain glare is often confused as an effect of the non-uniformity of the illumination or product of non standard conditions in the acquisition setup, in which spatial difference of the illumination can cause errors in the spectral acquisitions e.g. sensor saturation or exposure errors. Nevertheless, these problems can easily be solved, controlled or reduced modifying the acquisition setup, despite glare which is systematic and unavoidable. Glare effect, in fact can be increased by the presence of non-uniform lighting or wrong acquisition conditions, but can not be prevented. Another characteristic of glare, in comparison to other

FIGURE 4.3: Glare effect in photographic acquisitions. On the left it is visible the effect of glare caused by the light source in the scene. On the right the contrast variation caused by the coverage of the light source.

camera noise sources, is that glare produces alterations in data acquisition which can be higher of orders of magnitude and way bigger than the effect of non-uniform illumination. In this field, glare effect has been studied mainly in High Dynamic Range applications because it reduces the general image details [113]–[116]. In these studies, it has been demonstrated that glare causes an unwanted changes in pixel values limiting the radiance range which can be acquired in a shot. In [42], [43] and [115] authors reports an extensive explanation of glare in HDR images. Nevertheless these studies, glare affects systematically every image acquisition which uses lenses (see 4.3) and today there is still a lack of studies in hyperspectral imaging. This fact seems in contrast with the wide diffusion of hyperspectral imaging to make accurate measurements for materials identification and characterization. Furthermore, imaging techniques are becoming increasingly popular in many application fields such as cultural heritage, for its ability to combine spectroscopy with digital imaging [117]–[123].

In literature, different attempts to remove glare are described. One of the main solutions was presented by Talvala et al. in [124], where the use of an occlusion mask was found successful in the reduction of glare effect. Nevertheless this solution could be unpractical for many applications. Furthermore, in [125], Gianini et al. analyze the glare formation and for each step a corresponding influence is analyzed as ill-posed and ill-conditioned problem.

4.3.1 Evaluation and assessment of tones reproduction in hyperspectral imaging systems

In the acquisition pipeline, many factors can contribute to the production of noise, errors and artifacts in the output and today there are just few solutions to these problems. In order to assess and measure the presence of glare in acquisition systems, here I present an experiment that I recently published in [23].

In this experiment is presented the analysis of an hyperspectral acquisition system with a particular focus on the phenomenon of glare. The scope of this experiment is to analyze the effect of glare in realistic acquisition setups with different

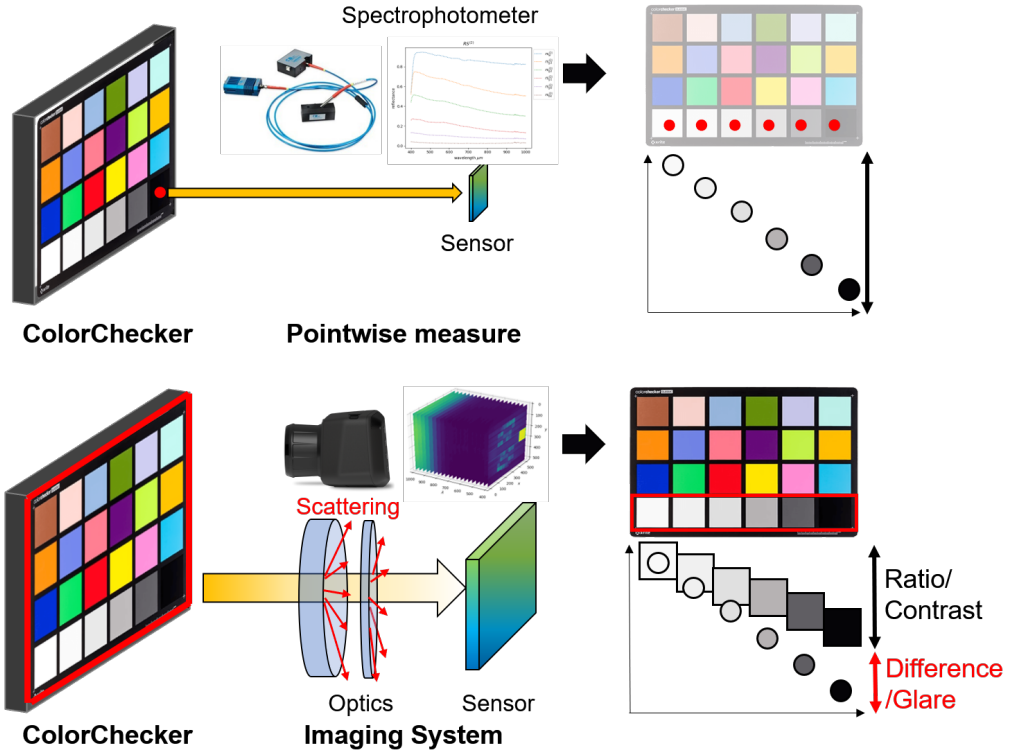

FIGURE 4.4: Glare effect. On the top, a graphical representation of a pointwise measure of reflectance. In this system, the reflectance spectrum is acquired directly from a portion of the surface in standard colorimetric conditions (illumination geometry, direction of observation, and light source). On the bottom, a graphical representation of an imaging system, where the scene information is acquired through a sensing pipeline which requires optics. Thus, the scattering phenomena can induce the glare effect and decrease the contrast of the final image. In this work, to provide a measure of the glare effect, we performed a comparison between the ratio of the grayscale patches acquired through a pointwise system and the ratio of the grayscale patches acquired through a hyperspectral image (HSI) system. Figure reproduced from [23].

geometries, light sources and backgrounds. Thanks to this it has been possible to report the prevail of glare effect in presence of other factors and source of errors. With this study and analysis I arise awareness of glare effect in imaging acquisition, especially when used for cultural heritage applications such as materials identification. For this purpose, two Color Checkers have been acquired in three different lighting conditions, with different background and orientations, to verify how much glare can affect an hyperspectral image also in standard conditions. The hyperspectral output has been compared with point-wise reference measures. Since glare mainly affects the final contrast in the acquired image/output it has been compared the contrast of the grayscale patches of the Color Checker in the hyperspectral acquisition with the contrast of the point-wise measure (see Figure 4.4). This measure has been called: Glare Effect index (GE).

More details and about this study and application are published in [23].

Experimental set-up

In this study the hyperspectral camera under analysis is a SpecimIQ camera, which is capable to acquire a wide range of wavelengths, from 400 to 1000nm with a spectral resolution of 7nm. This camera is equipped with a camera calibration software and with a service RGB camera, which helps the user in composing the frame. An immediate RGB color visualization of the acquired data cube is obtained combining three reference wavelengths: 598nm (R), 548nm (G) and 449nm (B). More details about the hyperspectral camera hardware and software can be found in [126].

In this work, I will refer to the hyperspectral data cube as:

$$\begin{aligned} HSI = X \times Y \times L \rightarrow \mathbb{R} \\ x, y, l \mapsto HSI(x, y, l) \end{aligned} \tag{4.4}$$

where,

$$\begin{aligned} X = Y = \{0, \cdots, 511\} \\ \Lambda = \{0, \cdots, 203\} \end{aligned} \tag{4.5}$$

Here X and Y refers to the spatial coordinates of the data cube and L is the set of corresponding wavelengths.

The output data from the hyperspectral imaging system are: the raw data-cube (R_{DC}), the black (dark current) frame (D_F) and the white reference spectrum (W_R). The white calibration spectrum is derived from a reference white target with a reflectance of $> 99\%$ over the whole acquired range of wavelengths. The final pixel-wise reflectance values $R(x, y, l)$ obtained in each hyperspectral acquisition are computed with the following calibration formula:

$$R(x, y, l) = \frac{R_{DC}(x, y, l) - D_F(x, l)}{W_R(l) - D_F(x, l)} \tag{4.6}$$

The main limit of Equation 4.6 is that the white calibration, as in many acquisition systems, is made on through the average of the spectrum in a reduced area, so the non-homogeneity of the illumination cannot be compensated.

In this experiment 23 hyperspectral images have been acquired, all in the same room with the same artificial light sources (a room neon lamp and two halogen spotlights). Here, three set-ups have been used (see Figures 4.6). **Setup 1** (images from 01 to 14): in this setup the Color Checkers have been placed on the same plane. Images from 03 to 08 presents a black background, while all the others have a white background.

Setup 2 (images from 15 to 21): here the two Color Checkers have been places on different planes and a LED lamp was placed between them on a upper plane. All the images have a black background. **Setup 3** (images from 22 to 23): in this acquisition the setup is similar to Setup 2 but without the LED lamp.

In these images, the Color Checkers have been named respectively *CCA* for the first Color Checker to the right or from the top of the image, and *CCB* for the one on the left or on the image bottom. Every image name is coded using the following naming pattern:

N{·}S{·}B{·}D{·}-T{·}

Where, $N\{\cdot\}$ refers to the image number, $S\{\cdot\}$ refers to the setup, $B\{\cdot\}$ indicates the image background (*B0* - black background and *B1* - white background), $D\{\cdot\}$ refers

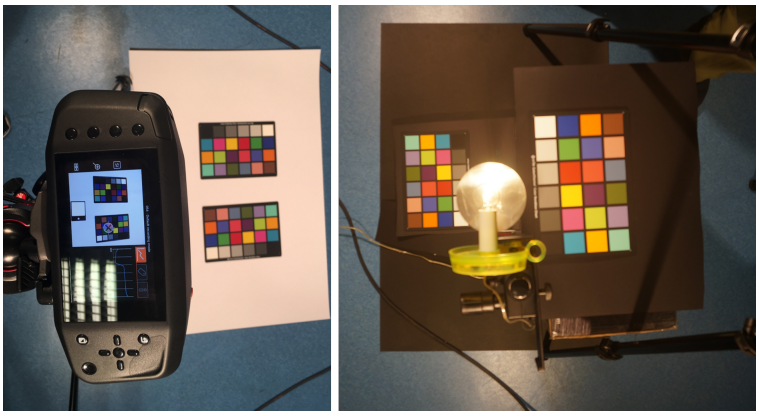

FIGURE 4.5: Pictures of the experimental setups.

to the grayscale orientation (*D0* - toward the image center and *D1* - toward the image borders) and $-T\{\cdot\}$ indicates the exposure time (expressed in *ms*).

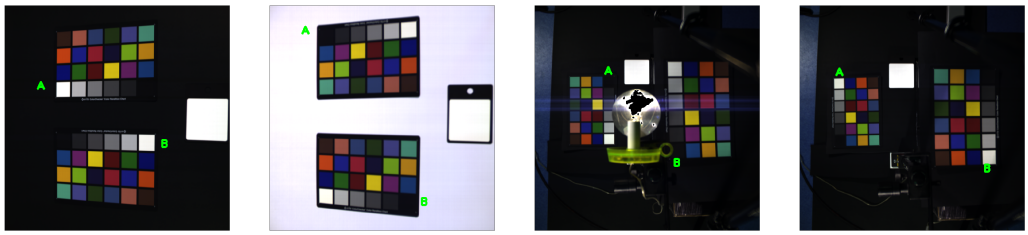

(A) (B) (C) (D)

FIGURE 4.6: Some examples of experimental setups, in Figures a, b two image from setup 1 are shown, one with with dark background and the other with white background. In Figures c, d one image from setup 2 and another from setup 3 are shown. Figure reproduced from [23].

In this experiment, the focus is on the grayscale patches of two original Color Checkers (see the notation is reported in Table 4.1).

Official Name	**Used Name**
white 9.5	*w*
neutral 8	*g3*
neutral 6.5	*g2*
neutral 5	*g1*
neutral 3.5	*g0*
black 2	*bk*

TABLE 4.1: Color Name Notation. Table reproduced from [23].

As presented in Figure 4.4 in this study the contrast of the hyperspectral images obtained in different conditions, have been compared with the contrast obtained through point-wise measures. In particular we selected two point-wise reference data. The first references are tabulated data published by Pascale in [82], here named RS^1. This standard reference has been used to compute the glare effect in the visible range (from 400 to 700nm). Furthermore, since the hyperspectral system acquired a wider range of wavelengths, a second point-wise reference dataset has been used,

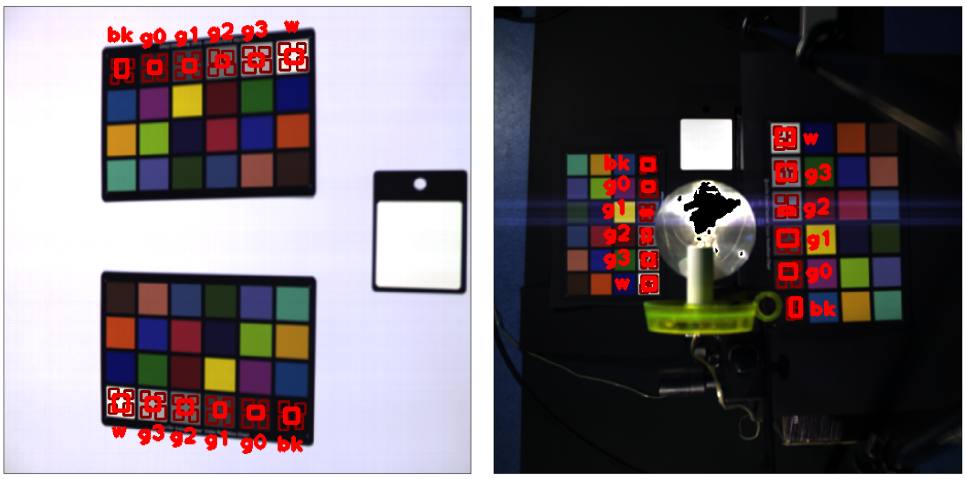

(A) (B)

FIGURE 4.7: Red boxes denotes the patch regions in which spectra are collected in Figure a for image 'N09' and in Figure b for image 'N17'. Figure reproduced from [23].

here named RS^2. This dataset is obtained through a spectrophotometer Ocean Optics HR4000 (the spectral measures are the same used for the original Color Checker in the experiment presented in Section 3.2) and has a sensitivity range from 200 to $1000nm$. This second reference has been used in the comparison of the infra-red region of the graylevel color patches.

Glare Effect index

In each hyperspectral acquisition, for each patch of the grayscale level in the Color Checkers five spectra have been extracted. The five spectra came from five different region in the patch: one at the center and four in the patch corners (Figure 4.7). Then, the five spectra of each patch have been compared with the references, one from the tabulated values RS^1 and the other from the spectrophotometer RS^2. An example of spectral acquisition in image 09 is reported in Figure 4.8.

From the comparison of contrast between the grayscale patches in the hyperspectral acquisitions and in the references it has been possible to measure the Glare Effect index (GE). Supposing that the main glare contribution is given by the proximity to a light source or a bright area, as a consequence the black and dark patches must be the most affected by this effect. To measure this phenomenon, at first it has been measured the ratio between the spectrum of a graylevel patch and the spectrum of its corresponding white patch in the same Color Checker. Then, this ratio has been compared with a second ratio obtained from the spectrum of the same graylevel patch and the corresponding white in one of the references (a graphical explanation is presented in 4.9). If the first ratio (hyperspectral image) is higher than the second ratio (reference point-wise measure) glare has affected the acquisition. This reasoning can be formalized as following. Considering the spectrum of each grayscale patch (s_c) and the corresponding spectrum of the white patch (s_w), the first ratio ($r_{c,w}$) is:

$$r_{c,w}(l) = \frac{s_c(l)}{s_w(l)} \tag{4.7}$$

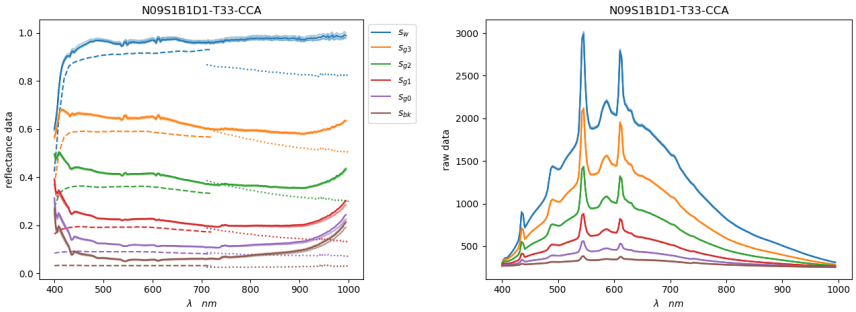

(A) (B)

FIGURE 4.8: Spectra extracted from the CCA grayscale on the image N09S1B1D1T33. In (Figures a) and (Figure b) the solid lines represent the mean reflectance and raw acquired values respectively. In (Figure a) the dashed lines represent the reference RS^1 in 400 nm to 700 nm and the dotted lines represent the reference RS^2 in 700 nm to 1000 nm. Figure reproduced from [23].

To analyze the glare effect in specific regions of the considered wavelengths (l), an interpolation has been performed:

$$s(\hat{\lambda}) = \frac{1}{|\hat{\lambda}_{l_0} - \hat{\lambda}_{l_1}|}(|\hat{\lambda} - \hat{\lambda}_{l_1}|s(l_0) + |\hat{\lambda} - \hat{\lambda}_{l_0}|s(l_1)) \tag{4.8}$$

where, $\hat{\lambda}_{l_0}$ and $\hat{\lambda}_{l_1}$ are the nearest wavelengths to the needed wavelength $\hat{\lambda}$, and $s(l_0)$ and $s(l_1)$ are the corresponding values. From this, the Glare Effect index is computed as:

$$GE^j_{\lambda_{min},\lambda_{max}}(c) = \frac{f_{\lambda_{min},\lambda_{max}}(s_c, s_w)}{f_{\lambda_{min},\lambda_{max}}\left(RS^j_c, RS^j_w\right)} \tag{4.9}$$

where, c refers to the grayscale patch w, $g3$, $g2$, $g1$, $g0$, bk, λ_{min} and λ_{max} refers to the considered range of wavelengths and $j = (1, 2)$ indicates the reference dataset. As explained before the numerator and denominator in GE index are both ratios between a grayscale patch and the corresponding white, but the numerator is derived from the hyperspectral images and the denominator from the reference point-wise spectra. For instance we expect an increasing GE index going from white ('w') to black ('bk'), with a minimum value of 1 for the white patch.

In the GE index it is possible to take into account spectral values relatives to a single wavelength or a range of wavelengths. Thanks to this, it has been possible to produce different results combining the hyperspectral data with the two reference datasets in defined spectral ranges. An example is reported in Figure 4.9. For this experiment, it has been chosen to obtain the GE index in the visible range (from 400 to 700nm) using the first reference dataset (RS^1), and the GE index in the IR range using the second reference dataset (RS^2). This decision has been made because the reference measures were acquired with different instruments and different light sources, so it is present a mismatch among the spectra (see Figure 4.8). As consequence, to limit the error propagation it has been decided to use the second reference dataset (RS^2) just in the IR range of wavelengths. I will refer to the GE index computed in the visible range as $GE^1_{400,700}$ and to the GE index computed in the IR range as $GE^2_{700,1000}$.

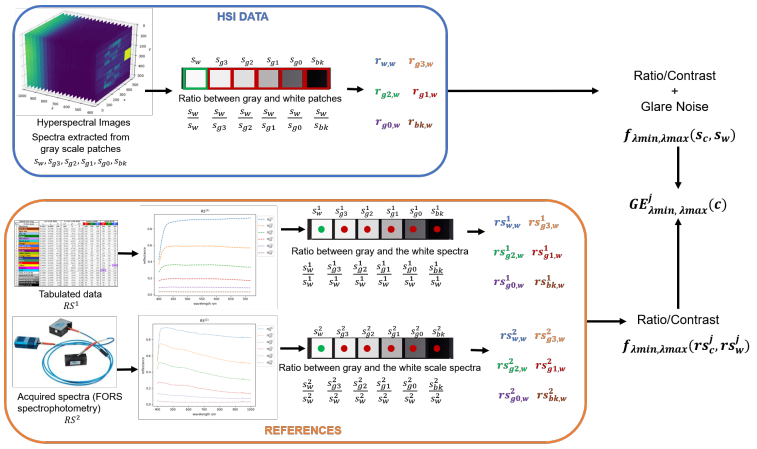

FIGURE 4.9: Graphical explanation of the Glare Evidence (GE) formula. The numerator is the ratio between the gray and white patches of the HSI system, which includes the glare effect introduced by the lenses in the imaging system. The denominator is the ratio between the gray and white spectra obtained from the two references (point-wise measuring systems). Thus, GE measures the noise introduced by the imaging system which is represented by the difference between the two computed ratios. Figure reproduced from [23].

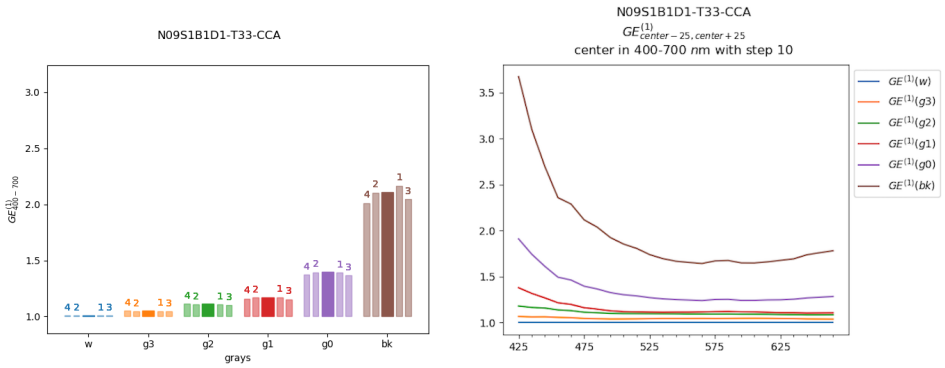

(A) (B)

FIGURE 4.10: Example of GE^1 plot representation of the CCA on image *N09S1B1D1-T33*. Plot a represents average values of glare effect of each grayscale patch in a range from 400 nm to 700 nm. The central solid color bar represents the GE values obtained from the central region of the grayscale patch; the labels 1,2,3,4 refers to the GE values obtained from data of the regions toward the patch corners (see patch regions in Figure 4.7). In Figure b the average values of GE^1 are represented for each wavelength from 400 nm to 700 nm and smoothed by applying a sliding window in the considered interval. Figure reproduced from [23].

Results and Discussion

Setup 1

The results obtained in the first setup (*'S1'*) are presented in Tables 4.2 and 4.3 where $GE^1_{400,700}$ and $GE^2_{700,1000}$ are considered respectively for the images with exposure time of $41ms$. Furthermore, in Table 4.4 are presented the results of GE index using different exposure times. In the first setup (*'S1'*), the Color Checkers have been acquired with a black (*'B0'*) or a white (*'B1'*) background and with an exposure time

of 41ms. As already explained, the Glare Effect in the visible range ($GE^1_{400,700}$) has been measured using as reference the tabulated data of RS^1 and the GE index in the IR range ($GE^2_{700,1000}$) has been computed using as reference the measured point-wise spectra of RS^2 dataset.Results are reported in the following Tables:

HSI Number	w	g3	g2	g1	g0	bk
N01S1B0D0-T41-CCA	1.00	0.99	1.01	0.98	1.02	1.29
N01S1B0D0-T41-CCB	1.00	1.06	1.10	1.13	1.27	1.56
N02S1B0D1-T41-CCA	1.00	1.04	1.08	1.10	1.22	1.52
N02S1B0D1-T41-CCB	1.00	1.03	1.01	0.98	1.05	1.28
N07S1B1D1-T41-CCA	1.00	1.04	1.11	1.18	1.42	2.22
N07S1B1D1-T41-CCB	1.00	1.03	1.04	1.06	1.25	1.90
N08S1B1D0-T41-CCA	1.00	1.00	1.03	1.04	1.18	1.80
N08S1B1D0-T41-CCB	1.00	1.07	1.12	1.19	1.43	2.14

TABLE 4.2: $GE^1_{400,700}$. To make the table (of the glare effect in each acquisition) easier to read the values between 1 and 1.19 are highlighted in gray, the values between 1.20 and 1.79 in light blue, the values between 1.80 and 2.39 in green . Table reproduced from [23].

HSI Number	w	g3	g2	g1	g0	bk
N01S1B0D0-T41-CCA	1.00	0.87	0.81	0.87	0.95	1.55
N01S1B0D0-T41-CCB	1.00	0.96	0.91	1.08	1.23	2.02
N02S1B0D1-T41-CCA	1.00	0.92	0.90	1.02	1.20	2.01
N02S1B0D1-T41-CCB	1.00	0.91	0.82	0.91	0.98	1.58
N07S1B1D1-T41-CCA	1.00	0.94	0.95	1.16	1.49	2.98
N07S1B1D1-T41-CCB	1.00	0.93	0.87	1.05	1.28	2.49
N08S1B1D0-T41-CCA	1.00	0.88	0.85	0.97	1.17	2.27
N08S1B1D0-T41-CCB	1.00	0.97	0.95	1.19	1.46	2.82

TABLE 4.3: $GE^2_{700,1000}$. To make the table (of the glare effect in each acquisition) easier to read the values between 1 and 1.19 are highlighted in gray, the values between 1.20 and 1.79 in light blue , the values between 1.80 and 2.39 in green and the values over 2.40 in orange. Table reproduced from [23].

Considering the visible range of the first setup, the GE index grows as expected along the grayscale, from the white to the black patches. The only exception is represented by the Color Checker B (CCB) in the image 'N02'. Furthermore, in this setup the Glare Effect increase when the black patches are near to the white reference or surrounded by the white background. As example of this effect can be noticed looking at Table 4.2, where it is clearly visible that in *'B1'* condition the gray values 'g3', 'g2' and 'g1' have similar GE values than in condition *'B0'*, but the Glare Effect in 'g0' and 'bk' is considerably higher. In Table 4.2 the black patches with higher GE values are the ones in 'N07-CCA' and 'N08-CCB'. In this case both the hyperspectral images have a white background and the grayscales of the Color Checkers are oriented toward the image borders. The high values of GE in these black patches is probably caused by the non-uniformity of the lighting, which is more intense on the left side of the image and which contribute to the increase of glare in this region. In this case it is important to notice that, the non-uniformity of the illumination contribute to the

increase of glare effect, which affects all the black patches, even the ones oriented in the opposite direction or with a black background. Considering now the results in the IR range presented in Table 4.3, it is possible to see that the data trend is similar to the visible range. In this case, the mismatch problems of the reference spectra explained in the previous Section are more visible and, in some cases, cause a decrease of GE values under 1. Nevertheless, also in this range the black patches present high GE values, which in most cases grow over 2 and the highest glare values are reported in the images 'N07-CCA' and 'N08-CCB'.

All the images used to analyze the Glare Effect in the first setup and reported in Tables 4.2 and 4.3 use an exposure time of $41ms$. This time has been empirically defined. To support this decision in the following Table are reported the GE values obtained with different exposure times (*'T41'*, *'T33'*, *'T14'*), but with the same setup, background and direction:

HSI Number	w	g3	g2	g1	g0	bk
N01S1B0D0-T41-CCA	1.00	0.99	1.01	0.98	1.02	1.29
N01S1B0D0-T41-CCB	1.00	1.06	1.10	1.13	1.27	1.56
N03S1B0D0-T33-CCA	1.00	0.99	1.00	0.97	1.02	1.28
N03S1B0D0-T33-CCB	1.00	1.06	1.10	1.12	1.26	1.58
N05S1B0D0-T14-CCA	1.00	0.99	1.00	0.97	1.03	1.30
N05S1B0D0-T14-CCB	1.00	1.05	1.09	1.12	1.27	1.57

TABLE 4.4: $GE^1_{400,700}$. To make the table (of the glare effect in each acquisition) easier to read the values between 1 and 1.19 are highlighted in gray, the values between 1.20 and 1.79 in light blue. Table reproduced from [23].

As showed in this Table, if the exposure time changes, the results are nearly unchanged with an average variance is 0.02 circa. Thus, the use of an exposure time of $41ms$ is validated.

Setup 2

The results of the second setup (*'S2'*) are presented in Tables 4.5 and 4.6, where the values of $GE^1_{400,700}$ and $GE^2_{700,1000}$ are computed for hyperspectral images with exposure time from 11 to $44ms$.

In the second setup (*'S2'*) all the hyperspectral images have been acquired with a black background with a LED lamp between the two Color Checkers. The Glare Effect in the visible range ($GE^1_{400,700}$) has been computed using the tabulated reference dataset RS^1 and in the IR range ($GE^2_{700,1000}$) it has been computed using the measured reference dataset RS^2.

As reported in Tables 4.5 and 4.6 in this setup have been used different exposure times. In this case, the presence if a LED lamp between the Color Checkers, in some acquisitions, caused the saturation of the camera sensors. In this setup, as in *'S1'* the GE values increase along the grayscale and the black patches present the highest values of glare. In this setup the Color Checker are disposed vertically. In the direction *'D0'* the Color Checkers have both the grayscale near the LED lamp, and in *'D1'* the grayscale is toward the image borders. In *'D0'* condition the highest values of GE have been registered for the black patches. Thus, as expected, the presence of a lamp between the Color Checkers produced a strong glare increase. Furthermore, the GE index grows also in the *'D1'* condition and this fact demonstrate that glare affects all the regions in the image, not just the ones near the light source. The data trend in the IR range of the second setup (see Table 4.6) is similar to the visible range and the

HSI Number	w	g3	g2	g1	g0	bk
N13S2B0D1-T44-CCA	—	—	—	—	—	—
N13S2B0D1-T44-CCB	—	—	—	—	—	—
N14S2B0D0-T42-CCA	—	—	—	—	—	—
N14S2B0D0-T42-CCB	1.00	1.19	1.78	1.54	1.86	2.37
N15S2B0D0-T42-CCA	—	—	—	—	—	—
N15S2B0D0-T42-CCB	—	—	—	—	—	—
N16S2B0D0-T42-CCA	—	—	—	—	—	—
N16S2B0D0-T42-CCB	—	—	—	—	—	—
N17S2B0D0-T11-CCA	1.00	1.05	1.07	1.63	1.29	1.76
N17S2B0D0-T11-CCB	1.00	0.96	1.57	1.44	1.82	2.37
N18S2B0D0-T11-CCA	1.00	1.07	1.12	1.59	1.60	2.61
N18S2B0D0-T11-CCB	1.00	0.99	1.57	1.63	2.24	3.48
N19S2B0D1-T11-CCA	1.00	1.05	1.17	1.15	1.25	1.59
N19S2B0D1-T11-CCB	1.00	1.08	1.16	1.36	1.30	1.70
N20S2B0D1-T11-CCA	1.00	1.03	1.13	1.09	1.19	1.55
N20S2B0D1-T11-CCB	1.00	1.07	1.15	1.29	1.29	1.65
N21S2B0D1-T11-CCA	1.00	1.03	1.07	1.09	1.18	1.55
N21S2B0D1-T11-CCB	1.00	1.06	1.12	1.15	1.22	1.59

TABLE 4.5: $GE^1_{400,700}$. To make the table (of the glare effect in each acquisition) easier to read the values between 1 and 1.19 are highlighted in gray, the values between 1.20 and 1.79 in light blue, the values between 1.80 and 2.39 in green and the values over 2.40 in orange. Table reproduced from [23].

highest glare values are registered in the images where the grayscale has orientation *'D0'*.

Setup 3

The results of the third setup (*'S3'*) are reported in Tables 4.7 and 4.8 and computed in images obtained with exposure time from 11 to 21ms.

In the last setup (*'S3'*) the hyperspectral images have been acquired in the same condition as setup 2, but without the LED lamp. In the following Tables are reported the values of ($GE^1_{400,700}$) and ($GE^2_{700,1000}$)

In setup 3 two exposure times have been used, respectively 12 and 11ms. Also in this last setup the growth of GE along the grayscale is confirmed. This setup is particularly useful to define the contribution in glare produced by the LED lamp in setup 2 and determine that glare remains also without the presence of a light source. Considering the results reported in Table 4.7, it is possible to see that glare is present also with black background and without a light source in the image. The presence of white patches in the images is sufficient to produce glare and decrease the general contrast in the acquired images. This causes a general increase of black reflectance of 1.50 circa.

HSI number	w	g3	g2	g1	g0	bk
N13S2B0D1-T44-CCA	—	—	—	—	—	—
N13S2B0D1-T44-CCB	—	—	—	—	—	—
N14S2B0D0-T42-CCA	—	—	—	—	—	—
N14S2B0D0-T42-CCB	1.00	1.08	1.89	1.56	1.89	2.91
N15S2B0D0-T42-CCA	—	—	—	—	—	—
N15S2B0D0-T42-CCB	—	—	—	—	—	—
N16S2B0D0-T42-CCA	—	—	—	—	—	—
N16S2B0D0-T42-CCB	—	—	—	—	—	—
N17S2B0D0-T11-CCA	1.00	0.96	0.92	2.01	1.35	2.33
N17S2B0D0-T11-CCB	1.00	0.86	1.74	1.47	1.89	2.90
N18S2B0D0-T11-CCA	1.00	1.01	1.08	2.05	2.31	5.05
N18S2B0D0-T11-CCB	1.00	0.96	1.71	1.98	3.11	6.34
N19S2B0D1-T11-CCA	1.00	0.96	1.05	1.18	1.28	2.01
N19S2B0D1-T11-CCB	1.00	0.95	0.97	1.41	1.30	2.12
N20S2B0D1-T11-CCA	1.00	0.94	0.97	1.09	1.20	1.99
N20S2B0D1-T11-CCB	1.00	0.95	0.95	1.24	1.25	2.00
N21S2B0D1-T11-CCA	1.00	0.93	0.91	1.07	1.19	1.99
N21S2B0D1-T11-CCB	1.00	0.94	0.93	1.05	1.16	1.91

TABLE 4.6: $GE^2_{700,1000}$. To make the table (of the glare effect in each acquisition) easier to read the values between 1 and 1.19 are highlighted in gray, the values between 1.20 and 1.79 in light blue, the values between 1.80 and 2.39 in green and the values over 2.40 in orange. Table reproduced from [23].

HSI Number	w	g3	g2	g1	g0	bk
N22S3B0D1-T21-CCA	1.00	1.02	1.03	1.07	1.17	1.49
N22S3B0D1-T21-CCB	1.00	1.05	1.12	1.04	1.14	1.48
N23S3B0D1-T11-CCA	1.00	1.03	1.04	1.07	1.16	1.50
N23S3B0D1-T11-CCB	1.00	1.03	1.09	1.04	1.14	1.44

TABLE 4.7: $GE^1_{400,700}$. To make the table (of the glare effect in each acquisition) easier to read the values between 1 and 1.19 are highlighted in gray and the values between 1.20 and 1.79 in light blue. Table reproduced from [23].

HSI Number	w	g3	g2	g1	g0	bk
N22S3B0D1-T21-CCA	1.00	0.93	0.86	1.04	1.16	1.89
N22S3B0D1-T21-CCB	1.00	0.93	0.92	0.92	1.09	1.78
N23S3B0D1-T11-CCA	1.00	0.93	0.87	1.04	1.16	1.92
N23S3B0D1-T11-CCB	1.00	0.91	0.90	0.93	1.09	1.74

TABLE 4.8: $GE^2_{700,1000}$. To make the table (of the glare effect in each acquisition) easier to read the values between 1 and 1.19 are highlighted in gray, the values between 1.20 and 1.79 in light blue and the values between 1.80 and 2.39 in green. Table reproduced from [23].

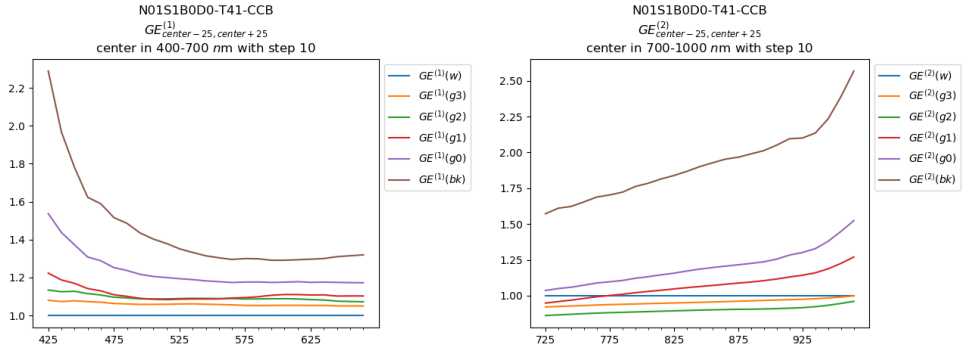

(A) (B)

FIGURE 4.11: GE^1 of the CCB of image *N01S1B0D0-T41* in Figure a range 400 nm to 700 nm and in Figure b in the interval 700 nm to 1000 nm, both evaluated for each wavelength and smoothed by applying a sliding window. Figure reproduced from [23].

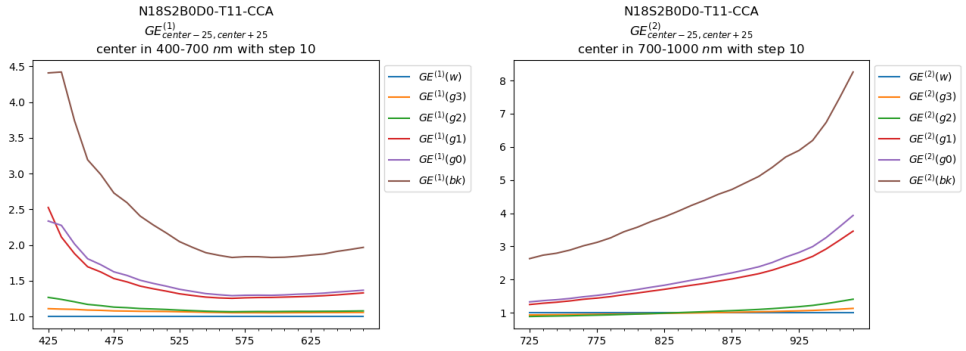

(A) (B)

FIGURE 4.12: GE^2 of the CCA of image *N18S2B0D0-T11* in Figure a range 400 nm to 700 nm and in Figure b in the interval 700 nm to 1000 nm, both evaluated for each wavelength and smoothed by applying a sliding window. Figure reproduced from [23].

Preliminary glare spectral analysis

Thanks to the possibility to select specific wavelengths ranges in the analysis of Glare Effect, in this Section is preliminary discussed the glare spectral response. In Figure 4.11 and 4.12 are represented respectively the GE^1 values for each grayscale patch the GE^2 values for each grayscale patch in the visible and IR range.

In Figure 4.11 Glare Effect is computed from the grayscale of Color Checker B in the first setup, with a black background and with the grayscale oriented toward the image center. The GE values in the visible range are reported in Figure 4.11a and the values in the IR range in Figure 4.11b. In the visible range the values of GE^1 are higher for short wavelengths (violet and blue regions) especially in for darker patches ('bk' and 'g0'). This trend is comparable in all the other wavelengths. In the IR range, the GE^2 values increase in the region from 900 to 1000nm and the black patch presents significantly high values in comparison to the other grayscale patches. In this context, the mismatch among the acquired spectra and the RS^2 dataset affects the reliability of the data. This results mainly in the decrease of GE values under 1 for some gray patches.

In Figure 4.12 Glare Effect is computed for the Color Checker B in the second setup, with black background and with the grayscale oriented toward the image center, near the LED lamp. The GE^1 values in the visible range are displayed in Figure 4.12a and the GE^2 values in the IR range are reported in Figure 4.12b. Considering the visible range, the GE values are higher for short wavelengths, also if the spectral trend is less smooth and shows a peak at 580 nm. In the IR range the GE values increase from 900 to 1000nm.

In both setups glare increases in the shortest and in the longest ranges of wavelengths, and the presence of the LED light source in the second setup cause a general growth in GE intensity.

This preliminary glare spectral analysis demonstrates that glare affects differently specific wavelengths ranges. Anyway this fact could be caused by different factors like the mismatch among the reference and the acquired spectra or some approximation error during the data normalization. Thus, the spectral analysis of glare effect require further attention and analysis.

Deal and manage glare

Glare is a systematic phenomenon which affects every imaging acquisition system which uses lenses. The main effect of glare can be seen in the use of the acquired data, where the general contrast and dynamic range presents an unwanted decrease. In this study is demonstrated that glare effect is present not only when a direct light source hits the acquisition system, but it can generate an alteration in the acquired data also in setups with limited dynamic range. Furthermore, glare has a spatial dependency, which makes it impossible to be predicted, estimated or modeled before the acquisition [127]. Furthermore, in the hyperspectral imaging field the acquired data are considered as quantitative measures and a system quality assessment or a calibration do not consider the glare effect and are not sufficient to avoid this phenomenon. Thus, it is fundamental to be aware of this phenomenon and make further research to find new compensation strategies. To this aim, in this work is presented a first way to measure this phenomenon, the $GlareEffectindex$, which aims at quantifying the amount of glare in hyperspectral images. Thanks to this metric it has been possible to make also a preliminary glare spectral analysis, but further research must be done in this field. Glare, in fact, is strongly data-dependent and its effect can be tolerated due to the acquisition purpose, use or application field.

Chapter 5

Image enhancement

5.1 Introduction

Image enhancement techniques are often used to improve the image *pleasantness* or to make it more *readable*. At this scope many filters can strongly affect the original acquisitions and each single pixel can be manipulated.

As presented in the previous Chapter, in cultural heritage, acquisitions are often made under specific constraints, because they can have not only a qualitative but also a quantitative significance (see Section 4.3.1). Similarly, every photos or graphical representation of objects of cultural and historical meaning, should be faithful to the originals and must respect their authenticity.

In Chapter 1 and Chapter 2 have been underlined the limits of standard colorimetry in the representation of 2D and 3D objects, where the strict constraints are no more respected and color is inserted in a spatial arrangement or in a complex scene. To this aim, there is the need to develop new models to compute color vision processes in complex scenes, like 2D or 3D scenes.

In this Chapter, I aim at proposing some preliminary solution to overcome the problems of standard colorimetry in image color restoration and enhancement resorting to the family of Spatial Color Algorithms. These algorithms enhance colors according to the spatial distribution of pixel values in the scene, thus aim at overcoming one of the main limit of standard colorimetry.

In the following Sections, after a brief overview of image enhancement techniques, I will present the main Spatial Color Algorithms, together with an overview of the main used and diffused, and I will present a speed-up of one of those algorithms: FACE.

5.2 Overview of image enhancement techniques

Image enhancement belongs to image processing methods, which aims at elaborating the image and convert it into a form that is more suitable for further analysis or applications [94]. Examples of processing operations are: color balancing [128]–[130], exposure correction [131], noise reduction [132], [133], contrast enhancement [134]–[136] and sharpness increasing [128], [137], [138]. Image enhancing methods are based on subjective image quality criteria. The main image enhancement methods can be divided in two groups: point processing and spatial filtering. The point processing methods are the simplest transformation, which manipulates each single pixel independently of its neighborhood and each output pixel depends only by the corresponding input pixel. The point processing operations involves among others, contrast, brightness enhancement, histogram equalization and image averaging. On the other hand, the spatial filtering involves area-based operators, and each pixel

value is recomputed due to a specific number of neighboring input values.The spatial filtering operations involves: linear filtering, non-linear filters, edge detection and zooming. In addition to those groups, the main image processing operations may involve also e.g., the Fourier transformations, pyramid and wavelets, geometric transformations and global optimization.

5.2.1 Point and Neighborhood operators

The point operators produce an output pixel value which depends only by the corresponding input value. In this transformations are included e.g., brightness and contrast adjustments, color transformations, pixel transforms and histogram equalizations. A image processing *operator* is a function which takes an input image and produces an output:

$$g(x) = h(f(x)) \tag{5.1}$$

where x is the 2D domain (for images) and the function f and g operate over a specific range (scalar or vector). In 2D images, the value x corresponds to the pixel locations, $x = (i, j)$. Starting from this notation, contrast and brightness are two of the most common point operations, and can be written as:

$$g(x) = af(x) + b \tag{5.2}$$

where $a, b > 0$ control contrast and brightness and are called *gain* and *bias* [94], respectively. Nevertheless, when elaborating color images, the relationship among gain/bias and the respective variation in contrast/brightness is not linear. For example, adding a constant to each RGB color channel not only increases the pixels intensity, but affects also the hue and saturation. Thus, it is wise to change color space, manipulate just the luminance Y channel and then re-compute the RGB image with same hue and saturation. The increase of contrast and brightness can be done subjectively increasing gain and bias until the desired appearance is reached. To do this operation automatically, it is possible to determine their best values. A first approach is done by looking at the darkest and brightest pixel in the image and mapping them to pure black [0,0,0] and pure white [255,255,255] (White Patch Assumption). Another approach, proposed for the first time by Evans in 1946 [139], consist in finding the average value in the image, push it towards middle gray [128,128,128] and expand the range (Gray World Assumption).

The image histogram is an interesting visualization system allowing to compute and show relevant statistics about the tones distribution in the image. Furthermore, to map the tones of the image in the full extent of the dynamic range it is possible to perform the *histogram equalization* (see Figure 5.1). Once found the original histogram $h(I)$, this function is integrated to obtain the cumulative distribution $c(I)$,

$$c(I) = \frac{1}{N}\sum_{i=0}^{I} h(i) = c(I-1) + \frac{1}{N}h(I) \tag{5.3}$$

where N is the number of pixels in the image. In this way for every intensity it is possible to find the corresponding percentile $c(I)$ and determine the final value.

Point based operators are the key feature for defining global filtering. Although global filtering is a simple and useful tool for manipulating different features of the image, it has shown to be unsatisfactory in different applications. Thus exploiting neighboring pixels for defining local filters may become mandatory in several situations.

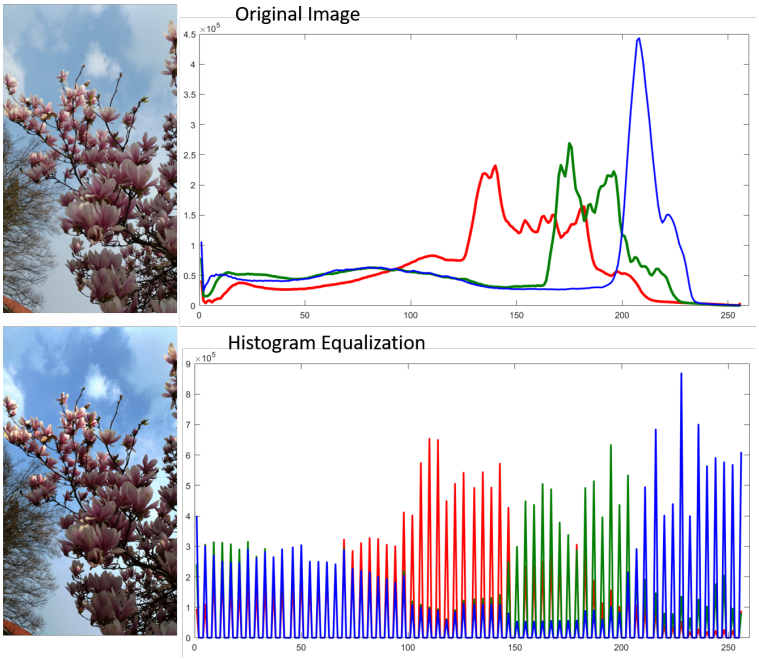

FIGURE 5.1: Histogram analysis and equalization.

The linear filtering is the most common neighborhood operator and involves weighted combinations of pixels in small neighborhoods which can be used to add e.g., soft blur, sharpen details, increase edges or remove noise. The linear filter is made such as the response to a sum of two signal is the same as the sum of the individual responses. It can be formalized as:

$$g(i,j) = \sum_{k,l} f(i+k, j+l) * h(k,l) = \sum_{k,l} f(k,l) * h(i-k, j-l) \tag{5.4}$$

where the output pixel value is the weighted sum of input pixel values. The values $h(k,l)$ are the weight mask and $g = f * h$ is called convolution operator.

Some frequently used linear filters are: the box filter, the Bartlett filter, the Gaussian kernel filter, low-pass kernels and unsharp masking filter. Furthermore, linear filtering can be used as a pre-processing stage to edge extraction and interest point detection algorithms [94].

Linear filters can perform a wide variety of image transformations. Nevertheless, non-linear combinations of neighboring pixels, in some application, may have a better performance or can output better results. Example of non-linear filters are e.g., median filter, bilateral filters, distance transforms [94].

The histogram equalization can be applied globally on the image, or locally. An example of locally histogram equalization is known as *Adaptive Histogram Equalization* (AHE) [140] and its contrast limited version is known as CLAHE [141].

5.3 SCAs - Spatial Color Algorithms

An interesting family of algorithms born in the '70 and spread widely in the last 10 years are the Spatial Color Algorithms (SCAs), which enhance colors according to the spatial distribution of pixels values in the scene. Examples of SCAs are Retinex [12], iCAM and its evolutions [142], [143], ACE [144], [145], STRESS [146], RSR [147].

As A. Rizzi and J.J. McCann explain in [148], all the SCAs have a two-phase structure. Firstly, each pixel is recomputed according to the spatial distribution of the other pixels in the image and this phase generates a matrix of a-dimensional values. Secondly, this matrix is remapped into the range available in the output device. Here, a Look-Up-Table (LUT) and/or gamma adjustment can be applied.

When using SCAs, the output is strictly characterized by the behavior of the single algorithm that presents the following features [148], the *local proprieties*, which defines how to explore and weight a set of neighboring pixels (e.g. using random sprays, convolution masks, paths), and a final *global scaling*, which defines the final dynamic range output. In general, in this step two main approaches are used: Gray World (GW) or White Patch (WP) assumptions.

Thanks to the local properties and global scaling, SCAs can target several applications e.g., color/contrast recovery, quantization, dequantization, gamut re-mapping, HDR to LDR, illuminant and reflectance estimation.

The SCA output depends basically on the parameters selection and the visual characteristics of the input image. Due to this, the outcome does not strictly rely to the physical values of the input, but presents an enhancement based on appearance reconstruction. Following these considerations, it is often challenging to measure and judge the performance of these algorithms.

5.3.1 From Retinex theory to the actual models

Celebrating almost 50 years, the Retinex theory proposed in 1971 by E.H. Land and J.J. McCann [12] has seen many and many evolutions.

The name *Retinex* is the union of the words *retina* and *cortex*, and the idea at the base of this model is that these two parts of the HVS realize a robust adjustment to compensate for the high photometric and colorimetric variability in the world surrounding us.

This model is based on three retinal cortical systems that process separately the low, the middle and the high frequencies of the visible spectrum. In this way, a separate image is formed from each process and determined by the relative lightness values of the various regions of a scene [13]. In this model, if the lightness is very different between two areas, the ratio is far from the value of 1, at the opposite it will tend to 1 if the lightnesses are equal. Furthermore, Retinex can discount chromatic casts, if the ratio tends to the average among the image.

In the original Retinex model [12], the relative channel lightness (L) at a point i is computed as the mean value of the relative channel lightnesses (l) along N random paths from point j to the point i:

$$L^i = \frac{\sum_{h=1}^{N} l_h^{i,j}}{N} \tag{5.5}$$

where:

$$l_h^{i,j} = \prod_{x=j}^{i} \delta_{x \in path} \left[\left(\frac{I_{x+1 \in path}}{I_{x \in path}} \right) \right] \tag{5.6}$$

where I_x is the lightness intensity of the pixel x, and I_{x+1} is the lightness intensity of the pixel $x+1$ and h is indicating the path. δ is the reset mechanism, which forces the chain of ratios to restart from the unitary value, considering the lightness value

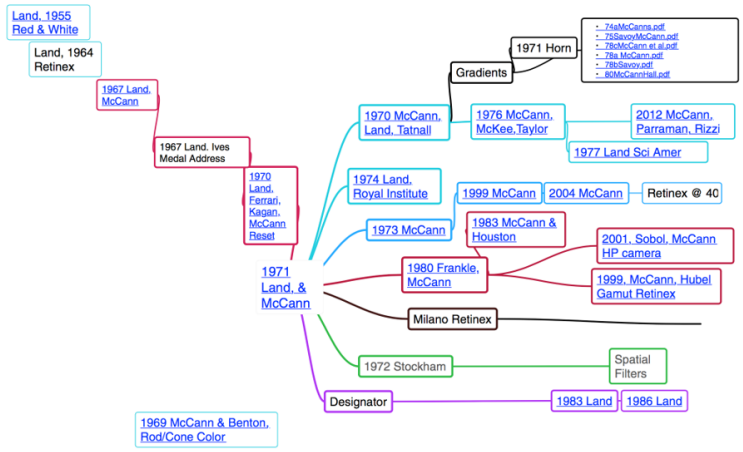

FIGURE 5.2: Retinex Family. Figure reproduced from: [14]

found at the reset point a new local reference white:

$$\delta_{x\in path} = \begin{cases} 1 & \text{if } \frac{I_{x+1\in path}}{I_{x\in path}} > T \\ \frac{I_{x+1\in path}}{I_{x\in path}} & \text{else} \end{cases}, \tag{5.7}$$

where T is a defined threshold.

In the original Retinex model the three color channel R, G and B are processed independently. In some Retinex implementations, along the process of ratio computation, called *ratio chain*, the use of a threshold is discussed. Thanks to the threshold, of the ratio does not differ from 1 more than a certain value, the ratio is set equal to 1, but its use it is not essential [42]. There are many variants derived from the Retinex model by Land and McCann. A general overview is given in [14].

5.3.2 The extended Retinex family

In [149] the Retinex family of algorithms (see Figure 5.3 see orange upper branch) is divided in three classes based on the computational model and the way the image is explored:

1. Random-based: use paths or extract random pixels around the pixel of interest.
2. Scale-based: compute values over the image with convolution masks or weighting distances.
3. Variational-based: use differential mathematical techniques based on Poisson-type equations and variational approaches.

Inside the Random-based group there are the Milano-Retinex algorithms [150]. Those algorithms are derived directly from Retinex, but instead of modeling vision aims at enhancing images. The idea at the base, is always the same of performing spatial comparison among regions of the input image and then computing a chain of ratio-product-reset. This last mechanism is the core of Milano-Retinex family. In this algorithm the ratio-product-reset is computed at each step, like in Retinex, but the computed value is used to change only the last pixel, and this gives to the path a different meaning [150]. In this way the final value of the pixel is the ratio of all the

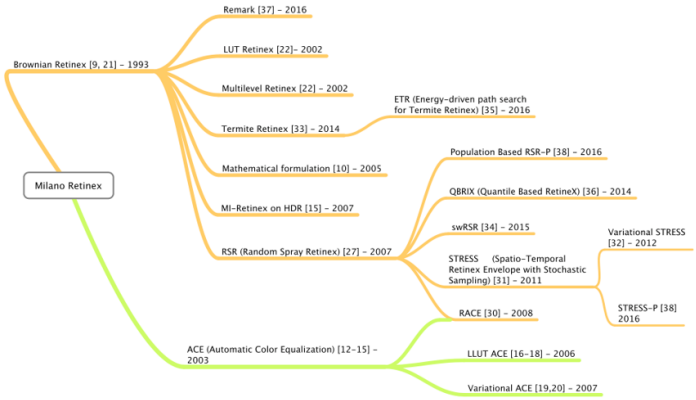

FIGURE 5.3: Milano Retinex Family. Figure reproduced from: [150]

ratio-chains computed along every other path ending in the pixel of interest, so the ratio of the pixel of interest to the pixel with maximum value found in the path.

The main difference between Retinex and Milano-Retinex is, at first the sampling of the input image, then the ratio-product-reset produces a different normalization and at the end the output has an average form. in [151] Provenzi et al. presented a first mathematical description of Milano Retinex. Through the years, Milano Retinex evolved mainly with changes in the image sampling methods, and in the following Sections are presented some algorithms of this family.

Spray sampling

The first Milano-Retinex algorithm that involved a spray sampling stage was RSR (Random Spray Retinex) presented by Provenzi et al. in 2007 [147]. This algorithm substitute the path counts made by Milano-Retinex with a random sampling (called sprays) made through the use of spray points around the input pixel. The RSR implementation is based on the studies made in [152], where the authors have proven the redundancy of the Milano-Retinex approach and have proposed a simplified reformulation, where paths are replaced with sprays in the image. Also in this case, this exploration aims at finding the pixel with the maximum value in the spray that is used as local white to rescale the original pixel value.

Starting from those consideration, for each pixel in each channel p_t are generated N random sprays with n pixels. To incorporate the idea of locality the sprays are computed using polar coordinates with an isotopic points distribution, so the pixels are more dense near the pixel p_t. The ratio-product-reset of Milano-Retinex is substituted by the research of the pixel with maximum intensity value s^{max} in the spray i and by the ratio between s^{max} and the original pixel p_t. As consequence, the new pixel value p_{new} is obtained:

$$p_{new} = \frac{1}{N} \sum_{i=1}^{N} \frac{p_t}{s_i^{max}} \tag{5.8}$$

In 2013 and 2015 two implementation of the RSR algorithm were presented: the LRSR (Light Random Spray Retinex) [153] and the SLRMSR (Smart Light Random Memory Spray Retinex) [154]. Another interesting implementation is the combination of ACE and RSR which generates the RACE algorithm [155].

A variant of RSR is STRESS (Spatio-Temporal Retinex-inspired Envelope with Stochastic Sampling) [146], which aims at calculating not only the local maximum intensity (reference white), but also the local minimum intensity (reference black) for each pixel in each chromatic channel.

Since s_i^{max} and s_i^{min} are the maximum and minimum values among the pixels p_j in the spray i, and since the sample pixel p_t is always $s_i^{max} \leq p_t \leq s_i^{min}$, the range of the sample r_i and the relative value v_i of the center pixel p_t are calculated as:

$$r_i = s_i^{max} - s_i^{min} \tag{5.9}$$

$$v_i = \begin{cases} 0.5 & \text{if } r_i = 0 \\ \frac{(p_t - s_i^{min})}{r_i} & \text{else} \end{cases} \tag{5.10}$$

Considering this, the new value p_{new} is obtained:

$$p_{new} = \frac{1}{N} \sum_{i=1}^{N} v_i \tag{5.11}$$

Another interesting implementation among the Milano-Retinex Family is Termite Retinex[156]. In this algorithm the paths are preserved but their creation is not completely random, but based on a swarm of agents called *termites*. The termites consider as the image contrast for the paths generation and travel all along the path. To avoid the use of the same pixels in the generation of further paths, the termites leave along the way a trace called *poison*. This core of this algorithm is the creation of a path based on the image content, following the idea that some areas in the image are more relevant for the final appearance, due to their contrast.

5.4 ACE - Automatic Color Equalization

The ACE algorithm is part of Milano Retinex family (see Figure 5.3 see green branch) and was presented for the first time in 2003 by Rizzi et al. in [144]. This family of algorithms tries to simulate some characteristics of the Human Visual System (HSV) reconstructing and enhancing images with a global and local approach, assuming that color sensation is the result of the ratios of the reflected light intensity in specific wavelengths bands computed between adjacent areas of the image. Among all the Retinex implementations, ACE algorithms focus on the reproduction of color and lightness constancy of the HVS to make a local filtering of the image, starting from the color spatial distribution. One of the main characteristics of ACE, presented in [144], is the integration of the Gray World (GW) and White Patch (WP) approaches. The WP mechanism was already used in the Retinex algorithm and tries to simulate the HVS adaptation to the mean luminance changes in the scene. The GW mechanism aims at estimating the lighting colour cast by looking at the average colour and comparing it to the average gray, so this mechanism helps in preserving the original naturalness of the image. ACE algorithm is composed by a two-step process. The first step is responsible for color constancy and contrast tuning and the second one performs lightness constancy through tone mapping. In the first stage, the chromatic and spatial adjustment produces a resultant image, in which every pixel is recomputed due to the image content. The integration of WP and GW performs a sort of lateral inhibition mechanism weighted by pixel distance, and this allows to a better

reconstruction of the HVS mechanism. In the second step of ACE algorithm the image dynamic range is maximized, by normalizing the white at a global level. The main advantage of ACE algorithm is that it does not require user supervision, statistic characterization, nor data preparation. It works by comparing every pixel p_t in the image I to every other pixel independently in the RGB channels and summing all the difference to compute the final value:

$$p_{new} = \frac{1}{k_t} \sum_{p_j \in I, p_j \neq p_t} r(p_t - p_j) d(t, j) \tag{5.12}$$

$$k_t = \sum_{p_j \in I, p_j \neq p_t} d(t, j) \tag{5.13}$$

Before the sum, each difference is modified by a non-linear function $r(\cdot)$ and weighted by $d(\cdot)$, the inverse of the Euclidean distance among the pixels (p_t and p_j). The normalizing factor k_t is used to make the weighting meaningful. The factor $r(\cdot)$ is the truncated gain function:

$$r(p_t - p_j) = \begin{cases} -1 & \text{if}(p_t - p_j) \leq -thr \\ \frac{(p_t - p_j)}{thr} & \text{if} -thr < (p_t - p_j) < thr \\ 1 & \text{if}(p_t - p_j) \geq -thr \end{cases} \tag{5.14}$$

This last function is a non-linear amplification of the normalized difference between pixel values, responsible of the final spatial re-arrangements. The filtering effect of ACE depends on the slope value of $r(\cdot)$ and the growth of the slope can be simplified as an increase in contrast. Due to its characteristics, ACE together with Retinex, is considered part of the SCA (Spatial Colour Algorithms) [148]. A comparison and first evaluation of the performance of the two main SCA, Retinex and ACE, is presented by Rizzi et al. in [145]. In this second paper, the new ACE algorithm is presented under a different light, and its computational model is compared with Retinex, in order to underline their peculiar characteristics and promote a more specific and aware use of those two algorithms. From this paper, can be derived that, the main difference between those two algorithms is in lightness equalization, in fact ACE is implemented with a GW compensation mechanism, while Retinex is based just on the WP algorithm. Due to this, for underexposed images both ACE and Retinex increase the mean lightness, but for overexposed scenes, only ACE reduces the mean lightness. Despite this main difference the two algorithms present similar properties of global and local enhancement for what concerns lightness, color constancy and dynamic range stretching, and when applied to visual illusions (like images of simultaneous contrast) both compute visual appearance presenting the same values of hue, but different brightness and saturation (see [145]). During years of applications ACE demonstrate promising results and has been implemented to archive better computational costs and automatic parameters tuning.

5.4.1 Use and diffusion of ACE algorithm

Since ACE first publication, this algorithm has been widely used, formalized, and implemented. ACE is particularly appreciated for pre-processing in different application fields and as standalone image enhancement. In order to identify and classify the available evidence on ACE, I performed a scoping study on this algorithms. This

work, still under publication at the time of writing this thesis, will report just preliminary conclusions and considerations of the spread of ACE algorithm.

The wide diffusion of this ACE may be linked to the correlation with the human visual system in the output, thus with the visual appearance of the resulting image [157]–[159]. Another advantage of ACE is that it can enhance images with different lighting conditions, thanks to its ability to normalize the effect of illumination. Furthermore, ACE algorithm can also be easily implemented in different programming languages and it presents few easily manageable parameters. To support the aforementioned theories and evaluate the effective diffusion of this algorithm, here is presented an overview of the published works which cite ACE algorithm.

This work is part of a scoping review which (at the time of writing this thesis) is still in preparation for its submission to a journal. The two funding paper presenting ACE are:

- Alessandro Rizzi, Carlo Gatta, Daniele Marini (2003). A new algorithm for unsupervised global and local color correction. Pattern Recognition Letters, 24(11), 1663-1677 [144].
- Alessandro Rizzi, Carlo Gatta, Daniele Marini (2004). From retinex to automatic color equalization: issues in developing a new algorithm for unsupervised color equalization. Journal of Electronic Imaging, 13(1), 75-85 [145].

To define the spread and the diffusion of ACE algorithms in the literature all the publication citing the two mentioned ACE papers have been considered and analyzed. To do so, Google Scholar and Scopus have been used. The preliminary research provided 826 results and after a selection phase based on criteria of language, type of publication, presence of duplicates and errors the papers included in the research became 312. In Table 5.1 is presented the count of publications which cite ACE algorithm.

Year	Journal	Proceedings	PhD Thesis	Chapter
2003	1	4	-	-
2004	-	4	-	-
2005	2	7	-	-
2006	5	11	-	-
2007	10	10	2	-
2008	2	6	-	-
2009	7	16	1	-
2010	6	10	-	-
2011	8	9	-	-
2012	8	5	1	1
2013	7	9	2	-
2014	16	5	-	1
2015	20	8	3	4
2016	16	10	-	1
2017	20	3	2	1
2018	21	8	2	-
2019	9	5	-	1

TABLE 5.1: Count of publications which cite ACE paper [144] and [145].

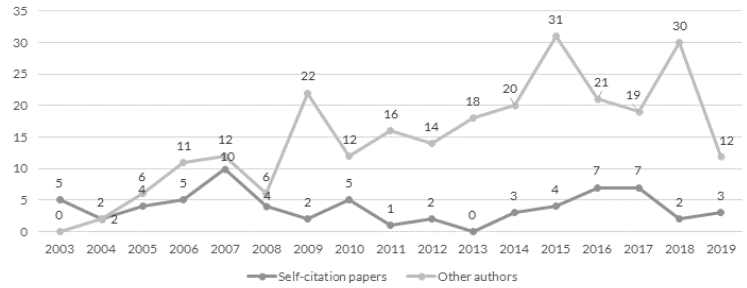

FIGURE 5.4: Distribution of papers over the years.

Application domain	Self-citation papers	Other authors
Advertising posters	1	0
Art	0	2
Astrophotography	4	1
Biology	0	1
Color	2	1
Computer vision	0	1
Cultural heritage	3	1
Film restoration	6	1
Fish behaviour monitoring	0	1
High Dynamic Range	1	0
Human Visual System	0	1
Image enhancement	2	22
Image fusion	0	1
Image quality	2	3
Interfaces	3	0
Machine vision	0	3
Medicine	0	3
Mobile images	0	2
Movies	4	2
Printing	1	0
Psychophysical studies	2	0
Security	0	1
Steel bridges	0	1
Stereo images	1	0
Underwater imaging	0	16
Virtual reality	1	0

FIGURE 5.5: Application Domains identified during the study and distribution of the papers according to this classification.

During the paper analysis, the works published by at least one of the authors of the reference papers Daniele Marini, Carlo Gatta, Alessandro Rizzi, have been tagged as *self-citations*. Among the 312 considered publications, only 66 have been tagged as self-citations (see Figure 5.4).

The considered publications have been subsequently classified by: application domain and roles. In Figure 5.5 are reported all the identified application domains and the corresponding publications distribution and in Figure 5.6 are reported the identified roles.

Considering the application domain just the 27.24% (85 papers) of papers have been associated with a specific field of application. In general image enhancement and underwater imaging are the fields in which ACE algorithm presents more citations. Concerning the role paper classification, so the description of the way in which ACE algorithm was used, six values have been selected: comparison, formalization, implementation, modification, state of the art/survey and use. The main role which ACE assume in the paper in which it is cited is state of the art/survey (up to 200 papers circa), followed by comparison (60 papers circa).

Thanks to this preliminary analysis it was possible to define and characterize the

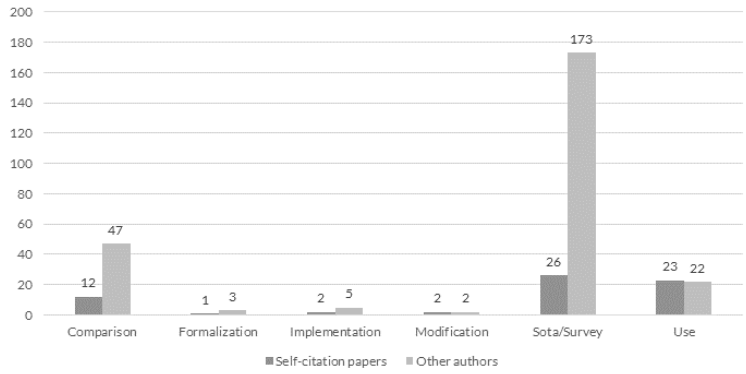

FIGURE 5.6: Roles identified during the study and distribution of the papers according to this classification.

wide diffusion of ACE algorithms during these years. This algorithms has demonstrated promising results among all the other SCAs, so that new implementations and optimized versions have been developed. The interest of the scientific community in ACE is growing and I hope that the field of colorimetry and spatial model algorithm will be even more able to deal with complex scenes, providing new global and local approaches.

5.5 FACE - Fast Automatic Color Equalization

The Fast Automatic Color Equalization (FACE) is an innovative speed-up of ACE algorithm modeled and developed during the writing this thesis and still under publication. For this reason, we will present just some preliminary results.

As presented in the previous Section, in recent years ACE has been employed for different field of application, from underwater imaging, to cultural heritage, from interfaces to astrophotography (see Figure 5.5). The main characteristic of ACE, in comparison to Retinex and the other SCAs, is that it executes the complete scan and analysis of all the pixels in every channel in the image. The main advantage of this approach is that it can enhance the image depending on the content, but, since ACE considers all the image pixels, the computational costs are $O(n^4)$ for a linear input image resolution of n. This limit was underlined in different works presented in Section 5.4.1 and this limits the applicability of ACE algorithm in video streams.

5.5.1 Related works

Considering Figure 5.5, the papers which applies ACE for film restoration in chronological order are: [26], [160]–[164]. Since the first application made by Chambah et. al in [160], new directions have been opened for an *appearance* color restoration using Spatial Color Algorithms and ACE among them. The success of ACE in image enhancement and more specifically for old film color restoration has been proven by different applications [25], [165], but the great computational time required limits its applicability, especially in video streams. As a consequence the full films which have been completely restored through ACE are a few, and its potential has been proven just on some frame or sequence (see examples and applications in Section 6.7). To provide lower computational costs and reduce the computational time, different implementations have been proposed. A first technique, proposed by Chambah et al.

[166], uses two linear techniques a Local Linear LUT (LLL) and a PC2D, for the enhancement of image sequences considering the spatial relationship between image areas. Lately, Bertalmío et al. [167] propose an alternative approach based on a Singular Value Decomposition (SVD) to create a filtering mapping function before the application of the ACE basic algorithm. This second method performed a speed-up of two orders of magnitude, but causes quality loss in the output images. In 2007 Bertalmío et al. [168] reduced ACE complexity to O($n^2 logn$) starting from the idea that the major cost of the algorithm is in the computation of the contrast modification function. This study was reported in another implementation presented in [169], where a new model named Kernel-Based Retinex (KBR) was proposed. A CUDA implementation of ACE for stereoscopic streams was published by Gadia et. al in [170], and an evaluation of gamut changes in the final image were analyzed by the authors. A reduction of ACE computational costs to O($n^2 logn$) was reported also by Getreuer [171] using a polynomial approximation of the contrast function to decompose the corresponding computation, and an algorithm based on the interpolation of the intensity levels. In conclusion, a further implementation of ACE algorithm through FPGA using VHDL was proposed by Romero et al. [172].

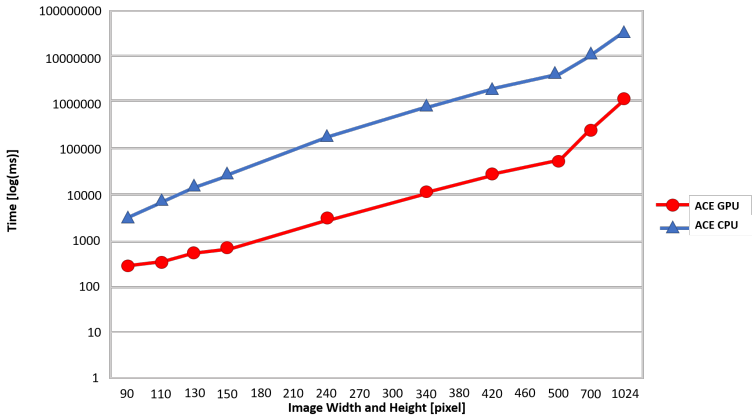

FIGURE 5.7: Comparison between ACE implementation on CPU and on GPU. "The CPU version has been implemented in C++, and the computational times are relative to single-core execution on an Intel Xeon Quad Core E5-2609 2.40GHz under Windows 7 operating system. The GPU version has been implemented using OpenCL API on a NVIDIA Quadro 4000, hosted on the same workstation. On the considered image sizes, the gain factor using GPU computation is between 10x and 80x (average gain factor 45x)" (Description reported from [173]). Figure reproduced from [173].

5.5.2 The proposed idea

The straightforward approach to ACE algorithm presented in Section 5.4 is quadratic with the number of pixels and the computational costs are $O(n^4)$ for a linear input image resolution of n. This approach is extremely slow, but this limit is also the potential of ACE because, by its nature, it is a global image function, where the entire image has an effect on each pixel. In this context, a first time-saving approximation can be to exclude, in the computation of the pixel p, all the pixels q further away than a given distance from p, so to define a threshold distance (as presented in ACE CPU version, where a pixel sub-sampling is applied [173]). Anyway this approximation would be excessive, because even if the contributions of the single pixels p at a given

distance decrease linearly, the number of total pixels at the same distance increase, making the total contribution constant at every distance. Thus, all the optimizations and speed-ups which compute ACE on a defined image-subset around the pixel p, are too rough and will reduce the output reliability. This observation motivates the effort of providing a speed-up of ACE algorithm which does not compromise the reliability of the output and which could provide an *a priori* error bounding. At this purpose, FACE is based on the a precomputed partitioning of the image around each pixel p. Thanks to this, the contribute of all the other pixels in the image q inside the precomputed pattern is approximated by dividing them by the average distance of every element in the pattern, instead of their individual distance. Furthermore, the Summed Area Tables (SAT) allow to quickly compute integrals on these area. Thanks to this approach, it is possible to define the error upper bound before the computation and ACE computational time on video streams can be optimized taking advantage of having images at the same resolution (video frames). In fact, the precomputed pattern can be calculate just one time for all the video stream frames and instead of computing the contributions for each pixel individually, the Summed Area Tables (SAT) can be used, to quickly get the total contributions coming from all pixels inside a given rectangular region of the pattern R, in constant time (regardless of the dimension of R).

5.5.3 Algorithm overview

Considering I and RGB image, where $I = [I_r, I_b, I_g]$, FACE computation is performed in each channel separately. Considering I and 8 bit image, every pixel in I can assume a defined set of possible values $i \in [0, ..., 255]$. FACE algorithm can be divided in three main steps (see Figure 5.5):

1. Preprocessing:
   (a) Rectangle pattern computation R
   (b) Computation of the per-pixel normalization N (see [174])
   (c) SAT computation for each pixel value $i \in [0, ..., 255]$:
      i. $F_i \leftarrow clamp(r(\cdot)(I - i))$, where $r(\cdot)$ is ACE slope (see Equation 5.14).
      ii. $S_i \leftarrow SAT(F_i)$, where SAT is computed as presented in [175].
2. Per-pixel ACE computation. For each rectangle r in the pattern R and for each pixel of coordinates p and of value p_i:

$$Output[p] \leftarrow \frac{S_{p_i}(r - p)}{dist(r - p)} \tag{5.15}$$

3. Normalization: $Output \leftarrow Output/N$

In the preprocessing step, the image I is divided in a set of rectangular regions r composing a pattern R. Thanks to this pre-partitioning of the global image around every pixel p, it is possible to approximate ACE Equation 5.12. Thanks to this, the contribution of the pixels in the rectangle (except p) is approximated by dividing the average rectangle r distance from the pixel p, instead of the individual pixel distance. This approximation depends on the precomputed rectangular pattern, in fact, the smaller (and numerous) are the rectangles, the smaller is the introduced error. As a consequence, the use of small and numerous rectangles allows to reduce

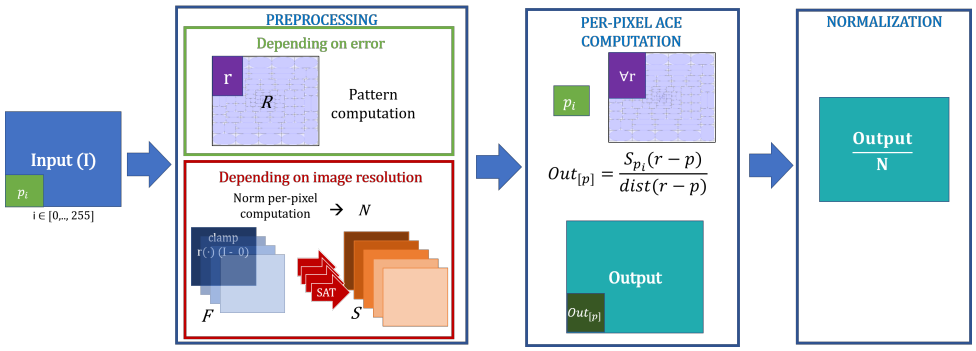

FIGURE 5.8: Graphical representation of FACE computation.

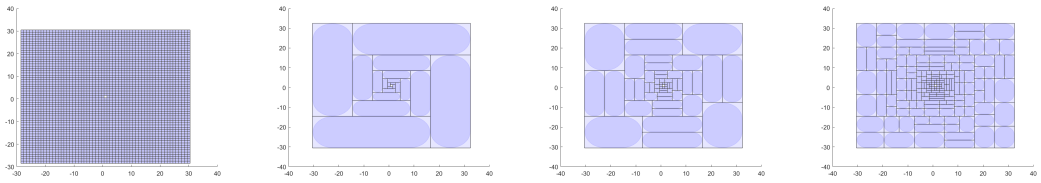

(A) (B) Basic pattern (C) $e = 0.5$ (D) $e = 0.05$

FIGURE 5.9: In Figure 5.9a an example of 30x30 pixel pattern. In Figure 5.9b the basic starting pattern, in Figure 5.9c the error-bounded pattern with $e = 0.5$ and in Figure 5.9d the error-bounded pattern with $e = 0.05$.

the approximation error, but the use of big and less numerous rectangles allows to increase the speed-up reducing the computational time.

In this context, the rectangle approximation error has a strict upper bound depending on its size, shape and distance from the considered pixel p, and do not depend on the image content. Thus, it has been possible to produce a pattern based on the upper bound error and for a given resolution, so applicable for all the images with the same dimension. This makes the FACE computation optimized for the application on all the frames of a movie, or on collections of images with the same resolution.

The computation of the pattern is based on a *basic pattern* (see Figure 5.9b) centered in p with concentric shape. Starting from this pattern the upper bounding error (the total error introduced by all rectangles) can be computed and the starting rectangles r in the basic pattern R are spitted vertically or horizontally in order to get a defined maximum error per rectangle (e) (in Figure 5.9c are reported examples of this pattern with $e = 0.5$ and $e = 0.05$).

Thanks to this method it is possible to pre-compute the pattern based on the upper-bounded error per-rectangle (e) and the SAT based on the image resolution. In this way, FACE can be easily applied to video streams.

5.5.4 Preliminary testing and results

This work (at the time of writing this thesis) is still under publication, so just some preliminary results are reported. FACE algorithm has been implemented in a preliminary version using MatLab R2018a. This implementation uses some built-in parallelization mechanisms of the Matlab suite, and some existing libraries [174], [175].

(A) Original (B) $e = 5.0$ (C) $e = 0.5$ (D) $e = 0.01$

(E) Original (F) $e = 0.5$ (G) $e = 0.1$ (H) $e = 0.01$

(I) Original (J) $e = 2.0$ (K) $e = 0.1$ (L) $e = 0.01$

FIGURE 5.10: Comparison among the original images (Figures 5.10a, 5.10e and 5.10i) and the FACE enhancement using different error values (see Table 5.2).

Image	Resolution	e	Computation Time (s)	Tot r
Lena	50×50	5	0.33	24
Lena	50×50	0.5	0.33	24
Lena	50×50	0.01	1.66	813
Angel	1024×682	0.5	30.48	40
Angel	1024×682	0.1	52.86	224
Angel	1024×682	0.01	283.97	2146
Flowers	901×901	2	33.85	40
Flowers	901×901	0.1	62.10	232
Flowers	901×901	0.01	302.94	2202

TABLE 5.2: Values of FACE computational time, total number or rectangles (r) in the pattern and upper-bounded error (e) for the images in Figure 5.10. All the images have been enhanced with slope 5.

(A) Original (B) $e = 0.5$ (C) (D) Sub sampling 8

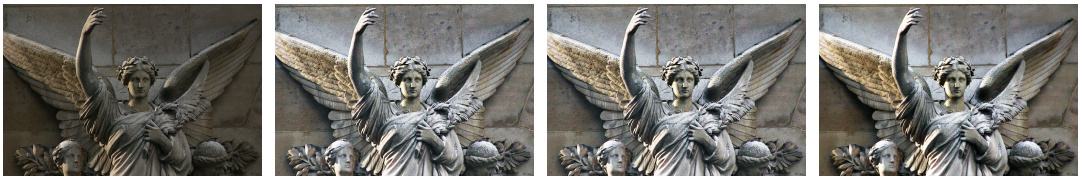

(E) Original (F) $e = 0.1$ (G) (H) Sub sampling 8

(I) Original (J) $e = 0.1$ (K) (L) Sub sampling 8

FIGURE 5.11: The original images are presented in 5.11a, 5.11e and 5.11i, the FACE enhancement are presented in 5.11b, 5.11f and 5.11j, the enhancements with ACE Brutal are presented in 5.11c, 5.11g and 5.11k and the ACE CPU enhancements are presented in 5.11d, 5.11h and 5.11l.

To assess the improvements of FACE speed up, the algorithm has been compared with a MatLab version of ACE (Section 5.4), here named *ACE Brutal*, and the CPU ACE version [173].

To preliminary assess the differences between the two considered speed-ups, FACE and ACE CPU, a comparison with ACE Brutal has been made. The images have been compared pixel-per-pixel and the maximum and average ΔRGB difference has been computed. With ΔRGB is intended the average difference between the RGB values of each pixel composing the image.

Algorithm	Image	Resolution	Parameters	Computation Time (s)
ACE Brutal	Lena	50×50	slope 5	0.98
ACE Brutal	Angel	1024×682	slope 5	104338.17 ($\approx$ 29 hours)
ACE Brutal	Flowers	901×901	slope 5	136087.31 (($\approx$ 37 hours)
ACE CPU	Lena	50×50	slope 5, sub-sampling 8	less than 1
ACE CPU	Angel	1024×682	slope 5, sub-sampling 8	18.00
ACE CPU	Flowers	901×901	slope 5, sub-sampling 8	15.00

TABLE 5.3: Values of computational time for ACE Brutal al ACE CPU. See images in Figure 5.11.

Algorithm	Image	Computation Time (s)	Avg ΔRGB	Max ΔRGB
FACE ($e = 5.0$)	Lena	0.33	0	0
FACE ($e = 0.5$)	Lena	0.33	0	0
FACE ($e = 0.01$)	Lena	1.66	0	0
ACE CPU	Lena	< 1	0	0
FACE ($e = 0.5$)	Angel	30.48	0.76	5.19
FACE ($e = 0.1$)	Angel	52.86	0.20	1.73
FACE ($e = 0.01$)	Angel	283.97	0.01	1.73
ACE CPU	Angel	30.48	9.80	18.00
FACE ($e = 2.0$)	Flowers	33.85	0.83	11.00
FACE ($e = 0.1$)	Flowers	62.10	0.10	1.73
FACE ($e = 0.01$)	Flowers	302.94	0.03	1.73
ACE CPU	Flowers	15.00	5.85	15.97

TABLE 5.4: Table of average and maximum ΔRGB error.

5.5.5 Final considerations

The presented preliminary experiments empirically confirm the expected result: FACE images are indistinguishable from ACE enhancement, so the presented speed-up can replace ACE in any context. At the same time, even if further evaluations and assessments are required, it is possible to assert that, the speed up provides a computation resulting in a $O(n^2 logn)$ with the linear image resolution against a $O(n^4)$ trivial algorithm.

In this work, it is demonstrated that the speed-up and the proposed approximation error, depend directly on the rectangle pattern used in the algorithm. Thus, fewer and bigger rectangles generate better speed-ups, and smaller and numerous rectangles produce lower error. In this context, a fixed optimized rectangle pattern can be constructed automatically in the preliminary step, and the user can set the pattern construction defining the maximum error per rectangle (i.e., the algorithm accuracy) for a specific resolution. In the future developments, the layout construction will be implemented to produce a pattern with a defined number of rectangles or with a defined image total error, instead of using just the parameter of error per-rectangle (i.e., upper-bounded error). In this way, FACE will be more usable and accessible also for non-pro users.

The definition of a number of rectangle, total error or error per-rectangle is the only parameter requested in FACE computation (in addition to ACE slope), and allow the user to define the balance between the algorithm speed and precision.

Furthermore, FACE algorithm offers for the first time the possibility to adopt ACE enhancement in a wider scenario, for example for video streams enhancement. In comparison to ACE CPU version which used a sub-sampling of pixels to perform a faster ACE computation, FACE algorithm introduces a lower error, resulting in a higher accuracy of the results.

As a future work, a better assessment, testing and evaluation of FACE algorithm will be proposed an published, together with a preliminary application on video streams and for film restoration purpose.

Chapter 6

Digitization and enhancement in film restoration

6.1 Introduction

Film restoration is a peculiar field, where the colorimetric constraints are often not considered, and the lack of scientific research caused weaknesses and problems between color measurements and color sensations, which are often solved through subjective assessment.

As part of the cultural heritage, films digitization, restoration and reproduction must be faithful to the original materials, but also to the coloring technique and projection process. In recent years, different efforts have been made to analyze original film dyes and create databases of film processes, but just few works have been published and there is still a lack of public technical data. Furthermore, as presented in Chapter 1, even if a standard colorimetric acquisition is made, the acquired data can be used just in point-wise standard conditions, and the integration in a spatial arrangement or in real conditions would make the effort worthless.

In this Chapter, I will present an overview of film restoration and I will report the actual best practices and standard workflow. After that, I will propose the application of Spatial Color Algorithms for film color and tones restoration in order to promote an innovative research direction in color movie restoration.

6.2 What is film restoration?

In 1980, the UNESCO commission recognized for the first time *moving images* as part of the World's cultural heritage.

All moving images of national production should be considered by Member States as an integral part of their 'moving image heritage'. Moving images of original foreign production may also form part of the cultural heritage of a country when they are of particular national importance from the point of view of the culture or history of the country concerned. Should it not be possible for this heritage to be handed down in its entirety to future generations for technical or financial reasons, as large a proportion as possible should be safeguarded and preserved. The necessary arrangements should be made to ensure that concerted action is taken by all the public and private bodies concerned in order to elaborate and apply an active policy to this end.[176]

Since that moment, the practices of conservation, restoration and valorization of films have been recognized.

Before that date, the terms *restoration* and *preservation* were synonymous of *duplication*. In fact, film duplication was the most immediate way to obtain a long-lasting copy, striving to minimize quality loss. This methodology was supported by the big instability of the first film bases, cellulose nitrate and cellulose acetate, which are subject to a very fast chemical-physical decay, if not duplicated on more stable supports. Film instability played a enormous role in the loss of early movies. For example, it has been estimated that the 90% of all American silent films has been lost, together with the 50% of American sound films made before 1950 [177].

Through the years, the process of film preservation has developed, and today it includes different operations of management, duplication, storage, access and valorization.

Since 1980, the different techniques has changed and, nowadays, film digital restoration has become the standard *de facto* in cinematographic restoration workflow. This recent evolution led to an increase of interest for the research in this field in order to set up new practices and innovative methods [178].

6.3 Objectives of film restoration

It is now established that like statues, frescoes and paintings, films deserve an adequate conservation and require precise restoration practices. However, in this domain, there is a lack of shared methodologies and ethical guidelines as for all the other forms of cultural heritages [19]. Nevertheless, in film restoration it is fundamental to define unambiguously the *original version* of a film; this is considered one of the top issue in the restoration activity.

Leo Enticknap in [19] defines the original version as *"definitive form of the film from which others can be considered deviations and which, if it is not known to exist, it is the restorer's aim to recreate"*. From this definition, we derive that the identification of the original version of a film is the first step for the restoration workflow. Since cinema is a serial art, for every movie or documentary exits different versions and/or editions even in contradiction to one another, but all equally legitimate. For example, for one single movie we can have: camera negative, camera positive, dupe positive (in original language, dubbed, with subtitles), dupe negative, dailies, work copies, intermediates, copies for television, scraps, censured scenes, alternative cuts. From the analysis of all these materials and of paper sources (i.e. censor's certificates, production documents, cinema magazines), it is usually possible to establish the existence of different versions of a movie and define which one is targeted for restoration.

Due to these considerations, it is more appropriate to talk about *film authenticity* instead of originality, because this term is more complete and includes the time of the work and certify an intention or a situation. Furthermore, the distinction between authenticity and originality could effectively help the work of the restorer in the definition of the copy to restore without occurring in philological constraints. In the rest of this work, with the term *original* I will refer to the film used for the restoration, that was considered the most *authentic* copy in a given restoration project.

The first first public projection in the production Country is usually chosen as reference. Whenever this version is not available, it could be legitimate the preservation of a foreign version or a later re-edition, but the restoration aim must always be explicitly stated and clear, in order to give to the audience the possibility of understanding the final decisions [179].

Another main difference between cinematographic works of art and other forms of plastic arts is that the restored copy is a new object, totally different from the original. This idea comes from the theories exposed by Cesare Brandi in [180], where the author underlines the difference in base, emulsion, methodology and techniques that a restored copy has in comparison to the original one. With the spread of the digital, the manipulation that a movie can undergo is completely different and the final restoration file must be considered a different object from the original.

In film restoration it is impossible to apply the concept of *reversibility* applicable, e.g. in the plastic arts, because every restored copy is a new and different object from the starting one. As consequence, it is fundamental to physically preserve the original materials also after the restoration process.

So far, we have discussed about the identification of the film to restore, but now it is important to clarify what *film restoration* is. In brief, it is a relatively young discipline, without a shared and recognized terminology. The Charter of Film Restoration [181] is one of the most authoritative document, approved by FIAF, defining as following:

Preservation is a set of activities that ensure the safeguarding and protection of film material from damage, destruction, and loss. (These activities imply, among others, storing under special conditions, regular inspection, and copying, the latter encompassing duplicating, restoration, or reconstruction.)

Restoration involves research, followed by the retrieval, repair, and preservation of elements of a film work for the purpose of saving that work.

Reconstruction is a further stage of restoration, of which the goal (in an ideal case) is the (re) creation from different elements of an original version of a film work.

These definitions give some guidelines about the terminology that concerns the restoration workflow of a film, but they remain general and do not specify the technical operations involved in the single actions. This weakness most always leads to every restoration laboratory and every restorer to follow its own guidelines according to their formation and experience.

Thus, the lack of shared definitions and technical references for film restoration is leading to the creation of students and experts specialized in the use of specific instruments and softwares, strictly dependent by the school and laboratory of origin. The following Sub-Section reports our interpretation of the film restoration workflow, and underlines its main limits and potentials.

6.3.1 Film restoration workflow

The main steps of the film restoration workflow can be summarized as:

1. Definition of the restoration project
2. Film analysis
3. Analog restoration
4. Film Digitization
5. Digital restoration
6. Archiving and cataloging

Once the copy to restore is identified, the next step is to define the restoration project, that begins with the curator's definition of the restoration aim. In general, a project can have different objectives: the *copy* (digital or analog), the *full restoration* or, the *re-editing*.

The *copy* aims at changing type of support of a damaged film. This can be made digitally, by scanning the film or in analog way by copying the film on a different film support. The copying process is a borderline film restoration procedure, because it does not substantially affect the film materials. The interventions that are generally made are: the white balancing in the digital media or the copying through a wet-gate printer, i.e. film scanning submerging it into a specific liquid with a suitably matched refractive index that reduces the effects of scratches on the film.

The second potential aim of a film restoration project is the *full restoration*. In this case, the original film follows the whole restoration workflow and the outcome simulate as much as possible the original appearance of the original material.

In conclusion, the *re-editing* aim concerns all the restoration processes that alters completely the nature of a film for valorization purposes. This subset includes all the colorization methods, i.e. any process that adds color to monochrome moving-picture images.

In general, all the main restoration laboratories and archives aims at making a full restoration, especially when working with editorial films. On the opposite, for many amateur films, the archive's funds and personnel are typically insufficient to supervise a complete restoration workflow, so they settle with copying restoration projects. In the definition of the restoration workflow, the next step consists in project planning, including the organization of the funds to employ, the timing, the instruments and staff to involve.

In the following, we describe the most complete version of restoration workflow, even if specific projects can decide to skip some steps.

After the definition of the restoration project, there is the film analysis, in which the film conservation state is assessed and the restoration procedure is defined. In this step, the film is analyzed frame by frame on manual rewinding table to have a first assessment of the chemical-physical status of the reel. In this way, it is possible to evaluate the quality of the print, identify the generation and, the photographic rendering. In certain cases [179], presence of specific defects reveal the origin of the copy thanks to the presence of some print defects. The film analysis and the analog restoration are strictly linked, because it is important to enable the original film to pass through scanners and printers without being damaged. To do so, during the analysis the film is repaired, e.g. the splices are substituted, glue is removed, perforations are checked. Any physical damage, on the perforations or on the actual images, is repaired and all the dirt areas are manually cleaned. This is the starting point of the analog restoration, but as reported in [182] the types of damage on a film can be different and more or less recoverable. In some restoration labs, like the one of "L'Immagine Ritrovata" (Bologna, Italy), it is possible to recover films subject to strong chemical decay through chemical treatment like drying, softening and re-hydration. The analog restoration can also include film washing through ultrasound cleaning, to delete the dirt that can not be removed manually.

The analog restoration is a long and complex procedure, typically done manually, to avoid damages during the film scanning or printing. This requires specialized staff and large amounts of time and funds. When a film is repaired, it can be printed on another film through specific printers, it can be digitized, or both. Today, the majority of film restoration laboratories opt for the digitalization, due to the high cost of

virgin film reels, but there are still laboratories specialized in analog restoration and re-print on film, such as the "Centro de Conservação - ANIM" (Lisbon, Portugal).

The mandatory step in the restoration workflow to convert analog to digital is the process of film scanning. Every film scanner has its own characteristics, but in general they are all instruments allowing to convert the analog frame in a digital image with defined properties (e.g. to assess resolution, dpi, bit per pixel). Anyway, before scanning a film, it is mandatory to assess the conservation state, to avoid damages and breakages during the scan. Since the analog restoration step requires specialized staff and instruments, today this process is often reduced to the quality control of the film necessary to allow the film scanning. In this way, the complete restoration process is performed digitally. Furthermore, the possibility to use new generation or wet-gate scanners, which washes away dust and conceals scratches during the scanning process, reduces digital cleaning times.

In the film scanning phase, each frame of the analog film is converted in a digital image. This is done through a gate, equipped with a LED source that digitize it using the defined parameters. At the end of the process, the digitized film is returned as uncompressed file usually in .DPX (Digital Picture Exchange). Today, the scanners used for film restoration uses standard resolution of 2K up to 4K. In [183], Fossati assesses that all the resolutions under 2K, are considered less than the analog film resolution. As well recent studies demonstrate that the minimum resolution of modern 35mm films, is circa $12.8x10^6$ pixel per frame, comparable to a 4K [179]. This topic will be better explained in Section 6.5.1, and is one of the main topic in the archival domain. In fact the choice of film resolution is always a trade-off between the accuracy of the acquired information, the data volume, the computing power required to elaborate the images, and the overall cost of the project.

During the digitization the standard film format is 16/9, typical of the modern 35mm frames, so it is common use to add lateral black border to older 4/3 film frames formats. In addition to this, due to the standard film speed of 24-25 fps, all the movies and documentaries shoot at lower speed are digitally standardized through interpolation processes.

After the film digitization, the following step is the digital restoration. Today, this phase was done through the use of specific softwares (the most used are Revival by Black Magic, Phoenix by Image System or Diamant by HS Ar), which allow for a manual, semiautomatic or automatic workflow, supported by a thorough control and a frame-by-frame correction carried out by specialists in this sector. In this way, the digital restoration phase can take several months and specialized professionals are required.

These softwares exploit dedicated algorithms able to identify and remove all the undesired elements in the film that are impossible to be removed through analog restoration (e.g. strains, flickering, graininess, dust and scratches). However, despite the great potential of digital restoration, these algorithms are not foolproof and user supervision is always needed. In fact, the instruments for defects identification are significantly less efficient than the human eye [19].

The digital restoration step in the workflow involves not only the restoration *per se*, as described above, but also the color correction. This phase corresponds to the negative printing in the photochemical production and aims at balance the film sequences to obtain homogeneity and photographic coherence. In this step it is possible to make all the corrections to re-create the original faded colors, giving to the aged film a recovered lightness and color grading. In this context, the digital technologies offer a wide range of color grading tools which, in the hands of an expert, can improve significantly the appearance of an old film colors. The employed

tools are the same softwares that today are used in movie post-production editing (the most used are Resolve by Black Magic or Premiere by Adobe). These softwares are all manual and are often composed by a control panel for color correction and a scope for the analysis and representation of the result.

As well as for all the other steps in the restoration workflow, also for digital restoration the used instruments and hardwares are fundamental, in fact is mandatory the use of a high quality calibrated monitor to edit and show the results of the restoration process. In some cases, in large laboratories the results are also projected in a standard and calibrated cinema.

The color correction process is a very sensitive step in the workflow, because it is really easily occurring in historical forgery. Thus, it is fundamental to establish in the restoration project which is the aim of the color correction. In many cases, the curator decides to be faithful to the original copy appearance, and just a white and black calibration is performed. In other common situations, the color correction is made comparing the digital frames with an analog positive print of the same film, used as reference. In this latter case the operator tries to simulate on the digital media the colors of the analog making a subjective comparison between frames. In order to perform this operation it is fundamental for the user to have a deep knowledge of the film original colors and using different references to obtain a trustworthy result. As already mentioned, this operation is really sensitive, because an arbitrary reading or a personal interpretation may compromise the philological fairness and the final outcome of the restoration process [19]. However, in this process there is always a subjective bias caused by the experience of the operator, its knowledge of the film material and the impossibility to recover a reference, also in good conservation state, that has been subject to deterioration and aging.

The result of the digital restoration process is a master intended to long-term conservation and distribution. This operation is done in the last step of the restoration workflow, the archiving and cataloging.

In order to maintain the integrity of film restoration final outcome for a long-term conservation an analog film print is the most preferable result. In fact, all the recent year research demonstrated that if conserved in appropriate condition of relative humidity (RH) and temperature, a new 35mm film in polyester has an estimated life of 500 centuries (in [184] and FIAF Technical Commission, Best Practices are reported the ideal conservation conditions at 5 C and 35% RH). Due to this, the best practices suggest printing the final outcome of the digital restoration on an analog film.

Despite this shared knowledge, many archives and restoration laboratories can not afford the expenses of an analog film printing and decide to preserve the digital format. This is the case of a restoration workflow that involves at minimum the analog restoration, due to the high costs in time and funds, and also in the case of archives that already struggle to maintain the original film in good conservation conditions because can not afford the expenses of new analog film copies.

Generally, the preserved digital copies are: the raw film scan, the intermediate and the final copies of the restoration workflow. The most diffuse technologies that suite this scope are the RAID (Redundant Array of Independent Disks) and the LTO (Linear Tape-Open). Anyway the obsolescence of the digital format is a key factor that contributes to the common state of conservation practices for which the preservation on analog film is often cheaper than its digital equivalent. In fact, all the digital technologies require an active approach, continuous maintenance and renewal of the software and hardwares, and this led to a strong need of constant data migration. The archival issues of the long-term conservation masters are an open problem

in film restoration and archiving domain and, today, the archives are still looking for a trade-off between analog and digital conservation.

On the other hand, the master for film distribution is DCP [179].

In the last step of film restoration, together with the archival, the cataloging of the restored film is included. Nowadays, the cataloging boards and guidelines give particular attention to the documentation of the analog process and just a few of them consider also the digital restoration process. In fact, many cataloging sheets, databases and guidelines, report just marginally the intervention made during the digital restoration, it is not satisfying [179].

Among the few points generally accepted in the restoration workflow, there is the ethical practice of reporting in details all the intervention made on the film, to create a complete record of all the decision took during the restoration. This action aims at giving the future end-users the reversibility of all the operations. As mentioned, this operation is commonly done for all the analog intervention, but not for the digital step.

This lack of documentation is one of the most important issues in the restoration workflow, because often it is not only impossible to reverse a digital intervention, but it is also impossible to know which enhancement or modification has been made on the film.

6.3.2 Ethics of film restoration

Film restoration is, fundamentally, a simulation. Thanks to the expertise of the film curator and the professionalism of the restorer, people try to reconstruct an image that has been lost over the years. Moreover, a film is not only a sequence of frame, but is an experience, made in a specific cinema, in a defined epoch, projected with certain projectors equipped with particular lights. This situation is even more complex when working with early cinema films, which were recorded and projected using colored filters that today are impossible to find, or which were tinted and handed to us in form of negatives or black and white positives. Today these issues are still a concern and at the center of many philological debates that attempt to define if the work of the restorer should aim at being faithful to the original materials and condition of projection, or aiming at a new fruition and valorization. In this debate the film ethics tries to define if it is more correct to re-create the *last will* of the film director or trying to modernize the film.

For this reason, it is fundamental to define at the beginning of the restoration workflow which is the aim of the restoration, because both the need of conservation and modernization are understandable. Every solution is a trade-off between the need of bringing the public closer to cinematography and its history, and preserving the original nature and significance of a movie. This compromise, is linked to the the goal of achieving the best quality possible for the fruition with current visualization devices, overtaking the technological limits typical of the period that the film was produced. A trade-off solution may suggest to restore the film defects staying as close as possible to the original. However, a movie is not only the film, but also the experience derived from the use of the theaters and projection technologies of that time, which, nowadays, are not available. Every movie has its own characteristics (i.e. colors, dynamic, light source) and all of them affect the approach to film restoration. Following these considerations, today, we can just try to simulate appearance of the original movie, using modern technologies.

Nevertheless, today, the new technologies and different approaches provide different methods to solve the ethical problems of film restoration, it is fundamental to

give awareness to the audience. The public must know that is attending to a new version of the original film, even different from the one that was presented to the public at the time of its release, in a brand new experience. In this case, it is fundamental to explain and document in details all the restoration workflow and the whole enhancements, modifications and restorations made on a film, to give to the public and the experts a full usability and awareness.

6.4 The Film material

The film is the cinematographic material allowing the shoot, the conservation and the projection of images obtained from a moving subject [185]. The two fundamental layers of a film base are the *support* and the *emulsion*. The support is the material on which is spread the emulsion that is photo-sensible. Other layers that can be find on a film base are the anti-halation layer and one or more subbing layers. A graphical representation of a film base is shown in 6.1.

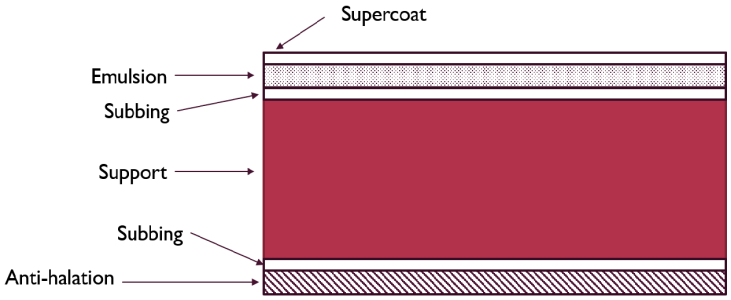

FIGURE 6.1: Graphical representation of the film base.

The support must have precise characteristics like perfect transparency, flexibility, good resistance to strain and durability. The film, in fact, should flow through different machines e.g., the projector and the developers. without damages. Furthermore, it should be stocked and wrapped in reels. A fundamental characteristic is the non-flammability, because the film is subjected to high temperatures, while passing through the projector's film gate.

Film stock with a nitrate base was the first transparent flexible plasticized base commercially available, thanks to celluloid developments by John Carbutt, Hannibal Goodwin, and Eastman Kodak in the 1880s. Unfortunately, nitrate also had the serious drawback that it was extremely flammable and decomposes after several decades into a no less flammable gas (leaving the film sticky and goo-like) and ultimately into dust. An example of nitrate fading is reported in Figure 6.2a.

Projection booth fires were common in the early decades of cinema and several incidents of this type resulted in audience deaths by flames, smoke, or the resulting stampede. An accident of this kind was recreated in the movie Cinema Paradiso (Giuseppe Tornatore, 1988).

As already said, during the years, many nitrate films have been copied and transferred to safety stocks and, today, the original nitrate films are stored in separate and safe bunkers to prevent fires.

The nitrate base was used to make all the major movies prior 1952, when Kodak began distributing *safety films*, made by acetate. This base was always used for amateur film format, like 8 mm and 16 mm, to minimize the risks for the public. The acetate base has all the characteristics of flexibility, good resistance to strain and

(A)

(B)

FIGURE 6.2: In Figure 6.2a a frame of 35mm nitrate film lost to silver oxidation. In Figure 6.2b a 35 mm dupe negative shrank and curled as the acetate base decayed. Figures reproduced from: [182].

durability, but does not have the same transparency as the nitrate. Furthermore, the acetate base does not burn, but melts under intense heat and could cause damages on the camera or projector if some issue occurs. Acetate films are also subject to decay and aging, and are well known for the *vinegar syndrome*, a degradation of the cellulose which forms the film base that release free acetic acid with a peculiar smell of vinegar. An example of degradation of acetate film is reported in Figure 6.2b.

The last developed film base is the polyester, first used in 1955 and become popular in 1990s. It has flexibility, strength, stability and optimal transparency. This film format inert to heat and strain is still in use today. The format was substituted in 2013 by the DCP (Digital Cinema Package) [179].

As explained before and represented in Figure 6.1 the emulsion is the layer in which the image is formed. Leo Enticknap in [19] defines the emulsion as:

Multiple layers of chemicals on the surface of photographic film which carry the image and, in the case of optical recording, sound information. Before exposure the emulsion is photosensitive, or 'raw'; after exposure it carries a latent image; and after processing it takes the form of visible dyes.

Those *layers of chemicals* is generally a suspension of a compound sensible to light (usually Silver Bromide - $AgBr$) in a gelatin binder. It is important for the gelatin to be strongly adhesive, colorless and inert to photochemical phenomena. In [185], Paolo Uccello, defines the main characteristics of the film emulsion. As stated before the emulsion is photosensitive, so the final image on a film is produced by the *exposure*, the amount of light per unit area reaching it, as determined by shutter speed, lens aperture and scene luminance. Due to this, the first fundamental characteristic of the emulsion is the light-sensitivity, so the capability of producing an image when a minimum light is applied for a defined time. The second characteristic is the chromatic sensitivity, i.e. the property of an emulsion of reproducing in correct gray-scale the different radiations coming from the visible spectrum. The relative chromatic sensitivities of different kind of emulsions are reported in Figure 6.3. As it is possible to see, the first photographic black and white plates were sensible just to blue, violet and UV light. This was resulting in blue skyes appearing as white and yellow, and reds appearing black when shooting a landscape. In this period, H. W. Vogel changed the dyes emulsion to extend the spectral chromatic sensitivity to the green and yellow lights. This new film, called *orthochromatic* made possible the reproduction of a larger range of colors in black and white films, and was available

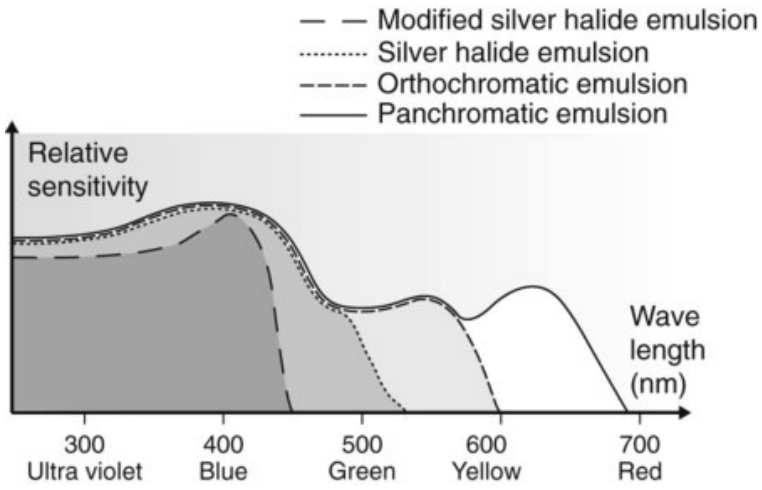

FIGURE 6.3: Relative Sensitivity of different kids of emulsions. Figure reproduced from: clinicalgate.com/image-receptors/

commercially from 1882 [186]. In 1894, the Lumière brothers introduced the *panchromatic* plate, which was sensitive to all colors including red. It must be clarified that all those emulsions were disproportionately sensitive to different wavelengths so, through the years, different attempts were made to produce more uniform plates. Furthermore, some of them required long exposure time and high quantity of light impressing the film. In addition to light-sensitivity and chromatic sensitivity, another fundamental property of the emulsion is the *contrast* intended as the ratio between the maximum value of white and black in an image [185]. Furthermore, it is important to evaluate the *exposure latitude* of an emulsion, as the extent to which a light-sensitive material can be overexposed or underexposed and still achieve an acceptable result. In conclusion the last two characteristics to consider when analyzing an emulsion are the *resolution*, the property to reproduce high frequent lines as distinguishable, and the *grain*, the dimension of the silver crystals. All those characteristics are studied and reported for all analog films and defines the characteristics of the final image.

The combination of technical characteristics of a given storage medium, like an analog film is the *format* [19]. In cinematography, the format is the width of the film expressed in millimeters. Today the official Academy standard format is 35 mm, but through the history, different experiments have been made to obtain a bigger image with higher resolution and lower grain (e.g. the 70 mm format). Smaller formats have always been used for the amateur films, and the most known and spread are the 16 mm, 8 mm and Super8.

In conclusion, a film has always perforations on the sides that for 35 mm format are standardized as four for each frame side. The 16 mm, 8 mm and Super8 have respectively one and two perforation per side that can be halved in presence of a soundtrack.

6.4.1 Main motion picture film process

The first cinematographic films can be easily identified as black-and-white. This film process includes all the orthochromatic and panchromatic emulsion used for motion picture film. This is the simplest film composed by concentrations of filamentary silver particles suspended in a gelatin binder. Since cinema invention, different attempts to color films were made and the first one consists in applying dyes by hand

(A) (B)

(C) (D)

FIGURE 6.4: In Figure 6.4a a 35 mm print, hand coloring. In Figure 6.4b a 35 mm print on nitrate, stencil color. In Figures 6.4c a 35 mm nitrate print tinting. In Figure 6.4d 35 mm print toned though silver sulphide. Figures reproduced from: [182], [187].

(see Figure 6.4a). Hand colored film could be colored overall, or just in some scene, to give to the audience a most spectacular and magic feeling. In 1903, the Pathe Company experimented the use of stencils to color prints. The use of stencils improved the time and precision in dyes application and led to a mechanization and large-scale production (see Figure 6.4b).

Between the 1910s and the 1920s a new technique called *tinting* spread all around the world. It consists in immersing the black-and-white print in a dye solution. In this way the dye is absorbed by the gelatin coloring the film (see Figure 6.4c). Since that period a wide variety of dyes were available and a single film could be made by different color selections individually dyed and then added together. Thanks to this method the first chromatic code began and specific colors started to represent defined scenes or emotions. For example, the blue dye was used to represent night scenes, or the red dyes for war or rage scenes.

The tinting effect was also used with *toning*. A toned film is, at the opposite of tinting, a colored image embedded in a colorless gelatin. This effect, in fact, affects only the developed parts of the image (see Figure 6.4d). The toning coloring could be made through two different process. The first is the metallic toning and involves the replacement of silver with another colored metal salt (e.g. iron ferrocyanide to produce blue images). The second process was known as mordant toning and consists in converting the image silver in a colorless salt, then treated in basic dyes solution. This second method allows to obtain a wider variety of colors.

After 1928, the advent of sound film determined the end of all those pseudo-chromatic systems. Since then, the film color systems can be divided in two big families: *additive* and *subtractive* processes. The additive system in general uses filters to shoot the subject to obtain a black-and-white image for each filter. The images are then superposed and projected using the same filters. A widely used additive method was the *Kinemacolor*, born in 1908, and allowing to photograph and project

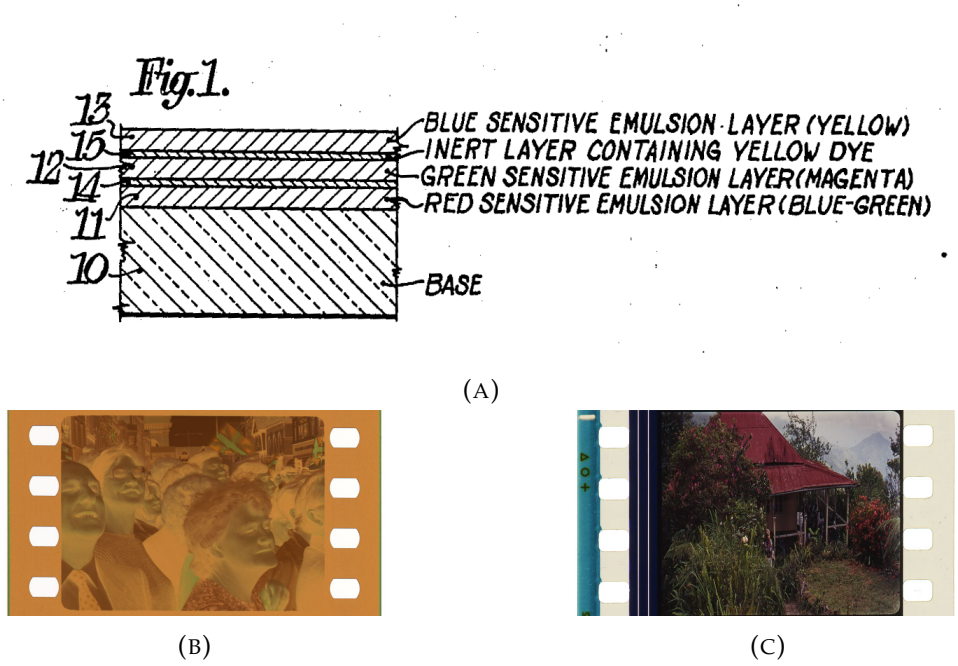

(A)

(B) (C)

FIGURE 6.5: In Figure 6.5a a graphical representation of the three-strip chromogenic emulsion presented by Kodak. In Figure 6.5b a 35 mm chromogenic negative. In Figure 6.5c 35 mm chromogenic positive. Figures reproduced from: [182].

a black-and-white film behind alternating red and green filters [186]. Another additive method is the *Kodacolor*, a three-color process used for amateur cinematography. In this process, the filters were substituted by microscopic cylindrical lenses so that the light was focused onto the tiny embossed lenses and refocused onto black-and-white emulsion as separate areas of red, green, and blue color information. The same banded filter was used during projection [182], [188]. The most innovative film system was the *Technicolor* Process 1, exploiting a beam-splitter behind the camera lens that allow to expose two consecutive frames of a single strip simultaneously (using a red and green filter). Despite the novelty of the beam-splitter the additive methods were all extremely complex and the result was often subject to spatial parallax. Due to this, when the first subtractive methods were invented, they quickly replaced the additive systems.

The subtractive process has the advantage of producing a film that self-containing the colors without the use of filters. One of the first attempts of creating a subtractive color system was made in the *Technicolor* Process 2, where as before the beam-splitter was used to expose the black-and-white film with green and red filter, but the negative was now used to produce a subtractive color print. The negative was used to print two black-and-white film, one obtained from the green filter and one by the red filter; after the development each print was toned to the color complementary to the filter (orange and cyan). At the end the two prints were cemented together to create a projection print.

This first preliminary method was then developed using the dye-transfer techniques and then using the monopack three-strip Technicolor. The production of color films using three primary colors in three emulsion layers on one strip was introduced by Eastman Kodak in United States and by Agfa in Germany. In this color system, the film is composed of three layers of gelatin, each containing an emulsion of silver halide, which is used as a light-sensitive material, and a different dye

coupler of subtractive color which together, that, when developed, form a full-color image [189].

It was the beginning of a rapid transformation from black-and-white to color movies and, since then, color motion production became available to the general public.

Today the chromogenic color system is still in use. It is important at the same time to remind another big improvement in the cinematographic world, the invention of the *Cineon* film system. It was invented by Kodak to solve the needs for developing digital post-production technology that could be used for film restoration and special effects. [190]. Cineon was resolution independent, because of the big amount of computer space needed to manage data from a whole 35 mm film (it was estimated that it would take 40 megabytes to reproduce a single frame).

Although this product is no longer available on the market, this format was commonly used in the film visual effect world, and formed the basis for the newer SMPTE-standardised Digital Picture Exchange (DPX) format.

6.4.2 Film analysis: sensitometry

Sensitometry is the science that studies the light-sensitive materials and permit to measure a film characteristics. In [19] is defined as:

The measurement of how quickly a permanent record is created on a photographic emulsion in response to a given intensity, duration and colour temperature of light exposure. Accurate knowledge of the sensitometry characteristics of a given film stock is essential in order to ensure consistent brightness, contrast and (if applicable) colour balance in photochemical duplication.

A sensitometric study of the film allows to describe how a film will react to type of lightning, exposure and developer. In cinematography the knowledge of sensitometry is not mandatory, because often using the right film speed and process will be sufficient. This science is much more useful for film restoration, because in order to obtain a faithful digital or analog reproduction of a film is fundamental to know the characteristics of the original base. For example, to make a correct copy of a nitrate film on a new polyester base, it is essential to study the sensitometry of the new film and study the right lightning and exposure time to obtain a copy faithful to the original.

The base of sensitometry is the plot of the film characteristic curve (see Figure 6.6) that represents the amount of exposure to the archived density. The film density, or radiographic density, is the amount of light absorbed by a given surface. It is the logarithm of the intensity of light incident on the film (I_i) and the intensity of light transmitted through the film (I_t):

$$D = \log \frac{I_i}{I_t} \tag{6.1}$$

The relationship between a material absorbance, trasmittance and reflectance is reported in Chapter 2.

In order to obtain the values of density to plot, the virgin film should be exposed in a *densitometer*, a light source allowing to expose each film frame at growing exposure values. Usually the film is exposed through 21 equally spaced lights, and the resulting densities are then measured and the density plot is built. An example of sensitivity curve is reported in Figure 6.6.

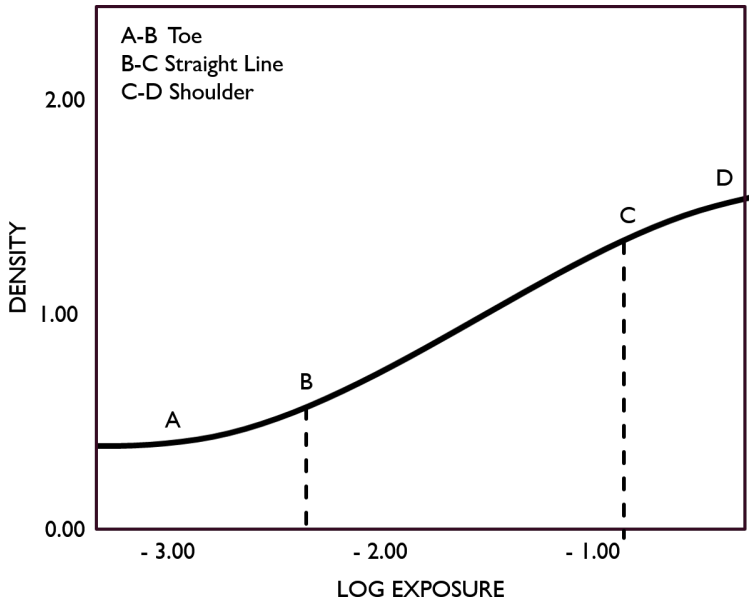

FIGURE 6.6: Film sensitometric characteristic curve.

The curve can be divided in three main parts: toe, straight line and shoulder. Generally, the toe represent the under-exposed area, the straight line the area of right exposition and the shoulder the over-exposed zone. It is important to specify that, for negative films the dark portion of the scene are the light part of the negative, so an over-exposed image will be completely dark.

The sensitometric curve has a characteristic "S" shape because the film does not reproduce dark and light areas linearly like for the midtones. This is extremely important because also the human eye response to light intensity produces a similar shape and in the darker/lighter areas has not the same sensitivity than in the middle ones (see Chapter 2).

The Toe of the curve represents the area of under-exposure. In the first part (around -3.00 log exposure) the exposition is not sufficient to impress the emulsion and can occur the phenomenon of *chemical fogging*. It takes place because during the development, some silver halide crystals will spontaneously develop, even with no exposure. In this area, can be individuated the *speed point* of the film, so the exposure required to obtain a perceivably minimum density. This point is empirically defined.

The most interesting area of the sensitivity plot is the straight line, where the increase of log exposure is directly proportional to the increase of density. In this area a correct exposure of the subject can be obtained. The slope and the steepness of this line define the main characteristics of the film. As reported in [190], from the area of correct exposure two measurements of contrast can be defined:

Gamma (γ), is a numeric value determined from the straight-line portion of the curve. Slope refers to the steepness of a straight line, determined by taking the increase in density from two points on the curve and dividing that by the increase in log exposure for the same two points.

$$\gamma = \frac{\Delta D}{\Delta log exposure} \tag{6.2}$$

Average Gradient is the slope of the line connecting two points bordering a specified log-exposure interval on the characteristic curve. The location of the two points includes portions of the curve beyond the straight-line portion. Thus, the Average Gradient can describe

contrast characteristics in areas of the scene not rendered on the straight-line portion of the curve.

These definitions are shared also in [185], and in [191], where we can find specific definitions of contrast, gamma and average gradient:

Contrast curve is the slope of the characteristic curve (in the straight line area).
The Gamma value is the maximum slope of the characteristic curve.
The average gradient is the average slope between two designated density values.

All these definitions and assertions are strictly linked to an analog film and to the study of this material starting from the sensitometric curve. This will be extremely important in the identification of the main features for image quality assessment in digital images. One significant example between these definitions in analog domain in comparison to the digital one is the concept of gamma. In the digital field, in fact, the gamma is a transformation used to encode and decode luminance values in video or still image systems. This concept is completely different from the gamma intended above.

In conclusion, the last part of the curve, the shoulder, represents the area of over-exposure.

Color sensitivity and spectral sensitivity

As explained and reported in Figure 6.3 the color sensitivity is describes the film sensitivity to the electromagnetic radiation in specific areas of the spectrum.

Panchromatic films and color films are sensitive to the whole wavelengths of the visible spectrum, but with different sensitivity. The spectral sensitivity describes the relative sensitivity of a specific emulsion [190]. Considering the density (D) formula presented before as the logarithm of the intensity of light incident on the film (I_i) and the intensity of light transmitted through the film (I_t), we can define the *opacity* term (o) as the inverse of the coefficient of transparency of the film (t), where:

$$t = \frac{It}{Ii}, \tag{6.3}$$

$$o = \frac{1}{t}, \tag{6.4}$$

$$D = \log o = \log \frac{1}{t} = \log \frac{Ii}{It}. \tag{6.5}$$

So, the film density to specific wavelengths (D_λ) can be described as:

$$D_\lambda = 1 - \log t_\lambda, \tag{6.6}$$

where, t_λ is the specific film transparency to specific wavelengths. This value is fundamental to study the sensitometry in color film emulsion. As explained, color films obtained through subtractive process, are generally made by three different layers sensitive to different wavelengths. Usually the dyes are Yellow, Magenta and Cyan [19], [185], [190], [192].

The diffuse spectral densities curves, represented in Figure 6.7, indicate the absorption by each color dyes at specific wavelengths and the visual neutral density (at 1.0) obtained by the combination of the three layers. The plot in Figure 6.7 is computed for an illuminant at 3200K.

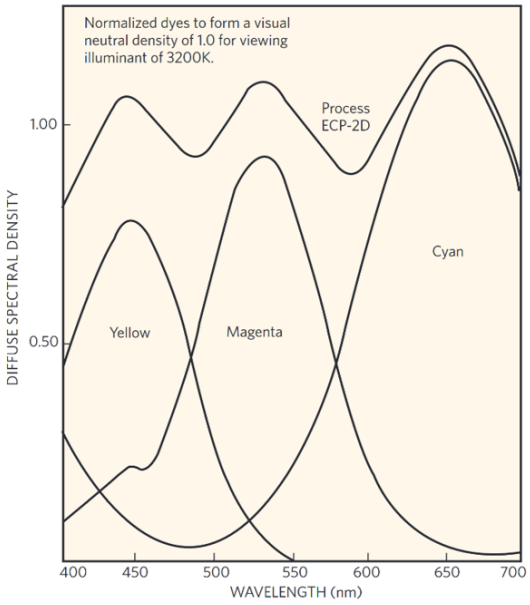

FIGURE 6.7: Diffuse spectral densities curves of color dyes and visual neutral sensity (at 1.0). Figure reproduced from: [190]

The main issue of sensitometry for color film is that ideally a dye should absorb only at specific wavelengths without cross the other dyes. However, all color dyes absorb some wavelengths in other regions of the spectrum and this unwanted absorption could led to uncontrolled color reproduction when films are printed. Usually, this effect was corrected manually from the film manufacture, using couplers that provided automatic *masking* to prevent unwanted dye absorption when the negative is printed.

Furthermore, the superimposition of the dyes makes the sensitometry computation extremely tricky. The dyes density curve is usually obtained through filters with transparency limited to specific areas of the spectrum. Those filters are given by the manufacturers and every producer establish the wavelengths to make densitometry analysis. Thanks to the study of the densities of the three layers it is possible to establish the relationship between the principal and the parasitic absorbance that will be useful in the definition of the corrections to make (i.e. masking) or to study the materials and their properties.

In Figure 6.8 are presented two sensitivity curves from two different film stocks. In the image, the yellow, cyan and magenta spotted lines are useful to visually understand how much two film stocks could be different.

6.5 Best practices for a correct film restoration

As seen in the previous Sections, the restoration workflow usually involves: the analysis of film materials, the historical and philological research, an analog restoration of the support, the digitization, the digital restoration and, finally, the valorization, archiving and cataloging of the material. It is a multidisciplinary process that deals with different issues linked to the preservation of materials characteristics in the digital copy, the determination of standard protocols to acquire the film, a correct reproduction of colors and many other aspects. In order to solve these problems, it is important to have an interdisciplinary background connecting the material, with

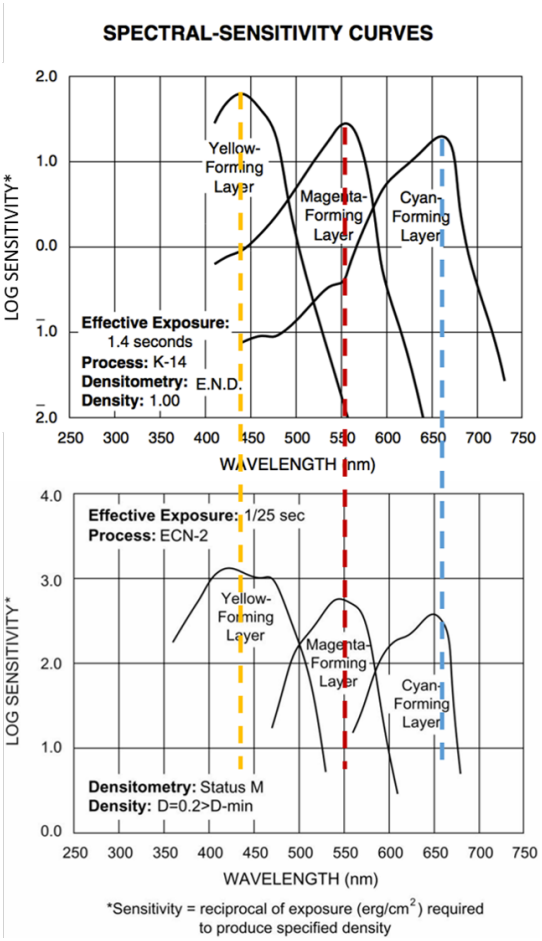

FIGURE 6.8: Sensitivity curves of two different film stocks. Figure reproduced from: [193]

color reproduction and visual perception. In this Section, we will analyze the main issues that concern the restoration workflow process that often can be solved following some best practices and standard, but sometimes still need the definition of better procedures.

6.5.1 Film digitization

Film scanning and imaging industry have always been driven by the commercial marketplace, and during the '90s many manufacturer companies like Kodak started making their own scanners [194]. So, digitization has undergone a deep transformation, in particular legacy systems built on scanning have been replaced with modern instant capture systems, furthermore archives and restoration laboratories are adopting guidelines to ensure high digitization quality standards. In this context, the TIFF (Tagged Image File Format) workflow is being replaced by RAW workflow, which allows to handle larger volumes, fast image enhancements and permits many derivatives (like TIFF or JPEG2000).

Anyway this transformation requires new hardwares, softwares and digitization workflows.

The obstacle to film and cultural heritage digitization in general, is the high volume of material to scan. This may lead to many problems in digitization workflow, because the scanning made by Operator 1 in the morning is often very different from the one made by Operator 2 in the evening. This is due to the lightning conditions in the archive that may change during the day, but also by the methodology used by different operators, or the documents/photos/frames positions in the scanners. This translates in intra-image variations that can be reduced through the use of appropriate instruments and a correct workflow.

In archives and cultural heritage domain, the most highly regarded guidelines concerning digitization are Federal Agency Digitization Guidelines Initiative (FADGI) [195], a US based inter-agency government effort and METAMORFOZE [196], a venture between the National Library and National Archive of the Netherlands. Both these guidelines are based on the ISO Standards.

Being based on the same Standards, those guidelines are very similar and many institutions decided to adopt those guidelines to plan their own digitization program. Both FADGI and METAMORFOZE classifies the quality of digitization using different layers, which aim at identifying digitization executed at less-than preservation-grade quality [197]. Among those two guidelines, just FADGI has a thorough and specific section relating to *Photographic Transparencies* and *Motion Picture Film*, instead of METAMORFOZE, which presents just guidelines for photos digitization and scanning. As already mentioned, FADGI Guidelines classify the digitization quality using four main tires: 1-star, 2-star, 3-star, and 4-star. In order to reach a tier of quality, the digital outcome must overcome a variety of quality metrics like sharpness, light uniformity, color accuracy, and many others. In this context, the FADGI guidelines are particularly useful for film scanning because they consider the wide variety of film materials to be digitized, from 8 mm to 35 mm and above, with their peculiar characteristics of gauges, aspect ratio, formats and configurations. Then, the guidelines gives advices about the output formats, considering the digitized copies as surrogates, and not as replacement of the originals. In this way, they contribute to create awareness about the process of film restoration and digitization. Furthermore, the guidance provided by FADGI are technology-aware and updated on the newest relevant standards (like the SMPTE standards). These characteristics make

Photographic Transparencies Larger than 4" x 5"

Performance Level:

	1 Star	2 Star	3 Star	4 Star
Master File Format	TIFF	TIFF	TIFF	TIFF
Access File Formats	All	All	All	All
Resolution	500 ppi	1000 ppi	1500 ppi	2000 ppi[1]
Bit Depth	8	8	16	16
Color Space	Grey Gamma 2.2 SRGB Adobe 1998 ProPhoto ECIRGBv2	Grey Gamma 2.2 SRGB Adobe 1998 ProPhoto ECIRGBv2	Grey Gamma 2.2 Adobe 1998 ProPhoto ECIRGBv2	Grey Gamma 2.2 Adobe 1998 ProPhoto ECIRGBv2
Color	Grayscale or Color as appropriate	Grayscale or Color as appropriate	Grayscale or Color as appropriate	Grayscale or Color as appropriate
Measurement Parameters				
Highlight/Shadow Density	245/10 > + - 5	245/10 > + - 5	245/10 > + - 5	245/10 > + - 5
Dynamic Range	3.5	3.8	3.9	4.0
Illuminance Non-Uniformity	<8%	<5%	<3%	<1%
Color Channel Misregistration	<1.2 pixel	<.80 pixel	<.50 pixel	<.33 pixel
MTF10 (10% SFR)	sampling efficiency > 60% and SFR response at half sampling frequency < 0.4	sampling efficiency > 60% and SFR response at half sampling frequency < 0.4	sampling efficiency > 80% and SFR response at half sampling frequency < 0.3	sampling efficiency > 90% and SFR response at half sampling frequency < 0.2
MTF50 (50% SFR)	50% of half sampling frequency: [25%,95%]	50% of half sampling frequency: [30%,85%]	50% of half sampling frequency: [35%,75%]	50% of half sampling frequency: [40%,65%]
Reproduction Scale Accuracy	<+/- 3% of AIM	<+/- 3% of AIM	<+/- 2% of AIM	<+/- 1% of AIM
Sharpening (Maximum MTF)	<1.3	<1.2	<1.1	<=1.0

1. Large format films may have actual resolutions that exceed this specification, but imaging at higher resolutions may exceed practical file sizes.

FIGURE 6.9: FADGI Guidelines for digital quality evaluation on Photographic Transparencies Larger than 4"x5" [195].

the FADGI guidelines an optimum starting point for an archive in the definition of its own digitization program of motion picture films.

In Figure 6.9 is reported an example from [195] about the evaluation of digital quality on Photographic Transparencies Larger than 4"x5". As mentioned, the FADGI guidelines include a wide variety of film materials, but all of them should be converted into a digital format. One of the proposed output formats is the SMPTE's Standards for File Format for Digital Moving-Picture Exchange (DPX) format (SMPTE ST 268:2003, and Amd 1:2012). This format is particularly suitable for motion picture films, because it creates a separate file for each frame of the film sequentially numbered. Furthermore the DPX includes embedded metadata options.

Together with the DPX format, it is suggested to produce also a video output, so an HD digital video file. This solution has lower costs than the DPX image+audio file and is easier to manage, so many users tend to prefer this solution. Despite this, the resultant image quality is lower than in the DPX format, and many archives

in the future will need to rescan the material. Following these consideration, the suggestion is always to create a DPX preservation file, and then, when needed, a diffusion *video* file.

This subject concerns also the choice of resolution of the final output, that influences the level of detail of the acquired information, the volume of data that should be archived, the computing power and the final cost of the project [19]. Today, the scanners used for film restoration uses standard resolution of 2K up to 4K, while for the digital cinema 4K and 8K. Digital cinema and UHDTV is pushing producers through higher levels of resolution and drive the demand for film scanning at these levels. The FADGI guidelines tend to identify some handful cases of film digitization to help archives in identifying the best scanning resolution for their purpose [195]. For what concerns the format of the digitization, the 16/9 is the suggested one, and it is common use to add black bands when scanning old 4/3 film formats. The standard acquisition frame-rate is 24-25 fps.

When digitizing movies/photo/films/objects that have artistic – cultural relevance and are intended as cultural heritage objects, the institutions are responsible for providing all the descriptive, technical and provenance information in the files metadata. The main metadata standards for archiving and motion picture films are: EBUCore, EAD (Encoded Archival Description), PBCore and RAD (Rules for Archival Description). In general the metadata can be divided in: Descriptive Metadata, Provenance Metadata, Technical Metadata, Structural Metadata, hence metadata concerns not only the acquisition process, but the whole restoration projects. In this context, the metadata produced in the acquisition step include not only the technical data of exportation format and parameters, but must contain also information about the digitization hardware and software. In fact, the aim of producing correct metedata is the reversibility of the digitization protocol and the documentation of all the digitization/restoration workflow. FADGI provides also guidelines about embedding metadata in DPX files.

Therefore, easy to understand, when planning a digitization workflow it is fundamental to define the scanners or image capturing systems that will be adopted. This is particularly important when working with transparencies, like in motion picture films, because the wide film density range (from 4.0 to 0.05) requires the best optics and imaging sensors. In this context, the lack of dynamic range in a scanning system can result in poor details in highlights/shadows, and low quality color reproduction. These phenomena can be caused specifically by the scanner lenses and the lightning (internal or external) that could cause flare and glare that reduce the dynamic range in the output. Before the acquisition is fundamental a selection of the instruments, and the selection of image capturing systems that employs lenses for film scanning applications that must be, following the FADGI guidelines, of flat field design. After the instrument selection the aperture and exposure time should be defined. This is often done through several experiments and tests. At this point, to guarantee a correct color and contrast reproduction it is fundamental to perform the instruments calibration through targets. Today many systems are available and the majority of them uses the Q60-IT8 target for scanner color management. In addition, it is fundamental also the monitor calibration, in order to let the operator to supervise immediately the correct acquisition output.

Depending on the film digitization system, it can be necessary to set up also an image processing step, to perform color calibration through object target, like a Color Checker, to balance the white and make the first corrections. The post-processing is highly dependent to the project goals and it may involve the creation of derivate files and metadata.

Starting from the FADGI guidelines, one of the most diffuse systems for the specific capture of cultural heritage is the *Standard Raw Digitization Workflow* used in the workspaces of *Capture One CH* elaborated by *Digital Transitions Division of Cultural Heritage* (DTDCH). The workflow in [197] is structured as follows:

1. Pre-Flight Stage
    - Establishing PPI (camera distance, lens selection, focus)
    - Calibration (LCC, exposure, white balance)
2. Production Stage
    - Object Handling (aka staging)
    - Capture (naming, capture)
    - Initial Quality Control (object completeness, organic exclusion, focus)
    - Process Control (neutrality, exposure)
3. Processing Stage
    - Cropping (auto or manual)
    - Final Quality Control (set completeness, cropping, consistency)
    - Processing PDOs (TIFF or JPG2000)

This workflow is built to capture losslessly compressed RAW files, and is well known for performing a fast capturing and image transferring. This system outputs a file much smaller than a 16-bit TIFF and containing more information. This translates in a faster device capture and file transfer that provides an immediate preliminary image quality control.

Although the *Standard Raw Digitization Workflow* is thought for the acquisition of documents/photos in RAW format, this structure can be easily applied for the digitization of film frames and motion picture films.

Considering the Italian law system, the digitization of cultural heritage is regulated by the Ministry of Cultural Heritage and Activities (Ministero per i Beni e le Attività culturali e per il turismo - MiBACT), in particular by the Central Institute for Cataloguing and Documentation (Istituto Centrale per Catalogo e Digitalizzazione - ICCD) and the Central Institute for the Union Catalogue (Istituto Centrale per il Catalogo Unico - ICCU). The guidelines given by the government concern mainly the digitization of documents and just in a few cases the photographic and cinematographic materials. In particular, the most interesting document concerning the digitization of film are: the "Normativa per acquisizione digitale di immagini" [198] by ICCD and the "Linee di indirizzo per i progetti di digitalizzazione del materiale fotografico" [199] by ICCU. The ICCD regulation dates back to 1998 and, like the FADGI guidelines, classifies different levels of digitization quality. Considering the digitized film materials as *«high-resolution images, to be used for printing and as high-quality digital reference of the original (through the use of professional scanners)»* [translation from the Italian of [198]], the quality-level of the digitization must be the highest one. Here, the suggested resolution is 3072x3072 pixel, the bit-depth in black and white is 8 bit or 24 bit in RGB and the suggested conservation format is PNG. In this document there is also a paragraph focused on the calibration of the instrument. Since it is dated back to 1998, the suggested format is PNG, instead of TIFF, because at the time this second format was not largely diffused.

The ICCU guidelines refer to the ICCD's ones, but date back to 2004. In this documentation the only difference from the ICCD's regulations is the final conservation format that is updated to TIFF. Here, there is also the suggestion to use the JPEG as compression format and the idea of keeping constant the conservation conditions of temperature and relative humidity also during the digitization step, to do not affect the sensible photographic materials.

Comparing the national regulations and the FADGI guidelines, it was found that FADGI provides more detailed and specific procedures for the digitization of film materials, with respect to the Italian regulation. Therefore, in this context, the FADGI normative are a trustworthy starting point to plan the digitization workflow of a film.

On the other hand, when digitizing cultural heritage, especially documents or old books, other interesting regulations to consider when planning the scanning workflow are: International Federation of Library Associations and Institutes (IFLA) [200], the European program Minerva [201] and the regulation of the single region/department (like Regione Lombardia [202]) or by the single archive.

6.5.2 Color reproduction

Thousands of different kind of film formats, emulsions and color systems have been used throughout the history. Of course many experts in the field tried to classify and study them. One attempt of creating a complete database was made in 2012 by Barbara Flueckiger at the University of Zurich [186]. She tried to provide a comprehensive survey about the different color emulsion and processes used through the history. In the database is possible to see high resolution photos of original film frames and consult the documentation about the film processes (for some items are reported also spectral information from the different emulsion layers). Nevertheless, it is not possible to download the reflectance/emittance spectra and unfortunately perform research on the frames of the database, due to copyright protections. This database is strongly used by students and researchers to make comparisons and learn about specific processes, but cannot be used to extract data to model and study the used colors.

Another approach was tried by Nicola Mazzanti, co-founder of the festival "Il Cinema Ritrovato" and of the laboratory "L'immagine ritrovata" and now director of the Royal Belgian Film Archive (Cinematek). He is trying to create a database of the different color systems used through the history to study which one can be correctly reproduced today. Until now he catalogued around 280 color systems, and he found out that just the 2% of them can be digitally reproduced [203]. The amount of reproducibly films is so low due to the lack of sensitometry documentation and technical reports made through the history, but also to the physical limitation of recent emulsions to reproduce older ones (see the example in Figure 6.8).

In the last years, the advent of digital intermediate improved the post-production technology and the film restoration process. Due to the high manageability and reversibility of digital intermediate many archives made huge digitization campaign to make more accessible copies of stored films and increase their usability. This support migration opened different issues about the color reproducibility in digital systems that present the same problems of the analog ones, as underlined by Mazzanti.

When talking about color reproduction in digital systems it is fundamental to define the concept of *color gamut*. A color gamut is the set of colors that can be reproduced by a specific device (i.e. monitor, film, printer). Each media has a different

color gamut, so some colors that we see in a monitor can not be reproduced by a printer or by a film. A common way to compare different color gamuts is through the x y coordinates of the chromaticity diagram. The gamuts of a CRT monitor, a DCP projector and the red, yellow, green, cyan, blue and magenta color of a typical film are compared in 6.10a. It is important to notice that unlike the monitor and the projector, the film gamut assumes an hexagonal shape, because it is a subtractive system.

Comparing the three color gamuts it is already clear that some colors represented in the film, are not reproducible by a monitor or a projector.

In [204], Harald Brendel took a set of 12x12x12 equally spaced density values and recorded them to a negative film, printed them and measured the resulting colors. The ones that can not be represented by the digital display (i.e. that are outside the CRT gamut) are marked. Then, he compared the film colors also with the DLP projector. The results are reported in Figures 6.10b 6.10c.

The film print can produce a wider range of darker colors, especially in the blue and cyan regions. On the other hand, the monitor and projector reproduce more saturated and brighter colors in the red, green and blue regions. For the reproduction of the yellow, both the DLP and CRT presents some limits, but the projector gamut is better than the monitor one.

This experiment shows that color reproduction in digital intermediate is not fully faithful to the original film, essentially because of the different performance of the additive and subtractive process, in fact this latter method reaches the maximum saturation in lower lightness levels, at the opposite of the additive one. Furthermore the lack of sensitivity information of films, underlined by Nicola Mazzanti, makes impossible the reconstruction of different film process gamut, and so their comparison with the digital intermediate. For this reason, nowadays, the comparison between films and digital media is made subjectively by visual comparison. This method has some practical advantages in its applicability, but the main limit is that it is not possible to identify precisely how much the reproduction and the original differs. If mathematical models and simulations are not available it is impossible to reproduce precisely a film gamut and the only way to do so is trying to simulate the original perception of the film. Furthermore it is fundamental to develop a system to identify the color corrections made on a film, to make the restoration reversible and transparent.

6.6 Digital color correction in the restoration pipeline

In Chapter 4 is presented a summary of the restoration workflow that is commonly shared between the main laboratories and archives. In this Section the idea is to focus on the color and contrast recovery in digital images as well as in digital film restoration, with a particular focus on the traditional manual softwares for color correction and the most innovative methods for color recovery and enhancement.

The digital color correction step aims at balancing the various sequences of the film and providing photographic consistency. In this step can be made all the corrections that aim at simulate the original faded colors, restore the original contrast and balance the lightness.

Today, the tools used in film digital color correction are the same used by the colorists to grade new movies in post-production and they can be personalized to deal with specific restoration projects. Despite the possibilities of customization, the softwares used in this phase require human expertise and interaction to be used: the

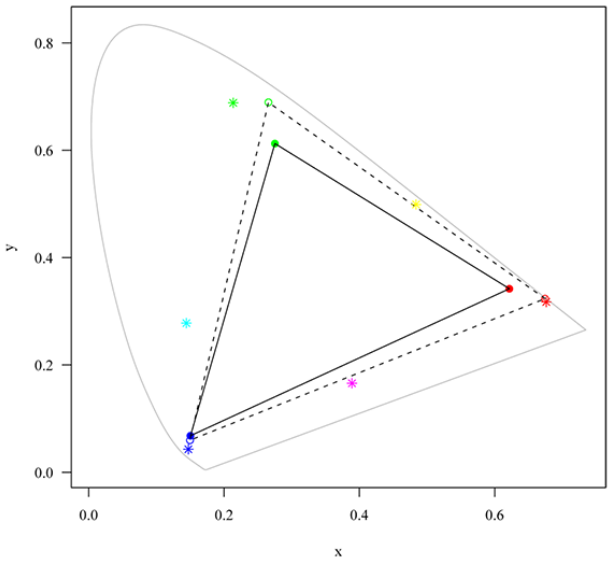

(A)

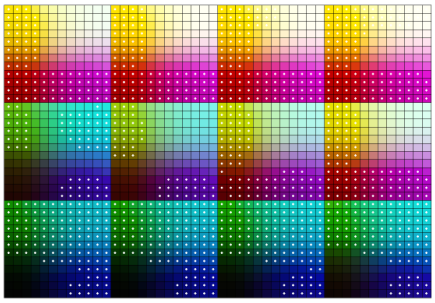

(B)

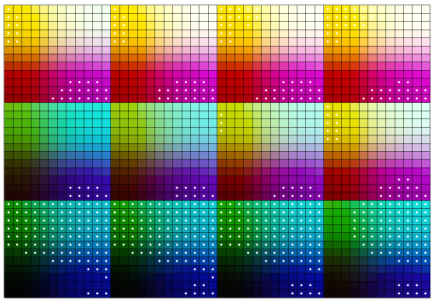

(C)

FIGURE 6.10: In Figure 6.10a the CIE chromaticity diagram in which is represented the gamut of a CRT monitor (solid lines) and the gamut of a DLP projector (dashed lines). The asterisks mark the locations of the red, yellow, green, cyan, blue, and magenta color of a typical motion picture print film projected with a Xenon lamp. Figure reproduced from: [204]. In Figure 6.10b the film colors displayed on a CRT monitor. The colors marked with a white point are outside of the monitor's gamut. Figure reproduced from: [204]. In Figure 6.10c the film colors displayed on a DLP projector. The colors marked with a white point are outside of the monitor's gamut. Figure reproduced from: [204].

operator has a control panel for color correction, a tool for analyzing and reading the signal (*scopes*) and a high-quality monitor for viewing the images, which can be often projected digitally on the big screen, to have a perfect vision of the final result in the cinema.

In order to simulate the original colors and without running the risk of creating "fabrication of history" it is of fundamental importance to have a well-preserved positive copy or at least have all the sensitometric data of the original film, to control the final color gamut and be as faithful as possible to the original. This is fundamental because, an arbitrary reading or a personal interpretation could definitively compromise the philological accuracy and the restoration outcome.

Generally the color correction process is splitted into two phases: the primary and the second color correction. The primary color correction permits to eliminate any chromatic dominants in the film and uniform the colors. In this step the contrast is enhanced, to make more evident the artifacts and the alterations in the image more evident (like the presence of dust and scratches), simplifying their identification and removal in the subsequent work phases. The secondary color correction, takes place after the film restoration *per se*, in which the images are restored and the artifacts, dust and scratches are removed. At this point the frames should be further more uniformed and the final adjustments of contrast and saturation are made.

The main difference between the first and the secondary color correction is that in the first step are removed the principal color casts and the white balance is made. Sometimes, during the film scanning the white balance is made automatically and the curator can decide to reduce the film color correction at this step. It is in the secondary color correction that the colors can be enhanced in brightness and saturation and, due to this, it is fundamental to have a trustworthy reference to follow.

Except for the primary color correction tools liked to the film scanners, it is really hard to find a software which allows at making the color correction automatically and, also if an automatic color balance is possible, it is fundamental to supervise the tools and make manual corrections when necessary.

6.7 Spatial Color Algorithms for digital color restoration

The mainly used digital color correction techniques involves a significant human intervention, a constant supervision and the use of expensive tools. Many softwares used in film restoration are designed for video editing, thus include functions and operations which produces information loss or alterations in the final image. For this reason it is fundamental to perform a constant visual supervision, and the film frames are often controlled singularly and subjectively. In addition to this problem, today, the dependency on a consumer software led to an extreme specialization of the restoration users on specific tools. This is leading also to a tool-dependent education, without any comprehension of digital imaging.

Today, a manual and subjective color restoration made by film experts appears to be the most suitable solution because, in many cases, the original reference is missing. In this context also a colorimetric approach is improper, because there are just a few datasets which include sensitometric and colorimetric dyes characterization to perform a colorants identification and reconstruction. In addition, even if a precise colorimetric characterization is available, is important to consider the gamut differences across the acquisition and fruition devices, which can make the effort worthless.

In this complex context, the use of Spatial Color Algorithms (presented in Section 5.3) can be an alternative approach to film color restoration. The SCA family is particularly suitable for film restoration, because allows at enhancing and restoring the original appearance of color rather than the original color signal. I remind to the reader that SCAs are inspired by the capabilities of the Human Visual System and produce results which are coherent to the original appearance of a scene, in particular thanks to the ability of simulate lightness constancy and color constancy. The aim behind film restoration through SCAs is to restore each frame by estimating the original scene color appearance. This idea was presented at first by Rizzi et al. in [164], and developed in [26], [173]. In film restoration, the proposed method can be used for complete restoration processes or as unsupervised kickoff process followed by manual refinements. This procedure allow at reducing the times and cost of a restoration workflow and at producing a objective unsupervised color enhancement.

SCAs parameters tuning and selection

SCAs perform an unsupervised frames enhancement almost based on small sets of parameters. In general the parameters tuning is made depending on the image content, but a initial set of values could contribute to speeding up the final tuning. In Figure 6.11 are displayed different SCAs filtering with different parameters settings. In RSR and STRESS is suggested a value between 20 and 40 of number of spray per pixel, and the default value of points in each spray can be between 100 and 800. The main scope of parameters selection in RSR and STRESS is to have an adequate sampling around the pixel to compute. The use of lower values of spray per pixel and points per spray could lead to reduce the computational time, but could increase the noise in the output. In ACE algorithm the increase of the slope parameters led to an increase of perceived contrast in the output and a lower slope value produce a lower contrast. In general, 5 can be an appropriate starting value of slope and a more extensive discussion about ACE paramaters tuning for film restoration can be found in [161], [205].

As in the traditional color correction, to apply an algorithm of image enhancement on a full film, it is sufficient to tune the parameters on each scene key frame. To do so, it is fundamental to split the whole video in shot, extract or select the key frames, tune the algorithms parameters on the selected frames and then filter the whole scenes. After these steps it could be necessary to assess the final quality of the enhancement and eventually perform a final re-editing or harmonization step.

6.7.1 Application of ACE algorithm for film restoration

In this Section different applications of ACE algorithm for film restoration are presented. All those works have been basic applications for different publications that I made as journal papers (see [25], [26]), as book chapters (see [173], [206]–[208]) and at national and international conferences (see [165], [209]–[214]).

In this Section, the quality of the results will be evaluated only visually. In Chapter 7, an extensive discussion on film restoration quality assessment will be provided and the results will be evaluated objectively through different methods.

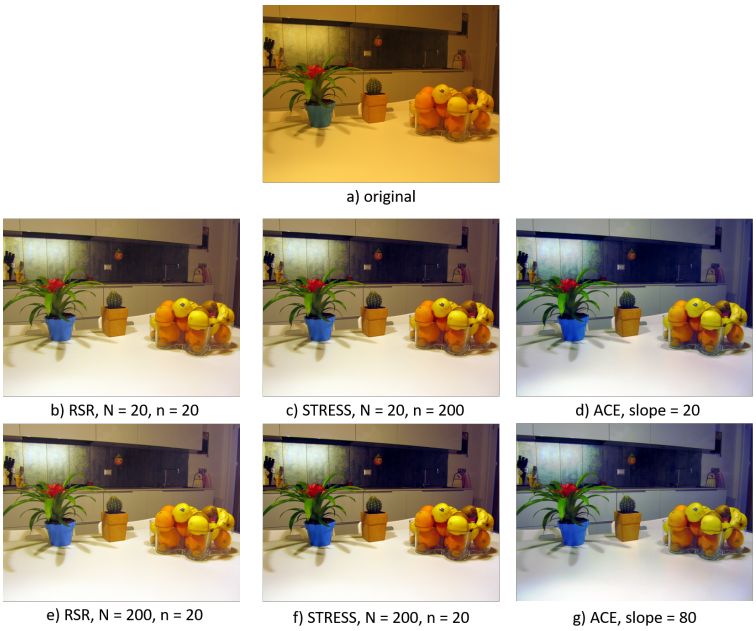

FIGURE 6.11: Filtering examples using RSR, STRESS, and ACE with different parameters settings. Figure reproduced from [173].

"Raccolta della carta nelle scuole"

The amateur video "Raccolta della carta nelle scuole" ("Paper collection at school") is a super8 mm film shot around December 1980 by different citizens of Brescia (Italy). This video has been archived by ASM foundation and is a rare historical documents about one of the first awareness campaigns on the theme of paper collection, recycling and sustainability. The analog film was in good conditions and has been digitized through a Reflecta Super8 Scanner [215]. The film has been scanned through a LED calibrated light with a color temperature of 3200 K to simulate the halogen lights usually used on Super8 projectors. The film digital color correction has been performed through ACE algorithm. To do so, the digitized film has been automatically divided in sequences and for each scene a key frame has been extracted and used to tune ACE parameter (see Figure 6.12).

In ACE parameters tuning it is important to set a value of slope which allows at enhancing the color contrast and at removing the fading caused by the aging, without occurring in over-saturated or noisy frames.

In Figure 6.13 are reproduced two key frames restored with ACE algorithm. Here it is possible to see that ACE algorithm removes the aging patina on the frames surface, and more details are now visible in the scenes. In this application ACE algorithm was used to perform the full restoration of the video. The restoration involved just one user and it required around 100 machine/hours. ACE parameters selection was supported by the video curator assessment. Thanks to this restoration it has been possible to archive and divulge a fundamental moment for the industrial and ecological history of Brescia.

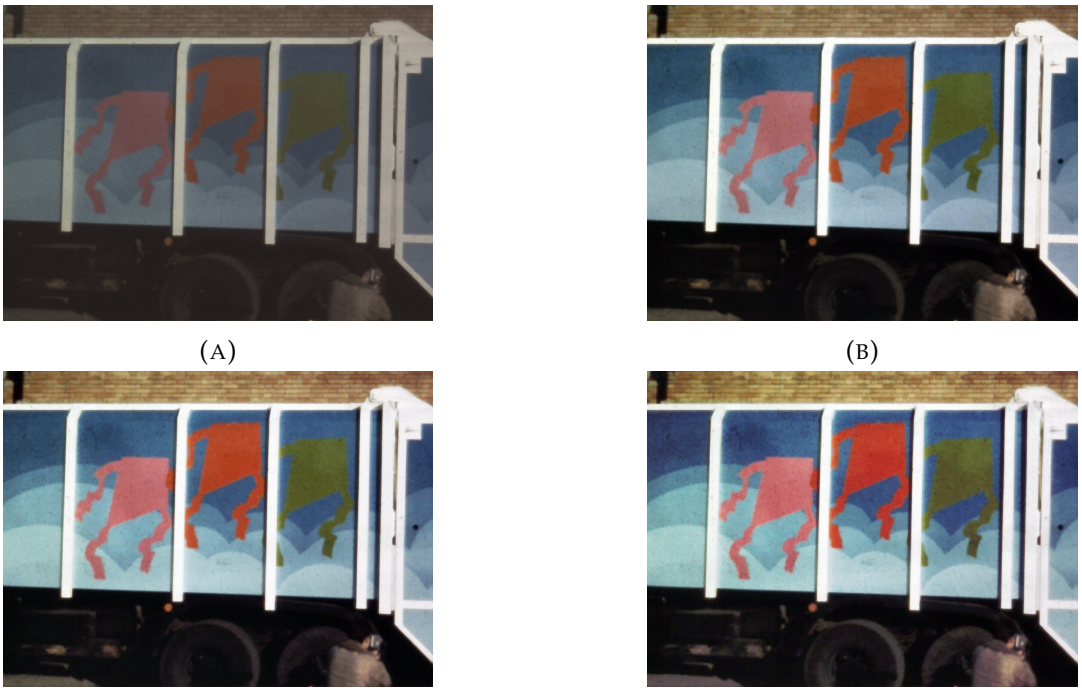

(A) (B)

(C) (D)

FIGURE 6.12: Example of the same frame restored through three different values of ACE parameter. In 6.12a the original frame, in 6.12b ACE with slope 5, in 6.12c ACE with slope 10, in 6.12d ACE with slope 20.

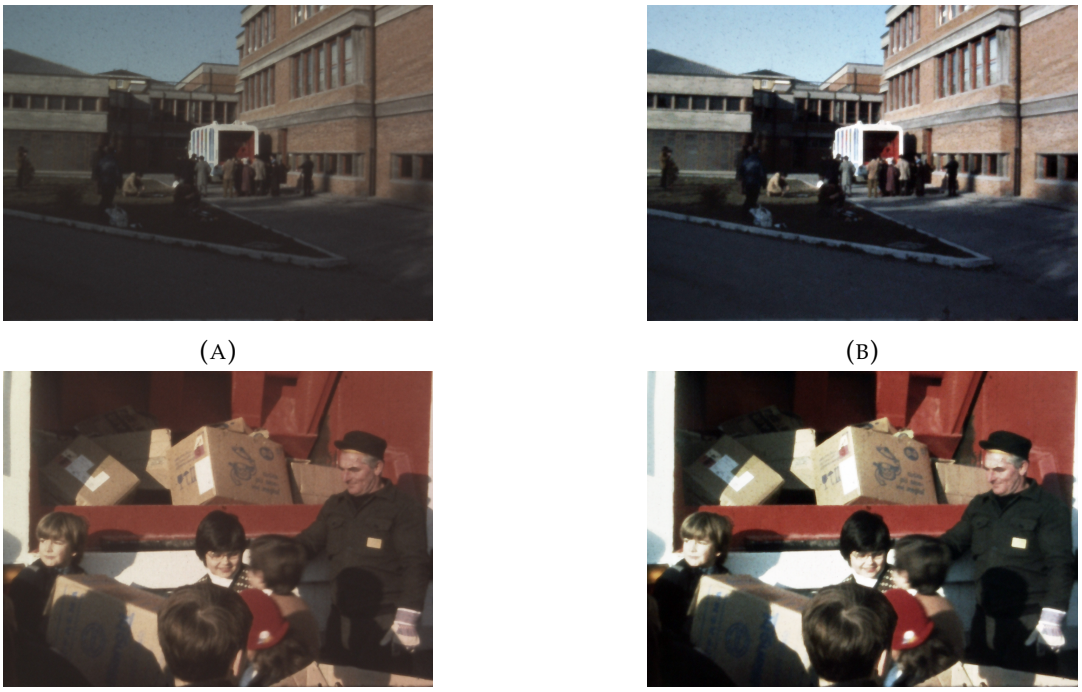

(A) (B)

(C) (D)

FIGURE 6.13: Example of frame restoration through ACE. Figures 6.13a and 6.13c are the original frames, and 6.13b and 6.13d the ones restored with ACE algorithm (slope 3).

"The funerals of the bombing of Piazza della Loggia in Brescia"

The 28th May 1974, a tragic event signed the history of the city of Brescia: a terroristic attack that will be later called "Strage di Piazza della Loggia" ("Bombing of Piazza della Loggia"). From that day, all the documents regarding the bombing, the subsequently events and the processes are safeguarded by the "Casa della Memoria" association, that aims to keep alive the memory of this tragic event and that every year is in charge of its commemoration. Thanks to an important collaboration between the University of Milan, "Casa della Memoria" association and ASM foundation, an important video concerning the funerals of the bombing of Piazza della Loggia has been restored. The video in Super8 format is the only proof in colors of the funerals celebrated in Brescia on 31st May 1974. The incomparable historical value of this video comes also from a recent discovery, in fact looking at the digitized video, it has been found that the first 30 seconds of the film were took by Mario Bertoli right before the bombing. Than the shoot was interrupted, and the record restarted the day of the funerals. The video has a length of 19 minutes and 50 seconds and a frequency of 18 fps. The video in general was well conserved and presented common problematics like: scratches, dust, film joining, instability and color degradations. The video has been digitized using the Reflecta Super8 Scanner [215]. The digitization took 15 hours circa of no-stop scanning. This phase is automatically controlled by the scanning hardware and for this film, resulted 21343 frames. In order to compare a restoration through SCAs, with a traditional restoration workflow, the video has been restored manually through different restoration softwares, and in parallel the frames have been enhanced through ACE algorithm.

Manual Restoration

For the color film editing and the color correction the software Da Vinci Resolve 14 was employed [216]. With this software it was possible to join the single frames to compose the entire video, and then divide it in scenes. With the same software it was made the primary color correction, the secondary color correction and the final editing of the video. For the digital restoration the software Phoenix Finish 2017 [217] was employed. This specific software presents various tools for film restoration, in particular functions of stabilization, dust and scratch removal. Both the software were used on PCs with calibrated Eizo monitors. The manual restoration was divided in three main step: first color correction, digital restoration and secondary color correction. The first color correction was made with Da Vinci Resolve 14, which allows also the automatic division of the video in sequences. The 120 obtained scenes were then divided between the operators which performed in each scene the white balance, the color saturation correction and a contrast enhancement. The white balance was performed manually balancing the RGB primary bars and acting in each single channel. The contrast and saturation were made subjectively and each operator, increased or decreased those values manually. The main disadvantage of this step of the workflow is that each worker tends to correct the scenes following his personal judgment and taste. Thus, this lead to the need of a scene matching and harmonization step. After the color correction the video was exported into scenes for the digital restoration step. In the digital restoration phase, was made using Phoenix Finish. This is a professional software which requires higly-specialized operators and PCs with performing graphic cards and a large amount of RAM memory. In this step for each scene the following operations were made: Video Stabilization, Dust Removal and Scratch Removal. For the stabilization, the software automatically makes the scene steady by translating the single frame along the horizontal and vertical axis. Despite this, this operation could lead to information loss, but in

this case it was considered necessary due to the high instability of the original image. After the stabilization, the video was cleaned by dust and scratches. In this step it was fundamental to set up the right parameters, because a too strong clean up may lead to the formation of artifacts or to the removal of elements in the image (like jackets' buttons or little details). Furthermore, in this step it is alway necessary a supervision of the automatic work and the manual removal of the remaining marks. In this case, the percentage of manual removal is high: around the 50% of dust and scratch were removed manually. In conclusion, the secondary color correction had the principal role of matching all the different scenes between them. In the Table below are reported the technical data relative to the manual restoration of the film "The funerals of the bombing of Piazza della Loggia in Brescia":

Film Title	"The funerals of the bombing of Piazza della Loggia in Brescia"
Duration	19 min 50 sec
Restoration hardware	5 Computers: DELL XPS, Intel Core i7 – 7700 3.60 GHz, RAM 16 GB. 5 Monitors: EIZO CS2420, NVIDIA GTX 1060 GB, resolution 1920 x 1200.
Software	Color correction: Da Vinci Resolve 14 Digital Restoration: Phoenix Finish 2017
Personnel	5 students and 3 video editors
Time	200 man/hour

TABLE 6.1: Technical data concerning the manual restoration of the film "The funerals of the bombing of Piazza della Loggia in Brescia"

ACE color restoration

The color correction of the digitized video of "The funerals of the bombing of Piazza della Loggia in Brescia" was made also with ACE algorithm. In the following table are reported the relative technical data:

Film Title	"The funerals of the bombing of Piazza della Loggia in Brescia"
Duration	19 min 50 sec
Restoration hardware	1 Computer: DELL XPS, Intel Core i7 – 7700 3.60 GHz, RAM 16 GB. 1 Monitor: EIZO CS2420, NVIDIA GTX 1060 GB, resolution 1920 x 1200.
Software	Color correction: ACE CPU version
Personnel	1 student
Time	90 machine/hour

TABLE 6.2: Technical data concerning the ACE restoration of the film "The funerals of the bombing of Piazza della Loggia in Brescia"

In Figure 6.14 are presented some comparison among the original film frame, the manual and ACE restoration. Despite the quality assessment, discussed in the following Chapter, here is important to notice the great improvement which an algorithm like ACE could give in the restoration workflow. Clearly in the ACE color

(A) (B) (C)

(D) (E) (F)

(G) (H) (I)

FIGURE 6.14: Example of three frames restored manually and through ACE. 6.14a, 6.14d and 6.14g are the original frames, 6.14b,6.14e and 6.14h are the frames restored manually, and 6.14c, 6.14f and 6.14i are the frames restored with ACE.

correction the digital restoration (scene stabilization, dust and scratch removal) is not performed, but the improvements provided by this unsupervised algorithm are still significant. The manual restoration is a delicate operation which must always be done with the supervision of a curator or of a film restoration expert, because it can lead to major errors (like artifacts, information loss or non-uniformity of the results). Furthermore, it requires a huge amount of time and expertise, and as consequence of resources. Thanks to the ACE algorithm, but more in general to SCAs, it is possible to perform complete restorations reducing the restoration time of the 90% circa.

"Le isole della Laguna"

"Le isole della laguna" is a black and white documentary directed by Luciano Emmer and Enrico Grass in 1948. Also in this application to evaluate ACE performances, the unsupervised filtering has been compared with a manual contrast restoration. The scene detection and the manual contrast enhancement have been made with Da Vinci Resolve 14 [216]. As mentioned in the previous Section the scene detection is automatic, but requires the constant supervision of the user. In Figure 6.15 is reported an example of scene cut detected manually in the supervision process.

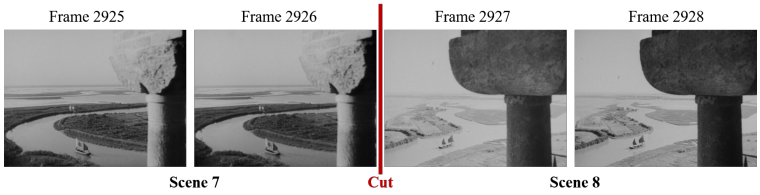

FIGURE 6.15: Example of scene cut not detected by the automatic software. Figure reproduced from [207].

Since the film under restoration is a black and white documentary it is fundamental to select for each scene the key frame which better represent the medium contrast and with the highest dynamic range. In fact on the key frames is performed the ACE parameter tuning as well as the manual color correction. In Figure 6.16 is reported an example of ACE slope tuning on the original frame and the comparison with the same frame enhanced manually.

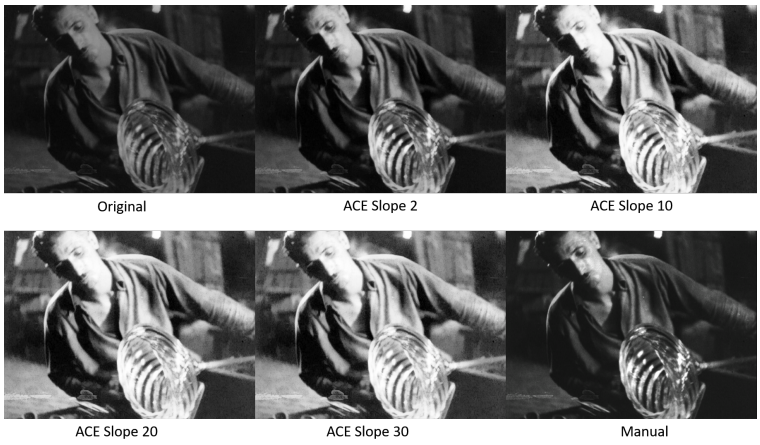

FIGURE 6.16: ACE parameter tuning. Figure reproduced from [207].

One challenge of this film, is the presence of many fade-in and fade-out effects introduced by the directors. This artistic feature must be preserved dring the restoration and must not be removed with the application of the ACE algorithm. In [164] Rizzi et al. presents some specific ACE functions, introduced in the second step of the filtering, which allow at preserving the luminance variance in artistic effects: Keep Original Gray (KOG), Keep Original Color Cast (KOC) and Keep Original Dynamic Range (KODR). KOG function preserves the original average value of each RGB channel in the image instead of recomputing the medium gray. This option was found useful to preserve the tonal characteristics of a low of high key image. KOC is useful to preserve the original color cast introduced for artistic purpose. In

this case the original color cast is computed and re-introduced in the output. In conclusion, KODR is useful when in the original image just a part of the dynamic range is used to obtain specific artistic effects. In this application, in presence of fade-in and fade-out sequences, KOG feature could provide the most effective results (see Figure 6.17).

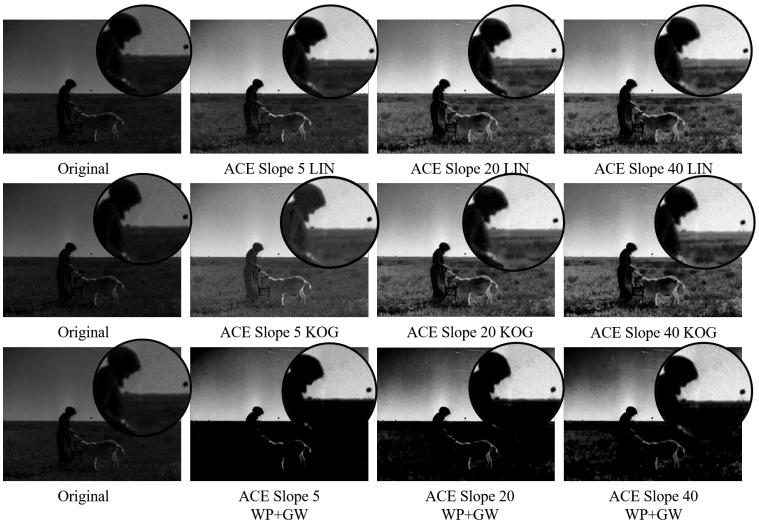

FIGURE 6.17: Example of ACE enhancement in a fade-in and fade-out sequence using different parameters. LIN denotes that the dynamic range re-computation fills linearly whole available range- WP+GW denotes the White Patch+Gray World function (see Section 5.3). Figure reproduced from [207].

After ACE parameter tuning step and the filtering process, in this application, 20 scenes have been restored through ACE algorithm. In the following Table are reported the enhancement statistics:

Function	Number of Scenes	Slope average	Slope variance
LIN	8	3.6	5.4
KOG	7	3.0	2.6
LIN	7	5.6	3.8

TABLE 6.3: Statistics of ACE filtering. Table reproduced from [207].

In Figures 6.19 and 6.18 is presented a visual comparison among the original film key frame, the ACE restoration using different parameters and the manual enhancement. The manual restoration concerned mostly a white balancing if the scenes and a visual correction of the contrast. In general, in a restoration workflow the final quality assessment is made by the film curator, who defines which scenes must be reworked or if some parameter must be adjusted. Clearly this final assessment is completely subjective and depends mainly by the experience of the operator and by the competences of the curator. To support the visual assessment and give to the operator a better control on the restoration operations, in this application the restored images have been combined with some basic objective quality metrics. Thanks to this, the restoration operators had the possibility to define ACE parameters and the resulting manual restoration not just on their visual assessment, but also based on some objective metrics. The first basic feature to assess the enhancement made by the restoration algorithm is the analysis of the image histogram [165]. Thanks to the representation of the image tonal distribution in the histogram, it has been possible

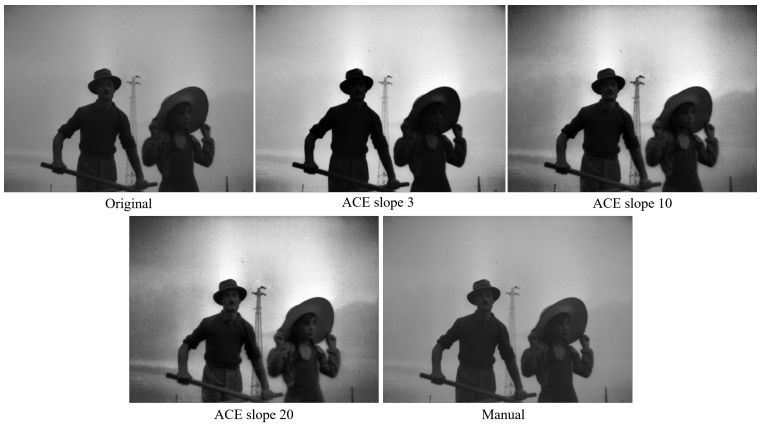

FIGURE 6.18: Key frame of "Le Isole della Laguna" scene 80 restored through different ACE parameters and manually.

to support the visual assessment made by the restoration operator and by the curator. The image histogram, is a really simple feature, that could be extremely useful especially when working on old faded films. When a film has aged and the colors or the contrast has faded, in the digital image the pure white is no more represented by the maximum value (255), but lowered proportionally to the fading [218] (see Figure 6.19). The image histogram is an optimal preliminary feature also to evaluate the different image enhancement methods and, in this case, the better ACE parameter tuning. In Figure 6.19 it is possible to see that the manual and ACE enhancement produce an increase of contrast in the image (i.e. ratio between the brightest and darkest value of luminance), but in the manual restoration the black and the white are not re-set at 0 and 255. On the other hand, ACE extends the luminance values using the whole dynamic range. Starting from this preliminary graphical evaluation of the results, which supported the work of the restorer and of the curator, in Chapter 7 a similar objective set of metrics will be presented. In this application the film "Le isole della laguna" has been a test-bed for alternative methods of contrast enhancement in aged films. Furthermore, the use of image algorithms set the base for new, objective and intuitive ways to assess the quality of restored films.

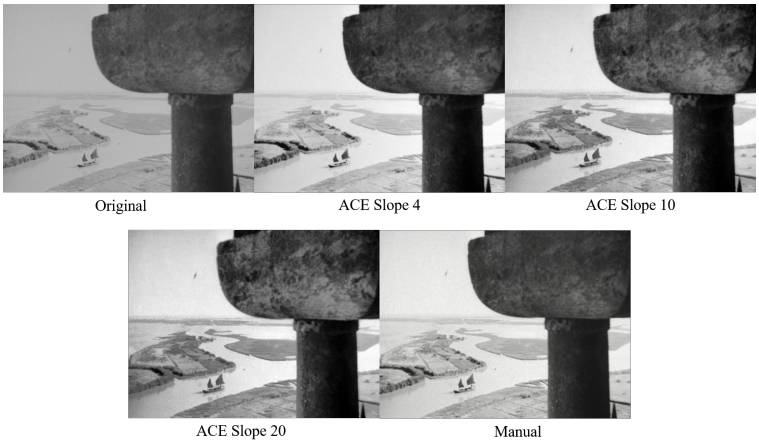

(A)

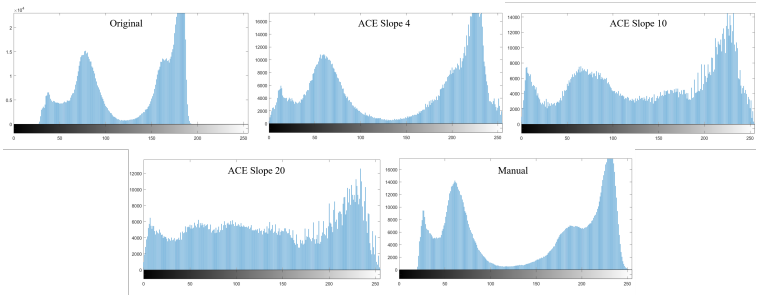

(B)

FIGURE 6.19: In Figure 6.19a, key frame of "Le Isole della Laguna" scene 6 restored through different ACE parameters and manually, and in 6.19b the relative image histograms. Images reproduced from [207].

Part III

Quality Assessment

Chapter 7

Image quality

7.1 Introduction

The International Organization for Standardization (ISO) defines quality as:

The totality of features and characteristics of a product or service that bear on its ability to satisfy stated or implied needs [219], [220].

In other words, quality is the conformance of the subject to one or more requirements. In the current literature it is possible to find several definitions of Image Quality which have already been deeply revised by Pedersen [221] and Simone [149]. A small selection of definition is reported here:

Yendrikhovskij 1998: *Image Quality is the degree of correspondence between the visual representation and the memory of a natural scene.[222]*

Janssen 1999: *Image Quality is (defined) in terms of two components, usefulness, that is, the precision of the internal representation of the image, and naturalness, that is, the degree of match between the internal representation of the image and representations stored in memory.[223]*

Engeldrum 1999: *Image Quality is the integrated set of perceptions of the overall degree of excellence of the image. [224]*

Fairchild 2002: *Image Quality is the perceptible visual differences from some ideal and the magnitude of such differences. [225]*

Keelan 2002 and ISO 2003: *Image Quality is the impression of the overall merit or excellence of an image, as perceived by an observer neither associated with the act of photography, nor closely involved with the subject matter depicted. [226], [227]*

International Imaging Industry Association (I3A) 2007: *Image Quality is the perceptually weighted combination of all significant attributes of an image when considered in its marketplace or application. [228]*

Image Quality as assessed by humans is a concept hard to be defined, since it relies on many different features, including both low level and high level visual characteristics. Image luminance, contrast, color distribution, smoothness, presence of noise or of geometric distortions are some examples of low level cues usually contributing top to image quality. Aesthetic canons and trends, displacement of the objects in the scene, significance and message of the imaged visual content are instances of the high level (i.e. semantic) concepts that may be involved in image quality assessment.

Following the definition given by I3A [228],it is mandatory to consider the application domain to assess the quality of an image. In fact, the final observer of an image

is not necessarily a human, but can be a machine vision system. As consequence the image quality can be considered the degree of adequacy to its function in a specific application field. Following this idea, De Ridder et al. presented in [229] the idea of three fundamental dimensions to define image quality: fidelity, usefulness and naturalness (see Figure 7.1). Fidelity is the degree of similarity of the acquired image with the original. Usefulness is the apparent suitability of the acquired image with respect to a task/domain. Naturalness defined the correspondence between the of the acquired image with the viewer's internal references.

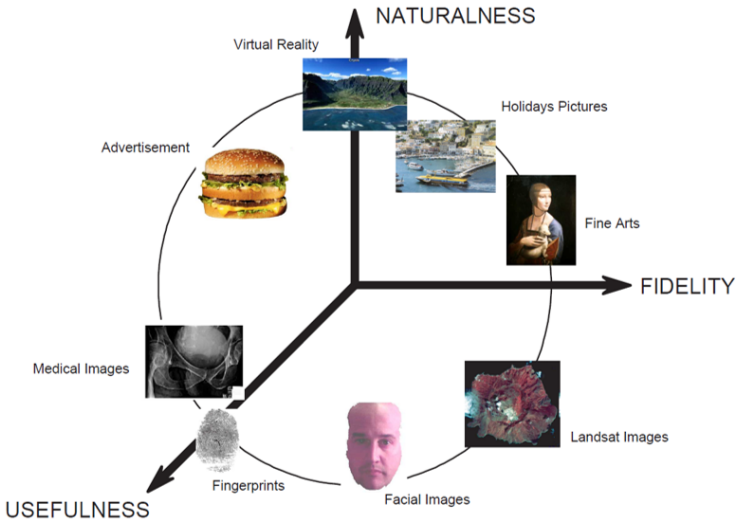

FIGURE 7.1: Fidelity-Usefulness-Naturalness (FUN) image quality representation. Figure reproduced from: [229]

Also if the quality dimensions are not independent, the image quality is usually evaluated as a single number weighting the individual components, due to the image type and field of application.

7.2 Image quality metrics classification

As presented in [230] different criteria can be used to classify IQ (Image Quality) assessments. The most popular criteria is to divide the methods into two main groups: subjective and objective Image Quality Metrics (IQMs) [226]. Subjective IQMs are based on experiments involving human observers. The techniques generally use a single or a double stimulus, and the standard for subjective IQMs assessments are defined by ITU-R BT 500-11 [231]. The subjective IQ assessment involves people and require big amount of time and resources especially when the dataset of images under test includes many items. Furthermore, this kind of analysis necessitate to take into account all the factors that influence human perception, like light source, environment, spatial arrangement, light geometry and so on.

Objective IQ assessment is known to be more efficient, compared to the subjective one, and it does not require the involvement of users. Those methods are generally based on computational models and measure the quality directly from the digital image. The objective IQA methods are classified in three groups, named Full-Reference (FR), Reduced-Reference (RR) and No-Reference (NR) metrics upon the availability of a visual model (*reference*) assumed as gold-standard [226]. In turns,

these metrics can be opinion-aware or opinion-unaware, according to the usage of not of human judgments.

The FR metrics compare the reference with the image under analysis. In this group are considered metrics like the ΔE, the Mean Square Error (MSE) or the Peack Signal to Noise Ratio (PSNR) [232]. Those metrics are widely used, but as demonstrated in [233], they are not correlated with human judgment and HVS. Due to this lack, during the years, those metric developed including also HVS features, like the perception of structures in the image, or computing the information loss or distortion, or also combining local image features. Several different research have classified Objective IQMs. Some classification are based on the information that the metric uses [234] (i.e. edge, contrast, spectral distance). Wang and Bovik in [235] divide the IQMs in three main categories based on the information about the original image, the distortion and the HVS. The three categories are: 1.Full-reference, no-reference and reduced reference metrics, 2.General-purpose and application specific metrics and 3.Bottom-up and top-down metrics. And other classifications were proposed by Le Callet et al. [236], Chandler et al. [237], Thung et al. [238], Seshadrinathan et al. [239].

An interesting classification was proposed in [240] by Fry et al., which classifies the Image Quality Metrics in four further genres, in addition to FR, RR and NR metrics: the STV-IQMs (Signal Transfer Visual-IQMs), CP-IQMs (Computational Metrics-IQMs), MF-IQMs (Multivariate Formalism-IQMs) and IF-IQMs (Image Fidelity-IQMs). The characteristic of each genre are reported in Table 7.1.

Metric Genre	Reference Type	Input Parameter	Output Data	Correlating Data
STV-IQM	No Reference	Test chart measurement	Quality or sharpness score	Perceived quality or sharpness score (JPD)
MF-IQM	No Reference	Univariate metric scores, from test chart measurements	Quality Score	Perceived quality score (JPD)
IF-IQM	Full Reference	Test Image + Reference Image	Fidelity Score or error map	Perceived fidelity score (JND), or probability of difference visibility
CP-IQM	Full/Reduced Reference No Reference	Test Image + Reference Image Test Image	Quality difference score Quality score	Differential Mean Opinion Score (DMOS) Mean Opinion Score (MOS)

TABLE 7.1: Summary of IQMs genres. Table reproduced from: [240].

Nevertheless the different classifications, in this work we will consider the one presented by Pedersen in [221].

7.2.1 Objective IQ assessments

In [221], Pedersen proposes a classification of Image Quality Metrics based on the implication of the HVS in the IQM computation. The IQM are classified in: mathematically - based assessments, low-level metrics, high-level metrics and other metrics. Following this classification, some example of mathematically - based assessments are MSE (Mean Square Error) and PSNR (Peack Signal to Noise Ratio); the low-level metrics are the ones like S-CIELAB (Spatial-CIELAB) [241] and the high-level metrics include the SSIM (Structural SIMilarity) [242] and VIF (Visual Image Fidelity) [243].

Full-Reference IQ assessments

The full-reference image quality metrics are the most diffuse and used in the literature. FR metrics are based on the comparison between the reference image and an enhanced one. Following the classification in [221], those metrics can be divided in two groups: the basic IQ metrics and the low- and high-level based metrics.

Basic IQ metrics

The basic IQ metrics, also defined mathematically - based assessments, apply statistical measures to assess the error between the reference and the enhanced image. Among these metrics the most diffused (especially in image compression and transmission) are the Mean Square Error (MSE) and the Peak Signal to Noise Ratio (PSNR) due to their physical meaning and to their simplicity and usability. Some of the main basic IQ metrics are: Mean Square Error (MSE) [17]:

$$MSE = \frac{1}{MN} \sum_{j=1}^{M} \sum_{k=1}^{N} (x_{j,k} - x'_{j,k})^2 \tag{7.1}$$

Peak Signal to Noise Ratio (PSNR) [17]:

$$PSNR = 10 \log \frac{(2^n - 1)^2}{MSE} \tag{7.2}$$

Normalize Cross Correlation (NK) [17]:

$$NK = \sum_{j=1}^{M} \sum_{k=1}^{N} (x_{j,k} \cdot x'_{j,k})^2 \tag{7.3}$$

Average Difference (AD) [17]:

$$AD = \frac{1}{MN} \sum_{j=1}^{M} \sum_{k=1}^{N} x_{j,k} - x'_{j,k} \tag{7.4}$$

Structural Content (SC) [17]:

$$SC = \frac{1}{MN} \sum_{j=1}^{M} \sum_{k=1}^{N} x_{j,k}^2 \tag{7.5}$$

Maximum Difference (MD) [17]:

$$MD = Max(|x_{j,k} - x'_{j,k}|) \tag{7.6}$$

Normalized Absolute Error (NAE) [17]:

$$NAE = \sum_{j=1}^{M} \sum_{k=1}^{N} |x_{j,k} - x'_{j,k}| \tag{7.7}$$

Low- and High-Level based IQ Metrics

The low- and high-level IQ metrics are based on the implication of some features of the Human Visual System in the metric computation. The most widely diffused IQ measures part of this group are: S-CIELAB, SSIM, FSIM, DRIM, HDR-VDP, HaarPSI and MAD.

The S-CIELAB [241] is derived from the ΔE color difference measure and performs two main step: at first simulate the HVS blurring applying a spatial filter on the image and then computes the basic CIELab consistency for large uniform areas. This metric is the spatial extension of ΔE and is particularly suitable to measure color difference of large and uniform color targets.

SSIM [242] is a metric based in the Universal Image Quality Index [233] and is based on the idea that the HVS adapts to extract information and structures from

the images. Thus, this metric evaluate the general structure of the image content from a set of defined structural attributes. A widely used variant of SSIM is the Multi Scale-SSIM (MS-SSIM) [244]. In this variant the SSIM metric is performed over multiple scales in a process of multiple sub-sampling of the image. The SSIM and MS-SSIM are considered among the most successful image quality metrics, due to the idea of evaluate the image quality based on its structure. Thus, those metrics are widely used in all the applications which use image features extraction or image compression.

The Feature SIMilarity metric (FSIM) [245] is based on the idea that the quality of an image is defined by its degree of understandability. More specifically, in this metric the phase congruency is used as the main feature which determine the ability of the HVS to read and understand an image. Usually, FSIM is used in image processing applications.

The Dynamic Range Independent Image Quality Assessment (DRIM) metric [246] is a metric which can operate on image pairs where both images have arbitrary dynamic ranges. This metric identifies the visible distortions, furthermore detect and classify the visible changes in the image structure. HDR-VDP II (High Dynamic Range Visual Difference Predictor) [247] is a metric tailored for High Dynamic Range images and is able to predict the visibility between two images. To do so, it uses a visual model suitable to identify different luminance conditions and derived from the contrast sensitivity measure. HaarPSI [248], the Haar wavelet-based Perceptual Similarity Index is an image quality index which aim assessing the perceptual similarity between two images based on the features of HSV. This metric is used for image transmission and compression. In conclusion MAD full-reference metric [249] consists in a dual strategy based on two different methods. First, a local luminance and contrast masking is used to estimate the perceived distortion in high quality images, second, a variation in the local statistics of spatial-frequency components is used to estimate the perceived distortion in low quality images.

No-Reference IQ assessments

In many cases and application, especially for restoration quality assessment, a reliable and undistorted reference is not available. In this case the no-reference IQ metrics are the only solution to assess the overall quality of an image. The no-reference IQ metrics compute quality scores based on expected image statistics or features. Two of the most used no-reference image quality metrics are BRISQUE and NIQE. BRISQUE (Blind Image Spatial QUality Evaluator) [250], [251] is a metric based on a default model trained on a dataset of natural images with the same type of distortions. This metric is limited to evaluating the quality of images which presents the same type of distortions. Furthermore this metric is opinion-aware, this means that each image in the training dataset is coupled with a subjective quality score. In this metric a smaller score indicates a better quality value. NIQUE (Natural Image Quality Evaluator) [252], as BRISQUE, is an image quality metric based on a model trained on a database of natural image. In this case the dataset is composed by pristine images without distortions. NIQE does not use subjective quality scores. Also in this case a smaller score indicates a better image quality. In addition to these two no-reference image quality metrics, I include in this group also basic statistical measures which aim at evaluating specific image features like brightness or contrast. Considering an image (I), the brightness can be evaluated as the is the mean value

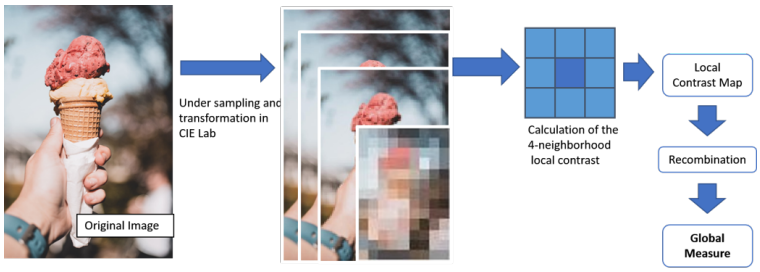

FIGURE 7.2: Graphical representation of local contrast measurement.

of the image intensities (S), i.e.:

$$B = \frac{1}{|S|} \sum_{x \in S} I(x) \tag{7.8}$$

Considering the CIELab color space the image brightness can also be measured as the mean luminance (L) of all the pixels in channel L^*. The image intensity can also be computed from its RGB channels, measuring the mean intensity of each channel of I, i.e. $I = [mR, mB, mG]$

Over the past few years it has emerged how difficult it is to measure and define contrast and how context-dependent its definition could be. Different approaches, like Michelson's formalization, operates just in controlled and point-wise situations under restrictive conditions. The traditional global contrast measures are unsuitable for many field of application, in fact they provide just a measure of the maximum difference in luminance and chromaticity. As a consequence, today, an unequivocal definition of contrast still does not exist [253]. The evaluation of image contrast is often made globally as the ratio between the brightest (P_{max}) and the darkest pixel (P_{min}) in an image.

$$C = \frac{P_{max}}{P_{min}} \tag{7.9}$$

The limits of contrast global measures in digital imaging, are underlined by the facts that this measure provides only a general evaluation of the maximum differences in luminance and chromaticity. Peli, in [254] and [255] proposes a local contrast measure. The locality of contrast measure makes it suitable for the use on natural images and after Peli's work many other measures which include local features have been developed [256]–[259]. In [253], [260], [261] an efficient and local algorithm for contrast evaluation has been presented.

$$C = \sum_{\forall levels} \left(\frac{\sum_{\forall pixels} \left(\frac{\sum_{8-neigh} \frac{|p_i - p_j|}{8}}{pixels} \right)}{\#levels} \right) \tag{7.10}$$

In this algorithm the local contrast at a pixel p_i is computed as the mean value of the L^1 distance between p_i and the eight pixels in its neighborhood (p_j). After the computation of the local contrast, the mean local contrast is computed, averaging the local contrast for each pixel in the image. After this step a multi-resolution local contrast is performed averaging the mean local contrast of a set of images obtained by sub-sequentially scaling the original image I. This operation is performed on the L^* channel. In Figure 7.2 is reported a graphical representation of this operation.

In Section 6.7.1 the histograms have been found useful to assess the global distribution of tones in an image. From this a measure of deviance from Histogram Flatness (HF) is proposed to evaluate the tones distribution in an image, in comparison compared with a uniform PFD. This measure is computed as the L_1 distance between the image histogram h and the histogram of a uniform PDF h. This distance is composed as:

$$HF = \frac{1}{255} \sum_{b=0}^{255} |h(b) - y(b)| \tag{7.11}$$

Thanks to this measure it is possible to evaluate the flatness of the tones distribution in the image I. Another important feature in image quality assessment is its structure and content. To do so I propose a metric of Local Variation, named Coefficient of Local Variation (CLV). This measure is the mean value of the relative standard deviation computed for each pixel in the L^* channel of an image. This basic statistical value is useful to measure the local dispersion of the probability distribution of L^*, and can be related to contrast and brightness informations, thus to the variance in image content.

7.2.2 Limits of a unique image quality index

Despite subjective evaluation of IQ is very popular in many applications e.g. image restoration, colorization and noise removal, in some cases, it may be poorly reliable since biased by the personal issues. Therefore, an objective evaluation, i.e. an image quality assessment based on visual features extracted from the image and mathematically modeled, is highly desirable, since it guaranties the repeatability of the results and enables the automation of the image quality measurement. Here the crucial point is the detection of the visual element salient for IQ. Many objective, numerical measures have been proposed in the literature. They differ to each other in the features considered to be relevant to IQ and in the presence of a reference image, i.e. and image of "perfect" quality with which to compare the image to be judged. By this way, the objective measures are broadly classified as full-reference, reduced-reference, and no-reference upon the availability of reference information. In Figure 7.3 are presented different enhancements of the same original image. To assess which enhancement provides a better quality different full-reference and no-reference measures have been compared and are reported in Table 7.2.

Considering the results reported in Table 7.2 RSR is the image enhancement method which reports more values of good quality according to measures like MSE, PSNR, MS-SSIM. Nevertheless, different image enhancement methods made on the original image provides good visual results and enhance different image features, like colors, details or luminance. Thus, due to the complexity of the IQ assessment process, a single measure may be not robust and accurate enough to capture and numerically summarize all the aspects concurring to IQ. Therefore, I propose to employ multiple objective IQ measures assembled in a cockpit of objective IQ measures. In this way, the use basic metrics to measure specific image features, like brightness or contrast, could be useful to assess which aspect is corrected or enhanced by a specific technique, and define why a specific result is more suitable for a determined field of application than an alternative one. An example is provided by the measures of brightness (B), contrast (C) or histogram flatness (HF) in Table 7.2. The image with higher brightness or contrast is not always the one with the better quality. As well an image with high deviance from histogram flatness is not always the one with the better tones distribution. However, if we use all those features together it is possible

Metric	Reference	Low Exposure	CLAHE L	CLAHE RGB	GREAT	LIME	NPEA	RSR	STAR
Full Reference Metrics									
MSE	-	849	2215	3059	3526	5160	4748	497	5992
PSNR	-	19	15	13	13	11	11	21	10
NK	-	1	1	1	1	2	2	1	2
AD	-	21.155	-29	-39	-55	-67	-62	-20	-74
SC	-	2.953	0.498	0.415	0.365	0.278	0.326	0.641	0.270
MD	-	117	176	177	65	22	48	31	61
NAE	-	0.396	0.662	0.838	1.074	1.254	1.175	0.367	1.405
S-CIELAB	-	0	106	107	0	0	174	0	0
MS-SSIM	-	0.875	0.657	0.589	0.806	0.729	0.594	0.878	0.767
FSIM	-	0.9253	0.7278	0.6911	0.8500	0.8182	0.7681	0.948	0.8335
HaarPSI	-	0.7598	0.4717	0.3987	0.5269	0.5696	0.4442	0.6004	0.4577
MAD	-	81.277	147.237	152.417	129.462	123.443	154.051	82.358	130.036
No-Reference Metrics									
BRISQUE	40.722	46.164	28.286	27.328	33.804	30.531	29.637	25.340	18.724
NIQUE	3.823	4.134	3.294	3.589	3.474	4.218	4.340	3.490	3.495
B	50.670	30.772	80.419	90.807	109.721	115.971	111.027	74.956	129.470
C	11.074	6.124	24.092	25.701	13.766	20.595	17.487	14.974	15.252
HF	0.005	0.006	0.003	0.002	0.005	0.003	0.004	0.004	0.004

TABLE 7.2: Results of different image quality metrics applied on the test images. Highlighted in green the values with higher quality for each metric.

to assess if a specific image enhancement method increases the color, the details or specific features in an image. For example thanks to this method it is possible to assess that CLAHE RGB (Figure 7.3d) provides the highest contrast and a high value of brightness, so in this image are visible more details than in the original image, but more noise can be present. This is just a preliminary assessment which will be developed in the following Sections, but the main idea is that a single image quality measure (even the more accurate) is not sufficient to assess the overall quality of an image. Thus I propose the idea of a framework to provide not only an extensive analysis and overview of features relevant to image quality, but also a tool to automate the selection of algorithms devoted to image enhancement.

7.3 The proposed framework

The aim of image quality assessment is to provide a measure of *readability* of the visual content. The IQMs must capture the visual properties of the images and translate them in a single value or a set of numbers. Since, as explained in Section 7.2.2, a single measure can hardly express all the features of quality of an image, I propose a different approach [25]: a cockpit of IQM (see Figure 7.4).

The proposed framework computes different measures of quality based on the different features of an image, and provides to the user a status of the image or video content, like the cockpit of a car or of an airplane. In this framework the user can control the performances of enhancement or restoration occurring in the image/video during he whole process, as a pilot controls the status of the airplane during the flight. In the IQM cockpit the measures are kept separated, and the interpretation of their semantic meaning is left to the user. Thus, in the cockpit is included a set of popular and intuitive no-reference objective measures, which capture basic visual perceptual features related to the image readability.

Since the needs of quality are different in every field of application, the main idea of the cockpit is to left the interpretation of the quality results to the expert user, who is free to add the IQM of the cockpit other non-visual features proper of the field

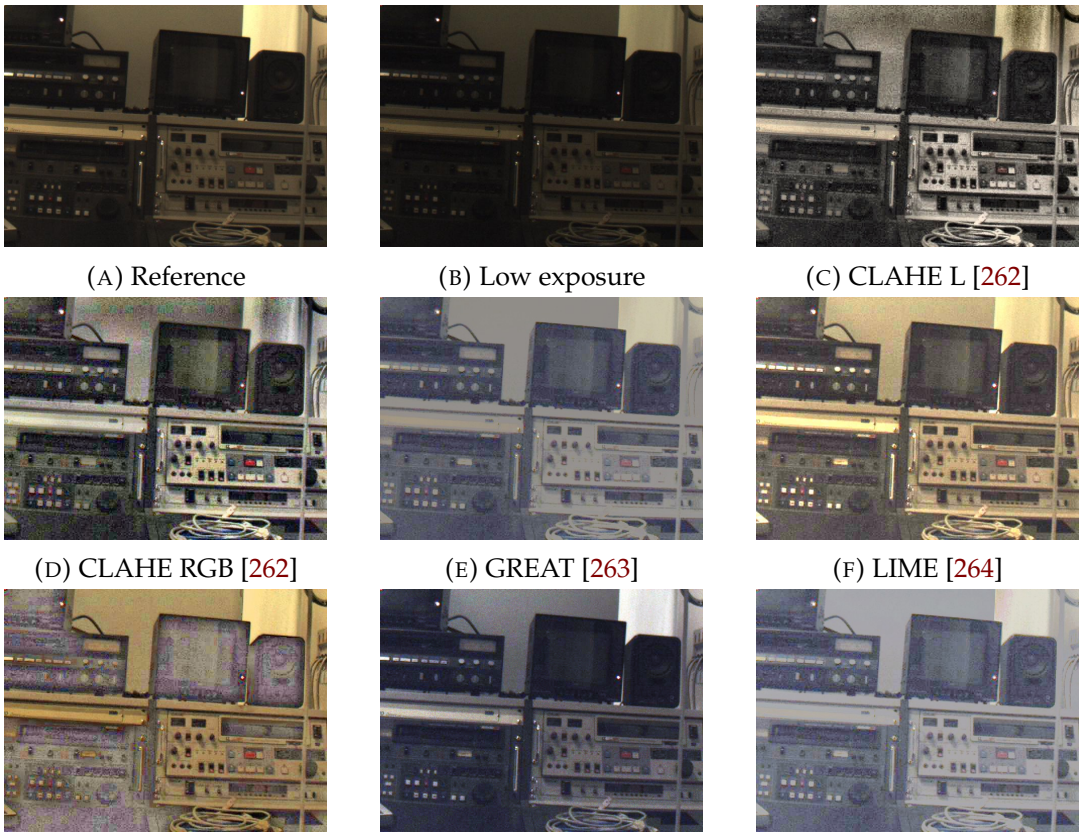

(A) Reference (B) Low exposure (C) CLAHE L [262]

(D) CLAHE RGB [262] (E) GREAT [263] (F) LIME [264]

(G) NPEA [265] (H) RSR N=20, n=200 (I) STAR [266]

FIGURE 7.3: Original image 7.3a used as reference in full-reference measures and subject to different image enhancement methods.

of application (e.g, image content, usability). In this way, the user and the quality dimensions (see [240]) are the center of the data interpretation process.

The cockpit approach differs greatly from the recent spreading approaches which tries to provide a single image quality measure by merging together different image features. The new systems uses vector regression models and machine learning systems, to extract the image features and merge them in a unique image quality index. The main limit of this approach is that the user is provided with just one quality value and the motivation behind the result are not provided. Thus, it does not considers the quality necessities of different field of applications, and if the user wants to improve the resulting image quality, he will never be able to understand which image characteristics have caused the achieved quality measure.

7.3.1 IQM Cockpit: a first prototype

The basic version of the cockpit proposed in this study takes as input a single image or a video (set of single images), and estimates some no-reference objective metrics. This is a basic version because the features that I propose are just a set of standard measures assessing image quality, and other features can be employed or added.

This framework strongly differs from recently spreading approaches, where different IQ measures describing specific image features are merged together to obtain a unique measure of visual quality. A representative example is presented by Gu et al in [267]. Here, the authors merge seventeen image quality measures using the LIBSVM (Library for Support Vector Machines) support regression model [268], which

FIGURE 7.4: The idea cockpit of image quality.

is trained on a set of automatically generated images. One of the main limits of this approach is that the unique IQ measure provided to this system is not justified, it provides just a number. As consequence, if this model provides a low IQ value, the user cannot be able to implement the image enhancement method, because it is extremely complex to deduce the image features which caused the given result. Furthermore, a machine learning approach must cope with the problem of training videos taking into account also non-visual features that may change over time. Let I be the RGB input image or a single video frame and let L^* be the luminance channel of the image converted in CIELAB color space (gamma 2.2 and D65 light source). The measures provided by the basic cockpit are:

- Mean Lightness (ΔL^*): it is the mean intensity of all the pixels in channel L^*.
- Mean RGB intensities ($\Delta R, \Delta G, \Delta B$): mean intensity of all the pixels in each channel of I.
- Contrast (C): the image local contrast is computed as exposed in Section 7.2.1.
- Histogram Flatness (HF): is the deviance from histogram flatness (see Section 7.2.1).
- Coefficient of Local Variation (CLV): it is the mean value of the relative standard deviation computed at each pixel of L^*.
- Color difference (ΔE): it is the normalized sum of color difference (CIE ΔE) between two consecutive images/frames.

The proposed set of NR measures is capable of describing the overall level of *readability* of the image content and at quantifying the perceptual difference between the original film and the restored versions [165]. The readability, i.e. the human understanding of the observed scene and of its details [25], can be modeled using five popular image features (see [269], [270]): brightness, contrast, color distribution, entropy, local color variation and color changes. Furthermore, the values of ΔL^*, C and HF can effectively correlate with human judgment as demonstrated in [266] and [270]. This framework has been called *cockpit*, because it acts exactly like a car or airplane cockpit, computing the parameters controlling the video or image status and the performances of the image enhancement workflow. Thanks to this, the IQ measures are kept separated and their semantic meaning is left to the expert operators, who merge and use them to assess the global performance of the enhancement

method, according to their experience and to the restoration aim. Thanks to this approach the expert or the curator are at the center of the data interpretation process [271] and they can interpret the IQ measure eventually considering other non-visual features. This concept is fundamental in film restoration quality assessment, where the enhanced image or video must be coherent with non-measurable features e.g., the original materials or technique, the historical period, the public.

7.4 Image quality in film restoration

In film restoration, quality control is always made and supervised by the curator, who defines the restoration pipeline based on the consecutive results obtained by each step of the restoration process. Its evaluation is based on its own professionalism and experience and controls are made comparing the restored films with the original film or with films from the same historical period, when the original is missing. The lack of trustworthy references in (digital) film restoration is one of the main limits in the application of the so called Full-Reference and Reduced-Reference metrics. Since FR methods assess the quality of restoration by comparing the restored image to the original reference image, while RR methods compare some features computed from the restored image to those computed on the original image. Unfortunately, even film stored in perfect conditions are subject to decay and aging, which makes impossible to have the original reference of a film from the age in which it was shoot (Figure 7.5). As a consequence, the No-Reference metrics, which do not need any reference, are the most suited for this purpose. Nowadays, many NR metrics are based on the use of Neural Networks (NN) and, synthetically, sort a quality value starting from a set of test images on which the NN is trained. Such metrics employ commonly used test images not effectively representing the range and variety of different scenes a director or artist may have recorded [26]. Furthermore, the film bases and technologies used during the years (e.g., Technicolor, Kinemacolor, Tinted and Toned films) present unique features and colors that differ fundamentally from natural pristine images or from existing image datasets. As consequence, today, the biggest restoration laboratories entrust film curators to assess the quality of restored movies, leaving the assessment of the whole restoration work to the subjective judgment of a film expert. Therefore, the subjective assessment made by domain experts could never be replaced by a single IQ measure, because the restoration process involves different enhancements on specific film features that cannot be synthesized by one metric. In this study, I focused mainly on the idea of using the a framework of IQ metrics to support the work of the curator or the restorer providing a set of low-level mathematical measures based on single image features (e.g., brightness, contrast, color) to assess the enhancement and the correction introduced during the restoration process. In Section 7.5 different examples are reported and the limits and potentials of this novel framework for the evaluation of IQ in film restoration applications are presented and analyzed .

7.4.1 “Raccolta della carta nelle scuole”

In Section 6.7.1 the restoration of the Super8 film “Raccolta della carta nelle scuole” (“Paper recycling at school”) has been presented. After the division in sequences and the key frame extraction the colors of the whole film have been restored using ACE algorithm. The original film is a home-video format (Super8) shoot during the ’80, so it is fundamental to preserve the aim and the mood of the original film, which

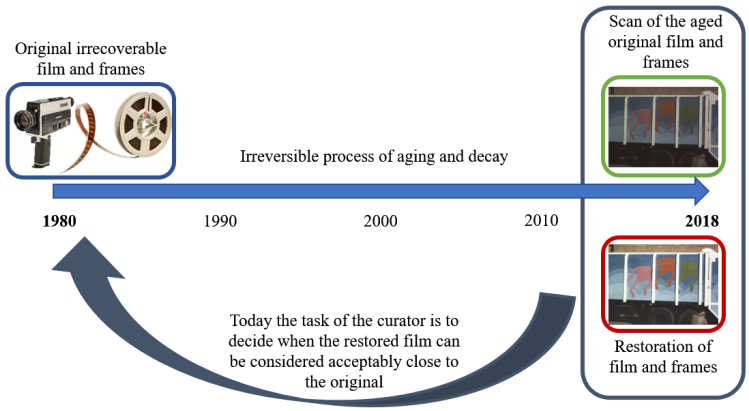

FIGURE 7.5: Graphic explanation of the problem of reference in film restoration. Figure reproduced from [26].

FIGURE 7.6: Example of the same frame restored through three different values of ACE parameter (slope 5, 10, 20 and 30). Figure reproduced from [26].

is radically different from current video quality. Thus, the main challenge of this work is to define how to correctly assess the quality of historical video restorations, without references and with unique features which cannot be compared with actual pristine images. The use of objective image quality metrics has been tested at first for ACE parameter tuning and secondly to assess the final image quality.

7.4.2 IQ metrics for ACE parameter tuning

The use of image quality metrics could be useful to objectively assess the best value of slope/contrast in ACE image enhancement. In Figure 7.6 is presented an example of an original frame of the video "Raccolta della carta nelle scuole" enhanced with slope 5, 10, 20 and 30.

To evaluate the best slope value for ACE enhancement at first some FR image quality metrics have been tested.

In Table 7.3 is possible to see that by increasing the slope, the difference between the reference and the enhanced image increases, but not linearly. Nevertheless, the FR values are generic and are useful to numerically express the difference between the enhancement and the reference, but are not decisive to tune the parameter. In general, all the IQ assessments reports an increase of image difference with the increase of ACE slope, except for S-CIELAB, which is not sensible enough to detect the variation among the images. As reported in Figure 7.7, some FR metrics report

Metric	Original	ACE 1	ACE 2	ACE 3	ACE 4
MSE	-	1.92E+07	2.07E+07	2.28E+07	2.36E+07
PSNR	-	153.00	149.62	145.44	144.04
NK	-	14.02	14.14	14.20	14.22
AD	-	-415.92	-415.99	-415.37	-415.39
SC	-	0.50	0.49	0.48	0.48
MD	-	-12.00	-2.00	10.00	14.00
NAE	-	0.48	0.48	0.49	0.49
S-CIELAB	-	0.00	0.00	0.00	0.00
MS-SSIM	-	0.94	0.89	0.84	0.82
FSIM	-	0.96	0.92	0.88	0.86
HaarPSI	-	0.64	0.58	0.53	0.51
MAD	-	76.18	94.37	107.55	111.06

TABLE 7.3: Values of full-reference IQ metrics for the original frame (reference) and the different enhancements (see Figure 7.6). Highlighted in green the values with higher quality for each metric. Table reproduced from [26].

a map of image difference between the reference and the enhancement. These maps could be the most useful for ACE parameter evaluation. In fact, thanks to the maps of difference it is possible to detect the areas in which the enhancement affects the frame the most and to evaluate the enhancement magnitude. For example, thanks to the maps of difference provided by SSIM and HDR-VDP, it is possible to determine whereas ACE excessively increase the image contrast producing burnings and artifacts. In this context, FR metrics can be useful to support the parameter choice in ACE algorithm, even if data interpretation is still required and if their performances are strictly dependent on the complexity of the scene. In the context of film restoration, the FR metrics could be particularly useful to identify operations of film restoration *per se* (e.g., dust and scratch removal).

To tune ACE parameter for film restoration, also some NR metrics have been proposed:

Metric	Original	ACE 1	ACE 2	ACE 3	ACE 4
C	0.1	0.12	0.13	0.13	0.13
L*	35.45	52.49	52.33	52.13	52.07
R	102.68	127.72	127.70	127.64	127.65
G	81.89	127.63	127.65	127.55	127.55
B	63.71	127.69	127.74	127.82	127.81
HF	10529.76	9568.74	6489.27	4069.6	3622.52
BRISQUE	38.68	36.9	30.4	27.01	26.65
NIQUE	4.39	3.89	3.94	3.95	3.89

TABLE 7.4: Values of contrast, brightness and deviance from histogram flatness for the original frame and its different enhancements (see Figure 7.6). Table reproduced from [26].

Considering the NR assessment of the images in Figure 7.6, it is possible to see that the $L*$ and RGB values increase quite constantly with the slope. On the other hand, the value of local contrast increase in ACE1 and ACE2 but then it remains

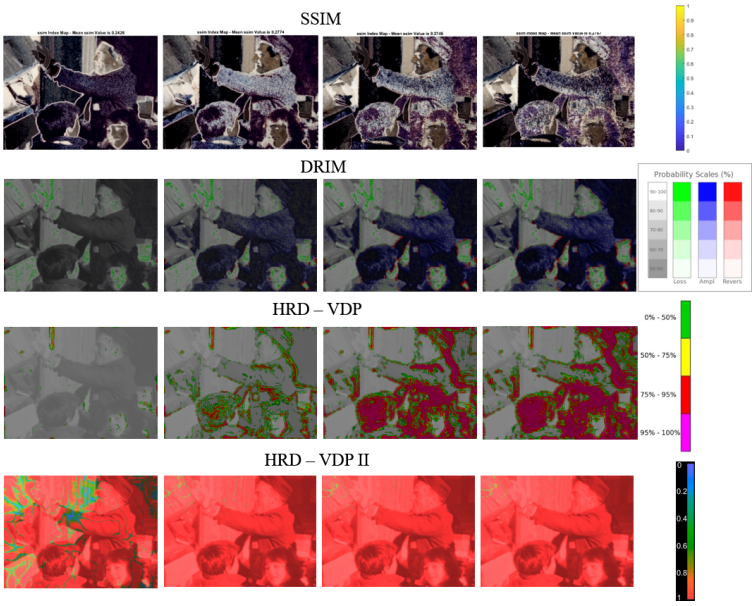

FIGURE 7.7: Maps of differences of some FR IQ metrics for ACE parameter evaluation (see Figure 7.6). Figure reproduced from [26].

constant for ACE3 and ACE4. The proposed values of brightness, contrast and divergence from histogram flatness are simple and intuitive. These values if considered singularly are not particularly significant, but together could provide a good overview of the enhancement provided by the increment of slope. For example it is possible to assess that an increment of slope, produces a decrease of $L*$, thus a darker image. Furthermore, the analysis of the single RGB channels allow to report a decrease of R and G values compensated by an increment of B channel. Considering now the BRISQUE and NIQE values, the best image is obtained with a slope of 30 and the original image is considered the worst one. The main limit of these IQ assessments is that use default training sets that neither include samples of movies from the '80 nor show typical film distortions. In addition, those metrics are complex and difficult to understand for non-expert users. The trend of BRISQUE and NIQE to associate higher quality to higher slope values (i.e. contrast) could also lead to wrong restorations, especially when the original frame presents faded colors and an excessive contrast could produce artifacts. Nevertheless, the combined use of basic NR metrics allow to support ACE parameter tuning and to support with objective measures the user's decisions.

7.4.3 IQ metrics for film restoration assessment

To assess the final quality of the restoration of the film "Raccolta della carta nelle scuole", some FR and NR metrics have been tested.

For ACE restoration evaluation, the basic FR metrics (MSE, PSNR, KN, AD, SC, MD, NAE) are too simple and general to have good overall quality evaluation, especially do to their non-correlation with the HVS. Also in this application, S-CIELAB provides a worthless result evidenced by the completely dark map of differences (Figure 7.9). The SSIM and DRIM maps of difference evidence an increment of contrast and brightness in the shadows and in the high lights. In the same way, HDR-VDP evidence an increment of contrast in the darkest area of the image. In general the FR metrics are suitable to detect the main changes introduced by ACE, but it

(A) (B)

FIGURE 7.8: Example of frame restoration through ACE. Figures 7.8a is the original frames and 7.8b the ones restored with ACE algorithm (slope 3). Figure reproduced from [26].

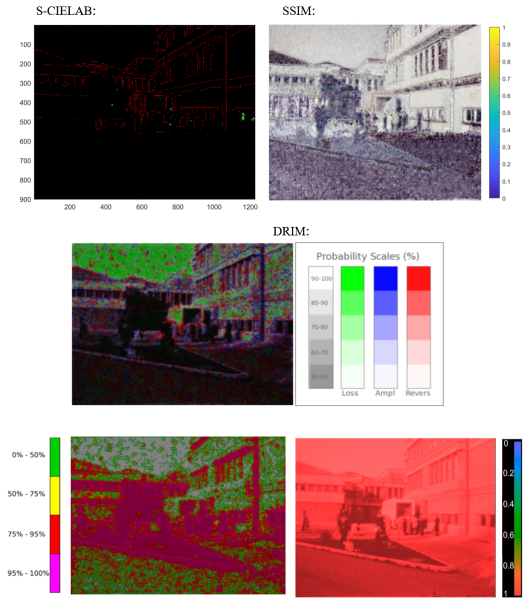

FIGURE 7.9: Maps of differences of some FR IQ metrics for ACE restoration evaluation (referred to frames in Figure 7.8). Table reproduced from [26].

Metric	Original	ACE
FR Metrics		
MSE	-	1.81E+03
PSNR	-	15.56
NK	-	1.44
AD	-	-21.33
SC	-	0.46
MD	-	41.00
NAE	-	0.46
S-CIELAB	-	160.00
MS-SSIM	-	0.82
FSIM	-	0.52
HaarPSI	-	0.61
MAD	-	114.18
NR Metrics		
C	0.07	0.15
L*	29.19	37.45
R	73.57	91.77
G	69.33	92.18
B	66.28	95.32
HF	13484	7823.96
BRISQUE	42.03	44.29
NIQUE	5.41	4.91

TABLE 7.5: Values of FR and NR IQ metrics for the original frame and its ACE enhancement (see Figure 7.8). Table reproduced from [26].

is not clear if the increment of contrast generated artifacts or error in the image, furthermore their performance is strictly dependent on image content. Considering now the NR metrics, an increment of contrast and brightness is reported. In this case, BRISQUE and NIQE values are representative of the best quality of the restored image and could be used for numerical evaluation. In this application, the use of IQ metrics is more complex than for parameters tuning, and the absence of a trustworthy reference leave the final quality assessment to the curator and to his subjective judgment. In fact, to assess the overall quality of a restoration, a single IQ metric can not be used as unique numerical judgment for a restoration process. It must be used as instrument to indicate the direction and the modifications introduced by an algorithms or a process of image enhancement. In this way the objective IQ assessment can support the work of technicians and curators, underlining the changes that restoration algorithms apply on frames. Nevertheless, the problem of a unique and correct quality measure for frames evaluation still persists, in this preliminary study, it has been demonstrated that some metrics exist and their combined use could give advice and support to the work of restorers.

7.5 IQ Cockpit for film restoration quality assessment

Image quality metrics are devised to assess standard images, so to help in researching their best possible quality. In film restoration the main goal is not the achievement of a perfect image, but of an image as close as possible to the original materials [26]. Thus, old movies present specific color gamuts or color casts, but also visual

defects peculiar of specific techniques which must be preserved and appreciated as an integral part of a film beauty. In the complex contest of film restoration, a single quality value can hardly provide a reliable assessment about the effect of the restoration operations. Due to this, a framework of IQ measures could support the work of restorers and curators in describing and evaluating the global and local visual properties of an image or a set of frames. In this work, the IQ Cockpit proposed in Section 7.3.1 will be tested and analyzed for film restoration applications. Here, the IQ Cockpit published in [165] and [26] has been developed, implemented and a Web application (named *MoReCo* - MOvie REstoration Cockpit) has been proposed and published in [25]. *MoReCo* has been implemented using HTML, Chart.js, PHP and Matlab R2018a, it is free and open source [1]. This web application gives to the users the possibility to upload and compare up to two videos using the cockpit NR measures of mI, mL, MRC, HF, CLV, and ΔE. This application took as input one or two videos and gives as output six charts. If only one video is uploaded as input, the charts show just the data relative to the single video, if two videos are uploaded the charts shows a frames comparison between the two videos. All the charts produced by this application can be downloaded as PNG images. To test and analyze the usefulness and reliability of the cockpit, the proposed framework has been tested on different films restored through one or more restoration algorithms (see Table 7.6).

Film	**Cardinality**	**Main Characteristics** Before Restoration	**Applied Enhancers (Parameters)**
Fiat 508 (1931)	888	Black and White movie Flickering Dust and Scratches Silver Fading	Phoenix (Manual) + ACE (slope 5)
La lunga calza verde (1961)	363	Animation Movie Colour Fading	STRESS ($M = 200$, $N = 20$)
La Ciudad en la Playa (1961)	125	Super8 movie Strong colour fading Dust and Scratches	RSR ($N = 200$, $n = 20$)
The funerals of the bombing of Piazza della Loggia in Brescia (1974) (see Section 6.7.1)	261	Super8 movie Colour fading Dust and Scratches Instability	Phoenix + DaVinci Resolve ACE (slope 3) CLAHE applied on L^* channel ($N = [0, 01]$)

TABLE 7.6: Title of the films, cardinality, principal characteristics, and the exploited enhancers with the values of their parameters. Table reproduced from [25].

As presented in Section 7.3.1, the cockpit framework employs five no-reference IQ measures. In this case four film scenes have been analyzed, thus these metrics have been applied frame-by-frame to measure the overall readability of the different enhancements. More specifically, these metrics have been implemented and computed as following. Let I be a frame of the video under analysis expressed in RGB coordinates and let L^* be the luminance channel derived from the conversion of the RGB coordinates of the image I in $CIEL^*a^*b^*$ color space (with a gamma of 2.2 and the D65 as reference illuminant):

- $mI = [mR, mB, mG]$: mean intensity of each RGB channel in the image I.
- mL: mean intensity of the L^* channel of I.
- MRC (Multi Resolution Contrast): in this implementation a scaling factor 4 has been applied, so the original image has been scaled for a maximum of 4

[1] MoReCo is available here: `http://159.149.129.182/moreco` Access credentials will be provided upon email request at: alice.plutino@unimi.it"

times ($K = 4$). The scaling factor is computed so that the minimum dimension of the scaled image is not less than 25 pixels. The size of the images among L^* (original) and L^*_4 (fourth scaling) is uniformly distributed between the sizes L^* and L^*_4.

- HF: the deviance from histogram flatness measures the entropy in L^*. In the original formulation [272] the value of HF is computed in each RGB channel. In this application the HF is computed in L^*, as in [270].
- CLV: the Coefficient of Local Variation is computed in a 9×9 window centered at each pixel in L^*. In this application, the neighborhood of pixels near the image borders is assumed having the same values of the nearest pixels in the border.
- ΔE: is the sum of color differences between two consecutive frames in $CIEL^*a^*b^*$ color space.

When using the IQ Cockpit it is important to notice that reference values of mI, mL, MRC, HF, CLV, ΔE do not exists, since these measures depend strictly on the image content. As consequence specific values of these metrics do not correspond to good or bad enhancements, but they can express if an image is over- or under-exposed, or if colors are faded or saturated, or if an enhancement method produced noise in the output. Thus, each measure must be interpreted and the intervention of an expert user is essential to define how to restore an image or a video.

The results of the application of the IQ Cockpit to the film presented in Table 7.6 are presented in Figures 7.10, 7.11, 7.12 and 7.13. The film "Fiat 508" (Figure 7.10) is a black and white video which presents faded contrast, flickering and a strong damage at the 435th frame. This video has been restored manually through Phoenix Finish Software [217] and the color correction has been made through ACE algorithm. The restoration increased the values of mI and mL, but the blue dominant (see mB value) of the original video is preserved also after the restoration. The local contrast in the frames has been increased as well as the overall HF. Thus, the histogram entropy has been increased by the growth of image contrast. The restoration of "La Lunga Calza Verde" was published in 2005 in [273] and made with STRESS algorithm [146]. The selected scene presents an animation, where the frames are uniformly colored in red (from the 80th and the 99th frames). This trend is confirmed by the mI plot (see Figure 7.11a), where mR curve strongly increase in correspondence of the red frames. In this application, STRESS increased the intensities of the three RGB channels in the image and of image contrast. In this scene the overall HF decreased and the color difference among frames (ΔE) remained constant, so even if STRESS produced more brighter and contrasted images, no flickering has been introduced. Considering now, "La Ciudad en La Playa" (see Figure 7.12), this film has been restored using RSR [147]. The original video presents strongly faded colors. The film restoration produced an increase of luminance in the scene, but it caused also an increase in the difference among mR, mG and mB producing a growth in the inter-frame variability of the R channel. This factor, combined with the strong increase of intra-frame ΔE suggested a possible introduction of flickering in the scene with an over-saturation of colors. Through RSR the local contrast, the deviance from histogram flatness and the coefficient of local variation have been increased, indicating that the restoration revealed more details in the image. In this case, the RSR enhancement may produce some errors in the output, so the cockpit allowed in identifying the pros and cons of this restoration algorithm. In conclusion, in this Section I analyze the restoration

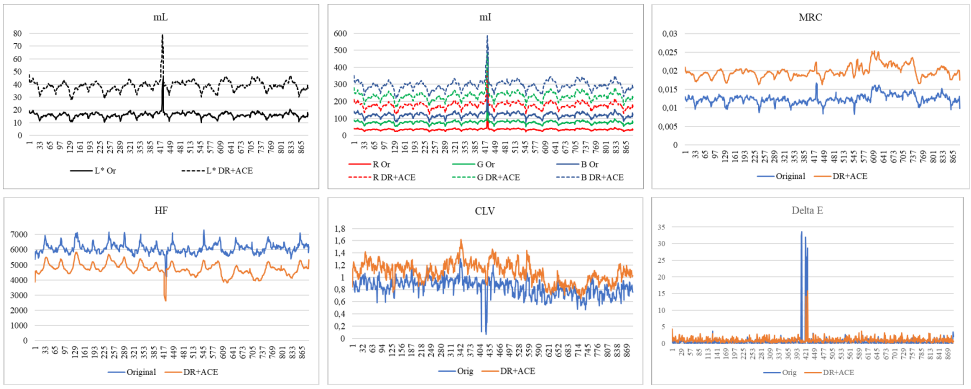

(A)

(B)

FIGURE 7.10: In Figure 7.10a, the plots of mL, mI, MRC (top), HF, CLV and ΔE (bottom) for frames of the video "Fiat 508", in Figure 7.10b. Figures reproduced from [25].

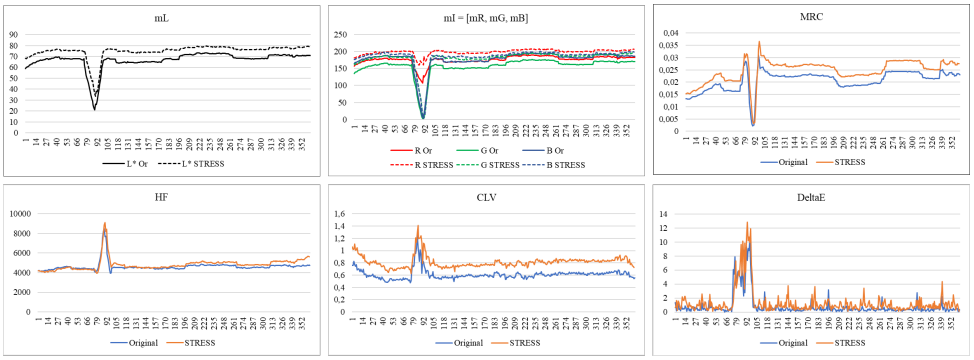

(A)

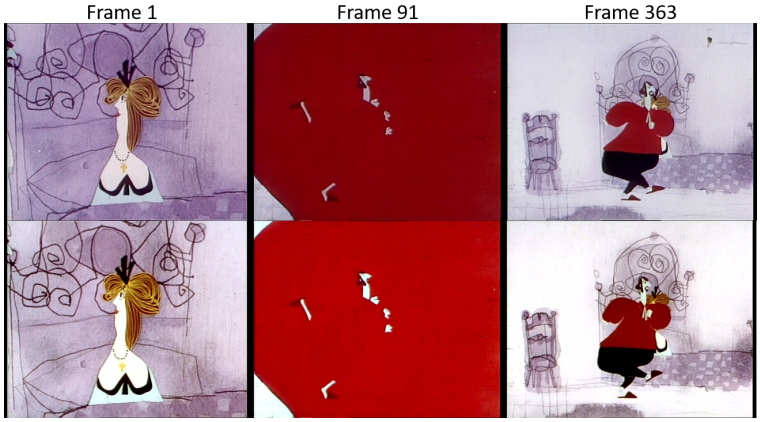

(B)

FIGURE 7.11: In Figure 7.11a, the plots of *mL*, *mI*, *MRC* (top), *HF*, *CLV* and ΔE (bottom) for frames of the video "La Lunga Calza Verde", in Figure 7.11b. Figures reproduced from [25]. Figures reproduced from [25].

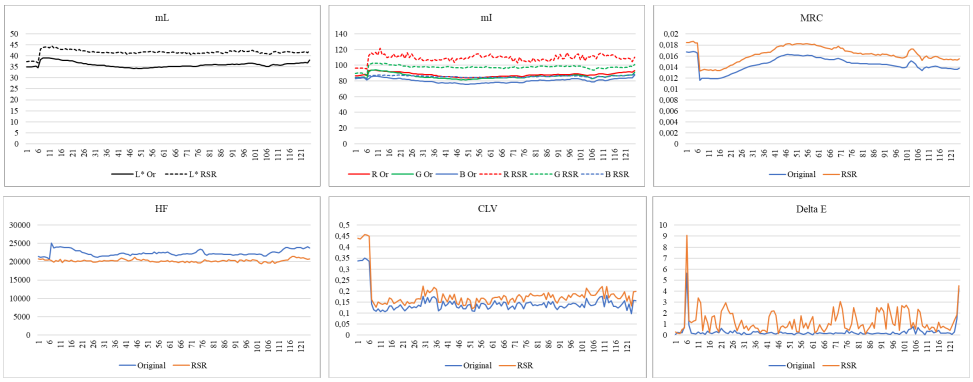

(A)

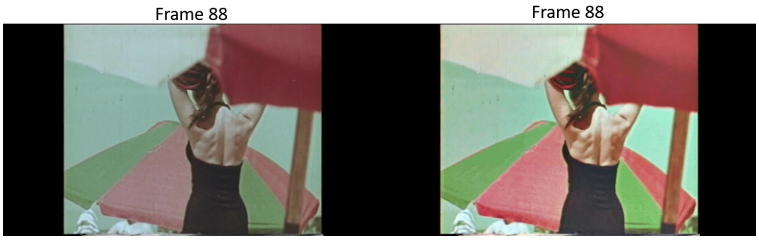

(B)

FIGURE 7.12: In Figure 7.12a, the plots of mL, mI, MRC (top), HF, CLV and ΔE (bottom) for frames of the video "La ciudad en la playa", in Figure 7.12b. Figures reproduced from [25].

of the video "The funerals of the bombing of Piazza della Loggia in Brescia" presented in Section 6.7.1. Here the manual and ACE restoration has been compared with the restoration through CLAHE algorithm [141]. In this application the manual restoration through Da Vinci and Phoenix Finish decreased the overall luminance mL, but increased the value of MRC. ACE produced a luminance similar to the original video, while CLAHE generated a great increase of mL. The greater value of HF is provided by CLAHE algorithm even if ACE and the manual restoration provided higher values of CLV. The manual restoration produced a strong color difference between frames especially around the 172th frame and the 197th frame. This strong difference could indicate some error caused by the subjective restoration. The application of the IQ cockpit to three different restoration of the video of "The funerals of the bombing of Piazza della Loggia in Brescia" demonstrate that different enhancement algorithms provide different results. Thus, the cockpit is a valuable instrument to guide operators and experts in the objective identification of the method which provides best results for the final restoration aim.

In this work, the cockpit has been found as a valuable alternative approach to assess image and video quality, which can support the work of the experts in film restoration assessment application. In my future work I aim at developing and expand the measures of the IQ cockpit inserting more IQ measures and eventually offering a clustering of the results.

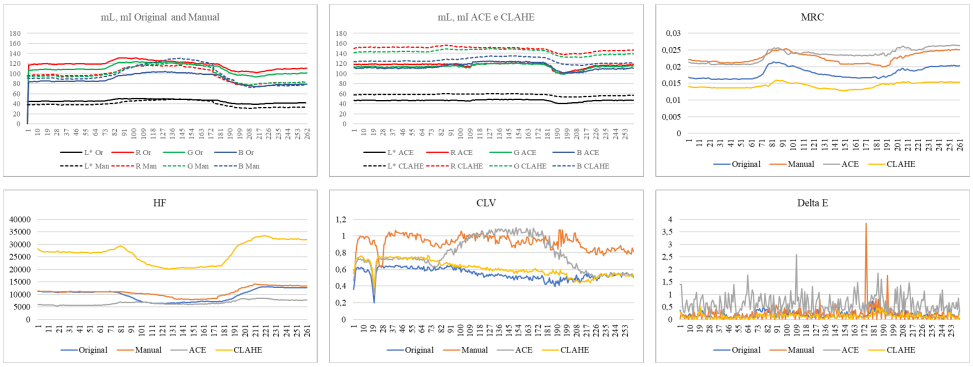

(A)

(B)

FIGURE 7.13: In Figure 7.13a, the plots of *mL*, *mI*, *MRC* (top), *HF*, *CLV* and ΔE (bottom) for frames of the video "The funerals of the bombing of Piazza della Loggia in Brescia", in Figure 7.13b. Figures reproduced from [25].

Chapter 8

Conclusion

In this work, among a wide variety of applications, the most common issues an limits of colorimetry have been analyzed, focusing mainly on the topics of: color assessment, color acquisition and processing and quality assessment.

Colorimetry is a science branch, which aims at studying and model the HVS, in order to specify color through numbers and objective measures. In Chapter 1, many questions concerning the adequacy of standard colorimetry have been highlighted, and its application in non-standard conditions has been critically analyzed and discussed. During the different historical phases of colorimetry, a series of specific assumptions and constraints have been developed and their use has become increasingly unpractical, so much that in everyday applications these constraints are often not respected or excessively approximated. Even the newest CAMs models are not applicable in many real conditions. Anyway, the actual need to measure and manage color led to approximations or non-compliance of the colorimetric constrains, producing mismatches between color measures and color sensations, as well as subjective assessments.

The field of cultural heritage is particularly suitable to underline the limits in the application of standard colorimetry, because in this context, color is never observed as isolated phenomenon, but always inside a spatial arrangement. In cultural heritage, in fact, colorimetry is used to analyze, reproduce and manage color limited to aperture mode (i.e., as isolated phenomenon), and its application is unpractical and erroneous whenever color sensation is the result of an high-level elaboration of the HVS. In this work, film digital restoration is the main field of application and different approaches and alternative methods have been proposed to overcome the limits of standard color analysis. In this thesis, the highlighted limits and the presented solutions characterize film restoration, as well as many other fields of application, where color analysis can not be limited to point-wise colorimetry. For this reason through this thesis, I aim at rising the awareness of the scientific community on this topic, to find new commonly shared methods and solutions leading to a wider applicable colorimetry and to a more accurate color acquisition, management and reproduction. The following Tables 8.1, 8.2 and 8.3 summarize the current colorimetric ground truth, the identified open issues and the novel proposed approaches for each considered topic.

In the first part of my thesis, starting from the current literature and the most recent developments, I presented a critical overview of colorimetry phases of color matching, color difference and color appearance.

The main limit of color matching is that all the phenomena consequent to cones activation are not considered and the aperture mode constraints strongly limits the application of psychophysical colorimetry in real conditions of observation. As a consequence, the color difference systems have been developed to provide color specification on uniform perceived scales and to present a first practical modeling

Ground Truth	Open Issues	Proposed approach
Color sensation depends on: the light source spectrum, the optical properties of the object surface and the spatial elaboration of the visual system.	The rigorous application of pointwise-based colorimetry is still insufficient to reproduce and manage colors faithfully, because it fails in scenes with non-standard illumination conditions, in real circumstances and for complex objects.	**Lighting for museums and collections** (Section 3.2) Color rendering indexes (CRI, TM-30) are not appropriate to measure the quality of the light sources. Proposal of a new model to assess the quality of the light sources based on Brilliance, Pleasantness and Satisfaction. Color difference measures (ΔE) are inappropriate to evaluate color in complex scenes. There is the need to develop new models which considers the higher-level elaboration of the signal made by the human visual system to assess color in complex spatial arrangements. **Assessing color of gemstones** (Section 3.3) Spectral measurements are insufficient to measure objects with pleochroism properties. Proposal of a new system for subjective gemstones color assessment based on visual comparison with the Munsell Atlas.

TABLE 8.1: Overview of the thesis contribution in the field of color assessment.

of color appearance. Even if these systems allow to overcome the aperture mode, they are approximative and inadequate to describe the complexity of color appearance. Psychometric colorimetry is extremely practical and widely used, but there is the strong need to develop new systems to model color perception in complex scenes, considering spatial interactions. In fact, even the more modern models of color appearance are limited to a small set of configurations.

In practical applications, standard colorimetry is extremely accurate in pointwise conditions of controlled illumination and standard direction of observation. Nevertheless, due to the complexity of the colorimetric Standard Systems, color analysis is often made without respecting the constraints and the colorimetric measures and indexes are used to reconstruct colors or assess the quality of light sources also in conditions of non-uniform illumination or complex scenes. In these contexts, the standard colorimetry fails, because the model on which it is based is limited to the transduction level (retina) of the human visual system and does not consider the higher-level elaboration of visual spatial processing. As a consequence, many indexes and measures (e.g., Color Rendering Index or color difference measures) are insufficient and imprecise when applied in complex scenes or non-standard conditions.

In order to present some limits of applicability of the colorimetric constraints and underline the need to develop new color computing methods applicable to real and complex scenes, a preliminary experiment involving human observers has been made. This application queries the adequacy of color rendering indexes to give an estimate of the perceptive quality of a light source or of an illumination set-up, especially for complex scenes like museums or expositions. Thanks to this application, it has been underlined the unsuitability of psychometric colorimetry for complex scenes analysis, like museums or collections, where phenomena of spatial processing occur. In this context, a first solution to have more accurate measure, based on Brilliance, Pleasantness and Satisfaction, has been proposed and the results have been discussed.

A second experiment, to assess the color in gemstones, has been made to test the suitability of standard spectroscopy in the analysis of objects which show phenomena of pleochroism. In this case, a subjective color assessment using the Munsell color Atlas as reference, has been found more suitable and precise at this purpose.

The second main topic of this thesis is color acquisition and processing. Today, many standard protocols, target and calibration methods exists to prevent the formation of artifacts and error in acquisition. Despite the many standardized instruments and tool to obtain a correct acquisition, there are no solutions for systematic errors occurring in all the acquisition systems which uses lenses (i.e., glare). In this work, a common hyperspectral imaging system has been tested and the phenomena of glare has been evidenced. This effect is systematic and unavoidable, and thanks to the use of a novel metric called *Glare Effect (GE)*, it has been possible to measure and analyze the systematic reduction of contrast in the acquired images. Therefore, in addition to new commonly shared metrics and methodologies to measure and control glare effect in imaging systems, it is fundamental to study and increase the research on this phenomenon, especially in fields like hyperspectral imaging, where data are considered quantitative spectral measures.

When working with cultural heritage, in particular in film restoration, the image processing and enhancement is a common practice to restore and retrieve the original colors. In literature, many algorithms for image enhancement have been presented, but many of them are made to enhance the colors for making them visually appreciable without considering the original information. Furthermore, in film restoration, the absence of references makes the work of the restorer even harder, and today colors in films are restored manually using video editing softwares. In this context, a novel approach to restore film color is proposed, in order to restore the original color appearance instead of the original physical colors. For this purpose, the Spatial Color Algorithms, derived from Retinex, have been found the most suitable for film restoration and color retrieval. This family of algorithms is appreciated for its capability of enhance the image contrast, revealing hidden details and being easily implementable, but has high computational costs. Among all the algorithms derived from Retinex, ACE has been considered for its wide diffusion and for its ability to enhance images depending on the content. Since ACE considers all the pixels in the input image, the computational costs are $O(n^4)$ for a linear input image resolution of n. In order to expand ACE applicability on a wider scenario, like video streams, a new speed-up named FACE has been proposed. FACE algorithm is based on the precomputed partitioning of the image around each pixel in the input image and allows an optimized computation of ACE algorithm defining the upper bound error. Thanks to this approach, it is possible to balance the algorithm accuracy with the computational time and, thanks to FACE structure, it is possible to optimize ACE application on image with the same resolution, like video streams.

Ground Truth	Open Issues	Proposed approach
To achieve a trustworthy qualitative and quantitative acquisition, it is fundamental to calibrate the system and compensate for the distorting effects. In imaging systems, the application of standard guidelines and the use of standard targets can not prevent the presence of systematic errors caused by the presence of lenses in the acquisition system.	The main effect occurring in imaging acquisitions is glare. This phenomenon is always present in imaging systems and produces a loss in contrast and information. Today, a commonly shared metric to measure glare still does not exist and this effect is usually neglected.	**Glare in HSI acquisitions** (Section 4.3) Glare effect is an unavoidable systematic error which occurs in every imaging system which uses lenses. A new measure (*Glare Effect (GE)*) to measure glare is proposed. A preliminary study on glare spectral trend is presented and new evidences on glare effect in HSI acquisitions are discussed.
Today, in cultural heritage and film restoration the image enhancement is performed subjectively and it is strictly dependent on commercial softwares. In film restoration the image/video enhancement must be faithful to the original materials and acquisition techniques.	It is necessary to define a more technical and objective approach for image restoration and enhancement in cultural heritage applications, in order to reduce the subjectivity and the software-dependency of the current methods.	**Spatial Color Algorithms for digital color restoration** (Section 6.7) The family of Spatial Color Algorithms, derived from Retinex, is the most appropriate for cultural heritage applications. A novel approach based on *appearance* restoration is proposed, using ACE (Automatic Color Equalization) algorithm. A new speed-up, FACE (Fast-ACE), has been proposed to extend the applicability of ACE algorithm on video streams.

TABLE 8.2: Overview of the thesis contribution in the field of color acquisition and processing.

In order to test and analyze the best methods to enhance and restore colors in film restoration, different objective image quality metrics have been studied and tested. The main limit in image quality assessment for film restoration is that there is a systematic lack of references, thus it is impossible to know the original appearance of a frame. Due to this, in this work I have proposed a novel framework, named Image Quality Cockpit, based on the use of different mathematically-based objective image quality metrics to assess some specific features of a restored image/video. This novel framework has been found useful for cultural heritage application, in particular as support for the restorers' work in the evaluation of the final quality of the image/video, or to assess the best method to perform an enhancement.

The work carried out in this Thesis has been both theoretical, including a deep analysis of the state of the art and literature reviews, but also practical, supporting

the theories and the statements with concrete applications and experiments.

Ground Truth	**Open Issues**	**Proposed approach**
To assess image quality in cultural heritage applications and film restoration, a single metric may not be robust and accurate enough to summarize all the aspects occurring in a enhancement and restoration process.	Today, image quality assessment in film restoration is performed subjectively by the film curator or the project manager. It is fundamental to define new methods and approaches in the context of cultural heritage and film restoration, where the references are systematically missing or untrustworthy (e.g., faded, aged, decayed).	**IQ Cockpit for film restoration quality assessment** (Section 7.5) Different objective image quality metrics to assess the quality of restored film frames have been tested. The limits of a unique image quality index have been presented. A new image quality metric framework (*IQ Cockpit*) has been proposed and tested on different film restoration datasets.

TABLE 8.3: Overview of the thesis contribution in the field of quality assessment.

8.1 List of publications

The current study led to the publication of several papers in international conferences and journals. Listed below are the main publications.

8.1.1 Journal Papers

Plutino A., Lanaro M. P., Liberini S., Rizzi A., "**Work memories in Super 8: Searching a frame quality metric for movie restoration assessment**", Journal of Cultural Heritage, 2019, DOI: 10.1016/j.culher.2019.06.008 [26].

Plutino A., Grechi L., Rizzi A., "**Evaluation of the perceived colour difference under different lighting for museum applications**", Color Culture and Science Journal Vol. 11 (2), 2019, DOI: 10.23738/CCSJ.110210 [8].

De Meo S., Plutino A. and Rizzi A., "**Assessing colour of gemstones**", Color Research and Application 2020, pp. 1-11, Wiley Periodicals Inc., 2020, DOI: 10.1002/col.22472 [22].

Barricelli B. R., Casiraghi E., Lecca M., Pluino A., and Rizzi A., "**A cockpit of multiple measures for assessing film restoration quality**", Pattern Recognition Letters, Pattern Recognition and Artificial Intelligence Techniques for Cultural Heritage special issue, available online: 8 January 2020, DOI: 10.1016/j.patrec.2020.01.009 [25].

Signoroni A., Conte M., Plutino A. and Rizzi A., "**Spatial-spectral evidence of glare influence on hyperspectral acquisitions**", Sensors 2020, 20(16), 4374; https://doi.org/10.3390/s20164374 [23].

Plutino A, Rizzi A. "**Research directions in color movie restoration**", Coloration Technol, Wiley-Blackwell, 2020; 00:1–5. https://doi.org/10.1111/cote.12488 [24] .

Plutino A. and Simone G., "**The Limits of Colorimetry in Cultural Heritage Applications**", Coloration Technology, 2020; 00: 1– 8 https://doi.org/10.1111/cote.12500 [21].

8.1.2 Books

Alice Plutino, "**Tecniche di Restauro Cinematografico – Metodi e Pratiche tra Analogico e Digitale**", Manuali n. 244, Dino Audino Editore, ISBN: 9788875274672, 2020 [274] .

8.1.3 Book Chapters

Rizzi A., Barricelli B. R., Bonanomi C., Plutino A., Lanaro M. P., "**Spatial Models of Colors for Digital Color Restoration**", Conservation, Restoration, and Analysis of Architectural and Archaeological Heritage, pp.386-404, IGI Global, 2019, DOI: 10.4018/978-1-5225-7555-9.ch015 [173] .

Plutino A. and Rizzi A., "**Algorithms for Film Digital Restoration: Unsupervised approaches for Film Frames Enhancement**", Moving Pictures, Living Machines, pp. 265-272, Editor: MIMES International, 2020, ISBN: 9788869772764, ISSN: 2420-9570 [206].

Plutino A. and Rizzi A., "**Alternative Methods for Digital Contrast Restoration**", Imagine Math 7 - Between Culture and Mathematics, Pages 73-87, edited by Michele Emmer and Marco Abate, Springer. ISBN 978-3-030-42653-8, [207] .

Bellotti S., Bottaro G., Plutino A. and Valsesia M., "**Mathematically-Based Algorithms for Film Digital Restoration**", Imagine Math 7 - Between Culture and

Mathematics, Pages 89-104, edited by Michele Emmer and Marco Abate, Springer. ISBN 978-3-030-42653-8 [208].

8.1.4 Conference Papers

Plutino A., Richard N., Deborah H., Fernandez-Maloigne C., Ludwig N. G., "**Spectral Divergence for Cultural Heritage applications**", 25th IS&T's Color and Imaging Conference (CIC), September 11-15 2017 Lillehammer (Norway), ISBN: 978-0-89208-328-2, [60] .

Plutino A., Lanaro M. P., Ghiroldi A., Cammarata R., Rizzi A., "**ACE for Super 8 movie restoration**", Poster Session, Mathematics for Computer Vision, Trento (Italy), February 15-16, 2018, [209] .

Plutino A., Lanaro M.P., Ghiroldi A., Bellotti S., Rizzi A., "**Work memories in Super8: the dawn of paper recycling in Brescia**", YOCOCU 2018: Dialogues in Cultural Heritage, Matera (Italy), May 23-25, 2018, [210].

Rizzi A., Bonanomi C., Melada J., Plutino A., "**The influence of Spatial arrangement of a scene in the stability of color appearance under different lights**", Balkan-Light2018, Sofia (Bulgary), 04-06 June 2018, [48] .

Rizzi A., Lanaro M.P., Plutino A., Liberini S., Simone G., Bellotti S., "**MIPS Lab**", CVPL, Vico Equense – Napoli (Italy), 30-31 August 2018, [275] .

Otto I., Plutino A., Lanaro M.P., Rizzi A., "**All the colours of a film: study of the chromatic variation of movies**", AIC Colours and Human Comfort, Lisboa (Portugal), 29-29 September 2018, ISSN: 2617-2410, [211].

Plutino A., Bellotti S., Lombardi C., Guerrini P., Rizzi A., "**The funerals of the bombing of Piazza della Loggia in Brescia: an example of rescue of an historical and amatorial document**", IX Conference "Diagnosis, Conservation and Valorisation of Cultural Heritage", Naples (Italy), 13-14 December 2018, [212] .

Rizzi A., Lecca M., Plutino A. and Liberini S., "**Designing a Cockpit for Image Quality Evaluation**", Transactions: Imaging/Art/Science - Image Quality, Content and Aesthetics, University of Westminster, London (UK), 26th April 2019, [165] .

Plutino A., Lecca M., Rizzi A., "**A cockpit of measures for image quality assessment in digital film restoration**", in New Trends in Image Analysis and Processing – ICIAP 2019, September 9-10 2019, Trento (Italy), DOI: https://doi.org/10.1007/978-3-030-30754-7, Springer, [213] .

Grechi. L., Plutino A., Rizzi A., "**Test percettivi per la valutazione della differenza cromatica sotto diversi illuminanti**", XV Color Conference, Gruppo del Colore, 5th – 7th September 2019, Macerata (Italy), https://gruppodelcolore.org/portfolio-articoli/macerata-2019/, [276] .

Rizzi A., Plutino A. and Rossi M., "**Fundamentals of color teaching in post-graduate education**", AIC Color and Landscape, 14 th-17th October 2019, Buenos Aires (Argentina) [277] .

Rossi M., Plutino A., Siniscalco A. and Rizzi A., "**Teaching color and color science: the experience of an international Master course**", IS&T Electronic Imaging, Color Imaging: Displaying, Processing, Hardcopy, and Applications, 26th-30th January 2020, Burlingame (California), [278] .

Plutino A. and Rizzi A., "**Film Restoration: closing the gap between humanities and hard sciences**", Science ABC hosted by Università La Sapienza di Roma, Rome, 19-21 February 2020, [279] .

Plutino A. and Rizzi A., "**Paper recycling consciousness into schools: an audio-visual evidence from the '80**", 12th Orphan Film Symposium - Water, Climate, &

Migration hosted by the 6th Eye International Conference, 23-27 May 2020, Amsterdam (NL). Online: https://wp.nyu.edu/orphanfilm/2020/06/05/brescia/, [214].

Cereda M., Rizzi A. and Plutino A., "**Quick Gamut mapping per la color correction**", XVI Conferenza del Colore 2020, 3-4 September 2020. https://gruppodelcolore.org/portfolio-articoli/bergamo-2020/, [280].

Sarti B., Plutino A. and Rizzi A., "**Glare ottico nelle immagini iperspettrali**", XVI Conferenza del Colore 2020, 3-4 September 2020. https://gruppodelcolore.org/portfolio-articoli/bergamo-2020/, [281] .

Barenghi F., Bittante M., Del Longo N., Mangano C., Plutino A. and Rizzi A., "**Uno studio sull'associazione colori, termini ed emozioni, basato sui colori primari di Lüscher**", XVI Conferenza del Colore 2020, 3-4 September 2020. https://gruppodelcolore.org/portfolio-articoli/bergamo-2020/, [282].

Gaspani M. F., Spada P. R., Plutino A. and Rizzi A., "**Un film in un frame: studio sulle variazioni cromatiche in film e video digitali**", XVI Conferenza del Colore 2020, 3-4 September 2020. https://gruppodelcolore.org/portfolio-articoli/bergamo-2020/, [283].

Scipioni S., Lombardi C. A., Giuliani L., Plutino A. and Rizzi A., "**Verso una più ampia comprensione del daltonismo: un test sulla discriminazione di colori in scene complesse**", XVI Conferenza del Colore 2020, 3-4 September 2020.https://gruppodelcolore.org/portfolio-articoli/bergamo-2020/, [284].

8.1.5 Work in progress

In Sections 5.4.1 and 5.5 are presented two works that are now in course of publication. The first, presented in Section 5.4.1 is a scoping review on the ACE algorithm. The second is FACE (Fast Automatic Color Equalization), an error-bounded approximation speed-up of ACE algorithm. Supplementary material or information can be required at: alice.plutino@unimi.it

Chapter 9

Ringraziamenti

In questi tre anni di dottorato ho avuto la possibilità di incontrare molti professionisti, studenti e insegnanti. Lavorare nell'ambito della ricerca non è da tutti, bisogna essere disposti a mettersi in gioco, ad ascoltare, a capire, a ragionare, a cambiare punto di vista e ad essere dinamici.

In questi tre anni di dottorato, che mi sembrano passati troppo velocemente, ho raggiunto molti traguardi di cui posso dirmi fiera, ma il più grande di tutti è stato l'imparare ad appezzare le correzioni e i consigli che mi sono stati dati. Dall'inizio del mio dottorato ho avuto modo di lavorare e confrontarmi con uomini e donne dalle personalità e dalle storie più disparate, e ogni giorno per me è stato occasione di crescita.

A livello scientifico e accademico, vorrei cominciare ringraziando "père Noël", ovvero la prima persona che ha creduto che io potessi avere un futuro nell'ambito della ricerca: Noël Richard. Lui fu il primo vero ricercatore con cui ho avuto la fortuna di lavorare a stretto contatto e mi ha insegnato che la ricerca non è una corsa in velocità, ma è una maratona continua, lungo la quale è necessario bilanciare le proprie energie per avere un ritmo costante. Mi ha insegnato ad appassionarmi agli argomenti di ricerca, a programmare e a godermi i week-end uscendo con gli amici e visitando i luoghi in cui mi trovavo, perché solo così si recuperano le energie per ricominciare a correre.

L'inizio del dottorato è stato strano, non conoscevo nessuno e le prime persone con cui ho avuto modo di confrontarmi sono stati i miei primi due colleghi di ufficio, Matteo e Cristian. Cristian era incredulo all'idea che una "non-informatica" fosse entrata al dottorato e, a causa del suo pessimismo cronico, mi ha descritto una strada in salita, tortuosa e piena di difficoltà che raramente mi avrebbe portata al successo. Cristian è un uomo straordinario, che ha sempre lavorato duramente e che è riuscito davvero a dare il suo contributo alla ricerca. Tutt'ora, anche se lavora in azienda e si è allontanato dal MIPS Lab, c'è sempre per qualsiasi necessità, e in laboratorio il suo posto non sarà mai occupato. Ringrazio anche Matteo, il mio vicino di scrivania per due anni, con cui ho avuto modo di confrontarmi e che mi ha aiutato a capire quali sono le priorità nel dottorato. Anche lui per me c'è sempre stato e alla fine sono riuscita ad esserci anche io per lui.

Oltre a questi due colleghi e amici, il MIPS Lab è sempre stato un punto di ritrovo per chi non sapeva dove andare e spesso mi chiedevo cosa avessero in comune tutti quei ricercatori che si occupavano di ambiti di ricerca così diversi. In laboratorio ho lavorato con Corrado, il dottorando con più esperienza che si sia mai visto, sempre schietto e diretto con tutti, ma anche estremamente generoso e disponibile, Simone, Serena, Fatima, Anton ed Elf, tutti con esperienze diverse da cui imparare. Il MIPS Lab è stato anche luogo di collaborazione, ma soprattutto amicizia con molti studenti, tra cui Luca, ovvero IL rappresentante degli studenti, che mi ha aiutato a conoscere il Dipartimento di Informatica, nelle sue persone e nelle sue fazioni

politiche. Con Luca ho condiviso risate, dispiaceri, the alla vaniglia, feste di Natale, conferenze da panico e moltissimi altri momenti di gioia e amicizia. Per questo lo voglio ringraziare individualmente, senza di lui il dipartimento di informatica sarebbe decisamente noioso e monotono.

Tra gli studenti voglio ringraziare anche Sara, che ho conosciuto prima da studentessa e poi da dottoranda, spero davvero che tu riesca a trovare la tua strada, e Manuel, il mio compagno di dottorato dall'inizio alla fine. È stato bello avere un collega con cui condividere le ansie e i dubbi sul dottorato, specialmente in quest'ultimo anno di COVID, con chiusure e proroghe; sei stato un compagno di avventura e spero che tu possa avere tutto il successo che ti meriti.

Parlando di studenti un immenso ed enorme grazie va a Serena, la mia futura arcinemica e concorrente nell'ambito del restauro cinematografico, con la quale un giorno andrò Festival del Cinema Ritrovato da donna ricca e impellicciata e ci sederemo al tavolo con registi, sceneggiatori e direttori della fotografia (e sarà Francis che vorrà abbracciare noi). È grazie a te che mi sono avvicinata al restauro cinematografico, e continuerò ad imparare da te, a starti accanto e a sostenerti in tutto ciò che farai. Sei brava, competente e appassionata, non lasciare mai che gli altri ti facciano sentire in difetto! Oltre a Serena voglio ringraziare anche Giulia, la "donna dell'ansia" che sta riuscendo veramente a fare carriera, che non si è mai lasciata abbattere e che è riuscita a tracciare la sua strada nell'archivistica. Spero che tu possa essere sempre felice, sappi che sono davvero fiera di tutto ciò che sei riuscita a fare.

Oltre a queste due compagne di avventura voglio ringraziare tutti gli studenti con i quali ho avuto a che fare per progetti, stage e tirocini. Sono davvero sincera quando dico che per me siete tutti davvero bravi quando vi appassionate ad un argomento. Adoro vedere i vostri occhi brillare quando vedete i risultati delle vostre ricerche che prendono forma, e quando realizzate che ciò che avete fatto è davvero importante. Quando si studia in università ci si dovrebbe sentire sempre così, perché ogni piccolo progetto, ogni analisi, ogni ricerca è importante e per quanto piccolo possa essere il passo che facciamo, ci conduce sempre più vicino all'ampliamento delle conoscenze, e non esiste una ricerca di serie A e una di serie B (anche se purtroppo molti ne sono ancora convinti). Io spero di essere riuscita ad essere un buon esempio per tutti i "miei" studenti e mi auguro di avervi trasmesso l'amore e la passione che ho per la ricerca. Devo ammettere, però, che in questo sono stata molto aiutata, da dei compagni che poi si sono trasformati in colleghi e amici con i quali spero di riuscire sempre a fare grandi cose. Mi riferisco a Laura, Jacopo O., Jacopo M., Miriam e Roberto. Insieme nel 2019 abbiamo fatto la prima conferenza "A Conservation Carol" e abbiamo iniziato un percorso che spero possa durare ancora per molti anni e che possa valorizzare sempre di più il lavoro dei Conservator Scientists. In particolare, voglio ringraziare Laura la nostra "capa", che è decisamente più un'amica che una collega. Grazie per esserci sempre stata per avermi seguita e supportata a volte anche nelle mie idee più pazze, spero di essere riuscita a fare lo stesso con te.

Dopo aver parlato dei miei colleghi e amici giunge il momento di ringraziare le cinque persone più importanti in assoluto per il mio dottorato e sappiate che in queste poche righe riuscirò a esprimere solo una parte di ciò che siete stati per me in questo percorso. Forse non tutti sanno che il primo activity report della mia attività di dottorato non è andato bene, sono stata valutata in modo sufficiente, ma nel mio sconforto mi è stato detto di non preoccuparmi, perché facevo parte di un ottimo gruppo di ricerca che sarebbe riuscito sicuramente a sostenermi e migliorarmi. Ed è stato esattamente così. Dopo quel momento di sconforto ho continuato a lavorare,

a pubblicare e ho avuto la soddisfazione di veder crescere il mio H-Index e i miei successi, e tutto grazie al miglior gruppo di ricerca che potessi desiderare.

In primis vorrei ringraziare Barbara, la mia co-supervisor. Ci tengo a dire che avevo pensato molto all'idea di trovarmi qualcuno a fianco di Rizzi per supervisionare il mio lavoro, e tu sei stata la scelta migliore. Quasi non ci conoscevamo quando sei diventata la mia co-supervisor, ma ho sempre ammirato la tua determinazione e la tua sicurezza. Da me hai sempre preteso il massimo e anche se per lunghi periodi non ci siamo sentite, mi ha sempre dato sicurezza, ho sempre saputo di poter contare su di te e mi sei stata accanto in ogni momento cruciale del mio dottorato. Grazie.

Oltre a Barbara vorrei dire un enorme grazie anche a Elena. Lavorare con te è sempre sorprendente ed entusiasmante! Sei una persona straordinaria, e sai rendere divertenti anche le commissioni di laurea. Sono felice di aver condiviso una grossa parte del mio percorso con te e spero di continuare a farlo.

Nel corso del mio ultimo anno di dottorato ho avuto modo di conoscere come collega e come amico anche Gabriele Simone, che devo assolutamente ringraziare per essermi stato accanto e avermi aiutato nelle mie indecisioni e nella stesura di questa tesi. Grazie a te ho imparato tanto sulla colorimetria di Oleari e la tua esperienza mi ha concretamente aiutata ad avere successo in quest'ultimo anno. Spero di poter presto festeggiare con te con un aperitivo sul nostro lago.

Oltre che con Gabriele ho lavorato tantissimo anche con Marco, che mi ha sopportata nella programmazione e con il quale ho giocato a costruire pattern sempre più belli per i nostri progetti di speed-up. Marco io ti ringrazio di cuore, perché credi e hai creduto in me e nelle mie potenzialità nonostante i miei limiti. Grazie perché sai apprezzare e vedere il potenziale nella mia natura di sirena, come dici tu, metà umanista e metà informatica. Oltre ad un ottimo professore e un ricercatore straordinario sei stato un amico e spero che la vita ci porterà a fare ancora tanti colorati progetti insieme. Grazie per la tua creatività, fantasia e genialità.

Infine, il ringraziamento più importante va al mio supervisor Alessandro Rizzi (che non riuscirò mai a chiamare solamente per nome). Quando abbiamo iniziato il nostro primo progetto insieme ho trovato in lui professore diverso da tutti gli altri, guidato dall'entusiasmo e dalla passione per ciò che spiega. Ci siamo subito trovati, nel modo di organizzarci, di pianificare e di progettare. In queste righe vorrei ringraziarla con il cuore in mano per tutte le energie che mi ha dedicato, per le volte in cui mi ha difesa e supportata, ma soprattutto per avermi spinta ad uscire dalla mia zona di comfort, ad osare, a parlare con altri ricercatori e professori e ad espormi. Lei ha saputo darmi tutta la sicurezza di cui avevo bisogno, mi ha mostrato come uscire dagli schemi e mi ha insegnato che i dubbi e le domande sono il primo punto di partenza per fare una buona ricerca. Come dico spesso per me questo dottorato è stata un'esperienza meravigliosa, che rifarei per altri tre anni, e il merito principale è suo. Ora che il dottorato è finito mi sa che dovrà sopportarmi ancora per qualche anno, perché io ho ancora troppe cose da imparare, progetti da continuare e bandi da vincere (**finger crossed**) e mi piacerebbe farlo con lei.

Giunta a questo punto sono felice di poter dire che voglio continuare a proseguire il mio cammino nella ricerca, che non mi farò abbattere dalle poche possibilità fondamentalmente perché tutte le persone che ho elencato fino ad ora mi hanno portata ad amare questo lavoro, ad appassionarmi ed entusiasmarmi, e con il sorriso in volto e dei compagni di viaggio come questi è molto più semplice affrontare le difficoltà.

A questo punto dei ringraziamenti, voglio dire grazie alle persone più importanti della mia vita. Il primo immenso grazie va a mia mamma, mio papà e Luca, coloro che mi sono sempre accanto in ogni momento della mia vita. Grazie soprattutto perché nonostante la mia scelta di studiare materie sempre più astruse e complicate

da spiegare, avete sempre cercato di capire, interessarvi e appoggiarmi in quello che facevo. Vi voglio immensamente bene.

Oltre a loro, vorrei ringraziare anche il membro più importante della nuova piccola famiglia di cui faccio parte, Matteo. Questi ultimi mesi si preannunciavano come terribili a causa della consegna della tesi e l'incertezza sul futuro, uniti ai lockdowns e alla pandemia mondiale in corso, insomma, non il periodo ideale per iniziare una convivenza. Così però non è stato, e tutti questi momenti si sono rivelati di una bellezza unica e rara, un fiore in un abisso. Hai saputo portare un sorriso nelle giornate più tristi, sei riuscito a tirarmi fuori dalle mie spirali di inquietudine e sei sempre stato qui, vicino a me, pronto a rasserenarmi con una carezza o un piccolo gesto di affetto. Hai sempre creduto in me e continui a farlo, ogni giorno. Questo mio successo è anche per te.

Ora che questi ringraziamenti volgono alla conclusione, e che finisce il mio percorso di dottorato, un pensiero va alla mia persona, alla mia migliore amica e a colei che so, che il giorno della mia proclamazione sarà felice anche più di me per questo successo. Lucilla. Spero che il tuo percorso di dottorato sia arricchente e positivo come è stato il mio e so già che la tua sezione di ringraziamenti a fine Tesi sarà ancora più lunga della mia per tutte le persone che ti avranno aiutato e supportato nei tuoi progetti. Ricordati di me quando prenderai il nobel e quando sarai ministro della Repubblica, perché sono sicura che per te il PhD sarà solo l'inizio. Eh si, che lo vogliamo o no, io e te abbiamo deciso che quello che abbiamo non ci basta e punteremo sempre più in alto. L'importante è continuare a farlo insieme.

It always seems impossible until it is done

[Nelson Mandela]

Bibliography

[1] Y. Ohno, "Cie fundamentals for color measurements", in *NIP & Digital Fabrication Conference*, Society for Imaging Science and Technology, vol. 2000, 2000, pp. 540–545.

[2] CIE, "International lighting vocabulary", CIE 17.4-1987, ISBN 978 3 900734 07 7D. Lgs. n.112/98 art. 150 comma 6, Tech. Rep., 1987.

[3] ——, "Cie publication n. 15:2004, colorimetry, 3rd edition", CIE Central Bureau, Kegelstrasse 27, A-1030, Wien, Austria, Tech. Rep., 2004.

[4] J. Schanda, *Colorimetry: understanding the CIE system*. John Wiley & Sons, 2007.

[5] C. Oleari, *Standard colorimetry: definitions, algorithms and software*. John Wiley & Sons, 2016.

[6] I. E. Society, "Ies methods for evaluating light source color rendition", pp. ISBN-13: 978-87995-379-9, Tech. Rep., 2018.

[7] S. Robinson, *System and method for light source identification*, US Patent App. 12/279,419, 2009.

[8] A. Plutino, L. Grechi, and A. Rizzi, "Evaluation of the perceived colour difference under different lighting for museum applications", *Cultura e Scienza del Colore-Color Culture and Science*, vol. 11, no. 02, pp. 90–97, 2019.

[9] G. Gauglitz and D. S. Moore, *Handbook of spectroscopy*. Wiley-VCH Weinheim, Germany, 2014.

[10] T. Theophile, *Infrared spectroscopy: Materials science, engineering and technology*. BoD–Books on Demand, 2012.

[11] J. C. Lindon, G. E. Tranter, and D. Koppenaal, *Encyclopedia of spectroscopy and spectrometry*. Academic Press, 2016.

[12] E. Land and J. McCann, "Lightness and retinex theory", *Journal of the Optical Society of America*, pp. 1–11, 1971.

[13] E. Land, "The retinex theory of color vision", *Sci. Amer*, pp. 108–128, 1977.

[14] J. J. McCann, "Retinex algorithms: Many spatial processes used to solve many different problems", *Electron. Imaging*, 1–10, 2016.

[15] M. D. Fairchild and L. Reniff, "Propagation of random errors in spectrophotometric colorimetry", *Color Research and Application*, vol. 16, no. 6, pp. 360–367, 1991. DOI: 10.1002/col.5080160605.

[16] A. R. Robertson, "Colorimetric significance of spectrophotometric errors", *JOSA*, vol. 57, no. 5, pp. 691–698, 1967. DOI: 10.1364/JOSA.57.000691.

[17] C. F. Hall and E. L. Hall, "A nonlinear model for the spatial characteristics of the human visual system", *IEEE Transactions on systems, man, and cybernetics*, vol. 7, no. 3, pp. 161–170, 1977.

[18] H. Hofer, B. Singer, and D. Williams, "Different sensations from cones with the same photopigment", *Journal of Vision*, vol. 5, no. 5, pp. 444–454, 2005. DOI: 10.1167/5.5.5.

[19] L. Enticknap, *The culture and science of audiovisual heritage*. Palgrave MacMillan, 2013.

[20] C. Haine, *Color Grading 101: Getting Started Color Grading for Editors, Cinematographers, Directors, and Aspiring Colorists*. Routledge, 2019.

[21] A. Plutino and G. Simone, "The limits of colorimetry in cultural heritage applications", *Coloration Technology, Special Issue: Challenges and Open Problems in Colorimetry Special Issue*,

[22] S. De Meo, A. Plutino, and A. Rizzi, "Assessing color of gemstones", *Color Research & Application*, vol. 45, no. 2, pp. 224–234, 2020.

[23] A. Signoroni, M. Conte, A. Plutino, and A. Rizzi, "Spatial–spectral evidence of glare influence on hyperspectral acquisitions", *Sensors*, vol. 20, no. 16, p. 4374, 2020.

[24] A. Plutino and A. Rizzi, "Research directions in color movie restoration", *Coloration Technology, Special Issue: Challenges and Open Problems in Colorimetry Special Issue*,

[25] B. R. Barricelli, E. Casiraghi, M. Lecca, A. Plutino, and A. Rizzi, "A cockpit of multiple measures for assessing film restoration quality", *Pattern Recognition Letters*, vol. 131, pp. 178–184, 2020.

[26] A. Plutino, M. P. Lanaro, S. Liberini, and A. Rizzi, "Work memories in super 8: Searching a frame quality metric for movie restoration assessment", *Wournal of Cultural Heritage*, 2019, ISSN: 1296-2074. DOI: 10.1016/j.culher.2019.06.008.

[27] R. Cajal, *Histologie du systéme nerveux de l'homme et des vertébrés*. Paris - Maloine, 1911, vol. 1, p. 1012.

[28] M. F. Bear, B. W. Connors, and P. M.A., *Neuroscience: Exploring the Brain*. Lippincott Williams & Wilkins, 1996.

[29] G. Osterberg, *Topography of the layer of rods and cones in the human retina*. Acta Ophthalmol, 1935.

[30] C. A. Curcio, K. R. Sloan, R. E. Kalina, and A. E. Hendrickson, "Human photoreceptor topography", *Journal of Comparative Neurology*, vol. 292 (4), 497–523, 1990. DOI: 10.1002/cne.902920402.

[31] J. Bowmaker and H. Dartnall, "Visual pigments of rods and cones in a human retina.", *The Journal of Physiology*, vol. 298, pp. 501–511, 1980. DOI: 10.1113/jphysiol.1980.sp013097.

[32] C. Oleari, *Misurare il Colore*. Hoepli, 2015.

[33] CIE, "Cie proceedings", Tech. Rep., 1951, p. 37.

[34] A. Rizzi, "Colour after colorimetry", *Coloration Technology*, 2020.

[35] ——, "What if colorimetry does not work", in *Color Imaging XXVI: Displaying, Processing, Hardcopy, and Applications*, IS&T Electronic Imaging 2021, 2021.

[36] M. Plank, *The Theory of Heat Radiation*. Blakiston's Sons & Co., 1912.

[37] G. Sharma and C. E. Rodríguez-Pardo, "The dark side of cielab", in *Color Imaging XVII: Displaying, Processing, Hardcopy, and Applications*, International Society for Optics and Photonics, vol. 8292, 2012, p. 82920D.

[38] M. E. Chevreul, *The principles of harmony and contrast of colours, and their applications to the arts*. Longman, Brown, Green, and Longmans, 1855.

[39] W. Davis and Y. Ohno, "Toward an improved color rendering metric", vol. 5941, 2005, pp. 1–8. DOI: 10.1117/12.615388.

[40] N. Moroney, M. D. Fairchild, R. W. G. Hunt, C. Li, M. R. Luo, and T. Newman, "The ciecam02 color appearance model", in *Color and Imaging Conference*, Society for Imaging Science & Technology, vol. 2002, 2002, pp. 23–27.

[41] N. Sándor and J. Schanda, "Visual colour rendering based on colour difference evaluations", *Lighting Research and Technology*, vol. 38, no. 3, pp. 225–239, 2006.

[42] J. McCann and A. Rizzi, *The art and science of HDR imaging*. Jan. 2012. DOI: 10.1002/9781119951483.ch8.

[43] V. Vonikakis, A. Rizzi, and J. J. McCann, *HDR Scene Capture and Appearance*. Jan. 2017. DOI: https://doi.org/10.1117/3.2315540.ch1.

[44] M. H. Brill, "Irregularity in ciecam02 and its avoidance", *Color Research & Application: Endorsed by Inter-Society Color Council, The Colour Group (Great Britain), Canadian Society for Color, Color Science Association of Japan, Dutch Society for the Study of Color, The Swedish Colour Centre Foundation, Colour Society of Australia, Centre Français de la Couleur*, vol. 31, no. 2, pp. 142–145, 2006.

[45] M. H. Brill and S. Süsstrunk, "Repairing gamut problems in ciecam02: A progress report", *Color Research & Application: Endorsed by Inter-Society Color Council, The Colour Group (Great Britain), Canadian Society for Color, Color Science Association of Japan, Dutch Society for the Study of Color, The Swedish Colour Centre Foundation, Colour Society of Australia, Centre Français de la Couleur*, vol. 33, no. 5, pp. 424–426, 2008.

[46] M. H. Brill and M. Mahy, "Visualization of mathematical inconsistencies in ciecam02", *Color Research & Application*, vol. 38, no. 3, pp. 188–195, 2013.

[47] M. D. Fairchild, *Color appearance models*. John Wiley & Sons, 2013.

[48] A. Rizzi, C. Bonanomi, M Jacopo, and A. Plutino, "The influence of spatial arrangement of a scene in the stability of color appearance under different lights", in *Balkan Conference and Exhibition on Lighting*, 2018.

[49] S. Grusche, "Basic slit spectroscope reveals three-dimensional scenes through diagonal slices of hyperspectral cubes", *Applied optics*, vol. 53, no. 20, pp. 4594–4603, 2014.

[50] F. France, "Advanced spectral imaging for noninvasive microanalysis of cultural heritage materials: Review of application to documents in the u.s. library of congress", *Applied Spectroscopy*, vol. 65, no. 6, pp. 565–574, 2011. DOI: 10.1366/11-06295.

[51] T. Peery and D. Messinger, "Msi vs. hsi in cultural heritage imaging", vol. 10768, 2018. DOI: 10.1117/12.2320671.

[52] C. Cucci and A. Casini, "Hyperspectral imaging for artworks investigation", *Data Handling in Science and Technology*, vol. 32, pp. 583–604, 2020. DOI: 10.1016/B978-0-444-63977-6.00023-7.

[53] C. Oleari, "Colorimetria e beni culturali - prefazione", ser. Atti dei convegni di Firenze 1999 e Venezia 2000 - Società italiana di ottica e fotonica, Gruppo di Lavoro in Colorimetria e Reflectoscopia, Firenze 1999 e Venezia 2000.

[54] G. Bitossi, R. Giorgi, M. Mauro, B. Salvadori, and L. Dei, "Spectroscopic techniques in cultural heritage conservation: A survey", *Applied Spectroscopy Reviews*, vol. 40, no. 3, pp. 187–228, 2005.

[55] A. Cosentino, "Identification of pigments by multispectral imaging; a flowchart method", *Heritage Science*, vol. 2, no. 1, pp. 1–12, 2014.

[56] F. Casadio, C. Daher, and L. Bellot-Gurlet, "Raman spectroscopy of cultural heritage materials: Overview of applications and new frontiers in instrumentation, sampling modalities, and data processing", *Analytical Chemistry for Cultural Heritage*, pp. 161–211, 2017.

[57] M. Bacci, S. Baronti, A. Casini, P. Castagna, R. Linari, A. Orlando, M. Picollo, and B. Radicati, "Detection of alteration products in artworks by non-destructive spectroscopic analysis", vol. 352, 1995, pp. 153–159.

[58] R. Giorgi, L. Dei, M. Ceccato, C. Schettino, and P. Baglioni, "Nanotechnologies for conservation of cultural heritage: Paper and canvas deacidification", *Langmuir*, vol. 18, 21, pp. 8198–8203, 2002. DOI: 10.1021/la025964d.

[59] A. Bartoletti, R. Barker, D. Chelazzi, N. Bonelli, P. Baglioni, J. Lee, L. Angelova, and B. Ormsby, "Reviving whaam! a comparative evaluation of cleaning systems for the conservation treatment of roy lichtenstein's iconic painting", *Heritage Science*, vol. 8, 1, 2020. DOI: 10.1186/s40494-020-0350-2.

[60] A. Plutino, N. Richard, H. Deborah, C. Fernandez-Maloigne, and N. Ludwig, "Spectral divergence for cultural heritage applications", IS&T/SID Color Imaging Conference, 25 September 2017, 2017, pp. 141–146.

[61] E. Grifoni, S. Legnaioli, P. Nieri, B. Campanella, G. Lorenzetti, S. Pagnotta, F. Poggialini, and V. Palleschi, "Construction and comparison of 3d multisource multi-band models for cultural heritage applications", *Journal of Cultural Heritage*, vol. 34, pp. 261–267, 2018. DOI: 10.1016/j.culher.2018.04.014.

[62] E. Grifoni, B. Campanella, S. Legnaioli, G. Lorenzetti, L. Marras, S. Pagnotta, V. Palleschi, F. Poggialini, E. Salerno, and A. Tonazzini, "A new infrared true-color approach for visible-infrared multispectral image analysis", *Journal on Computing and Cultural Heritage*, vol. 12, 2, 2019. DOI: 10.1145/3241065.

[63] F. Apollonio, M. Ballabeni, S. Bertacchi, F. Fallavollita, R. Foschi, and M. Gaiani, "Digital documentation and restoration tools reusing existing imagery: A multipurpose model of the neptune's fountain in bologna", *Applied Geomatics*, vol. 10, pp. 295–316, 2018. DOI: 10.1007/s12518-018-0210-x.

[64] M. Gaiani, F. Apollonio, and F. Fantini, "Evaluating smartphones color fidelity and metric accuracy for the 3d documentation of small artifacts", vol. 42, 2/W11, 2019, pp. 539–547. DOI: 10.5194/isprs-Archives-XLII-2-W11-539-2019.

[65] E. H. Land, "Color vision and the natural imahe. part i", *Proceedings of the National Academy of Sciences*, vol. 45, no. 1, pp. 115–129, 1959, ISSN: 0027-8424. DOI: 10.1073/pnas.45.1.115.

[66] ——, "Experiments in color vision", *Scientific American*, vol. 200, no. 5, pp. 84–99, 1959. DOI: http://dx.doi.org/10.1038/scientificamerican0559-84.

[67] X rite photo& video, *Colorchecker classic*, 2020. [Online]. Available: https://xritephoto.com/ph_product_overview.aspx?id=1192&catid=28 (visited on 11/25/2020).

[68] D. Camuffo, *Microclimate for Cultural Heritage: Conservation, Restoration, and Maintenance of Indoor and Outdoor Monuments: Second Edition*. 2014, pp. 1–526. DOI: 10.1016/C2013-0-00676-7.

[69] M. La Gennusa, G. Rizzo, G. Scaccianoce, and F. Nicoletti, "Control of indoor environments in heritage buildings: Experimental measurements in an old italian museum and proposal of a methodology", *Journal of Cultural Heritage*, vol. 6, no. 2, pp. 147–155, 2005. DOI: 10.1016/j.culher.2005.03.001.

[70] M. P.I.B. E. LE and A. CULTURALI, "Atto di indirizzo sui criteri tecnico-scientifici e sugli standard di funzionamento e sviluppo dei musei", Technical report, Italian Law, Tech. Rep., 2001.

[71] E. I. di Normazione, "Uni 10829/99 - beni di interesse storico e artistico. condizioni ambientali di conservazione. misurazione ed analisi", UNI, Tech. Rep., 1999.

[72] ——, "Uni cen/ts 16163:2014. conservazione dei beni culturali - linee guida e procedure per scegliere l'illuminazione adatta a esposizioni in ambienti interni", UNI, Tech. Rep., 2014.

[73] S. Boissard and M. Fontoynont, "Optimization of led-based light blendings for object presentation", *Color Research & Application: Endorsed by Inter-Society Color Council, The Colour Group (Great Britain), Canadian Society for Color, Color Science Association of Japan, Dutch Society for the Study of Color, The Swedish Colour Centre Foundation, Colour Society of Australia, Centre Français de la Couleur*, vol. 34, no. 4, pp. 310–320, 2009.

[74] P. D. Pinto, J. M. M. Linhares, and S. M. C. Nascimento, "Correlated color temperature preferred by observers for illumination of artistic paintings", *JOSA A*, vol. 25, no. 3, pp. 623–630, 2008.

[75] P. D. Pinto, J. M. Linhares, J. A. Carvalhal, and S. M. Nascimento, "Psychophysical estimation of the best illumination for appreciation of renaissance paintings", *Visual Neuroscience*, vol. 23, no. 3-4, pp. 669–674, 2006.

[76] M. Scuello, I. Abramov, J. Gordon, and S. Weintraub, "Museum lighting: Optimizing the illuminant", *Color Research & Application: Endorsed by Inter-Society Color Council, The Colour Group (Great Britain), Canadian Society for Color, Color Science Association of Japan, Dutch Society for the Study of Color, The Swedish Colour Centre Foundation, Colour Society of Australia, Centre Français de la Couleur*, vol. 29, no. 2, pp. 121–127, 2004.

[77] F. Viénot, G. Coron, and B. Lavédrine, "Leds as a tool to enhance faded colours of museums artefacts", *Journal of Cultural Heritage*, vol. 12, no. 4, pp. 431–440, 2011.

[78] S. M. Nascimento and O. Masuda, "Psychophysical optimization of lighting spectra for naturalness, preference, and chromatic diversity", *JOSA A*, vol. 29, no. 2, A144–A151, 2012.

[79] S. M. C. Nascimento and O. Masuda, "Best lighting for visual appreciation of artistic paintings—experiments with real paintings and real illumination", *JOSA A*, vol. 31, no. 4, A214–A219, 2014.

[80] D Vázquez, J. M. de Luna, A Alvarez, A Sánchez, and U Sedano, "Study of chromatic variations between metameres by varying the lighting in the painting" boy in a turban holding a nosegay" by michiel sweerts", in *Optical Systems Design 2012*, International Society for Optics and Photonics, vol. 8550, 2012, p. 855 035.

[81] A. Rizzi, C. Bonanomi, L. Blaso, O. Li Rosi, and S. Fumagalli, "The effect of lighting changes on simultaneous colour contrast: A new aspect of colour rendition", *Coloration Technology*, vol. 134, no. 3, pp. 214–221, 2018.

[82] D. Pascale, "Rgb coordinates of the macbeth colorchecker", *The BabelColor Company*, vol. 6, 2006.

[83] R. W. Hughes, W. Manorotkul, and E. B. Hughes, *Ruby & Sapphire: A Gemologist's Guide*. RWH Publishing, 2017.

[84] J. M. King, R. H. Geurts, A. M. Gilbertson, and J. E. Shigley, "Color grading" d-to-z" diamonds at the gia laboratory.", *Gems & Gemology*, vol. 44, no. 4, 2008.

[85] G. R. Rossman, "The geochemistry of gems and its relevance to gemology: Different traces, different prices", *Elements*, vol. 5, no. 3, pp. 159–162, 2009.

[86] A. H. Munsell, *A Color Notation*. G. H. Ellis Company, 1905.

[87] K. A. Valente, E. R. Reuter, and R. M. Wagner, *Gemstone evaluation system*, US Patent 5,615,005, 1997.

[88] P. Centore, "Shadow series in the munsell system", *Color Research & Application*, vol. 38, no. 1, pp. 58–64, 2013.

[89] Y. Sekita and M. Omodani, "Subjective assessment of color naturalness of objects illuminated by led light sources with various color rendering index and color temperature", 2013, pp. 48–51.

[90] E. Ioanid, A. Ioanid, B. Goraş, and L. Goraş, "Assessment of the cleaning effect of hf cold plasma by statistical processing of photographic image", *Measurement: Journal of the International Measurement Confederation*, vol. 46, no. 8, pp. 2569–2576, 2013. DOI: 10.1016/j.measurement.2013.03.020.

[91] M. Sammartino, C. Genova, S. Ronca, G. Cau, and G. Visco, "A cheap protocol for colour measure and for diagnostic in planning a cultural heritage restoration. case study: Main façade of palazzo governi (cagliari, sardinia, italy)", *Environmental Science and Pollution Research*, vol. 24, no. 16, pp. 13 979–13 989, 2017. DOI: 10.1007/s11356-016-8160-5.

[92] ——, "A cheap protocol for colour measure and for diagnostic in planning a cultural heritage restoration. case study: Main façade of palazzo governi (cagliari, sardinia, italy)", *Environmental Science and Pollution Research*, vol. 24, no. 16, pp. 13 979–13 989, 2017. DOI: 10.1007/s11356-016-8160-5.

[93] R. C. Gonzalez, R. E. Woods, *et al.*, *Digital image processing*. Prentice hall Upper Saddle River, NJ, 2002.

[94] R. Szeliski, *Computer Vision: Algorithms and Applications*. Springer-Nature New York Inc, 2010. DOI: ISBN-10:1848829345.

[95] G. Healey and R. Kondepudy, "Radiometric ccd camera calibration and noise estimation", *IEEE Trans. Pattern Anal. Mach. Intell.*, vol. 16, pp. 267–276, 1994.

[96] Y. Tsin, V. Ramesh, and K. T., "Statistical calibration of ccd imaging process", *IEEE International Conference on Computer Vision, year=2001, volume=1, pages=480-487*,

[97] C. Liu, R. Szeliski, S. Bing Kang, C. L. Zitnick, and W. T. Freeman, "Automatic estimation and removal of noise from a single image", *IEEE Transactions on Pattern Analysis and Machine Intelligence*, vol. 30, no. 2, pp. 299–314, 2008.

[98] S. Bianco, A. Bruna, F. Naccari, and R. Schettini, "Color correction pipeline optimization for digital cameras", *Journal of Electronic Imaging*, vol. 22, no. 2, 2013. DOI: 10.1117/1.JEI.22.2.023014.

[99] R. Ramanath, W. E. Snyder, Y. Yoo, and M. S. Drew, "Color image processing pipeline - a general survey of digital still camera processing", *IEEE Signal Processing Magazine*, no. 34-43, 2005.

[100] K. Takahashi, Y. Monno, M. Tanaka, and M. Okutomi, "Effective color correction pipeline for a noisy image", vol. 2016-August, 2016, pp. 4002–4006. DOI: 10.1109/ICIP.2016.7533111.

[101] G. Hong, M. Luo, and P. Rhodes, "A study of digital camera colorimetric characterization based on polynomial modeling", *Color Research and Application*, vol. 26, no. 1, pp. 76–84, 2001. DOI: 10.1002/1520-6378(200102)26:1<76::AID-COL8>3.0.CO;2-3.

[102] G. Finlayson, M. Mackiewicz, and A. Hurlbert, "Root-polynomial colour correction", 2011, pp. 115–119.

[103] G. Finlayson, M. MacKiewicz, and A. Hurlbert, "Color correction using root-polynomial regression", *IEEE Transactions on Image Processing*, vol. 24, no. 5, pp. 1460–1470, 2015. DOI: 10.1109/TIP.2015.2405336.

[104] P. Hung, "Colorimetric calibration in electronic imaging devices using a look-up-table model and interpolations", *Journal of Electronic Imaging*, vol. 2, no. 1, pp. 53–61, 1993. DOI: 10.1117/12.132391.

[105] K. L. Huang, S.-C. Hsieh, and H.-C. Fu, "Cascade-cmac neural network applications on the color scanner to printer calibration", vol. 1, 1997, pp. 10–15. DOI: 10.1109/ICNN.1997.611626.

[106] G. K. Wallace, "The jpeg still picture compression standard", *IEEE transactions on consumer electronics*, vol. 38, no. 1, pp. xviii–xxxiv, 1992.

[107] D. Le Gall, "Mpeg: A video compression standard for multimedia applications", *Communications of the ACM*, vol. 34, no. 4, pp. 46–58, 1991.

[108] D. Williams, P. D. Burns, and L. Scarff, "Imaging performance taxonomy", in *Image Quality and System Performance VI*, International Society for Optics and Photonics, vol. 7242, 2009, p. 724 208.

[109] I. E. D. Wueller, "Image engineering digital camera tests", 2006.

[110] W. van Bommel, "Glare", in *Encyclopedia of Color Science and Technology*, R. Luo, Ed. New York, NY: Springer New York, 2014, pp. 1–11, ISBN: 978-3-642-27851-8. DOI: 10.1007/978-3-642-27851-8_125-3. [Online]. Available: https://doi.org/10.1007/978-3-642-27851-8_125-3.

[111] J. J. McCann and A. Rizzi, "Retinal hdr images: Intraocular glare and object size", *Journal of the Society for Information Display*, vol. 17, no. 11, pp. 913–920, 2009.

[112] A. Rizzi and J. J. McCann, "Glare-limited appearances in hdr images", *Journal of the Society for Information Display*, vol. 17, no. 1, pp. 3–12, 2009.

[113] J. J. McCann and A. Rizzi, "Camera and visual veiling glare in hdr images", *Journal of the Society for Information Display*, vol. 15, no. 9, pp. 721–730, 2007.

[114] P. Hansen, J. Wienold, and M. Andersen, "Hdr images for glare evaluation: Comparison between dslr cameras, an absolute calibrated luminance camera and a spot luminance meter", in *Proceedings of the Conference on" Smarter Lighting for Better Life" at the CIE Midterm Meeting 2017*, CIE-International Commission on Illumination, 2017, pp. 553–563.

[115] A. Rizzi, B. R. Barricelli, C. Bonanomi, L. Albani, and G. Gianini, "Visual glare limits of hdr displays in medical imaging", *IET Computer Vision*, vol. 12, no. 7, pp. 976–988, 2018.

[116] J. J. McCann and A. Rizzi, "Veiling glare: The dynamic range limit of hdr images", in *Human Vision and Electronic Imaging XII*, International Society for Optics and Photonics, vol. 6492, 2007, p. 649 213.

[117] C. Fischer and I. Kakoulli, "Multispectral and hyperspectral imaging technologies in conservation: Current research and potential applications", *Studies in Conservation*, vol. 51, no. sup1, pp. 3–16, 2006.

[118] G. Lu and B. Fei, "Medical hyperspectral imaging: A review", *Journal of biomedical optics*, vol. 19, no. 1, p. 010 901, 2014.

[119] A. Signoroni, M. Savardi, A. Baronio, and S. Benini, "Deep learning meets hyperspectral image analysis: A multidisciplinary review", *Journal of Imaging*, vol. 5, no. 5, p. 52, 2019.

[120] M. Teke, H. S. Deveci, O. Haliloğlu, S. Z. Gürbüz, and U. Sakarya, "A short survey of hyperspectral remote sensing applications in agriculture", in *2013 6th International Conference on Recent Advances in Space Technologies (RAST)*, IEEE, 2013, pp. 171–176.

[121] C. Cucci, J. K. Delaney, and M. Picollo, "Reflectance hyperspectral imaging for investigation of works of art: Old master paintings and illuminated manuscripts", *Accounts of chemical research*, vol. 49, no. 10, pp. 2070–2079, 2016.

[122] J. Transon, R. d'Andrimont, A. Maugnard, and P. Defourny, "Survey of hyperspectral earth observation applications from space in the sentinel-2 context", *Remote Sensing*, vol. 10, no. 2, p. 157, 2018.

[123] J Striova, A Dal Fovo, and R Fontana, "Reflectance imaging spectroscopy in heritage science", *La Rivista del Nuovo Cimento*, pp. 1–52, 2020.

[124] E.-V. Talvala, A. Adams, M. Horowitz, and M. Levoy, "Veiling glare in high dynamic range imaging", *ACM Transactions on Graphics (TOG)*, vol. 26, no. 3, 37–es, 2007.

[125] G. Gianini, C. Bonanomi, C. Mio, M. Anisetti, and A. Rizzi, "Glare removal as an ill-conditioned problem", *Journal of Electronic Imaging*, vol. 28, no. 6, p. 063 014, 2019.

[126] J. Behmann, K. Acebron, D. Emin, S. Bennertz, S. Matsubara, S. Thomas, D. Bohnenkamp, M. T. Kuska, J. Jussila, H. Salo, *et al.*, "Specim iq: Evaluation of a new, miniaturized handheld hyperspectral camera and its application for plant phenotyping and disease detection", *Sensors*, vol. 18, no. 2, p. 441, 2018.

[127] ISO, "Iso 9358: 1994 (en). optics and optical instruments—veiling glare of image forming systems—definitions and methods of measurement.", Available online: https://www.iso.org/standard/17042.html, Tech. Rep., 1994.

[128] R. Eschbach and W. A. Fuss, *Image-dependent sharpness enhancement*, US Patent 5,363,209, 1994.

[129] S. Imai and K. Fukasawa, *Image color adjustment*, US Patent App. 12/590,981, 2010.

[130] D. Pettigrew, A. Bryant, J. C. Arndt, O. Fedkiw, and R. A. Gallagher, *Color balance*, US Patent 8,823,726, 2014.

[131] S. S. Saquib and J. E. Thornton, *Digital image exposure correction*, US Patent 7,283,666, 2007.

[132] R. A. Peters, "A new algorithm for image noise reduction using mathematical morphology", *IEEE transactions on Image Processing*, vol. 4, no. 5, pp. 554–568, 1995.

[133] I. Ovsiannikov, *Method and apparatus for image noise reduction using noise models*, US Patent 8,160,381, 2012.

[134] Y. Shimoni, *Image contrast enhancement arrangement*, US Patent 4,907,288, 1990.

[135] J. A. Stark, "Adaptive image contrast enhancement using generalizations of histogram equalization", *IEEE Transactions on image processing*, vol. 9, no. 5, pp. 889–896, 2000.

[136] D. S. Hooper, *Image contrast enhancement*, US Patent 8,014,034, 2011.

[137] T. Kawabata, K. Hosoe, N. Shinoda, S. Sakai, and T. Kinoshita, *Image sharpness detecting system*, US Patent 4,377,742, 1983.

[138] G. M. Johnson and M. D. Fairchild, "Sharpness rules", in *Color and Imaging Conference*, Society for Imaging Science and Technology, vol. 2000, 2000, pp. 24–30.

[139] R. M. Evans, *Method for correcting photographic color prints*, US Patent 2,571,697, 1951.

[140] S. M. Pizer, E. P. Amburn, J. D. Austin, R. Cromartie, A. Geselowitz, T. Greer, B. T. H. Romeny, and J. B. Zimmerman, "Adaptive histogram equalization and its variations", *Comput. Vision Graph. Image Process.*, vol. 39, no. 3, pp. 355–368, Sep. 1987, ISSN: 0734-189X. DOI: 10.1016/S0734-189X(87)80186-X.

[141] K. Zuiderveld, "Contrast limited adaptive histogram equalization", in *Graphics gems IV*, Academic Press Professional, Inc., 1994, pp. 474–485.

[142] M. D. Fairchild and G. M. Johnson, "The icam framework for image appearance, image differences, and image quality", *Journal of Electronic Imaging*, vol. 13, pp. 126–138, 2004.

[143] K. Jiangtao, Y. Hiroshi, L. Changmeng, M. J. Garrett, and M. D. Fairchild, "Evaluating hdr rendering algorithms", *ACM Trans. Appl. Percept.*, vol. 4, no. 2, p. 9, 2007, ISSN: 1544-3558. DOI: http://doi.acm.org/10.1145/1265957.1265958.

[144] A. Rizzi, C. Gatta, and M. D., "A new algorithm for unsupervised global and local color correction", *Pattern Recognition Letters*, vol. 24, no. 11, pp. 1663–1677, 2003.

[145] R. A., G. C., and M. D., "From retinex to automatic color equalization: Issues in developing a new algorithm for unsupervised color equalization", *Journal of Electronic Imaging*, vol. 13(1), pp. 75–84, 2004.

[146] O. Kolas, I. Farup, and A. Rizzi, "Spatio-temporal retinex-inspired envelope with stochastic sampling: A framework for spatial color algorithms", *Journal of Imaging Science and Technology*, vol. 55, Jul. 2011. DOI: 10.2352/J.ImagingSci.Technol.2011.55.4.040503.

[147] E. Provenzi, M. Fierro, A. Rizzi, L. De Carli, D. Gadia, and D. Marini, "Random spray retinex: A new retinex implementation to investigate the local properties of the model", *IEEE Transactions on Image Processing*, vol. 16, no. 1, pp. 162–171, 2007.

[148] A. Rizzi and J. McCann, "On the behavior of spatial models of color", *Proc SPIE*, vol. 6493, Jan. 2007. DOI: 10.1117/12.708905.

[149] G. Simone, "Measuring and enhancing the contrast and quality of digital images", *Doctoral Dissertation at the Faculty of Mathematics and Natural Sciences at the University of Oslo*, 2016. [Online]. Available: https://www.duo.uio.no/handle/10852/65413.

[150] A. Rizzi and C. Bonanomi, "Milano retinex family", *Journal of Electronic Imaging*, vol. 26, no. 3, pp. 031 207–031 207, 2017.

[151] D. Marini and A. Rizzi, "A computational approach to color adaptation effects", *Image Vision Computing*, vol. 18(13), 1005–1014, 2000.

[152] E. Provenzi, L. De Carli, A. Rizzi, and D. Marini, "Mathematical definition and analysis of the retinex algorithm", *Journal of Optical Society America A*, vol. 22, no. 12, pp. 2613–2621, 2005. DOI: 10.1364/JOSAA.22.002613.

[153] N. Banic and S. Loncaric, "Light random sprays retinex: Exploiting the noisy illumination estimation", *IEEE Signal Processing Letters*, vol. 20, pp. 1240 – 1243, 2013.

[154] ——, "Smart light random memory sprays retinex: A fast retinex implementation for high-quality brightness adjustment and color correction", *Journal of Optical Society America A*, vol. 32, pp. 2136 –2147, 2015.

[155] E. Provenzi, C. Gatta, M. Fierro, and A. Rizzi, "A spatially variant white-patch and gray-world method for color image enhancement driven by local contrast", *IEEE Transactions on Pattern Analysis and Machine Intelligence*, vol. 30, no. 10, pp. 1757–1770, 2008, ISSN: 1939-3539. DOI: 10.1109/TPAMI.2007.70827.

[156] G. Simone, G. Audino, I. Farup, F. Albregtsen, and A. Rizzi, "Termite Retinex: a new implementation based on a colony of intelligent agents", *Journal of Electronic Imaging*, vol. 23, no. 1, pp. 1 –14, 2014. DOI: 10.1117/1.JEI.23.1.013006.

[157] A. Rizzi, D. Fogli, and B. R. Barricelli, "A new approach to perceptual assessment of human-computer interfaces", *Multimedia Tools and Applications*, vol. 76, no. 5, pp. 7381–7399, 2017.

[158] C. Parraman and A. Rizzi, "User preferences in colour enhancement for unsupervised printing methods", in *Color Imaging XII: Processing, Hardcopy, and Applications*, International Society for Optics and Photonics, vol. 6493, 2007, 64930U.

[159] C Parraman and A Rizzi, "Searching user preferences in printing: A proposal for an automatic solution", *Printing Technology SpB06*, 2006.

[160] M. Chambah, A. Rizzi, C. Gatta, B. Besserer, and D. Marini, "Perceptual approach for unsupervised digital color restoration of cinematographic archives", in *Color Imaging VIII: Processing, Hardcopy, and Applications, Santa Clara, CA, USA, January 20, 2003*, 2003, pp. 138–149. DOI: 10.1117/12.472019. [Online]. Available: https://doi.org/10.1117/12.472019.

[161] A. Rizzi, M. Chambah, D. Lenza, B. Besserer, and D. Marini, "Tuning of perceptual technique for digital movie color restoration", in *Visual Communications and Image Processing 2004, VCIP 2004, San Jose, California, USA, 18-22 January 2004*, 2004, pp. 1286–1294. DOI: 10.1117/12.525789. [Online]. Available: https://doi.org/10.1117/12.525789.

[162] A. Rizzi and M. Chambah, "Perceptual color film restoration", *SMPTE Motion Imaging Journal*, vol. 119, no. 8, pp. 33–41, 2010.

[163] A. B.M. T. Islam and I. Farup, "Spatio-temporal colour correction of strongly degraded movies", in *Color Imaging XVI: Displaying, Processing, Hardcopy, and Applications*, vol. 7866, 2011, 78660Z. DOI: 10.1117/12.872105.

[164] A. Rizzi, A. J. Berolo, C. Bonanomi, and D. Gadia, "Unsupervised digital movie restoration with spatial models of color", *Multimedia Tools and Applications*, vol. 75, no. 7, pp. 3747–3765, 2016.

[165] A. Rizzi, M. Lecca, A. Plutino, and S. Liberini, "Designing a cockpit for image quality evaluation", in *Transactions: Imaging/Art/Science: Image Quality, Content and Aesthetics*, 2019.

[166] M. Chambah, C. Gatta, and A. Rizzi, "Linear techniques for image sequence processing acceleration", in *Color Imaging X: Processing, Hardcopy, and Applications*, International Society for Optics and Photonics, vol. 5667, 2005, pp. 263–274.

[167] A. Artusi, C. Gatta, D. Marini, W. Purgathofer, and A. Rizzi, "Speed-up technique for a local automatic colour equalization model", in *Computer Graphics Forum*, Wiley Online Library, vol. 25, 2006, pp. 5–14.

[168] M. Bertalmío, V. Caselles, E. Provenzi, and A. Rizzi, "Perceptual color correction through variational techniques", *IEEE Transactions on Image Processing*, vol. 16, no. 4, pp. 1058–1072, 2007.

[169] M. Bertalmío, V. Caselles, and E. Provenzi, "Issues about retinex theory and contrast enhancement", *International Journal of Computer Vision*, vol. 83, no. 1, pp. 101–119, 2009.

[170] D. Gadia, D. Villa, C. Bonanomi, A. Rizzi, and D. Marini, "Local color correction of stereo pairs", in *Stereoscopic Displays and Applications XXI*, International Society for Optics and Photonics, vol. 7524, 2010, 75240W.

[171] P. Getreuer, "Automatic color enhancement (ace) and its fast implementation", *Image Processing On Line*, vol. 2, pp. 266–277, 2012.

[172] J. S. Romero, L. M. Procel, L. Trojman, and D. Verdier, "Implementation and optimization of the algorithm of automatic color enhancement in digital images", in *2017 IEEE International Autumn Meeting on Power, Electronics and Computing (ROPEC)*, IEEE, 2017, pp. 1–6.

[173] A. Rizzi, B. R. Barricelli, C. Bonanomi, A. Plutino, and M. P. Lanaro, "Spatial models of color for digital color restoration", in *Conservation, Restoration, and Analysis of Architectural and Archaeological Heritage*, IGI Global, 2019, pp. 386–404.

[174] MathWorks. (). "Norm", [Online]. Available: https://it.mathworks.com/help/matlab/ref/norm.html#d122e878195 (visited on 11/21/2020).

[175] ——, (). "Integralimage", [Online]. Available: https://it.mathworks.com/help/images/ref/integralimage.html (visited on 11/21/2020).

[176] UNESCO, "Recommendation for the safeguarding and preservation of moving images", *Technical report*, 27 October 1980.

[177] K. Dave, "Film riches, cleaned up for posterity", *New York Times*, 2010.

[178] S. Bellotti, *Analisi dei punti critici e dei problemi organizzativi nel processo di restauro digitale di pellicole, per lo sviluppo di un protocollo guida*. Università degli Studi di Milano, 2017, vol. Master thesis.

[179] S. Dagna, *Perchè Restaurare i film?* Edizioni ETS, 2014.

[180] C. Brandi, *Teoria del restauro*. Einaudi, 1963.

[181] V. Boarini and V. Opela, "Charter of film restoration", *Journal of Film Preservation*, vol. 83, pp. 37–39, 2010.

[182] R. Image Permanence Institute, *Film care*, 2019. [Online]. Available: https://www.filmcare.org/ (visited on 10/23/2019).

[183] G. Fossati, *From Grain to Pixel*. Amsterdam University Press, 2009.

[184] N. Fairbairn, P. M.A, and T. Ross, *The FIAF Moving Image Cataloguing Manual*. Edited by Linda Todic for the FIAF Cataloguing and Documentation Commission, 2016.

[185] P. Uccello, *Cinema. tecnica e Linguaggio*. Edited by San Paolo, 1997.

[186] B. Flueckiger, *Timeline of historical film colors*, 2011-2013. [Online]. Available: https://filmcolors.org/ (visited on 10/24/2019).

[187] *Women film pioneers, french film colorists*, 2019. [Online]. Available: https://wfpp.columbia.edu/essay/french-film-colorists/ (visited on 10/24/2019).

[188] J. Capstaff and M. Seymour, "The kodacolor process for amateur color cinematography", *Transactions of the Society of Motion Picture Engineers*, vol. 12, no. 36, pp. 940–947, 1928.

[189] *L'atelier de restauration et de conservation des photographies de la ville de paris - chromogenic prints*, 2013. [Online]. Available: https://www.parisphoto.com/en/Glossary/chromogenic-prints/ (visited on 10/24/2019).

[190] Kodak, *The Essential Reference Guide for Filmmaker*. 2019.

[191] P. Sprawls, *Physical Principles of Medical Imaging*. Medical Physics Publishing Corporation, 1995.

[192] A. Cornwell-Clyne, *Colour cinematography*. Chapman and Hall, 1936.

[193] Kodak, "Kodak vision2 500t color negative film 5218 / 7218", *Technical Data*, 2002.

[194] P. Siegel and D. Peterson, *Film scanning*, 2015.

[195] FADGI, *Federal agencies digital guidelines initiative - guidelines*, 2016. [Online]. Available: http://www.digitizationguidelines.gov/guidelines/ (visited on 12/02/2019).

[196] H. van Dormolen, *Metamorfoze preservation imaging guidelines*, 2012. [Online]. Available: https://www.metamorfoze.nl/english/digitization (visited on 12/02/2019).

[197] D. Cultural Heritage, *Digital transitions division of cultural heritage*, 2019. [Online]. Available: https://dtculturalheritage.com/ (visited on 12/02/2019).

[198] ICCD, "Normativa per l'acquisizione digitale delle immagini fotografiche (regulation regarding the digital acquisition of photographic images)", *Roma*, 1998.

[199] ICCU, "Linee di indirizzo per i progetti di digitalizzazione del materiale fotografico (giodelines regarding projects for the digitization of photographic materials)", *edited by Gruppo di lavoro sulla digitalizzazione del materiale fotografico*, 2004.

[200] IFLA, "Guidelines for planning the digitization of rare book and manuscript collections", *International Federation of Library Associations and Institutes*, 2014.

[201] M. Project, "Technical guidelines for digital cultural content creation programmes", *Minerva Project by UKOLN, University of Bath, in association with MLA The Council for Museums, Libraries and Archives*, 2004.

[202] R. Lombardia, "Dematerializzazione - linee guida per gli enti locali", *Agenda Digitale Lombardia*, 2012.

[203] N. Mazzanti, *Ciname colors, now and then*, 2019.

[204] H. Brendel, *The ARRI Companion to Digital Intermediate*. Arnold, Richter Cine Technik GmbH, and Co Betriebs KG, 2005.

[205] M. Chambah, C. Saint-Jean, F. Helt, and A. Rizzi, "Further image quality assessment in digital film restoration", in *Image Quality and System Performance III*, International Society for Optics and Photonics, vol. 6059, 2006, 60590S.

[206] A. Rizzi and A. Plutino, "Algorithms for film digital restoration: Unsupervised approaches for film frames enhancement", in *Moving Pictures, Living Machines: Automation, Animation and the Imitation of Life in Cinema and Media*, 2019.

[207] A. Plutino and A. Rizzi, "Alternative methods for digital contrast restoration", in *Imagine Math 7*, Springer, 2020, pp. 73–87.

[208] S. Bellotti, G. Bottaro, A. Plutino, and M. Valsesia, "Mathematically based algorithms for film digital restoration", in *Imagine Math 7*, Springer, 2020, pp. 89–104.

[209] A. Plutino, M. Lanaro, G. Alfredo, R. Cammarata, and A. Rizzi, "Ace for super 8 movie restoration", in *Mathematics for Computer Vision*, 2018.

[210] ——, "Work memories in super 8: The dawn of paper recycling in brescia", in *YOCOCU*, 2018.

[211] O Isabella, A. Plutino, M. Lanaro, and A Rizzi, "All the colours of a film: Study of the chromatic variation of movies", in *AIC Lisboa 2018: color and human comfort*, 2018.

[212] A. Plutino, S. Bellotti, C. Lombardi, P. Guerrini, and R. A., "The funerals of the bombing of piazza della loggia in brescia: An example of rescue of an historical and amatorial document", in *IX Conference "Diagnosis, Conservation and Valorisation of Cultural Heritage"*, 2018.

[213] A. Plutino, M. Lecca, and A. Rizzi, "A cockpit of measures for image quality assessment in digital film restoration", in *International Conference on Image Analysis and Processing*, Springer, 2019, pp. 159–169.

[214] A. Rizzi and A. Plutino, "Paper recycling consciousness into schools: An audiovisual evidence from the '80", in *12th Orphan Film Symposium - Water, Climate, & Migration hosted by the 6th Eye International Conference,*, 23-27 May 2020, Amsterdam.

[215] ScanDig. (). "Reflecta super8 scanner test report", [Online]. Available: https://www.filmscanner.info/en/ReflectaSuper8Scanner.html (visited on 12/21/2018).

[216] B. M. Design, *Da vinci resolve 16*, 2019. [Online]. Available: https://www.blackmagicdesign.com/it/products/davinciresolve/ (visited on 07/11/2019).

[217] D. Vision, *Phoenix film restoration software*, 2019. [Online]. Available: http://www.digitalvision.tv/products/phoenix_film_restoration/ (visited on 07/11/2019).

[218] S. Zuffi, R. Cereda, and A Rizzi, "Valutazione automatica di interventi di restauro del colore in opere cinematografiche", in *Conferenza Nazionale del Gruppo del Colore*, Centro editoriale toscano, 2007.

[219] I. O. for Standardization, *ISO 8402: 1994: Quality Management and Quality Assurance-Vocabulary*. International Organization for Standardization, 1994.

[220] I. ISO, "9000: 2000—quality management systems—fundamentals and vocabulary", *International Organization for Standardization (ISO), Switzerland*, 2004.

[221] M. Pedersen, "Image quality metrics for the evaluation of printings workflows", *Doctoral Dissertation submitted at the Faculty of Mathematics and Natural Sciences at the University of Oslo*, 2011, ISSN: 1501-7710.

[222] S. Yendrikhovskij, "Color reproduction and the naturalness constraint", *Doctoral Dissertation submitted at Eindhoven: Technische Universiteit Eindhoven.*, 1998.

[223] ——, "Computational image quality", *PhD thesis, IPO, Center for User-System Interaction*, 1999.

[224] P. G. Engeldrum, "Image quality modeling: Where are we?", in *PICS*, 1999, pp. 251–255.

[225] M. Fairchild, "Image quality measurement and modeling for digital photography", 2002.

[226] B. W. Keelan, *Handbook of Image Quality - Characterization and Prediction*. New York, NY: Marcel Dekker, 2002. DOI: Inc.ISBN978-0-8247-0770-5.

[227] B. W. Keelan and H. Urabe, "Iso 20462: A psychophysical image quality measurement standard", in *Image Quality and System Performance*, International Society for Optics and Photonics, vol. 5294, 2003, pp. 181–189.

[228] I. I. I. Association *et al.*, "Cpiq initiative phase 1 white paper: Fundamentals and review of considered test methods", *Director of Standards, I3A*, 2007.

[229] H. de Ridder and S. Endrikhovski, "33.1: Invited paper: Image quality is fun: Reflections on fidelity, usefulness and naturalness", in *SID Symposium Digest of Technical Papers*, Wiley Online Library, vol. 33, 2002, pp. 986–989.

[230] M. Pedersen and J. Yngve Hardeberg, "Full-reference image quality metrics: Classification and evaluation", *Foundations and Trends(R) in Computer Graphics and Vision*, vol. 7, pp. 1–80, Jan. 2012. DOI: 10.1561/0600000037.

[231] I. R. Assembly, "Recommendation itu-r bt.500-11 - methodology for the subjective assessment of the quality of television pictures", *Technical Report*, vol. 500-11, 2002.

[232] S. Grgic, M. Grgic, and M. Mrak, "Reliability of objective picture quality measures", *Journal of Electrical Engineering*, vol. 55, pp. 3–10, 2004, ISSN: 335-3632.

[233] Z. Wang and A. C. Bovik, "A universal image quality index", *IEEE Signal Processing Letters*, vol. 9, no. 3, pp. 81–84, 2002, ISSN: 1070-9908. DOI: 10.1109/97.995823.

[234] I. Avcibaş, B. Sankur, and K. Sayood, "Statistical evaluation of image quality measures", *Journal of Electronic imaging*, vol. 11, no. 2, pp. 206–223, 2002.

[235] Z. Wang and A. C. Bovik, "Modern image quality assessment", *Synthesis Lectures on Image, Video, and Multimedia Processing*, 2006. DOI: 10.2200/S00010ED1V01Y200508IVM003.

[236] P. Le Callet and D. Barba, "A robust quality metric for color image quality assessment", in *Proceedings 2003 International Conference on Image Processing (Cat. No. 03CH37429)*, IEEE, vol. 1, 2003, pp. I–437.

[237] D. M. Chandler and S. S. Hemami, "Vsnr: A wavelet-based visual signal-to-noise ratio for natural images", *IEEE transactions on image processing*, vol. 16, no. 9, pp. 2284–2298, 2007.

[238] K.-H. Thung and P. Raveendran, "A survey of image quality measures", in *2009 international conference for technical postgraduates (TECHPOS)*, IEEE, 2009, pp. 1–4.

[239] K Seshadrinathan and A. Bovik, "The encyclopedia of multimedia", *Chapter Image and Video Quality Assessment*, pp. 8–17, 2009.

[240] E. W. S. Fry, S. Triantaphillidou, R. E. Jacobson, J. R. Jarvis, and R. B. Jenkin, "Bridging the gap between imaging performance and image quality measures", *Electronic Imaging*, vol. 2018, no. 12, pp. 231–1, 2018.

[241] X. Zhang and B. A. Wandell, "A spatial extension of cielab for digital color-image reproduction", *Journal of the Society for Information Display*, vol. 5, no. 1, pp. 61–63, 1997. DOI: 10.1889/1.1985127.

[242] Z. Wang, A. C. Bovik, H. R. Sheikh, and E. P. Simoncelli, "Image quality assessment: From error visibility to structural similarity", *IEEE transactions on image processing*, vol. 13, no. 4, pp. 600–612, 2004.

[243] H. Sheikh and A. Bovik, "Image information and visual quality", *IEEE Transactions on Image Processing*, vol. 15, no. 2, pp. 430–444, 2006, ISSN: 1057-7149. DOI: 10.1109/TIP.2005.859378.

[244] Z. Wang, E. P. Simoncelli, and A. C. Bovik, "Multiscale structural similarity for image quality assessment", in *The Thrity-Seventh Asilomar Conference on Signals, Systems & Computers, 2003*, Ieee, vol. 2, 2003, pp. 1398–1402.

[245] L. Zhang, L. Zhang, X. Mou, and D. Zhang, "Fsim: A feature similarity index for image quality assessment", *IEEE Transactions on Image Processing*, vol. 20, no. 8, pp. 2378–2386, 2011, ISSN: 1057-7149. DOI: 10.1109/TIP.2011.2109730.

[246] O. Tunç, R. Mantiuk, K. Myszkowski, and H. Seidel, "Dynamic range independent image quality assessment", *ACM Trans. Graph.*, vol. 27, no. 3, 69:1–69:10, Aug. 2008, ISSN: 0730-0301. DOI: 10.1145/1360612.1360668.

[247] R. Mantiuk, K. J. Kim, A. G. Rempel, and W. Heidrich, "Hdr-vdp-2: A calibrated visual metric for visibility and quality predictions in all luminance conditions", *ACM Trans. Graph.*, vol. 30, no. 4, 40:1–40:14, Jul. 2011, ISSN: 0730-0301. DOI: 10.1145/2010324.1964935.

[248] R. Reisenhofer, S. Bosse, G. Kutyniok, and T. Wiegand, "A haar wavelet-based perceptual similarity index for image quality assessment", *Signal Processing: Image Communication*, vol. 61, pp. 33 –43, 2018, ISSN: 0923-5965. DOI: https://doi.org/10.1016/j.image.2017.11.001.

[249] E. C. Larson and D. M. Chandler, "Most apparent distortion: Full-reference image quality assessment and the role of strategy", *Journal of electronic imaging*, vol. 19, no. 1, p. 011 006, 2010.

[250] A. Mittal, A. K. Moorthy, and A. C. Bovik, "Blind/referenceless image spatial quality evaluator", in *2011 Conference Record of the Forty Fifth Asilomar Conference on Signals, Systems and Computers (ASILOMAR)*, 2011, pp. 723–727. DOI: 10.1109/ACSSC.2011.6190099.

[251] ——, "No-reference image quality assessment in the spatial domain", *IEEE Transactions on Image Processing*, vol. 21, pp. 4695–4708, 2012.

[252] A. Mittal, R. Soundararajan, and A. C. Bovik, "Making a "completely blind" image quality analyzer", *IEEE Signal Processing Letters*, vol. 20, pp. 209–212, 2013.

[253] A. Rizzi, T. Algeri, G. Medeghini, and D. Marini, "A proposal for contrast measure in digital images", *Conference on Colour in Graphics, Imaging, and Vision*, vol. 2004, no. 1, pp. 187–192, 2004.

[254] E. Peli, "Contrast in complex images", *JOSA A*, vol. 7, no. 10, pp. 2032–2040, 1990.

[255] ——, "In search of a contrast metric: Matching the perceived contrast of gabor patches at different phases and bandwidths", *Vision Research*, vol. 37, no. 23, pp. 3217–3224, 1997.

[256] R. Eschbach, B. L. Waldron, and W. A. Fuss, *Image-dependent luminance enhancement*, US Patent 5,450,502, 1995.

[257] G Boccignone, "Visual contrast controlled by diffusion", in *Proc. International School of Biocybernetics, Downward Processing in the Perception Representation Mechanisms*, 1996.

[258] P Renegal and A. Zador, "Natural scene statistics at the center of gaze", *Network: Comput. Neural Syst*, vol. 10, pp. 1–10, 1999.

[259] Y Tadmor and D. Tolhurst, "Calculating the contrasts that retinal ganglion cells and lgn neurones encounter in natural scenes", *Vision research*, vol. 40, no. 22, pp. 3145–3157, 2000.

[260] M. Pedersen, A. Rizzi, J. Y. Hardeberg, and G. Simone, "Evaluation of contrast measures in relation to observers perceived contrast", in *CGIV/MCS*, 2008, pp. 253–258.

[261] A. Rizzi, G. Simone, and R. Cordone, "A modified algorithm for perceived contrast measure in digital images", in *CGIV 2008 and MCS'08 Final Program and Proceedings*, 2008, pp. 249–252.

[262] N. Nahvi and D. P. Mittal, "Medical image fusion using discrete wavelet transform", *International Journal of Engineering Research and Applications*, vol. 4, no. 9, pp. 165–170, 2014.

[263] M. Lecca, A. Rizzi, and R. P. Serapioni, "Great: A gradient-based color-sampling scheme for retinex", *JOSA A*, vol. 34, no. 4, pp. 513–522, 2017.

[264] X. Guo, Y. Li, and H. Ling, "Lime: Low-light image enhancement via illumination map estimation", *IEEE Transactions on image processing*, vol. 26, no. 2, pp. 982–993, 2016.

[265] S. Wang and G. Luo, "Naturalness preserved image enhancement using a priori multi-layer lightness statistics", *IEEE transactions on image processing*, vol. 27, no. 2, pp. 938–948, 2017.

[266] M. Lecca, "Star: A segmentation-based approximation of point-based sampling milano retinex for color image enhancement", *IEEE Transactions on Image Processing*, vol. 27, no. 12, pp. 5802–5812, 2018.

[267] K. Gu, D. Tao, J.-F. Qiao, and W. Lin, "Learning a no-reference quality assessment model of enhanced images with big data", *IEEE transactions on neural networks and learning systems*, vol. 29, no. 4, pp. 1301–1313, 2017.

[268] C.-C. Chang and C.-J. Lin, "Libsvm: A library for support vector machines", *ACM transactions on intelligent systems and technology (TIST)*, vol. 2, no. 3, pp. 1–27, 2011.

[269] M. Lecca, G. Simone, C. Bonanomi, and A. Rizzi, "Point-based spatial colour sampling in milano-retinex: A survey", *IET Image Processing*, vol. 12, no. 6, pp. 833–849, 2018, ISSN: 1751-9659. DOI: 10.1049/iet-ipr.2017.1224.

[270] M. Lecca and S. Messelodi, "Super: Milano retinex implementation exploiting a regular image grid", *JOSA A*, vol. 36, no. 8, pp. 1423–1432, 2019.

[271] B. R. Barricelli, G. Fischer, D. Fogli, A. Mørch, A. Piccinno, and S. Valtolina, "Cultures of participation in the digital age: From" have to" to" want to" participate", in *Proceedings of the 9th Nordic Conference on Human-Computer Interaction*, 2016, pp. 1–3.

[272] M. Lecca and A. Rizzi, "Tuning the locality of filtering with a spatially weighted implementation of random spray retinex", *JOSA A*, vol. 32, no. 10, pp. 1876–1887, 2015.

[273] A. Rizzi, C. Gatta, C. Slanzi, G. Ciocca, and R. Schettini, "Unsupervised color film restoration using adaptive color equalization", in *Visual Information and Information Systems, 8th International Conference, VISUAL 2005, Amsterdam, The Netherlands, July 5, 2005, Revised Selected Papers*, 2005, pp. 1–12. DOI: 10.1007/11590064/_1.

[274] A. Plutino, *Tecniche di Restauro Cinematografico – Metodi e Pratiche tra Analogico e Digitale*. Dino Audino Editore, 2017.

[275] A. Rizzi, M. P. Lanaro, A. Plutino, L Simone, S Gabriele, and B Serena, "Mips lab", in *Computer Vision, Pattern Recognition e Machine Learning*, 2018.

[276] L. Grechi, A. Plutino, and R. A., "Test percettivi per la valutazione della differenza cromatica sotto diversi illuminanti", in *Conferenza Nazionale del Gruppo del Colore*, XV Color Conference, Gruppo del Colore, 5th – 7th September 2019, Macerata (Italy), 2019.

[277] A Rizzi, A Plutino, and M Rossi, "Fundamentals of color teaching in postgraduate education", in *International Color Association*, International Color Association (AIC), 2019, pp. 538–542.

[278] M. Rossi, A. Plutino, A. Siniscalco, and A. Rizzi, "Teaching color and color science: The experience of an international master course", *Electronic Imaging*, vol. 2020, no. 15, pp. 165–1, 2020.

[279] A Rizzi and A Plutino, "Film restoration: Closing the gap between humanities and hard sciences", in *Science ABC hosted by Università La Sapienza di Roma*, Rome, 19-21 February 2020.

[280] M. Cereda, A. Plutino, and A. Rizzi, "Quick gamut mapping per la color correction", in *Conferenza Nazionale del Gruppo del Colore*, 3-4 September 2020, 2020.

[281] B. Sarti, A. Plutino, and A. Rizzi, "Glare ottico nelle immagini iperspettrali", in *Conferenza Nazionale del Gruppo del Colore*, 3-4 September 2020, 2020.

[282] F. Barenghi, M. Bittante, N. Del Longo, C. Mangano, A. Plutino, and A. Rizzi, "Uno studio sull'associazione colori, termini ed emozioni, basato sui colori primari di lüscher", in *Conferenza Nazionale del Gruppo del Colore*, 3-4 September 2020, 2020.

[283] M. F. Gaspani, P. R. Spada, A. Plutino, and A. Rizzi, "Un film in un frame: Studio sulle variazioni cromatiche in film e video digitali", in *Conferenza Nazionale del Gruppo del Colore*, 3-4 September 2020, 2020.

[284] S. Scipioni, C. A. Lombardi, L. Giuliani, A. Plutino, and A. Rizzi, "Verso una più ampia comprensione del daltonismo: Un test sulla discriminazione di colori in scene complesse", in *Conferenza Nazionale del Gruppo del Colore*, 3-4 September 2020, 2020.